2015

FERROCENE-FUSED DERIVATIVES OF ACENES, TROPONES AND THIEPINS

Bidhya L. Maharjan
University of Kentucky, bidhya2006@gmail.com

STUDENT AGREEMENT:

I represent that my thesis or dissertation and abstract are my original work. Proper attribution has been given to all outside sources. I understand that I am solely responsible for obtaining any needed copyright permissions. I have obtained needed written permission statement(s) from the owner(s) of each third-party copyrighted matter to be included in my work, allowing electronic distribution (if such use is not permitted by the fair use doctrine) which will be submitted to UKnowledge as Additional File.

I hereby grant to The University of Kentucky and its agents the irrevocable, non-exclusive, and royalty-free license to archive and make accessible my work in whole or in part in all forms of media, now or hereafter known. I agree that the document mentioned above may be made available immediately for worldwide access unless an embargo applies.

I retain all other ownership rights to the copyright of my work. I also retain the right to use in future works (such as articles or books) all or part of my work. I understand that I am free to register the copyright to my work.

REVIEW, APPROVAL AND ACCEPTANCE

The document mentioned above has been reviewed and accepted by the student's advisor, on behalf of the advisory committee, and by the Director of Graduate Studies (DGS), on behalf of the program; we verify that this is the final, approved version of the student's thesis including all changes required by the advisory committee. The undersigned agree to abide by the statements above.

Bidhya L. Maharjan, Student

Dr. John P. Selegue, Major Professor

Dr. Dong-Sheng Yang, Director of Graduate Studies

FERROCENE-FUSED DERIVATIVES OF ACENES, TROPONES AND THIEPINS

DISSERTATION

A dissertation submitted in partial fulfillment of the
requirements for the degree of Doctor of Philosophy in the
College of Arts and Science
at the University of Kentucky

By
Bidhya Laxmi Maharjan
Lexington, Kentucky
Director: Dr. John P. Selegue, Professor of Chemistry
Lexington, Kentucky

2015

ABSTRACT OF DISSERTATION

FERROCENE-FUSED DERIVATIVES OF POLYACENES, TROPONES AND THIEPINS

This research project is concentrated on tuning the properties of small organic molecules, namely polyacenes, tropones and thiepins, by incorporating redox-active transition metal centers π-bonded to terminal cyclopentadienyl ligands. Organometallic-fused acenequinones, tropones, thiepins and cyclopentadiene-capped polyacenes were synthesized and characterized. This work was divided into three parts: first, the synthesis of ferrocene-fused acenequinones, cyclopentadiene-capped acenequinones and their subsequent aromatization to polyacenes; second, the synthesis of ferrocene-fused tropones, thiotropones and tropone oxime; and third, the synthesis of ferrocene-fused thiepins.

Ferrocene-fused quinones are the precursors to our target complexes. Our synthetic route to ferrocenequinones involved two-fold aldol condensation between 1,2-diformylferrocene and naphthalene-1,4-diol or anthracene-1,4-diol, and four-fold condensation between 1,2-diformylferrocene and 1,4-cyclohexanedione. Reduction of ferrocene-fused quinones with borane in THF resulted in ferrocene-fused dihydroacenes. Attempts to reduce ferrocene-fused acenequinones with sodium dithionite led to metal-free cyclopentadiene- (Cp-) capped acenequinones. Cp-capped acenequinones were aromatized to bis(triisopropylsilyl)ethynyl polyacenes by using lithium (triisopropylsilyl)acetylide (TIPSC≡CLi) with subsequent dehydroxylation by stannous chloride. The compounds were characterized by using spectroscopic methods and X-ray crystallography. Further, the electronic properties of these compounds were studied by using cyclic voltammetry and UV-visible spectroscopy. Cyclic voltammetry showed oxidation potentials of Cp-capped TIPS-tetracene and bis-Cp-capped TIPS-anthracene as 0.49 V and 0.61 V, respectively (vs. ferrocene/ferrocenium). The electrochemical band gaps were 2.15 eV and 2.58 eV, respectively. Organic thin-film transistor device performance of Cp-capped polyacenes was studied using solution deposition bottom-contact, bottom-gate (BCBG) device architecture and the resulting performance parameters are described herein.

Similarly, we are also interested in potential applications of metallocene-fused tropones and derivatives as organic electronic materials. Condensation of 1,2-diformylferrocene with acetone or 1,3-diphenylacetone in the presence of KOH resulted in the ferrocene-fused tropone (η^5-2,4-cyclopentadien-1-yl)[(1,2,3,3a,8a-η)-1,6-dihydro-6-oxo-1-azulenyl]iron (**1**, R = H, E = O) and its 5,7-diphenyl derivative **(1,** R **=** Ph, E = O) as previously reported by Tirouflet. The use of piperidine as base resulted in Michael addition of piperidine to one of the carbon-carbon double bonds of the tropones. Lawesson's reagent converted the ferrocene-fused tropones to either a thiotropone (**1**, R = H, E = S) or a detached 5,7-diphenylazulenethiol (**2**). Reaction of the ferrocene-fused thiotropone with hydroxylamine gave the corresponding oxime (**1**, R = H, E = NOH). Products were characterized by using spectroscopic methods and X-ray crystallography. Their electronic properties were studied by using cyclic voltammetry and UV-visible spectroscopy.

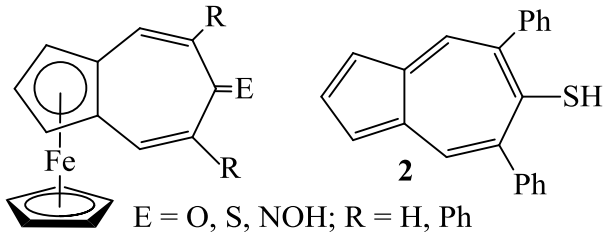

1 E = O, S, NOH; R = H, Ph **2**

The third project involved the two-fold aldol condensation of 1,2-diformylferrocene with dimethylthioglycolate S-oxide in the presence of freshly distilled triethylamine, which gave mono- and di-dehydrated products. Deoxygenation of the ferrocene-fused thiepin S-oxide with 2-chloro-1,3,2-benzodioxaphosphole in the presence of pyridine resulted in the corresponding thiepin. The ester groups of the thiepin and thiepin S-oxide were hydrolyzed under basic conditions to give carboxylic acids, which were converted into acid chlorides using oxalyl chloride. Attempts to decarboxylate the thiepin and thiepin S-oxide diacids resulted in decomposition.

KEYWORDS: ferrocene, aldol condensation, organometallic, acenequinone, tropone, thiepin

Bidhya Laxmi Maharjan

06/17/2015

FERROCENE-FUSED DERIVATIVES OF POLYACENES, TROPONES AND THIEPINS

By

Bidhya Laxmi Maharjan

Dr. John P. Selegue

Director of Dissertation

Dr. Dong-Sheng Yang

Director of Graduate Studies

6/17/2015

Date

To

My Parents

ACKNOWLEDGEMENTS

I am grateful to many people for their guidance, time, effort and patience in helping to further my scientific aspirations. I first and foremost would like to thank wholeheartedly my advisor, Professor John P. Selegue for his constant guidance, motivation, constructive criticism, dedication and commitment to scientific research. I am very grateful for his tremendous effort, time and patience in training me how to be an independent researcher.

I would like to express my sincere thanks to my advisory committee members, Professors Arthur Cammers, David Atwood, Bruce J. Hinds, and Douglass Kalika for their support, constructive criticism and helpful ideas throughout my Ph.D. studies. I would like to thank professor H Peter Spielmann for serving as the external examiner during my final defense.

I am thankful to Dr. Sean Parkin for his help with X-ray crystallography. I would also like to thank Mr. John Layton for his time and energy spent in acquiring NMR data and Dr. Jack Goodman for mass spectra services. I would also like to express my thanks to Mr. Art Sebesta (electronics) and Mr. J. Babbitt (glassware) for their time and effort in maintaining and keeping the instrument in workable condition. Without their prompt support, my research would not have gone smoothly.

I am grateful to Prof. John E. Anthony for allowing me to work in his lab and to use the cyclic voltammeter and UV spectrometer independently. I would like to thank his graduate student Dr. Matthew J. Bruzek for teaching me how to use electronic and optical instruments. I would also like to thank Professor Aram Amassion and Muhammad Rizwan Khan Niazi from King Abdullah University of Science and Technology, Saudi Arabia for providing the OFET studies of our compounds.

I am thankful for all my former and current group members Uttam, Rituraj, Mahendra, Deepshikha, Surya and Ilya for their friendliness, support and help in the lab, sharing their ideas and skills and also for creating an excellent working environment. I would like to extend my sincere thanks to my loving friends for their endless help.

I would like to express my deepest gratitude to my parents, Madan and Kamala Maharjan, my husband, Ishwor Maharjan and sisters and brother for their support in all rough times. Without their love, supervision and encouragement, I could not be who I am today. Also, I am very thankful to my husband's family for their support and understanding.

Table of Contents

List of Figures

List of Charts

List of Schemes

List of Tables

List of Abbreviations and Symbols

General

Å	angstrom, 10^{-10} m
Anal.	Analysis
[°]	degrees
η^5	pentahapto
n-BuLi	*n*-butyllithium, $CH_3(CH_2)_3Li$
Bu_4NPF_6	tetrabutylammonium hexafluorophosphate
Cp	cyclopentadienyl
°C	degree Celsius
d_{calc}	calculated density, Mg/m^3
dec	decomposed
DMF	N,N-Dimethylformamide
EI MS	electron impact mass spectrometry
Fc	ferrocenyl
Fc/Fc^+	ferrocene/ferrocenium
G	grams
GCMS	gas chromatography-mass spectrometry
GOF	goodness of fit
h	hours
kJ	kilojoules
M^+	molecular ion

Me	methyl, CH_3
mg	milligrams
min	minutes
mL	milliliters
μL	microliters
mmol	millimoles
mp	melting point
MS	mass spectra
m/z	mass-to-charge ratio
Ph	phenyl
R	R-factor (for X-ray crystallography)
Rw	weighted R-factor
s	seconds
t	time
T	temperature
THF	tetrahydrofuran, C_4H_8O

For nuclear magnetic resonance (NMR) spectra

δ	chemical shift (in parts per million)
d	doublet
dd	doublet of doublets
dt	doublet of triplets
Hz	hertz, s^{-1}
J	coupling constant

m	multiplet
NMR	nuclear magnetic resonance
ppm	parts per million
s	singlet
t	triplet
For infrared (IR) spectra	
ATR	Attenuated total reflectance
br	broad
cm^{-1}	wavenumbers
FT IR	Fourier Transform Infrared Spectra
s	strong
w	weak

Chapter 1 Organic Semiconductors

Inorganic semiconductors such as silicon (Si) and germanium (Ge) have dominated applications in the area of light-emitting diodes (LEDs), thin-film transistors (TFTs) and photovoltaic cells for the past few decades. However, recent contributions from several research groups in the field of organic semiconductor materials has enabled the use of organic molecules in optoelectronic applications, including organic light-emitting diodes (OLEDs), organic field-effect transistors (OFETs), organic photovoltaic cells,[1a-1c] sensors,[2] flat-panel displays[3] and radio-frequency identification tags (RF-IDs).[4] Organic semiconductors are of interest due to their ease of purification and large-scale, more flexible, lower temperature solution processing and lower cost of manufacture.[5] The ideal candidate should be stable under ambient conditions, suitable for solution processing, and possess high charge mobility.

Two important classes of organic semiconductors are conjugated polymers and linearly fused aromatic rings (polyacenes). These molecules are used for the charge-transport layer in organic electronic devices due to their extended π-conjugation, which lowers the energy gap between the highest occupied molecular orbital (HOMO) and lowest unoccupied molecular orbital (LUMO). Acenes have well-defined molecular weights, highly ordered crystalline structures and exhibit high charge carrier mobility. Polymers, on the other hand, suffer from undefined molecular weights and fewer purification techniques. These limitations affect the electronic properties of polymers.[6]

Unlike inorganic semiconductors, both polymers and acenes[6,7] can be processed by solution-phase fabrication methods such as inkjet printing, spin-casting, drop-casting and blade-coating, allowing future technological devices to be smaller, thinner and more

flexible as well as lowering the manufacturing cost of electronics. These advantages of organic conjugated small molecules may satisfy the increasing demand for cheaper, wide-area coverage, flexible devices that can be processed at lower substrate temperature than conventional silicon- and germanium-based semiconductors.[8]

Acenes have disadvantages such as poor solubility in common organic solvents and instability toward atmospheric oxygen, moisture and light. Many of these obstacles have been circumvented by functionalizing the acenes.[6] The environmental stability of organic semiconductors is the most important aspect for commercialization. Environmental sensitivity of these materials can be overcome by operating devices under inert conditions; but this could shrink the cost-savings of moving to organic semiconductor materials from inorganic semiconductors. Therefore, the application of organic semiconductors in the market still suffers from two major issues, life span and performance.

Thin-film transistors (TFTs) are the logic units for modern day microelectronic devices. In the Si and Ge semiconductors, the atoms are bonded closely with strong covalent interactions (100–400 kJ/mol)[9] and form highly ordered three-dimensional crystal lattice structures with better atomic orbital overlap than organic semiconductors, which causes charge carriers to transport in highly delocalized, band-like mechanisms.[10] While in organic semiconductors, namely acenes and heteroacenes, organic molecules are held together by weak van der Waals interactions (< 5 kJ/mol), π–π intermolecular (0–50 kJ/mol), and hydrogen bonding (10–65 kJ/mol).[9] Therefore, the atomic orbital overlap in organic semiconductor materials is weak, which results in poor charge-carrier transport.

Organic thin-film transistors (OTFTs) are also known as organic field-effect transistors (OFETs). Transistors can act as switches and amplifiers with the current flow between the source and drain electrodes controlled by an applied electric field to the gate electrode. OTFT devices consist of three major components called dielectric, semiconductor and three electrodes (gate, source and drain). The source and drain electrodes are commonly gold (Au); however other metals such as Ag, Pt, Pd, Al, Ca, Mg and polymers such as PEDOT:PSS and poly(aniline)[11] have been used, depending on the nature of organic molecules (p- or n-types). The gate electrode can be a metal or a conducting polymer, but highly doped silicon is often used. Inorganic insulators such as SiO_2, Al_2O_3, Si_3N_4, [11] HfO_2,[12] and polymer insulators such as poly(methyl methacrylate), (PMMA), poly(4-vinylphenol) (PVP) and polyvinyl alcohol (PVA)[13,14] have been commonly used as the dielectric layer.

The semiconducting layer is either vacuum-deposited or solution-phase fabricated by spin-coating, drop-coating or inkjet printing. Depending on how organic molecules are deposited relative to one another, two common device configurations are used in OFETs: one is bottom-contact, bottom-gate and the second is top-contact, bottom-gate. Although top-contact, bottom-gate device configuration gives better device performance[8, 15] because it has low contact resistance due to the large area for charge injection from the electrode to semiconductor, bottom-contact, bottom-gate device configuration is often preferred because develop metal electrodes on the top contact can damage the underlying organic semiconducting layer.[16`]

The distance between source and drain electrodes is called channel length, denoted by *L*. The width of source and drain electrodes is called channel width, denoted

by *W*. The voltage applied between source and gate electrodes, gate voltage (V_g) results in the accumulation of charge carriers at the dielectric-semiconductor interface. The voltage applied between source and drain electrodes, source-drain voltage (V_{ds}), results in the conduction of charge carriers in the accumulation layer, and this is known as the *on* state of the device. Ideally, when no V_g is applied, the conductance of the semiconducting layer should be zero because there is little to no current flow between the electrodes. Therefore, the device enters the *off* state. If the voltage applied to the gate electrode is enough to overcome the threshold voltage (V_{Th}), drain current (I_d) can be measured. If the voltage applied to the gate electrode is not enough to overcome V_{Th}, the current measured is the leakage current ($I_{Leakage}$) resulting from charge carrier tunneling through the insulating dielectric.[17]

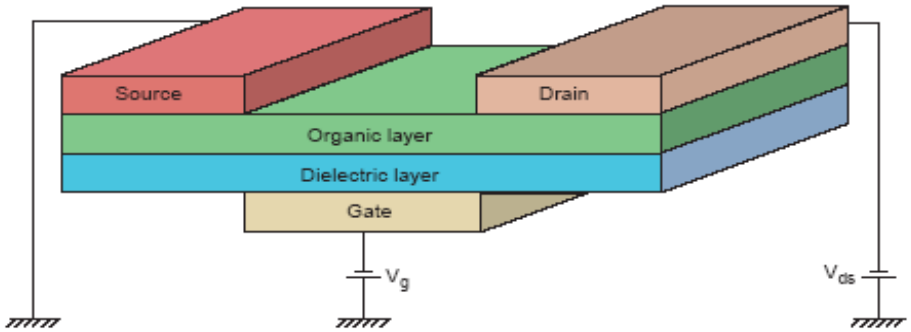

Figure 1.1 Schematic diagram of an OTFT.[18]

An OTFT's performance can be characterized by plotting drain current versus drain voltage at various gate voltages. At a low source-drain voltage ($V_{ds} << V_g$) the current flowing through the device is directly proportional to applied voltage (V_{ds}) and is known as linear regime (Figure 1.2). The current (I_d) flowing through the channel is given by

$$I_d = (W/L)\mu_{lin}C_i(V_g - V_{Th})V_{ds} \quad (1)$$

where W = channel width,

L = channel length

C_i = capacitance of the insulator

μ = charge carrier mobility

V_g = gate voltage

V_{Th} = threshold voltage

V_{ds} = drain voltage

As the applied V_{ds} increases, the device deviates from ohmic behavior. With further increase in voltage, the current flowing through the channel reaches a constant value as the device enters saturated regime (Figure 1.2).

The current flowing through the channel is given by equation 2.

$$I_d = (W/2L)\mu_{sat}C_i(V_g - V_{Th}) \quad (2)$$

$$\sqrt{I_d} = \sqrt{\{(W/2L)\mu_{sat}C_i\}}(V_g - V_{Th}) \quad (3)$$

Using equations (1) and (2), charge-carrier mobility can be calculated in the linear and saturated regimes. The mobility calculated from the linear and saturation methods may not be the same. The difference is a property of contact effects since the mobility is dependent on the gate-source bias that is related to the carrier density in the accumulation layer.

Another method to characterize the output of OTFTs is to plot both the square root of drain current ($\sqrt{I_d}$) and log(I_d) versus V_g. Equation 3 implies that the charge carrier mobility of the device in the saturation regime can be obtained from the slope of the plot

of $\sqrt{I_d}$ versus V_{gs} and the *x*-intercept gives the V_{Th} of the device. The plot of $\log(I_d)$ versus V_g gives the *on*/*off* current ratio.

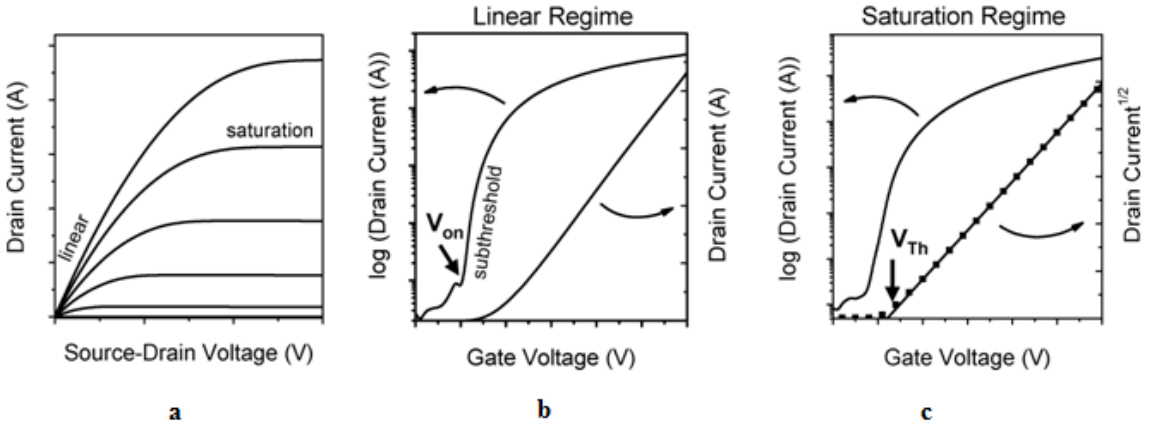

Figure 1.2 a) Output of OFET, b) $\sqrt{I_d}$ and $\log(I_d)$ vs. V_g in the linear regime, c) $\sqrt{I_d}$ and $\log(I_d)$ vs. Vg in the saturation regime [11]

The performance of an OFET is determined by the following parameters.

a) Charge carrier mobility (μ): A measure of the drift velocity of a charge (electron or hole) per unit of applied electric field. Mobility should be greater than 0.5 $cm^2/(V\ s)$ for commercial application.[6]

b) *On*/*off* current ratio ($I_{on/off}$): The ratio of current flowing between source and drain electrode in the *on* state and the *off* state of the device. For real world application, *on*/*off* current ratio should be greater than 10^5.[6]

c) Threshold voltage (V_{Th}): The gate voltage at which a conducting channel is formed in the semiconducting layer between the source and drain electrodes. V_{Th} should be close to zero for potential application.[6]

Based on the nature of charge carriers formed in the conducting channel of the device, organic semiconductors are classified into two types known as n-type and p-type.

In OFETs, positive gate voltage is required to turn on an n-type device, while negative gate voltage is required to turn on a p-type device.[15] Organic semiconductor materials that are able to conduct both electrons and holes depending on the sign of the gate bias are categorized as ambipolar materials (Chart 1.1). Most organic semiconductors are π-electron-rich species, which have a higher tendency to lose an electron to form the more stable radical cation. Most of the organic semiconductor materials reported in the literature are p-type. However, the addition of electron-withdrawing groups such as cyano, fluoro and nitro can convert p-type materials into n-type materials. Since n-type semiconductors have an electron deficiency, these materials tend to gain electrons to form a more stable radical anion. For example, complete fluorination of p-type pentacene converts it into a n-type organic semiconductor , perfluoropentacene, with an electron mobility of 0.22 $cm^2/(V\ s)$.[19]

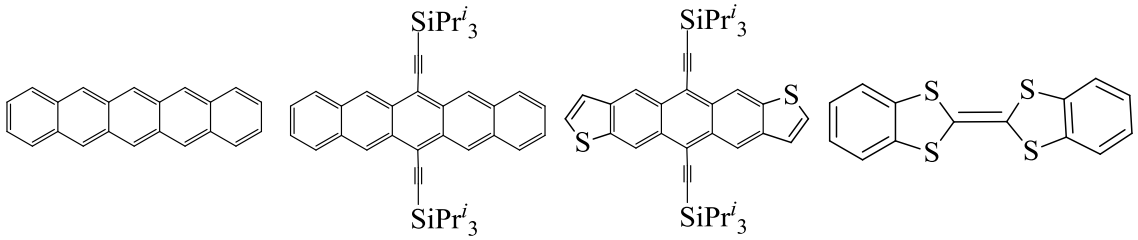

p-type Organic Semiconductors

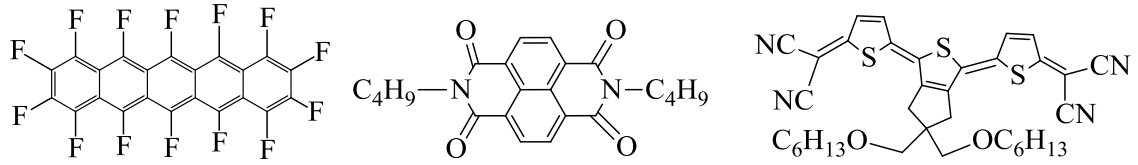

n-type Organic Semiconductors

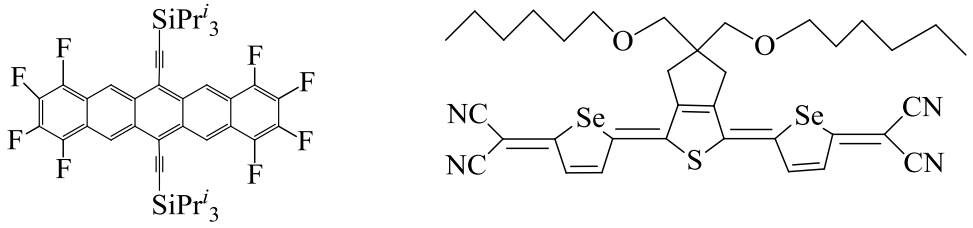

Ambipolar Semiconductors

Chart 1.1 Examples of p-type, n-type and ambipolar organic semiconductors

Polycyclic aromatic hydrocarbons (acenes), the most studied small organic semiconductors, can be synthesized to a high degree of purity with highly ordered crystallinity.[7] Acenes possess relatively high charge carrier mobilities, high *on*/*off* current ratio and low threshold voltage in OFETs, which are the required features of semiconductors. The vapor-deposited thin film of pentacene, a benchmark material, has shown hole carrier mobility greater than 3 $cm^2/(V\ s)$ in a OTFT.[20] However, some acenes exhibit poor solubility in common organic solvents and undergo decomposition in the presence of air and light. Acenes typically undergo decomposition either through photo-induced endoperoxide formation or through "butterfly" dimerization (Figure 1.3) of the

aromatic rings. Pentacene undergoes degradation by forming a symmetric butterfly dimer in light and endoperoxide formation in the presence of oxygen.[6,7]

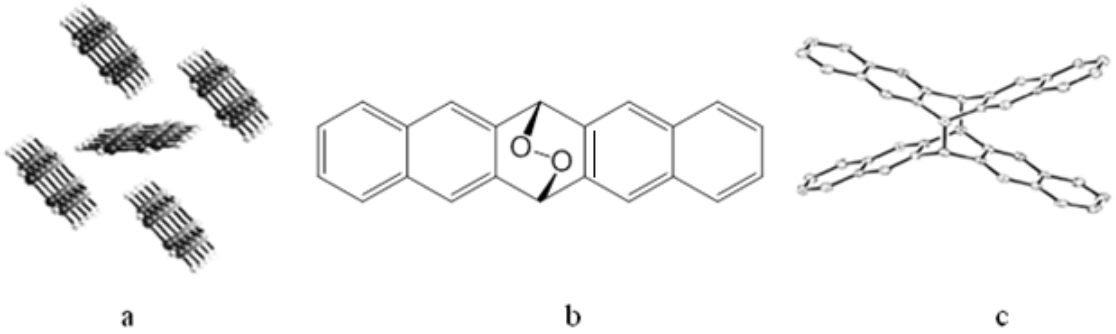

Figure 1.3 a) Herringbone packing, b) an endoperoxide, c) butterfly dimer[21]

To overcome the solubility issues and to take advantage of solution processing techniques (spin- and drop-casting), several research groups synthesized soluble adducts as pentacene precursors (Chart 1.2). The solubility of the pentacene adduct precursor in common organic solvent allows drop-casting of thin films of those materials, which are then converted into pentacene films by UV radiation followed by annealing at high temperature (150–200 °C) under an inert atmosphere. A thin film of pentacene prepared by this method produced reasonable charge carrier mobilities of 0.89 $cm^2/(V\ s)$.[19,22,23,24,25]

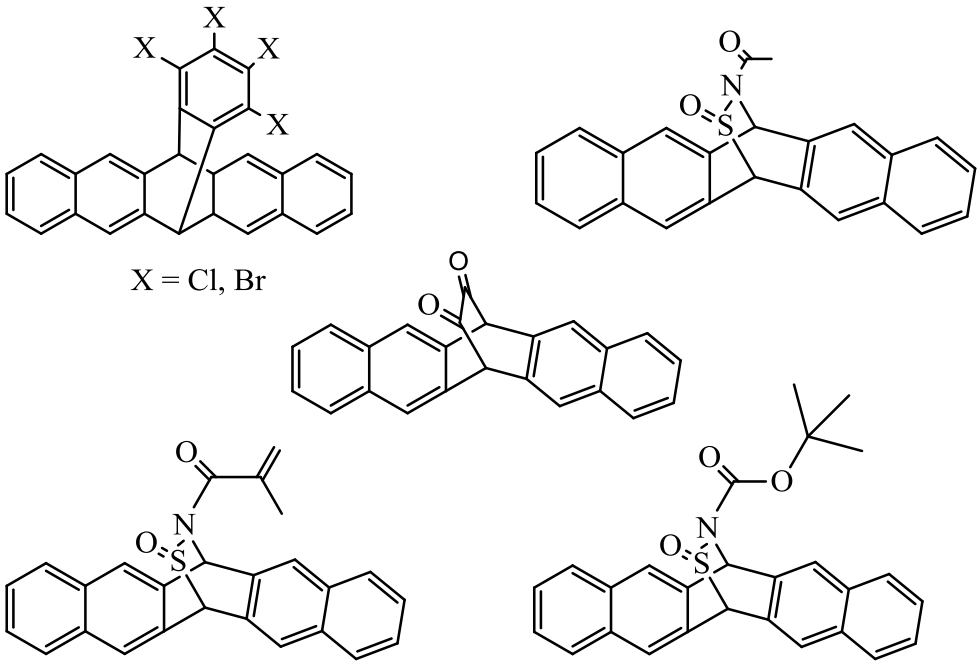

Chart 1.2 Soluble pentacene adducts

Another way to improve the solubility of acenes in organic solvents is to introduce solubilizing alkyls[26] or aryls[27,28] groups on the acene core. Wudl *et al.* reported the synthesis of methyl-substituted pentacene at the terminal rings to improve the solubility, stability and electronic properties of pentacene. Methyl substitution has shown a significant improvement in solubility and a decrease in oxidation potential versus unsubstituted pentacene, which leads to improving charge injection in electronic devices and shows hole mobility as high as 0.3 $cm^2/(V\ s)$, I_{on}/I_{off} of 6×10^3 from thermally deposited film; and methyl-substituted pentacene also leads to herringbone arrangement identical to the parent pentacene.[24]

Functionalization of acenes with solubilizing groups not only increases their solubility but also improves their stability and intermolecular interaction in crystal packing. Anthony's group developed a methodology to functionalize the acene core at the

peri-positions with trialkylsilylethynyl groups. The size of trialkylsilylethynyl group not only enhances the solubility and stability of acenes but also improves the π interaction between molecules in the solid state. The functionalization of pentacene at the central aromatic ring by triisopropylsilylethynyl (TIPS) groups resulted in two-dimensional (2-D) π-π stacking in the solid state with an interplanar spacing of 3.36 Å, enabling the use of solution processing techniques for making thin films for electronic devices. A study of a drop-cast bis(triisopropylsilylethynyl)pentacene film OFET has shown a mobility of 1.8 $cm^2/(V\ s)$ and I_{on}/I_{off} of 10^7.[6] When the triethylsilylethynyl (TES) group was used to functionalize the pentacene, it exhibited one dimensional (1-D) π stacking with a maximum mobility of 1×10^{-4} $cm^2/(V\ s)$.[6] Among the functionalized pentacene derivatives, in general 2-D π stacking arrangement in the solid state has shown the highest charge carrier mobility.

After revising the effect of size of trialkylsilylalkynyl side groups on crystal packing for linear acenes, Anthony's group designed a roadmap for achieving 2-D π stacking for linear acenes. When the diameter of the spherical substituent (silyl derivative) is close to half that of the acene backbone, it results into 2-D π stacking. When the diameter of the substituent is less or greater than half, it results in 1-D π stacking. Similarly, when the diameter of the substituent is much greater than half of the acene, it results in herringbone stacking. Therefore, the size of trialkylsilylethynyl side groups plays a vital role for tuning electronic behavior of the molecule in the solid state.

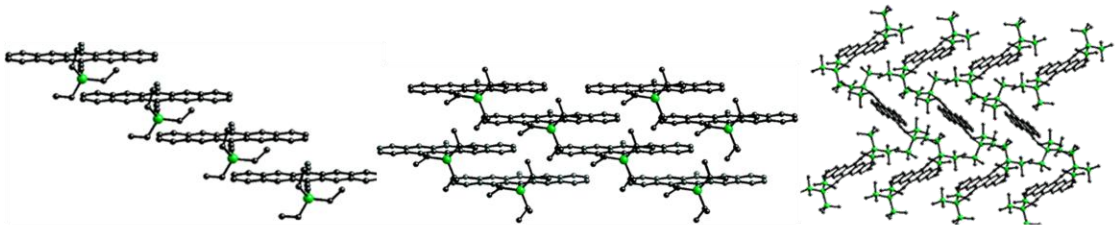

Figure 1.4 Arrangement of Pentacene derivatives in the solid state: a) one-dimensional triethylsilylethynylpentacene; b) two-dimensional π–stacking in triisopropylsilylethynylpentacene; c) herringbone in tris(trimethylsilyl)silylethynylpentacene[6]

Moreover, it is possible to improve the stability of acenes by adding bulky substituents, which hinder Diels-Alder reactions between a dienophile (multiple bonds of side group of one acene) and diene (central reactive aromatic ring of another acene).[6] To functionalize acenes through extension of the conjugation length in order to reduce band-gap and increase π-overlap, and through the improvement of charge injection by the modification of the HOMO energy level, Anthony's group has extended the acene backbone all the way to nonacene.[29]

Another strategy for improving the stability of functionalized pentacene is the partial halogenation of molecules and addition of electron-withdrawing cyano-groups that lower the HOMO energy level below that of the parent TIPS-pentacene.[30] Moreover, another approach to enhance the stability of acene molecules is to introduce heteroatoms to the acene core.[31,32] Katz and co-workers synthesized anthradithiophene (ADT) in two steps as an alternative to pentacene. They reported the synthesis and device studies of vacuum-deposited thin films of alkyl derivatives of ADT and found mobilities as high as

0.15 $cm^2/(V\ s)$.[33] Heteroacenes are of interest for electronic materials because their high HOMO energies lead to high resistance to dimerization and oxygen degradation.[34]

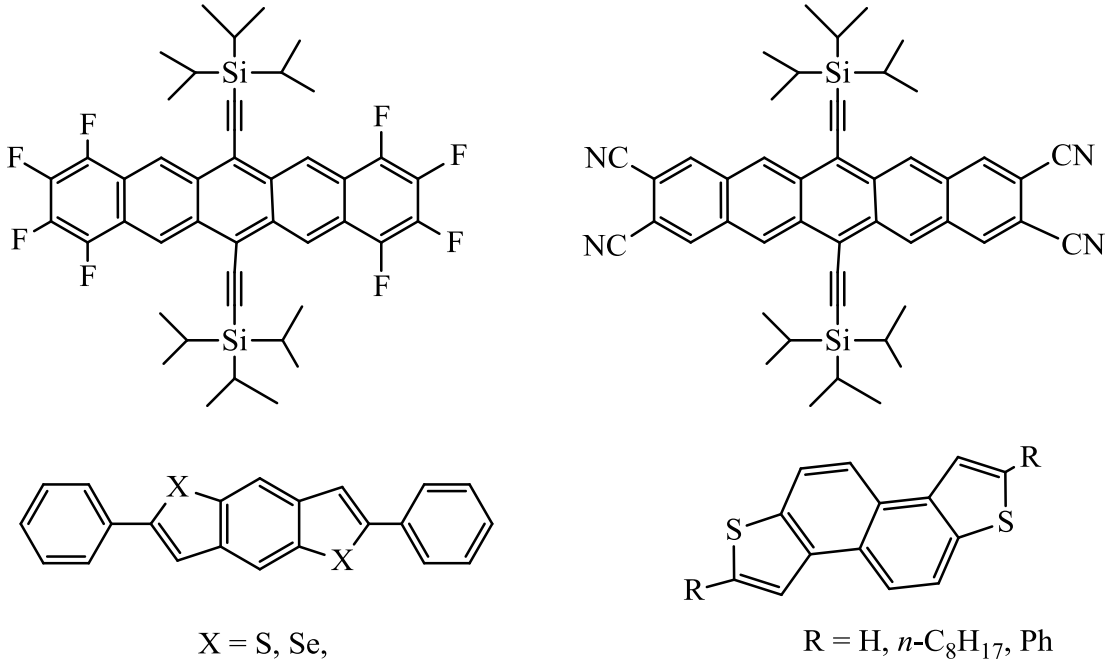

Chart 1.3 Acenes and heteroacenes with electron-withdrawing groups

Similar to the approach used for pentacene functionalization, Anthony's group utilized the trialkylsilylethynyl group at the peri position of anthradithiophene to improve stability, solubility and crystal arrangement of this material. The modification at the central ring of anthradithiophene with triethylsilylethynyl group resulted in isomeric mixtures of bis(triethylsilylethynyl) anthradithiophene (TES-ADT) and crystal arrangement showed 2-D π- interaction with a lower interplanar distance of 3.25 Å as compared to TIPS-pentacene. Device study of a drop-cast film of TES-ADT showed mobility of 1 $cm^2/(V\ s)$ and *on-off* current ratio of 10^7.[35] Even though TES-ADT has a high oxidation potential (0.91 vs. SCE) and large HOMO-LUMO energy gap, this material did not show a significant improvement in its photostability.[6]

Bao and coworkers reported the synthesis of two monothiophene acene derivatives, namely tetraceno[2,3-*b*]thiophene, and anthra[2,3-*b*]thiophene (Chart 1.4), and observed the mobilities of those materials on OTS/SiO_2/Si. Tetraceno[2,3-*b*]thiophene has shown mobility as high as 0.47 cm^2/(V s), whereas anthra[2,3-*b*]thiophene has a mobility of 0.1 cm^2/(V s).[36] Furthermore, Bao and coworkers modified the molecular structure of asymmetric linear heteroacenes by introducing trialkylsilylethynyl side groups to examine their impact on the π stacking and charge carrier mobilities. A field-effect transistor made from a vacuum-deposited thin film of bis(triisopropylsilylethynyl)tetracene[2,3-b]thiophene exhibited mobility as high as 1.25 cm^2/(V s), while vacuum-deposited TIPS-pentacene exhibited significantly lower mobility of 0.4 cm^2/(V s).[6] Moreover, Neckers *et al.* functionalized TIPS-tetraceno[2,3-*b*]thiophenes at the 6,11 and TIPS-pentacene at the 5,14 positions with methoxy groups to design the highly soluble and more photostable acenes. The enhanced photostability of these materials may be due to the methoxy groups hindering the approach of oxygen (O_2).[37, 38]

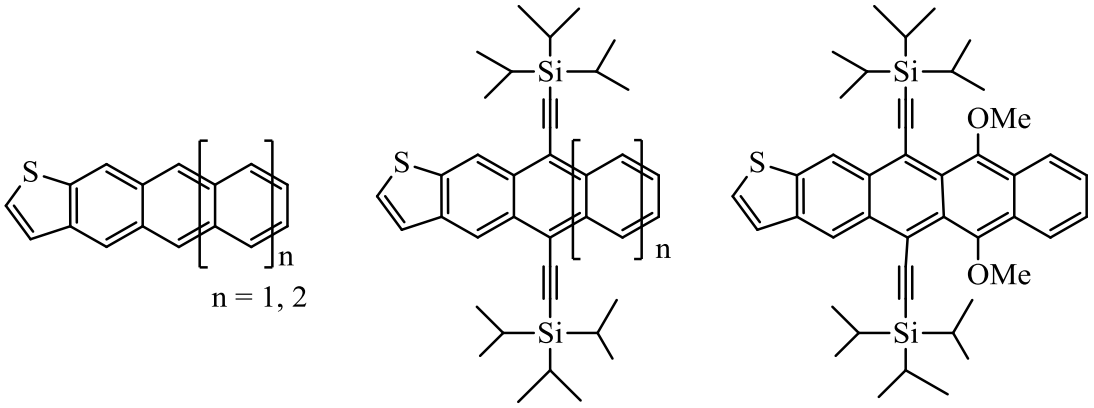

Chart 1.4 Asymmetric linear unsubstituted and trialkylsilylalkynyl substituted heteroacenes derivatives

Several research groups used different substituents to functionalize the acenes core namely alkyl, aryl and trialkylsilylethynyl. Yip et al. used a platinum ethynyl with different auxiliary ligands (Figure 1.5) to functionalize the pentacene core in order to tune emission energy and also studied the effect of metal coordination on electronic and optical properties, and packing arrangement of the complexes in the solid state.[39,40]

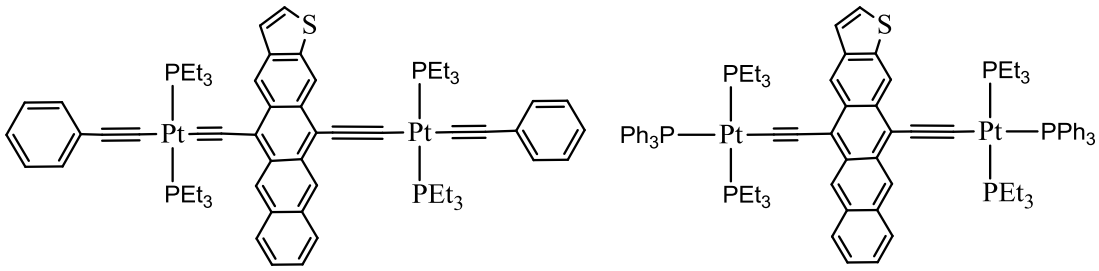

Figure 1.5 Platinum complex of ethynyl substituted acenes

Organometallic semiconductors may offer interesting characteristics that combine the physical and electronic properties of all-organic semiconducting materials with the physical, electronic, optical and catalytic properties inherent to organometallic complexes.[41] Organometallic groups can undergo oxidation and reduction processes that can be tuned by the choice of metal and ancillary ligand. If one portion of the organometallic polymer is oxidized or reduced, it can significantly impact the electrochemical properties of the polymer.[42,43] Furthermore, if the oxidation potential of metal is sufficiently matched to the reduction potential of the receiving ligand, there is an efficient conduction of electrons from a metal donor to an organic ligand. Electron communication between a metal center and an organic ligand can be used to design novel electroactive organometallic conductors.[44,45,46] Organometallic conductors may display environmental stability as well as unique redox properties due to the presence of a metal center in their molecules, which may act as a switch by changing its oxidation state. The

electronic properties of these materials can be tuned by altering the ligands attached to the transition metal center.[38]

1.1 Organometallic Complexes

Cyclopentadienyl and benzannulated cyclopentadienyl such as indenyl (Ind) and fluorenyl (Flu) are important ligands in organometallic chemistry. After the discovery of ferrocene,[47] investigations of the coordination chemistry of polycyclic aromatic compounds such as indenyl and fluorenyl intensified because of the application of those complexes in catalysts for olefin polymerization.[54-56,48] The higher reactivity of indenyl complexes than that of cyclopentadienyl complexes[49] is attributed to the ability of the indenyl ring to slip into η^3 bonding to C1–C3, aromatizing the C4–C9 ring.[50] This $\eta^5 - \eta^3$ haptotropic slip, termed the indenyl ligand effect by Basolo and Rerek,[51] opens a coordination site on the metal center, which is particularly useful for binding an additional two-electron ligand.[52]

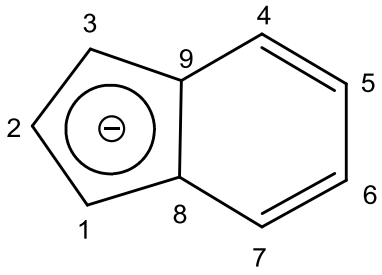

Figure 1.6 Numbering scheme of the indenyl ring

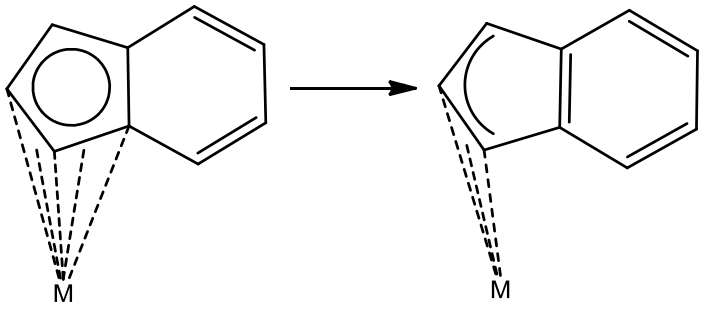

Figure 1.7 η^5 to η^3 haptotropic slip of the indenyl[53]

In 1954, Pauson and Wilkinson prepared bis(indenyl)iron(II) [Fe(η^5-$C_9H_7)_2$], by reacting indenyllithium with ferric chloride.[54] In 1964, King and Bisnette synthesized cyclopentadienylindenyliron(II), [Fe(η^5-C_5H_5)(η^5-C_9H_7)], by reacting sodium indenide, sodium cyclopentadienide and ferrous chloride.[55] Westcott et al. later reported the molecular structures of [Fe(η^5-$C_9H_7)_2$], [Co(η^5-$C_9H_7)_2$] and [Ni(η^5-$C_9H_7)_2$], demonstrating the unsymmetrical bonding modes of the five-membered ring of the indenyl group to metal. The slip parameter (ΔM–C) is defined as the difference in the average bond lengths of metal to carbon atoms C1, C2, and C3 and metal to the adjacent carbon atoms C8 and C9. The slip parameter of bis(indenyl)iron(II), (ΔFe-C) is 0.0495 Å. This value is not large enough to consider the indenyl group as significantly less than η^5 as in η^3 [Ni(η-$C_9H_7)_2$] ((Δ_{Ni-C} = 0.44 Å),[50] leading to a true η^5 coordination of a metal center in [Fe(η-$C_9H_7)_2$].

Recently, Crisp et al. synthesized bis(2-trimethylsilylindenyl)manganese(II), 1,3-bis(trimethylsilylindenyl)manganese(II) and 1,3-bis(isopropylindenyl)manganese(II) complexes (Chart 1.5) with Δ_{Mn-C} slip parameters of 0.14 Å and 0.12 Å respectively,[56] larger than that found in bis(indenyl)iron(II).

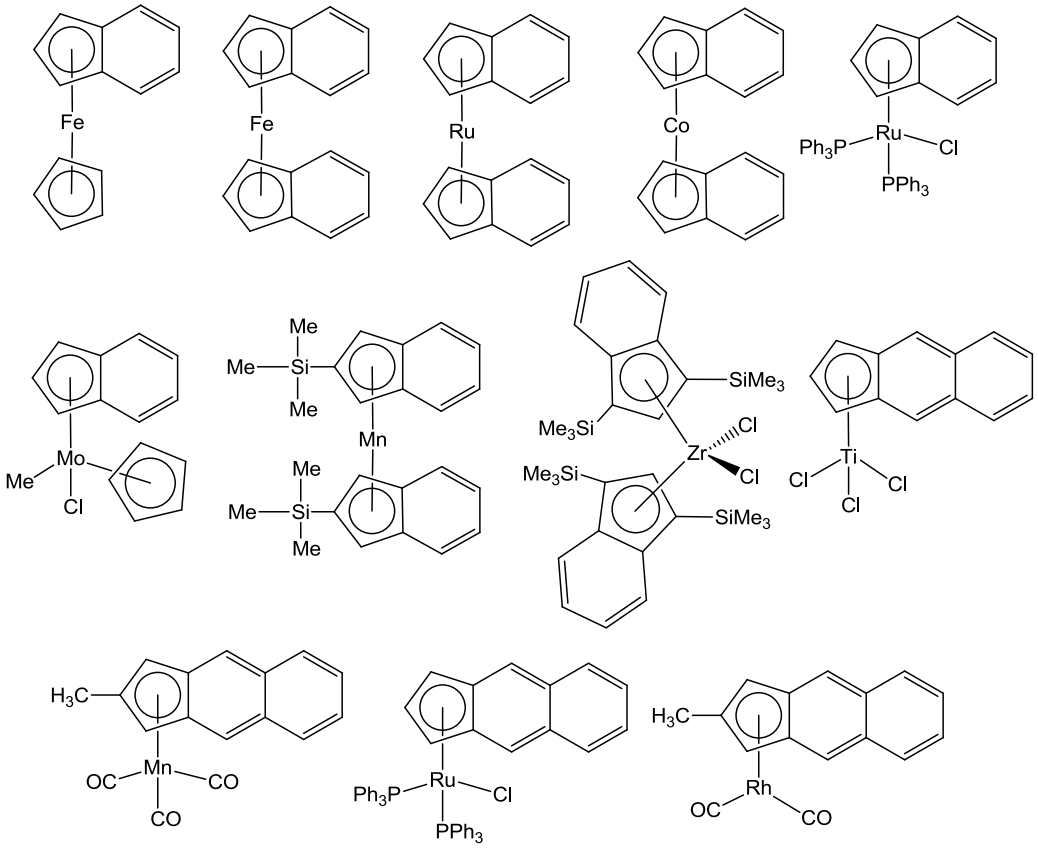

Chart 1.5 Representative indenyl and benz[*f*]indenyl complexes of transition metals

The replacement of cyclopentadienyl by benz[*f*]indenyl in homogeneous group 4 Ziegler-Natta polymerization catalysts has received much interest due to the ability of an annulated benzo ring to improve both stereocontrol and catalytic turnover. Bradley et al. prepared sterically hindered indenyl ligands, which can reversibly stabilize the Zr(II) center by toggling between η^5 and η^6 coordination modes.[57] Similarly, Kim and Foster et al. studied the catalytic activities of benz[*f*]indenyl complexes of group IV metals for the polymerization of ethylene to high molecular weight linear polymer.[58,59] Goncalves et al. synthesized mixed-ring indenyl complexes of molybdenum and studied their electrochemical properties.[60]

Fluorenyl can be considered either as a benzo-substituted cyclopentadienyl ligand or as a CH^--bridged biphenyl.[61,62] The main problem of these fluorenyl complexes is their limited solubility low stability in donor solvents. This low stability may be due to the weak bond interaction between metal and carbon, which increases the lability of ligands and allows solvent coordination with the loss of ligands.[62] Alkylation on the rings of fluorenyl complexes shows a significant improvement in their solubilities.[63]

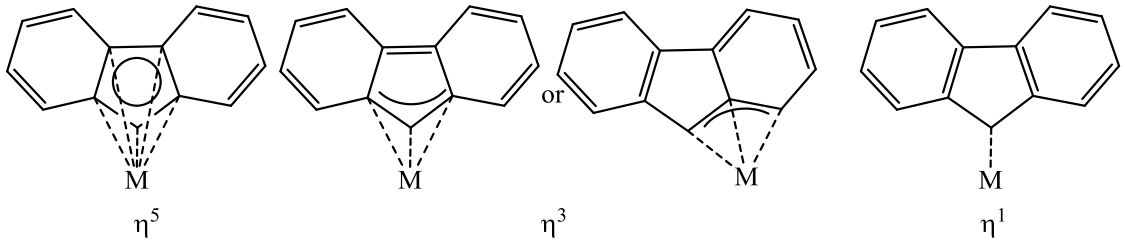

Figure 1.8 Haptotropic rearrangement of fluorenyl complexes

In 1965, Samuel and Setton synthesized bis(fluorenyl)dichlorozirconium(IV), $[ZrCl_2(C_{13}H_9)_2]$[64], which was structurally characterized by Kowala and coworkers in 1974.[65] In 1970 King and Efraty synthesized the first pentahapto-fluorenyl complex, $[Mn(CO)_3(\eta^5\text{-}C_{13}H_9)]$,[66] which was structurally characterized by Bottomley in 2002.[67] Fluorenyl complexes of alkaline earth and rare earth metals have also been synthesized (Chart 1.6).[61] In 1992 Schleyer and coworkers reported the first structurally characterized $[Ba(NH_3)_4(C_{13}H_9)_2]$ by reacting two equivalents of fluorene with barium in liquid ammonia at −80 °C with a high yield.[68] Moreover, fluorenyl complexes of a rare earth metal, $[Yb(THF)_2(C_{13}H_9)_2]$ and $[Yb(DME)(C_{13}H_9)_2]$, have also been synthesized from the metathesis approach and substitution method.[61] Several fluorenyl complexes of zirconium and hafnium with a hydrocarbon[69] or silicon[70,71] tether between two fluorenyl groups or a

fluorenyl and a cyclopentadienyl ligand have enhanced stability as well as the steric rigidity required for the regioregular catalysis of olefin polymerization.[72]

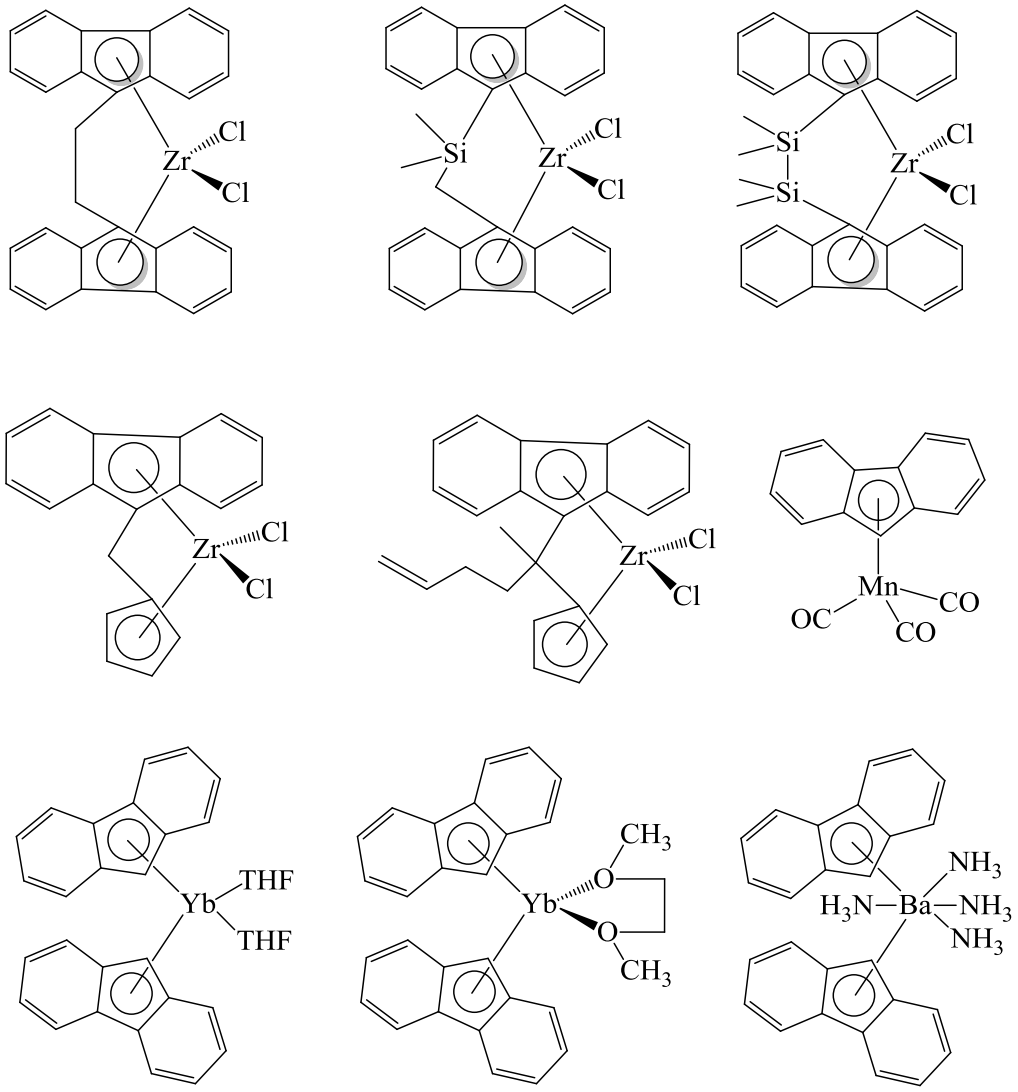

Chart 1.6 Some fluorenyl complexes of metals

In 1977, Johnson and Treichel observed an unexpected ring-slippage in an attempt to prepare fluorenyl complex of iron, [Fe(η^5-Cp)(η^5-$C_{13}H_{10}$)], where the metal was coordinated to a benzene ring instead of the Cp ring, with the formation of zwitterionic complex (Figure 1.8). This may be due to weak coordination of π extended Cp-type

ligand leading to ring slippage.[73] In 1994 Novikova et al. prepared fluorene complexes of iron, $[(\eta^6\text{-}C_{13}H_{10})Fe(\eta^5\text{-}Cp^*)]PF_6$ and $[(\eta^6\text{-}9\text{-}CH_3\text{-}C_{13}H_{10})Fe(\eta^5\text{-}Cp^*)]PF_6$, by the reaction of $Cp^*Fe(CO)_2Br$ with fluorene and 9-methylfluorene. They also observed ring slippage when $[Fe(\eta^5\text{-}Cp^*)\ (\eta^6\text{-}9\text{-}CH_3\text{-}C_{13}H_{10})]$ was heated in nonane at 150 °C with the formation of $[Fe(\eta^5\text{-}Cp^*)\ (\eta^5\text{-}9\text{-}CH_3\text{-}C_{13}H_{10})]$.[74] Similar results were obtained by the O'Hare group during the metathesis of ferrocene with Flu*H in the presence of $AlCl_3$ and Al powder.[62]

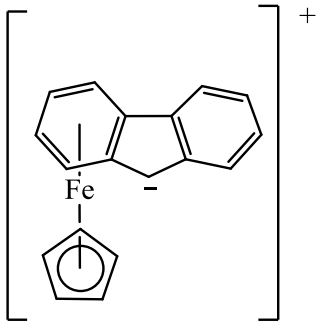

Figure 1.9 Ring slippage of iron center from η^5–Cp to η^6–arene

In 1979, Katz and Slusarek synthesized π-extended iron complexes, dicyclopenta[*a*,*h*]naphthalene and dicyclopenta[*c*,*g*]phenanthrene.[75] Further, Katz and Sudhakar synthesized π-conjugated iron complex with heptacyclic ligand (Chart 1.7) .[76]

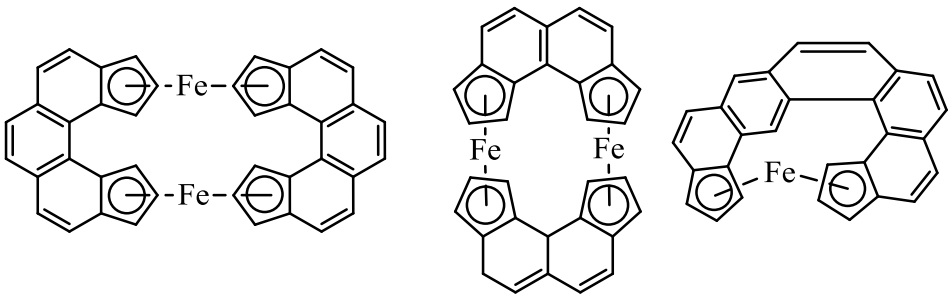

a **b** **c**

Chart 1.7 π-Conjugated iron complexes

Further annulations of benzene rings to fluorene leads to more extended π-systems. The extended π-systems of these ligands may give interesting physical properties which are important for organometallic novel material to use in the field of optoelectronic application similar to benzannulated aromatic compounds.[77] Beckhaus et al. reported a titanium complex with tetrabenzo[*a*,*c*,*g*,*i*]fluorene (Chart 1.8) and examined its application in the syndiospecific polymerization of styrene after activation with MAO.[78] The Thiel group prepared the first transition-metal complexes of the dibenzo[*c*,*g*]fluorenyl anion (Dbf^-) (**2** and **4** of Chart 1.8). A ligand, dibenzo[*c*,*g*]fluorenyl anion, can be considered as an analogue of the cyclopentadienyl anion (Cp^-). Thus, the negative charge on Dbf can stabilize a transition metal center as efficiently as cyclopentadienyl. This might be due to localization of a negative charge on the cyclopentadienyl moiety which leads to more covalent metal–ligand bond than in fluorenyl complexes.[79,80] Recently, the Toganoh group reported a double-decker ferrocene-type complex of N-fused porphyrin and compared its electronic structure with those of hypothetical π extended ferrocene derivatives to study their similarity.[81]

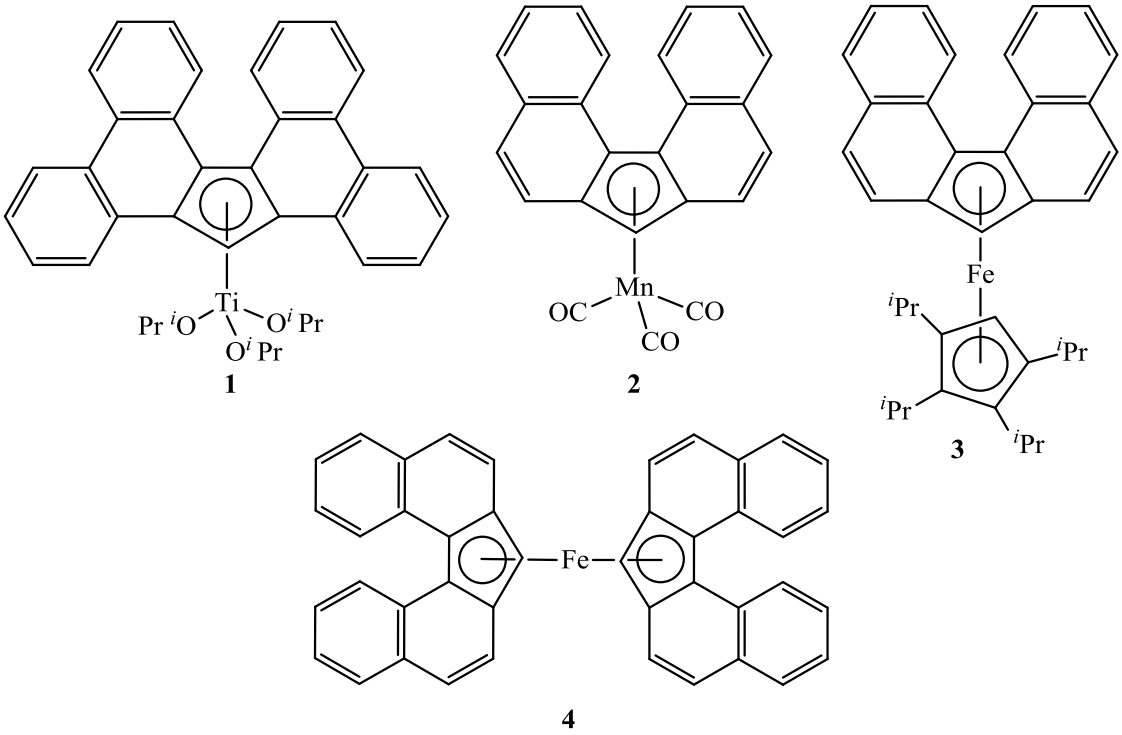

Chart 1.8 π–Extended complexes of transition metals

Although the indenyl iron complexes [Fe(η^5-C_5H_5)(η^5-C_9H_7)] and [Fe(η^5-C_9H_7)$_2$] were well characterized, there is no report of benz[*f*]indenyl or annulated benzo ring complexes of iron(II). This might be due to the weak interaction of a π extended aromatic backbone with an electron-rich iron center. Our group has a long-term interest in exploring the coordination chemistry of benzene annulated complexes of iron and examines the electronic properties of these complexes.

1.2 Overall Objectives of the Dissertation

The two-fold aldol condensation between dialdehyde and 1,4-dihydroxynaphthalene or 1,2-dihydroxyanthracene and four-fold aldol condensation between a 1,2-dialdehyde and 1,4-cyclohexanedione[82] have been used extensively in synthesizing organic acenequinones. The immediate objective of this dissertation is to

start with 1,2-diformylferrocene to extend those synthetic approaches to η^5-cyclopentadienyl-fused polycyclic quinone complexes with carbonyl groups at different positions of polycyclic backbone (**A**, Chart 1.9). Once we design the chemistry of Cp-capped quinone complexes, aromatization of the ligand can result in extension of π-conjugation to give new metallocene-fused polyacene complexes (**B**, Chart 1.9). These complexes may offer extra control of solubility, HOMO-LUMO gap, color, redox properties and solid-state packing, and utility in new electronic devices based on organometallic materials.

Similarly, the detachment of a polycyclic backbone from a metal center offers Cp-capped acenequinones. The functionalization of the resultant quinones with (trialkylsilyl)ethynyl groups gives Cp-capped substituted polyacenes (**C**, Chart 1.9). Then we investigate these complexes' structure, solid-state packing, redox and optical properties and their OTFT device performance to examine whether these complexes can fulfill the fundamental requirements of potential candidates of semiconducting materials for commercial optoelectronic applications.

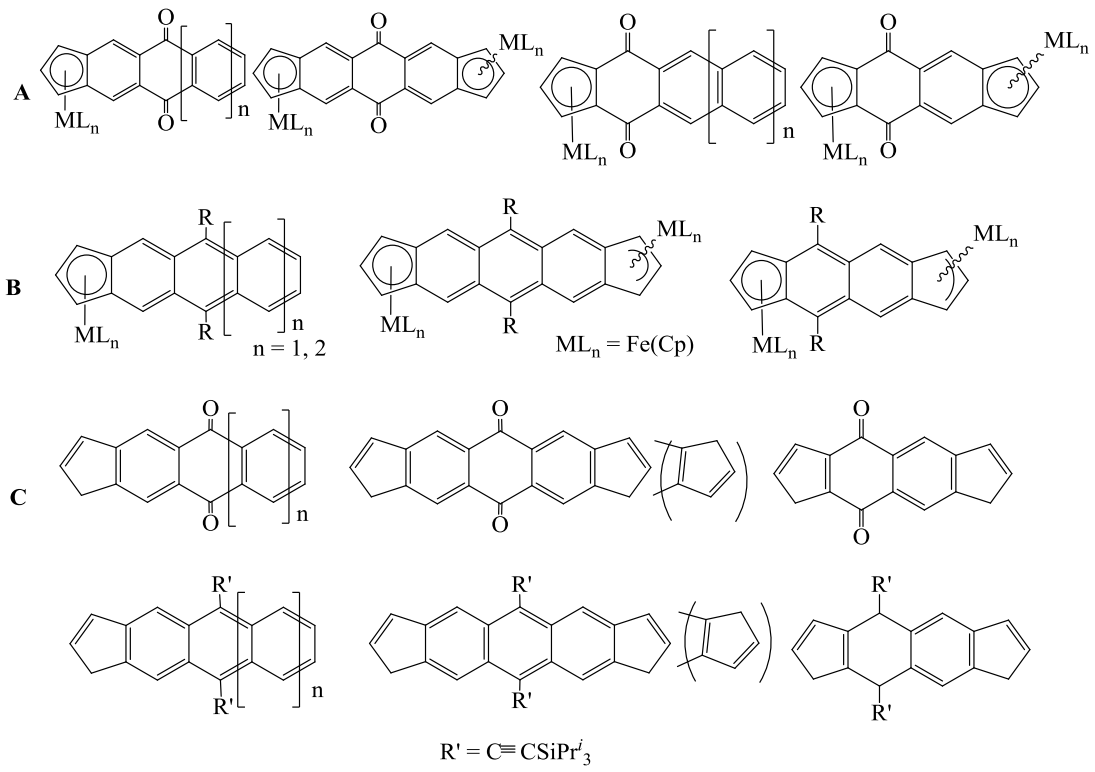

Chart 1.9 A) Organometallic acenequinones, B) organometallic polyacene, C) Cp-capped acenequinone and Cp-capped polyacenes

Chapter 2 Synthesis, Characterization and Reactivity of Ferrocene-Terminated Polyacenes

2.1 Introduction

Ferrocene is one of the most important and intensely studied robust organometallic compounds. It is the benchmark material for preparation of organometallic molecules and polymers because of its solubility in common organic solvents, availability, low cost, high stability and readily accessible reversible redox chemistry.[83] These advantages provide a tremendous stimulus for researchers to continue investigation as well as employment in diverse applications. Ferrocenes, due to high electron densities on their cyclopentadienyl rings, are well known nucleophiles that undergo electrophilic substitution reactions such as sulfonation, halogenation, Friedel-Crafts acylation and alkylation, metalation, arylation, formylation and aminomethylation more readily than benzene.[84]

Investigation of organometallic polymers has intensified in recent years, especially in light of their important electrical, optical and catalytic properties. Several synthetic methods for ferrocene-containing polymers have been reported including ring-opening metathesis polymerization, polycondensation and electropolymerization.[85] The well-studied redox reactions of ferrocene are often used as indicators in electrochemical measurements.[86] Ferrocene exhibits a fast and reversible one-electron transfer on gold and other electrodes, making ferrocene a good model for studying the electron transport phenomenon. Christopher's group utilized these advantages to functionalize silica nanoparticles with ferrocene, which offered a new material with a capacity of redox

charge storage up to 5×10^7 C/m^3 in the dry phase and 6×10^5 C/m^3 in the concentrated slurries.[87]

To meet our target, we started with commercially available ferrocene to get the precursor 1,2-diformylferrocene. The experimental procedure for 1,2-diformylferrocene is well known. The conventional route of making 1,2-diacylcyclopentadiene[88] cannot be extended to 1,2-diformylcyclopentadiene because of the lability of formyl chloride. Goetgheluck et al.[89] and Malfait et al.[90] reported that ortho-lithiation of N,N-dimethylaminomethylferrocene with *n*-BuLi, followed by formylation with DMF, results in N,N-dimethylaminomethylferrocene-carboxaldehyde, which on further oxidization with a mild oxidizing agent (activated manganese dioxide) gives 1,2-diformylferrocene. Marr *et al.*[91] reported that ortho-lithiation of N,N-dimethylaminomethylferrocene with *n*-BuLi and formylation with paraformaldehyde results in 1-hydroxymethyl-2-(dimethylaminomethylferrocene), which on reacting with methyl iodide gives Methanaminium,1-[2-(hydroxymethyl)ferrocenyl]-*N*,*N*,*N*-trimethyl-iodide. As the process is continued, further refluxing with the aqueous solution of potassium hydroxide leads to 1,2-bis(hydroxymethyl)ferrocene, and then oxidation with activated manganese dioxide results in 1,2-diformylferrocene.

Three classic organic reactions, Friedel-Crafts acylation, aldol condensation and the Cava reaction, are well known for preparing quinones, precursors of polycyclic aromatic hydrocarbons (acenes). Our long-term goal is to extend these reactions into the organometallic arena. Our group was mainly oriented in Friedel-Crafts acylation and aldol condensation. The acyl group being an electron-withdrawing group deactivates the cyclopentadienyl ring after first acylation, preventing the second acylation. To overcome

this problem, one of our group members applied Friedel-Crafts acylation between organometallic 1,2-dicarboxylic anhydride and diacyl chlorides with organic aromatic molecules (benzene, toluene, o-xylene, p-dimethoxybenzene) to synthesize several acenequinone complexes.[92]

The second route employed to prepare organometallic acenes is aldol condensation. Chart 2.1 shows some of our initial progress in synthesis of organometallic acenes.

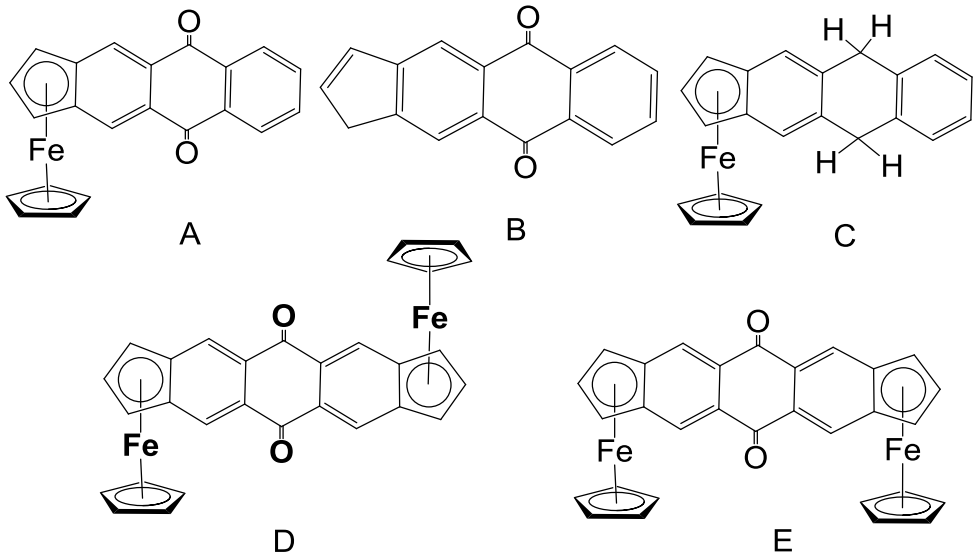

Chart 2.1 Some progress in organometallic acenes

2.2 Experimental

Reactions are carried out using standard Schlenk techniques under nitrogen. Solvents including ethyl ether, benzene, tetrahydrofuran (THF), hexane and toluene were dried over sodium benzophenone ketyl and distilled under N_2 before use. Dichloromethane and acetonitrile were dried and distilled over calcium hydride. $CDCl_3$, C_6D_6, DMSO-d_6, acetone-d_6 (Cambridge Isotopes), sodium, sodium dithionite (J.T. Baker), N,N,N',N-tetramethylmethylenediamine, butyllithium (2.5 M in hexane), N,N-dimethylformamide, 1,4-cyclohexanedione, naphthoquinone, 1 M borane solution in THF, aluminum chloride, trifluoroacetic anhydride (Aldrich), activated manganese dioxide (Acros), 1,4-dihydroxyanthraquinone (Alfa Aesar), sodium hydroxide (Fisher), potassium hydroxide, sodium borohydride (EMD), and mossy zinc (E.H. Sargent and Co.) were used without further purification. 1,4–Dihydroxynaphthalene and 1,4–anthracenediol were synthesized following the procedure reported by Oatis *et al.*[93] and Chen *et al.*[94] Triisopropylsilylacetylene was used as purchased from GFS chemicals. Organic phases were dried using either anhydrous sodium sulfate or anhydrous magnesium sulfate (Mallinckrodt). Flash chromatography was performed using 60 Å pore size, 230–400 mesh silica gel (Sorbent Technologies). ^{1}H and ^{13}C NMR spectra were recorded on a Varian Gemini–400 spectrometer at ca. 25 °C and were referenced to residual solvent peaks. Infrared spectra were recorded on an ATI–Mattson Galaxy™ Series 5000 FTIR15 spectrometer. Mass spectra were acquired by the University of Kentucky Mass Spectrometry Facility. Electron ionization (EI) mass spectra were recorded at 70 eV on a Thermo Finnigan Polaris Q (quadrupole ion trap). Samples were introduced via a heatable direct insertion probe. Melting points were taken in open

capillary tubes on a Thomas-Hoover or Electrothermal Mel-Temp melting point apparatus and were uncorrected. X-ray diffraction data were collected at 90 K on either a Nonius KappaCCD diffractometer or a Bruker-Nonius X8 Proteum diffractometer. Crystal indexing and data processing were performed with either DENZO–SMN (KappaCCD)[95] or Bruker APEX2 (X8 Proteum). The structures were solved and refined by using SHELXL-97.[96] UV–vis spectral analyses were performed on a Shimadzu UV–2501 PC. Electrochemical data were collected on a BAS CV–50 W voltammetric analyzer.

Synthesis of N,N-dimethylaminomethylferrocene (1). Phosphoric acid (43.2 g, 25. 6 mL, 0.44 mol) and glacial acetic acid (400 mL) were mixed in a 1 L three-necked round-bottom flask equipped with a magnetic stir bar, septum cap, water condenser and nitrogen inlet. The solution was cooled in an ice bath. Then N,N,N',N'–bis(dimethylamino)methane (43.2 g, 58.4 mL, 0.42 mol) was added dropwise via a syringe with continuous stirring. After the complete addition of amine, ferrocene (46.4 g, 0.25 mol) was added. The mixture was warmed to room temperature and slowly heated in an oil bath to 100 °C for 5 h. The dark amber solution was cooled to room temperature. The solution was diluted with 500 mL of water. Unreacted ferrocene was removed by extracting the solution with ethyl ether (3 × 300 mL). The aqueous phase separated from the organic phase and was cooled in ice water. NaOH (200 g, 5.00 mol) was added slowly to make the solution alkaline. The amine was separated from the alkaline solution as oil with some black tar. The mixture was extracted with 3 × 500 mL of ethyl ether. The ether solution was washed with water (3 × 100 mL) and dried over anhydrous sodium sulfate.[97] The solution was filtered through filter paper and evaporated under reduced

pressure to give a dark red liquid (39.0 g, 64.2%). **^{1}H NMR (400 MHz, $CDCl_3$, ppm):** δ 2.01 (s, 6 H, C*H*$_3$), 3.25 (s, 2 H, C*H*$_2$), 4.09 (t, 2 H, C*H*CC*H*), 4.04 (t, 2 H, C*H*C*H*CH), 4.09 (s, 5 H, C_5H_5).

Synthesis of N,N-dimethylaminomethyl-2-formylferrocene (2). An oven-dried 250 mL Schlenk flask equipped with a magnetic stir bar, nitrogen inlet and septum cap was cooled under N_2. N,N-Dimethylaminomethylferrocene (2.00 g, 8.22 mmol) was transferred through a syringe into a flask. Ethyl ether (80 mL) was added through a cannula. The solution was cooled with a dry ice/isopropanol slurry for 10 min. *n*-BuLi (2.5 M, 4.9 mL, 1.5 equiv) was added dropwise. After the complete addition of *n*-BuLi, the reaction flask was transferred to an ice bath and stirred for 5 h at 0 °C. DMF (1.3 mL) was added at 0 °C and the reaction mixture was brought to room temperature and stirred for 3 h. The reaction was quenched slowly with water. The organic phase was separated from the aqueous phase and extracted with ethyl ether (3 × 15 mL). The combined organic phase was washed with brine (2 × 20 mL). The organic phase was dried with anhydrous magnesium sulfate and the solvent rotary evaporated. The crude product was purified by chromatography on a silica column with hexane:ethyl ether:triethylamine (6:3:1) as an eluent to give a red-brown, liquid product (1.25 g, 56.1%). **^{1}H NMR (400 MHz, $CDCl_3$, ppm):** δ 2.18 (s, 6 H, C*H*$_3$), 3.25 (s, 2 H, C*H*$_2$), 4.08 (d, 2 H, ^3J = 3.6 Hz, C*H*CHC*H*), 4.09 (s, 5 H, C_5H_5), 4.14 (t, 1 H, ^3J = 3.6 Hz C*H*CHC*H*), 10.07 (s, 1 H, C*H*O). **IR (ATR, cm^{-1}):** 1671 (CHO). The compound was fully characterized by Goetgheluck et al.[89]

Synthesis of 1,2-diformylferrocene (3). In a 200 mL Schlenk flask, N,N-dimethylaminomethyl-2-formylferrocene (1.00 g, 3.96 mmol) was dissolved in toluene

(50 mL) under N_2. Active manganese dioxide (6.41 g, 20 equiv) was added. The slurry was allowed to reflux for 2 h and then cooled to room temperature. The manganese dioxide was removed by vacuum filtration on Celite 545, and the solvent was evaporated under reduced pressure. The crude product was chromatographed on silica with hexane:ethyl ether (1:1) as an eluent to give a dark red solid (450 mg, 50.4%). **^{1}H NMR (400 MHz, $CDCl_3$, ppm):** δ 4.39 (s, 5 H, C_5H_5), 4.92 (t, 1 H, ^3J = 2.4 Hz, CHC*H*CH), 5.2 (d, 2 H, ^3J = 2.4 Hz, C*H*CHC*H*), 10.36 (s, 2 H, C*H*O). **IR (ATR cm^{-1}):** 1664 (CHO). **Mp**: 111–113 ˚C (Lit. 112 ˚C). The compound was fully characterized by Malfait et al.[90]

Synthesis of 1-(3-carboxypropionyl)ferrocene (4). In a 500 mL Schlenk flask, ferrocene (16 g, 86 mmol) and succinic anhydride (4.3 g, 43 mmol) were dissolved in 125 mL of CH_2Cl_2 under N_2. Anhydrous $AlCl_3$ (11.5 g, 86.0 mmol) was dissolved in 125 mL of CH_2Cl_2. The solution of ferrocene and succinic anhydride was added dropwise from a dropping funnel to the $AlCl_3$ solution within 50 min. The purple solution was stirred to room temperature for 7 h. The solution was acidified with 50% HCl to pH 3–4. The organic phase was separated from the solution. The aqueous solution was further extracted with 20 mL aliquots of CH_2Cl_2 until the extract was colorless. The organic solution was reduced from 1 L to 600 mL and extracted with NaOH (2 M, 3 × 250 mL). The solution was cooled to 5 °C and 50 % phosphoric acid was added dropwise until the precipitation was complete. The solution was filtered and the orange, viscous solid was purified by hot water filtration. The solid was dried under vacuum to give 8.1 g (66%) of **4**. **^{1}H NMR (400 MHz, acetone-d, ppm):** δ 2.62–2.66 (m, 2 H, CC*H*$_2$CH$_2$), 3.08–3.11 (m, 2 H, CCH$_2$C*H*$_2$), 4.28 (s, 5 H, C_5H_5), 4.53 (t, 2 H, ^3J = 1.6 Hz, CHC*H*CH), 4.83 (t, 2 H, ^3J = 1.6 Hz, C*H*CHC*H*). **IR (ATR, cm^{-1}):** 2596–2916 (br, -COOH), 1714, 1655 (CO).

Mp: 164–166 °C (lit. 166.5–167.5 °C). The product was characterized by Rinehart et al.[98]

Synthesis of 1-(3-carboxypropyl)ferrocene (5). In a 100 mL round-bottom flask, zinc (6.0 g, 90 mmol), mercuric chloride (0.60 g, 2.2 mmol), water (10 mL) and conc. HCl (0.30 mL) were added. The solution was shaken manually for 5 min followed by stirring for 5 more min.[99] The solution was decanted and zinc was washed with water. This obtained zinc was put in a 200 mL Schlenk flask equipped with nitrogen inlet, and H_2O (3.8 mL), Conc. HCl (8.8 mL), toluene (20 mL) and 1-(3-carboxypropionyl)ferrocene (4.0 g, 14 mmol) were added serially. The resultant solution was heated at 90 °C for 9 h, cooled to room temperature and diluted with water (20 mL). The organic phase was separated and the aqueous layer was extracted with ethyl ether (2 × 10 mL). The combined organic phase was washed with water (2 × 10 mL) and dried with anhydrous $MgSO_4$. Rotary evaporation of the solvent gave a yellow crude product. The crude product was purified by silica column chromatography with petroleum ether:ethyl acetate (8:2) to yield a yellow solid (3.26 g, 85.7%). **^{1}H NMR (400 MHz, acetone-d_6, ppm):** δ 1.79–1.84 (m, 2 H, CH_2CH_2CH_2), 2.29–2.41 (m, 4 H, CH_2CH_2CH_2), 4.04 (t, 2 H, ^3J = 1.6 Hz, C*H*CC*H*), 4.09 (t, 2 H, ^3J = 1.6 Hz, CHC*H*C*H*), 4.11 (s, 5 H, C_5H_5). **IR (ATR cm^{-1}):** 3095–2595 (br, –COOH), 1705 (CO). **Mp:** 115 °C (lit. 115–116 °C).[100]

Synthesis of α-keto-1,2-tetramethyleneferrocene (6). A solution of **5** (3.00 g, 11.0 mmol) in 100 mL CH_2Cl_2 was added dropwise to a solution of trifluoroacetic anhydride (13.2 mmol, 1.93 mL) in 100 mL CH_2Cl_2 at 0 °C. The solution was stirred at this temperature for an additional 5 h and poured into water (50 mL) saturated with

$NaHCO_3$. The organic layer was separated and the aqueous phase was extracted with CH_2Cl_2 (2 × 20 mL). The combined organic phase was washed with water (2 × 30 mL) and dried with anhydrous $MgSO_4$. After the removal of solvent under reduced pressure, the residue was chromatographed on silica with petroleum ether:dichloromethane (5:95) to yield a dark red solid (2.58 g, 92.1%). **^{1}H NMR (400 MHz, $CDCl_3$, ppm):** δ 2.05–2.66 (m, 6 H, CH_2CH_2CH_2), 4.16 (s, 5 H, C_5H_5), 4.45 (d, 2 H, C*H*CHC*H*), 4.80 (s, 1 H, CHC*H*CH). **IR (ATR, cm^{-1}):** 2837, 2887, 2938 (sp^3 C–H), 1662 (CO). **Mp:** 80 °C (lit. 85–85.5 °C).[101]

Synthesis of ferroceno[*b*]benzoquinone (7). In a 200 mL Schlenk flask, MnO_2 (3.42 g, 30.0 equiv) was added to **6** (500 mg, 1.97 mmol) in chloroform (30 mL). The slurry was refluxed for 9 h with additional MnO_2 (3.42 g) added after 3 and 6 h. The solution was allowed to cool to room temperature and filtered through a thin pad of Celite 545. The removal of the solvent gave a dark purple solid (250 mg, 43.9%). **^{1}H NMR (400 MHz, $CDCl_3$, ppm):** δ 4.30 (s, 5 H, C_5H_5), 5.09 (t, 1 H, ^3J = 2.4 Hz, CHC*H*CH), 5.37 (d, 2 H, ^3J = 2.4 Hz, C*H*CHC*H*), 6.64 (s, 2 H, CC*H*C*H*). **^{13}C{^{1}H} NMR (100 MHz, $CDCl_3$ ppm):** δ 70.41 (*CC*, *ipso*), 72.80 (*C*HCH*C*H), 74.09 (C_5H_5), 76.16 (CH*C*HCH), 139.71 (C*C*H*C*H), 190.59 (*C*O). **IR (ATR cm^{-1}):** 1650 (CO). **MS (EI):** m/z 266 (M^+). **Mp**: (146–148 °C). The compound was characterized by X-ray diffraction.

Synthesis of ferrocene-fused-1,4-cyclohexanedione (8): Compound **7** (100 mg, 0.38 mmol) was added into a solution of sodium dithionite (276 mg, 1.59 mmol) in *p*-dioxane (3 mL) and nitrogen-bubbled water (3 mL) under nitrogen. The reaction mixture was stirred at room temperature for 4 h, more sodium dithionite (151 mg) was added, the reaction mixture was stirred for an additional 4 h and then poured into 5 mL water.[94] The

solution was extracted with ethyl ether (4 × 15 mL). The combined organic phase was dried with anhydrous $MgSO_4$. After the removal of solvent under reduced pressure, the residue was chromatographed on silica with ethyl ether:hexane (3:1) to yield an orange solid (51.4 mg, 50.5%). **^{1}H NMR (400 MHz, $CDCl_3$, ppm):** δ 2.77–2.84 (m, 2 H, CC*H*$_2$CH$_2$), 2.99–3.07 (m, 2 H, CCH$_2$C*H*$_2$), 4.27 (s, 5 H, C_5H_5), 4.86 (t, 1 H, ^3J = 2.4 Hz, CHC*H*CH,), 5.18 (d, 2 H, ^3J = 2.4 Hz, C*H*CHC*H*). **^{13}C{^{1}H} NMR (100 MHz, $CDCl_3$ ppm):** δ 71.02 (C*C*H$_2$*C*H$_2$), 72.49 (*C*$_5$H$_5$), 72.58 (*C*HCH*C*H), 75.66 (CH*C*HCH), 78.89 (*CC*, *ipso*), 201 (*C*O). **IR (ATR, cm^{-1}):** 2850, 2921, 2956 (sp^3 C–H), 1671 (CO). The compound was recrystallized by slow evaporation of dichloromethane solution in a stream of hexane-saturated N_2 through a cannula and analyzed by single X-ray crystal diffraction.

Synthesis of ferrocene-fused anthracenequinone (9): In a 25 mL two-necked round-bottom flask with a magnetic stir bar, phthalaldehyde (20.0 mg, 0.07 mmol) was dissolved in absolute ethanol (2 mL). Compound **8** (9.01 mg, 0.07 mmol) was added, followed by 15% KOH (1 drop). The solution was allowed to stir overnight at room temperature. The ethanol was evaporated to get a crude product, which was purified by silica column chromatography with ethyl ether:hexane (1:1) to yield a reddish purple solid (16.0 mg, 62.5%). **^{1}H NMR (400 MHz, $CDCl_3$, ppm):** δ 4.17 (s, 5 H, C_5H_5), 5.12 (t, 1 H, ^3J = 2.4 Hz, CHC*H*CH), 5.52 (d, 2 H, ^3J = 2.4 Hz, C*H*CHC*H*), 7.65–7.67 (m, 2 H, CCHC*H*), 8.05–8.07 (m, 2 H, CC*H*CH), 8.77 (s, 2 H, CC*H*C). **^{13}C{^{1}H} NMR (100 MHz, $CDCl_3$, ppm):** δ 72.8 (*C*HCH*C*H), 73.5 (CH*C*HCH), 76.9 (*C*$_5$H$_5$), 79.1 (*CC*, *ipso*), 128.6, 129.6, 130.2, 131.8, 135.0 (Ar), 188.5 (*C*O). **IR (ATR, cm^{-1}):** 1658 (CO). **MS (EI):** m/z 366 (M^+). **Mp:** 240–260 ˚C (dec).

Synthesis of bis(ferrocene-fused) naphthoquinone (10): In a 125 mL Schlenk flask with a magnetic stir bar, 1,2-diformylferrocene (400 mg, 1.65 mmol) was dissolved in absolute ethanol (3 mL). Compound **8** (443 mg, 1.65 mmol) was added, followed by 15% KOH (0.10 mL). The solution was allowed to stir overnight at room temperature. The solution was filtered through a frit and washed with cold ethyl ether (100 mL). The purple solid was dried under vacuum, yielding 624 mg (79.5%) of a ca. 1:1 *syn*:*anti* isomer mixture. Analytically pure product was obtained by recrystallization from slow evaporation of dichloromethane solution in a stream of hexane-saturated N_2 through a cannula. **^{1}H NMR (400 MHz, $CDCl_3$, ppm)** δ 3.89, (s, 5 H, C_5H_5), 3.92 (s, 5 H, C_5H_5), 4.13 (s, 5 H, C_5H_5), 4.14 (s, 5 H, C_5H_5), 4.58 (2 H, Cp), 5.05 (2 H, Cp), 5.28 (4 H, Cp), 5.45 (4 H, Cp), 8.76 (s, 2 H, CC*H*C), 8.77 (s, 2 H, CC*H*C). **^{13}C{^{1}H} NMR (100 MHz, $CDCl_3$, ppm):** δ 66.15 (Cp), 66.20 (Cp), 69.38 (Cp), 69.68 (Cp), 72.13 (Cp), 72.31 (Cp), 73.16 (Cp), 73.34 (Cp), 75.80 (Cp), 76.42 (Cp), 76.49 (Cp), 79.47 (Cp), 79.79 (Cp), 86.55 (Cp), 86.78 (Cp), 129.45, 129.58, 134.49, 134.68 (Ar), 187.49, 187.87 (*C*O). **IR (ATR, cm^{-1}):** 1658 (CO). **Mp:** >240 ˚C.

Synthesis of anthra[2,3-*b*:6,7-*b*]ferrocene-5,10-dione (11). In a 25 mL Schlenk flask with magnetic stir bar, 1,2-diformylferrocene (500 mg, 2.06 mmol) was dissolved in 3 mL of absolute ethanol. 1,4-Dihydroxynaphthalene (331 mg, 2.06 mmol) was added, followed by 15% KOH (0.10 mL). The solution was stirred overnight at room temperature. The purple precipitate was filtered through a frit and washed with cold ethyl ether (100 mL). The purple solid was dried under vacuum, yielding 596 mg (78.8%) of **11**. **^{1}H NMR (400 MHz, $CDCl_3$, ppm):** δ 3.93 (s, 5 H, C_5H_5), 4.65 (t, 1 H, ^3J = 2.4 Hz, CHC*H*CH), 5.36 (d, 2 H, ^3J = 2.4 Hz, C*H*CHC*H*), 7.78–7.75 (m, 2 H, CCHC*H*), 8.37–

8.34 (m, 2 H, CC*H*CH), 8.87 (s, 2 H, CC*H*C). **^{13}C{^{1}H} NMR (100 MHz, $CDCl_3$, ppm):** δ 66.79 (*C*HCH*C*H), 69.54 (C_5H_5), 76.62 (CH*C*HCH), 87.02 (*CC*, *ipso*), 127.52 (CO*C*CH), 127.70 (CHCH*C*H) , 134.01 (C*C*HCH), 135.25 (CH*C*CO), 136.99 (C*C*HC), 182.17 (*C*O). **IR (ATR, cm^{-1}):** 1669 (CO). **MS (EI):** m/z 366 (M^+). **Mp:** >200 ˚C. Full characterization of the compound was performed by X-ray crystallography.

Synthesis of anthra[2,3-*b*:6,7-*b*]diferrocene-5,11-dione (12). In a 25 mL two-necked round-bottom flask with a magnetic stir bar, 1,2-diformylferrocene (300 mg, 1.24 mmol) was dissolved in absolute ethanol (2 mL). 1,4-Cyclohexanedione (69.6 mg, 0.680 mmol) was added, followed by 15% KOH (0.10 mL). The solution was allowed to stir overnight at room temperature. The purple precipitate was filtered through a frit and washed with ethyl ether cooled under liquid N_2 (50 mL). The purple solid was dried under a vacuum to yield 452 mg (69.6%) of a ca. 1:1 *syn*:*anti* isomer mixture. **^{1}H NMR (400 MHz, $CDCl_3$, ppm):** δ 3.90, 3.97 (s, 5 H, C_5H_5), 4.59 (t, 1 H, ^{3}J = 2.4 Hz, CHC*H*CH), 5.35 (d, 2 H, ^{3}J = 2.4 Hz, C*H*CHC*H*), 8.92, 8.94 (s, 4 H, CC*H*C). **^{13}C{^{1}H} NMR (100 MHz, $CDCl_3$, ppm):** δ 66.17, 68.20 (CH*C*HCH), 69.29, 69.30 (C_5H_5), 76.33, 76.38 (*C*HCH*C*H), 87.68 (*CC*, *ipso*), 128.72 (CH*C*CO), 136.39, 136.44 (C*C*HC), 181.44 (*C*O) .**IR (ATR, cm^{-1}):** 1657 (CO). **Mp:** >240 ˚C.

Synthesis of naphthacene[2,3-*b*]ferrocene-5,12-dione (13). In a 25 mL sidearm round-bottom flask with a magnetic stir bar, 1,2-diformylferrocene (500 mg, 2.07 mmol) was dissolved in absolute ethanol (3 mL). 1,4-Anthracenediol (434 mg, 2.07 mmol) and 15% KOH (0.10 mL) were added. The resulting solution was stirred overnight at room temperature. The purple precipitate was filtered and washed with cold ethyl ether (50 mL). The purple solid was dried under vacuum to yield 705 mg (81.5%) of **13**. **^{1}H NMR**

(400 MHz, CD_2Cl_2, ppm): δ 3.97 (s, 5 H, C_5H_5), 4.70 (t, 1 H, CHC*H*CH), 5.43 (d, 2 H, C*H*CHC*H*), 7.70 (m, 2 H, CCHC*H*), 8.14 (m, 2 H, CC*H*CH), 8.90 (s, 2 H, CC*H*C), 8.95 (s, 2 H, CC*H*C). **$^{13}C\{^1H\}$ NMR (100 MHz, CD_2Cl_2, ppm)**: δ 67.01 (*C*HCHC*H*), 69.79 (C_5H_5), 77.16 (CH*C*HCH), 87.70 (*CC*, *ipso*), 128.61 (CH*C*CH), 129.68 (CCHC*H*), 129.72 (C*C*HCH), 130.44 (C*C*HC), 131.87 (CO*C*CH), 135.79 (CH*C*CO), 137.12 (C*C*HC), 182.22 (*C*O). **IR (ATR, cm^{-1})**: 1665 (C=O). **MS (EI)**: m/z 416 (m^+). **Mp**: >240 ˚C. The compound was characterized by an X-ray diffraction study.

Synthesis of 5,10-dihydroanthra[2,3-*b*:6,7-*b*]ferrocene (14). In a 100 mL Schlenk flask with a magnetic stir bar, anthra[2,3-*b*:6,7-*b*]ferrocene-5,10-dione (200 mg, 0.55 mmol) was dissolved in THF (20 mL) under N_2. The solution was cooled to 0 °C in an ice bath. Borane-THF solution (1.00 M, 4.37 mL, 4.37 mmol) was added dropwise. The solution was warmed to room temperature and stirred for 8 h. The solution was quenched with methanol (10 mL). The solvent was evaporated and the crude product was chromatographed on alumina with hexane:dichloromethane (3:2). The red fraction was collected and removal of the solvent gave a pink solid (84.0 mg, 45.5%). **^1H NMR (400 MHz $CDCl_3$, ppm):** δ 3.70 (s, 5 H, C_5H_5), 3.98 (s, 4 H, CCH_2C), 3.98 (s, 1 H, CHC*H*CH), 4.83 (s, 2 H,C*H*CHC*H*), 7.42 (m, 2 H, CC*H*CH), 7.72 (s, 2 H, CC*H*C), 7.77 (m, 2H, CCHC*H*). **$^{13}C\{^1H\}$ NMR (100 MHz, $CDCl_3$, ppm):** δ 38.28 (C*C*H_2C), 61.31 (*C*HCHC*H*), 68.37 (C_5H_5), 69.84 (CH*C*HCH), 87.62 (*CC*, *ipso*), 124.83 (CCHC*H*), 125.44 (C*C*HCH), 127.43 (C*C*HC), 132.69 (CH_2*C*CH), 136.68 (CH*C*CH_2). **IR (ATR, cm^{-1}):** 2931 (sp^3 C–H), 3089 (sp^2 C–H). **Mp:** >200˚C. **MS (EI):** m/z 338 (M^+).

Synthesis of 5,11-dihydroanthra[2,3-*b*:6,7-*b*]diferrocene (15). In a 100 mL Schlenk flask with a magnetic stir bar, anthra[2,3-*b*:6,7-*b*]diferrocene-5,11-dione (100

mg, 0.19 mmol) was dissolved in THF (10 mL) under N_2. The solution was cooled to 0 °C in an ice bath. Borane-THF solution (1.00 M, 0.57 mL, 0.57 mmol) was added dropwise. The solution was warmed to room temperature and stirred for 1 h. The temperature was slowly raised to 50 °C using an oil bath and stirred for 5 h. The solution was allowed to cool at room temperature and an additional 1 mL of borane-THF solution was added dropwise. The temperature of the resulting solution was raised slowly to 50 °C and stirred for 2 h. The initial purple solution changed to a reddish color. The solution was cooled to room temperature and quenched with methanol (10 mL). The solvent was evaporated under reduced pressure and the crude product was purified by chromatography on silica with hexane:dichloromethane (3:2) as an eluent. The red fraction was collected and removal of the solvent gave a pink solid (40.0 mg, 42.4%), which is a 1:1 mixture of *syn:anti* isomers. ^{1}H **NMR (400 MHz, $CDCl_3$, ppm):** δ 3.65, 3.69 (s, 10 H, C_5H_5), 3.73 (s, 8 H, CCH_2C), 3.95–3.96 (m, 2 H, CHCHCH), 4.82 (br, 4 H, CHCHCH), 7.35 (s, 4 H, CCHC), 7.38 (s, 4 H, CCHC). **IR (ATR, cm^{-1}):** 3089 (sp^2 C–H), 29.46 (sp^3 C–H). **Mp:** >240˚C.

Synthesis of 5,12-dihydronaphthacene[2,3-*b*]ferrocene (16). In a 200 mL Schlenk flask, naphthacene[2,3-*b*]ferrocene-5,12-dione (100 mg, 0.24 mmol) was dissolved in THF (20 mL). The solution was cooled at 0 ˚C for 10 minutes. Borane in THF (1.0 M, 0.96 mmol, 0.96 mL) was added to the solution dropwise. After the complete addition of reagent, the ice bath was removed and the solution was allowed to stir at room temperature for 8 h. The reaction mixture was quenched by 10 mL of methanol. The solvent was removed by rotary evaporation. The obtained crude product was purified by alumina column chromatography and eluted with

hexane:dichloromethane (3:2). The first reddish-pink fraction was collected, and the solvent was removed under reduced pressure and dried under a vacuum to give a pink solid (27.0 mg, 40.0%). **^{1}H NMR (400 MHz, C_6D_6, ppm):** δ 3.69 (s, 5 H, C_5H_5), 3.80 (s, 4 H, CCH_2C), 3.91 (t, 1 H, ^{3}J = 2.4 Hz, CHC*H*CH), 4.79 (d, 2 H, ^{3}J = 2.4 Hz, C*H*CHC*H*), 7.29–7.32 (m, 2 H, CC*H*CH), 7.33 (s, 2 H, CC*H*C), 7.52 (s, 2 H, CC*H*C), 7.68–7.71 (m, 2 H, CCHC*H*). **^{13}C{^{1}H} NMR (100 MHz, C_6D_6, ppm):** 38.63 (CCH_2C), 61.87 (CH*C*HCH), 70.10 (C_5H_5), 88.88 (*C*HCH*C*H), 88.29 (*CC*, ipso), 125.40, 125.60, 125.88, 128.99, 133.52, 134.55, 136.95 (Ar). **IR (ATR, cm^{-1}):** 3089 (sp^2 C–H), 2931 (sp^3 C–H). **Mp:** >250˚C. **MS (EI):** m/z 388 (M^+).

Synthesis of 1H-cyclopenta[*b*]anthracene-5,10-dione (17). An oven-dried 200 mL Schlenk flask was cooled under nitrogen. Anthra[2,3-*b*:6,7-*b*]ferrocene-5,11-dione **(11)** (300 mg, 0.82 mmol) was dissolved in THF (40 mL). A saturated solution of sodium dithionite in N_2-purged water (40 mL) was added and stirred overnight, monitored by thin-layer chromatography. There was no conversion of starting material to product, so the reaction mixture was refluxed 5 h. The organic phase was separated and the aqueous layer was extracted with CH_2Cl_2 (2 × 30 mL). The combined organic phase was dried with anhydrous magnesium sulfate and the solvent was removed in vacuum. The crude product was purified on silica chromatography with hexane:dichloromethane (1:1) as an eluent to collect a yellow fraction. The solvent was evaporated under reduced pressure, and the residue dried under a vacuum. The product was further triturated with pentane and dried to give a yellow solid (119 mg, 49.0%). **^{1}H NMR (400 MHz, $CDCl_3$, ppm):** δ 3.59 (s, 2 H, CCH_2CH), 6.87–6.88 (m, 1 H, CH_2C*H*CH), 7.04–7.06 (m, 1 H, CH_2CHC*H*), 7.75–7.78 (m, 2 H, CCHC*H*), 8.28–8.31 (m, 2 H, CC*H*CH), 8.37 (s, 2 H, CC*H*C).

$^{13}C\{^1H\}$ NMR (100 MHz, $CDCl_3$, ppm): δ 40.11 (C*C*H_2CH), 139.95 (CH_2*C*HCH), 134.02 (CH_2CH*C*H), 119.66, 122.50 (C*C*HC), 127.34, 127.36 (CCH*C*H), 130.40 (CO*C*CH), 132.30, 134.15 (C*C*HCH), 133.25, 133.92 ((CH*C*CO), 149.76 (CH_2*C*CH), 150.84 (CH*C*CH), 183.81, 183.94 (*C*O). **IR (ATR cm^{-1}):** 1672 (C=O). **MS (EI):** m/z 246 (M^+). The compound was fully characterized by X-ray crystallography.

Synthesis of 1H,9H-dicyclopenta[*b,i*]anthracene-5,11-dione (18). In a 250 mL sidearm round-bottom flask with a magnetic stir bar, **12** (150 mg, 0.29 mmol) was dissolved in 20 mL of THF. A saturated solution of sodium dithionite in N_2-purged distilled water (30 mL) was added and stirred overnight. TLC indicated the presence of starting material, so the reaction mixture was refluxed for 7 h. The organic phase was separated and the aqueous layer was extracted with dichloromethane (2 × 20 mL). The combined organic phase was dried with anhydrous $MgSO_4$ and the solvent was removed under reduced pressure. The crude product was purified by silica chromatography with hexane:CH_2Cl_2 (1:1). The solvent was evaporated under reduced pressure and dried under a vacuum. The product was further triturated with pentane and dried to give a yellow solid (35 mg, 42%). **^1H NMR (400 MHz, $CDCl_3$, ppm):** δ 3.59 (s, 4 H, CC*H*$_2$CH), 6.85–6.87 (m, 2 H, CH_2*C*HCH), 7.04–7.05 (m, 2 H, CH_2CH*C*H), 8.29 (s, 2 H, C*C*HC), 8.37 (s, 2 H, C*C*HC). **$^{13}C\{^1H\}$ NMR (100 MHz, $CDCl_3$, ppm):** δ 40.08 (CH*C*H_2C), 119.56, 119.61, 122.41, 122.43 (C*C*HC), 131.10, 131.20, 133.40, 133.55 (CH*C*CO), 132.30, 132.33 ((CH_2CH*C*H), 139.66, 139.72 (CH2*C*HCH), 149.42, 149.58, 150.53, 150.65 (CH*C*CH), 192.66 (*C*O). **IR (ATR, cm^{-1}):** 1664 (C=O). **MS (EI):** m/z 284 (M^+).

Synthesis of 1H-cyclopenta[2,3-b]naphthacene-5,12-dione (19). An oven-dried 200 mL Schlenk flask was cooled under N_2. Naphthacene[2,3-*b*]ferrocene-5,12-dione

(100 mg, 0.24 mmol) was dissolved in THF (20 mL). A saturated solution of sodium dithionite in N_2-purged distilled water (20 mL) was added and stirred overnight. TLC showed remaining starting material, so the solution was refluxed for 7 h. The color of the solution changed from purple to brownish yellow. The organic phase was separated and the aqueous layer was extracted with CH_2Cl_2 (2 × 25 mL). The combined organic phase was dried with anhydrous magnesium sulfate and the solvent was removed in vacuum. The evaporation of the solvent under reduced pressure gave a crude product, which was purified by silica column chromatography with hexane:CH_2Cl_2 (1:1) as eluent. The solvent was evaporated under reduced pressure and the residue dried under vacuum. The product was further triturated with pentane and dried to give a yellow solid (37.0 mg, 52.1%). **^{1}H NMR (400 MHz, $CDCl_3$, ppm)**: δ 3.61 (s, 2 H, CC*H*$_2$CH), 6.87–6.89 (m, 1 H, CH_2C*H*CH), 7.06–7.07 (m, 1 H, CH_2CHC*H*) 7.65–7.67 (m, 2 H, CCHC*H*), 8.07–8.09 (m, 2 H, CC*H*CH), 8.36 (s, 1 H,CC*H*C), 8.45 (s, 1 H, CC*H*C), 8.83 (s, 2 H, CC*H*C). **^{13}C{^{1}H} NMR (100 MHz, $CDCl_3$, ppm):** δ 40.08 (C*C*H$_2$CH), 119.86, 122.73 (C*C*HC), 129.49, 129.52, 132.31(remaining Ar), 129.61, 130.22 (CH*C*CH), 130.29, 130.31 (C*C*HC), 131.89, 134.22 (CO*C*CH), 135.30 (CH_2*C*CH), 135.39(CH_2CH*C*H), 140.02((CH*C*CO), 149.84 (CH_2*C*CH), 150.91(CH*C*CH), 183.62, 183.74 (*C*O). **IR (ATR cm^{-1}):** 1666 (C=O). **MS (EI):** m/z 296 (M^+). Finally, the compound was characterized by an X-ray crystal structure.

Synthesis of 1H-cyclopenta-5,10-bis(triisopropylsilylethynyl)anthracene (20). *n*-BuLi (2.5 M, 0.82 mL, 2.1 mmol) was added dropwise to hexane (10 mL) and triisopropylsilylethyne (0.51 mL, 2.3 mmol) in an oven-dried 250 mL Schlenk flask cooled under N_2, and the mixture was stirred for 1 h. THF (2 mL) and additional hexane

(20 mL) were added into the reaction mixture, followed by addition of 1H-cyclopenta[*b*]anthracene-5,10-dione (100 mg, 0.41 mmol), then the mixture was stirred overnight. The reaction was quenched with 1 mL H_2O and $SnCl_2{\cdot}2H_2O$ (510 mg, 2.26 mmol) solution in 10% HCl (1 mL) was added. The mixture was heated to 40 ˚C for 8 h, and then cooled to room temperature. After the addition of 30 mL of water, the organic layer was separated and the aqueous layer was extracted with hexane (3 × 30 mL). The combined organic phase was dried over anhydrous $MgSO_4$. The volume of the solution was reduced to one-third of its original volume and poured onto a thick pad of silica. The product was eluted with distilled hexane. The removal of the solvent under reduced pressure yielded a yellow gummy product 119 mg (50.0%). Recrystallization was carried out using acetone and yielded 71.8 mg (30.2%) of **20**. **^{1}H NMR (400 MHz, $CDCl_3$, ppm):** δ 1.25–1.26 (m, 42 H, *i*-Pr), 3.63 (s, 2 H, CC*H*$_2$CH), 6.71–6.72 (m, 1 H, CH$_2$C*H*CH), 7.00–7.02 (m, 1 H, CH$_2$CHC*H*), 7.54–7.56 (m, 2 H, CC*H*CH), 8.59–8.61 (m, 2 H, CCHC*H*), 8.53 (s, 1 H, CC*H*C), 8.65 (s, 1 H, CC*H*C). **^{13}C{^{1}H} NMR (100 MHz, $CDCl_3$, ppm):** δ 11.79 (*C*H, *i*-Pr), 19.12(*C*H$_3$, *i*-Pr), 59.75 (C*C*H$_2$CH), 104.10, 104.15, 104.26, 104.52 (*CC*Si), 118.51, 121.39 (C*C*HC), 127.37, 127.27 (*C*CC), 126.56, 126.87 (CCH*C*H), 129.05, 129.93 (C*C*HCH), 132.09, 132.29 (C*C*CH), 131.75, 132.65 (C*C*HC), 132.79, 137.53 (CH*C*C), 136.49 (CH$_2$CH*C*H), 142.86 (CH$_2$*C*CH), 145.23 ((CH*C*CH), 150.25 (CH$_2$*C*HCH)). **IR (ATR cm^{-1}):** 3060 (sp^2 C−H), 2944, 2865 (sp^3 C−H), 2145 (C≡C). **MS (EI):** m/z 576(M$^+$). The X-ray crystal structure was highly disordered, so it was unable to be refined.

Synthesis of 1H,9H-dicyclopenta-5,11-bis(triisopropylsilylethynyl)anthracene (21). Hexane (20 mL) and triisopropylsilylethyne (0.59 mL, 2.6 mmol) were added to an

oven-dried 250 mL Schlenk flask equipped with a magnetic stir bar and cooled under N_2. *n*-BuLi (2.5 M, 0.98 mL, 2.5 mmol) was added dropwise and the mixture was stirred for 1 h. Hexane (40 mL), THF (2 mL) and 1H,9H-dicyclopenta[*b*,*i*]anthracene-5,11-dione (100 mg, 0.35 mmol) were added separately and the mixture was stirred overnight. The reaction was quenched with 1 mL H_2O and $SnCl_2{\cdot}2H_2O$ (397 mg, 1.76 mmol) in 10 % aqueous HCl (1 mL), and the solution was heated for 2 h at 60 ˚C, and then cooled to room temperature. After the addition of 30 mL H_2O, the organic phase was separated and aqueous phase was extracted with hexane (3 × 20 mL). The combined organic phase was dried over anhydrous $MgSO_4$ and filtered. The filtrate was evaporated under reduced pressure to reduce volume to one-third of its original volume and poured onto a thick pad of silica, then eluted with distilled hexane. The solvent was removed to yield 50.0 mg (23.0%) of product and recrystallized from acetone yielded 34.3 mg (15.8%). The compound was characterized by X-ray diffraction.**^{1}H NMR (400 MHz, $CDCl_3$, ppm):** δ 1.27–1.28 (m, 42 H, *i*-Pr), 3.63 (s, 4 H, CC*H*$_2$CH), 6.69–6.71 (m, 2 H, CC*H*CH), 7.01–7.02 (m, 2 H, CH_2CHC*H*), 8.53 (s, 2 H, CC*H*C), 8.64 (s, 2 H, CC*H*C). **^{13}C{^{1}H} NMR (100 MHz, $CDCl_3$, ppm):** δ 11.84 (*C*H$_{3,\ i}$-Pr), 19.14 (*C*H, *i*-Pr), 38.47 (C*C*H$_2$CH), 103.82 (C*C*Si), 104.68 (*C*CSi), 117.63, 117.74, 121.24, 121.34 (C*C*HC), 118.20 (C*C*C), 131.17, 131.37 (CH*C*HC), 132.20, 132.40 (CH_2*C*HCH), 132.69, 137.14, 137.18 (CH*C*C), 142.31 142.48, 144.72, 144.86 (CH*C*CH). **Mp:** 210 °C (dec). **IR (ATR cm^{-1}):** 3037 (sp^2 C−H), 2961, 2941, 2866 (sp^3 C−H), 2130 (C≡C). Analysis Calc. for: C, 82.02; H, 8.85. Found: C, 79.62; H, 8.98.

Synthesis of 1H-cyclopenta-5,12-bis(triisopropylsilylethynyl)naphthacene (22). Hexane (10 mL) and triisopropylsilylethyne (0.42 mL, 1.9 mmol) were added to an

oven-dried 250 mL Schlenk flask cooled under N_2, followed by the dropwise addition of *n*-BuLi (2.5 M, 0.68 mL, 1.7 mmol). The mixture was stirred for 1 h. Hexane (20 mL), THF (2 mL) and 1H-cyclopenta[2,3-*b*]naphthacene-5,12-dione (100 mg, 0.34 mmol) were added separately to the mixture. The reaction mixture was stirred overnight. The reaction was quenched with H_2O (1 mL) and $SnCl_2{\cdot}2H_2O$ (420 mg, 1.86 mmol) in 10 % aqueous HCl (1 mL), and the solution was heated at 40 ˚C for 8 h, and then cooled to room temperature. After the addition of 25 mL H_2O, the organic phase was separated and aqueous phase was extracted with hexane (3 × 20 mL). The combined organic phase was dried over anhydrous $MgSO_4$ and filtered. The filtrate was evaporated under reduced pressure to reduce volume to one-third of its original volume and loaded onto a thick pad of silica. The product was eluted with hexane, then the solvent was reduced to yield 123 mg (59.0%) and recrystallized from acetone yielded 105 mg (50.4%). **^{1}H NMR (400 MHz, $CDCl_3$, ppm):** δ 1.31–1.32 (m, 42 H, *i*-Pr), 3.66 (s, 2 H, C*C*H_2CH), 6.71–6.73 (m, 1 H, CH_2C*H*CH), 7.00–7.01 (m, 1 H, CH_2CHC*H*), 7.43 (m, 2 H, C*H*CHC*H*), 7.99 (m, 2 H, CHC*H*C*H*), 8.51 (s, 1 H, CC*H*C), 8.62 (s, 1H, CC*H*C), 9.27 (s, 2 H, CCHC). **^{13}C{^{1}H} NMR (100 MHz, $CDCl_3$, ppm):** δ 11.87 (*C*H, i-Pr), 19.18 (*C*H_3, i-Pr), 38.38 (C*C*H_2CH), 104.62, 104.72, 105.21, 105.50 (*CC*Si), 117.63, 118.27 (*C*CC), 118.27, 121.34 (C*C*HC), 128.80, 128.80 (C*C*HC), 132.23, 132.69 (C*C*CH), 132.04, 132.17 (CH*C*CH) 133.56 (CH_2CH*C*H), 137.83, 137.84 (CH*C*C), 142.75 (CH_2*C*HCH) 145.30 (CH_2*C*CH), 163.30 (CH*C*CH), 130.37, 130.19, 126.29, 126.16 (remaining Ar). **Mp:** 215–216 °C. **MS (EI):** m/z 626(M^+). **IR (ATR cm^{-1}):** 3050 (sp^2 C−H), 2942, 2864 (sp^3 C−H), 2133 (C≡C). Analysis Calc. for: C, 82.36; H, 8.68. Found: C, 80.96; H, 8.52.

2.3 Results and discussion

2.3.1 Synthesis. A goal in our research is to synthesize organometallic acenes. 1,2-Disubstituted metallocene is a precursor to prepare our target complexes. In order to synthesize the target complexes, the synthetic pathway was started with the following reaction scheme.

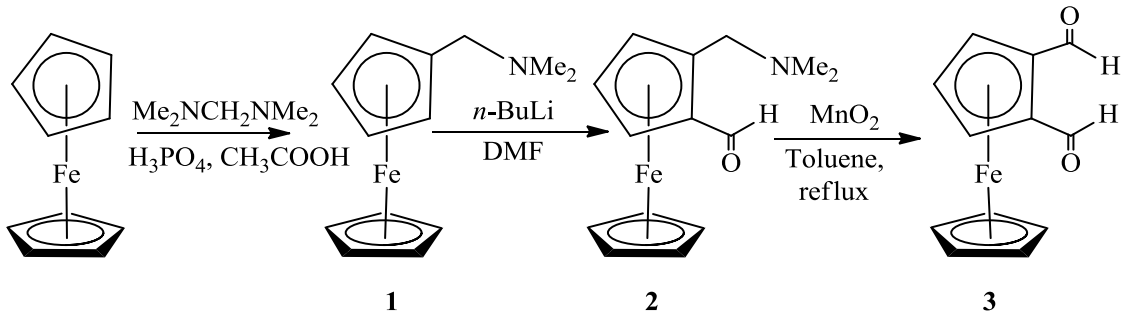

Scheme 2.1 Synthesis of 1,2-diformylferrocene

The reaction pathway involves the conversion of ferrocene to N,N-dimethylaminomethylferrocene by following the protocol developed by Lednicer and Hauser.[97] N,N-dimethylaminomethylferrocene **(1)** was prepared in 64.2% yield by reacting ferrocene with N,N,N',N'-tetramethylmethylenediamine under acidic conditions at 100 °C for 5 h. There are several approaches to prepare 1,2-diformyl ferrocene as described above. Among them, we used a procedure developed by the Brocard group.[89,90] On treating **1** with *n*-BuLi, it forms an ortho-lithiation complex, which on treatment with dimethylformamide forms N,N-dimethylaminomethyl-2-formylferrocene (**2**). Oxidation of **2** with activated MnO_2 yields 1,2-diformylferrocene (**3**), the precursor of our project. Unfortunately, we were unable to reproduce the reported 71% yield for conversion of **1** to **2**,[116] even with freshly dried solvent and oven-dried glassware cooled under nitrogen. The highest percentage of **2** we obtained under these conditions was 56%, but we typically

recovered around 50% of starting material (**1**)**.** In order to circumvent this issue, we attempted an alternative route to 1,2-diformylferrocene (Scheme 2.2) that avoids the lithiation step.

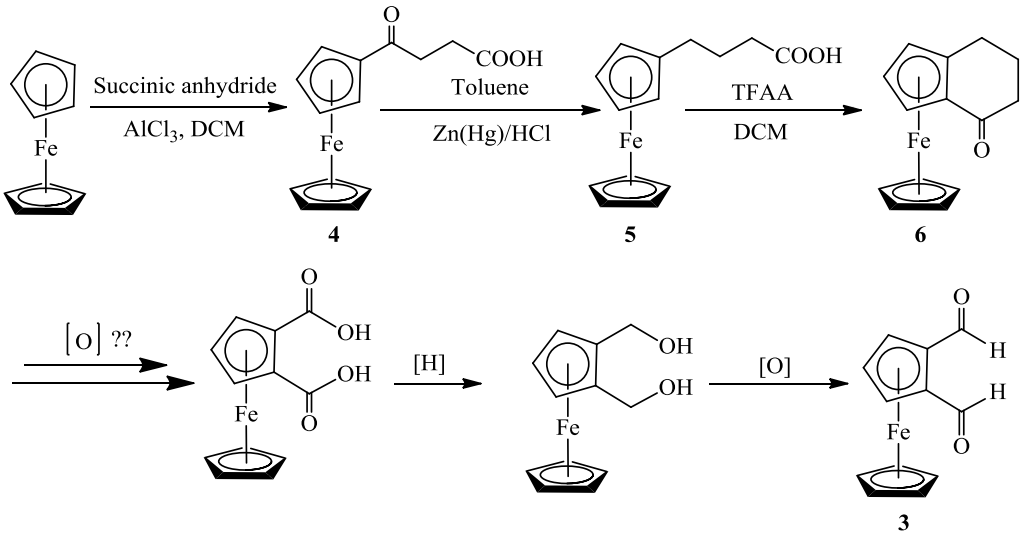

Scheme 2.2 Attempted synthetic route to 1,2-diformylferrocene

Following the reported procedure by Rinehart,[98] 1-(3-carboxypropionyl)ferrocene (**4,** 66%) was prepared by the Friedel-Crafts acylation between ferrocene and succinic anhydride in CH_2Cl_2 at room temperature. The keto group was reduced to methylene under the Clemmensen reduction to give desired acid (**5**, 85.7%).[99] Compound **5** was reacted with trifluoroacetic acid to prepare α-keto-1,2-tetramethylene ferrocene (**6,** 92.1%).[102]

Oxidation of **6** to 1,2-ferrocenedicarboxylic acid has not been achieved so far. Sotirious et al. reported aromatic 1,2-dicarboxylic acid prepared via oxidative cleavage of cyclic ketones fused to aromatic hydrocarbons using potassium superoxide in aprotic media in the presence of 18-crown-6-ether.[103] Oxidation of **6** under Sotirious' conditions resulted in intractable mixtures. Further, oxidation of acetylferrocene to

ferrocenecarboxylic acid is well known.[104,105,] Several attempts were carried out to oxidize ferrocenedicarboxylic acid using reagents such as Br_2/NaOH, I_2/NaOH , and reaction with bleach solution resulted in a decomposition.

Ferrocenedicarboxylic acid is the precursor to get the 1,2-diformylferrocene in two steps. The first step is the reduction of dicarboxylic acid to diol followed by oxidation to yield 1,2-diformylferrocene. We did not succeed in preparing 1,2-ferrocenedicarboxylic acid from **6**. Then, compound **6** was reacted with excess active manganese dioxide under reflux for 8 h to prepare ferrocene-fused-benzoquinone (**7**). The purple, gummy compound **7** was solidified by triturating with pentane under liquid N_2. The compound was characterized by ^{1}H NMR, ^{13}C NMR, IR and X-ray diffraction. IR shows a peak at 1650 cm^{-1} indicating the presence of a carbonyl group. Compound **7** was already reported by the Hill group,[101] but it had not been structurally characterized.

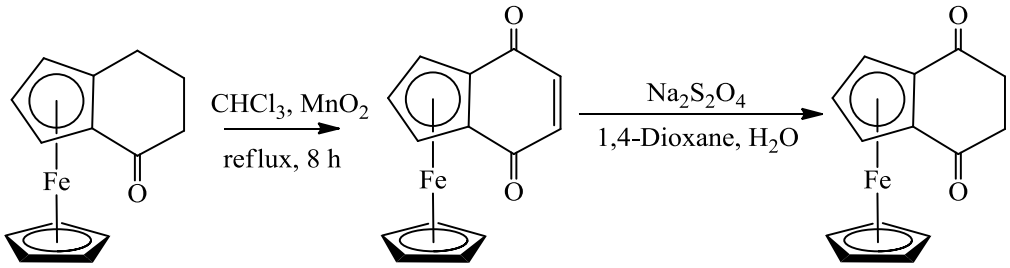

6 **7** **8**

Scheme 2.3 Synthesis of ferrocenebenzoquinone and ferrocene-fused cyclohexanedione

As our goal is to synthesize the ferrocenedicarboxylic acid, we attempted to oxidize ferrocene[*b*]benzoquinone (**7**) with the bleach solution in the dark at 50 ˚C for 6 h, with the addition of fresh bleach every 2 h resulted in decomposition. Compound **7** can be used to prepare acene analogous quinones under Cava conditions. An attempt to

prepare analogous acenequinones by the reaction of **7** with α,α,α',α'-tetrachloro-*o*-xylene under Cava conditions resulted in decomposition. However, reduction of ferrocene[*b*]benzoquinone (**7)** with sodium dithionite at room temperature for 7 h resulted in ferrocene-fused cyclohexanedione (8). Compound **8** is the stable form of the corresponding hydroquinone (enol tautomer). The dione is kinetically stable at room temperature but converts into phenolic form rapidly in presence of base.[106] The product was purified by chromatography on silica and crystallized by partial evaporation of ethyl ether solution in a stream of hexane-saturated N_2. The compound was characterized by a single X-ray crystal structure.

Compound **8** was reacted with phthalaldehyde, which underwent two-fold condensation in a base catalyst to give compound **9**. The quinone complex designed by this protocol has carbonyl groups at α- to cyclopentadienyl ring. Compound **9** had already been synthesized by one of our group members from the Friedel-Crafts acylation of ferrocene with 2-carbomethoxynaphthaloyl chloride in the presence of anhydrous $AlCl_3$ followed by the hydrolysis of an ester group, reduction of a carbonyl group, cyclization in presence of trifluoroacetic anhydride and oxidation of a cyclized product. The synthetic approach I have used to prepare **9** is not good as compared to one used by my former group member in termed of overall yield (7.38% vs. 44.7%) and number of reaction steps. The compound was characterized fully including a crystal structure.[107] Further, compound **8** was condensed with 1,2-diformylferrocene overnight at room temperature, which gave bimetallic acenequinone (**10**) (79.5%) with an equal mixture of two isomers (*syn* and *anti*). We were not able to separate the isomers chromatographically.

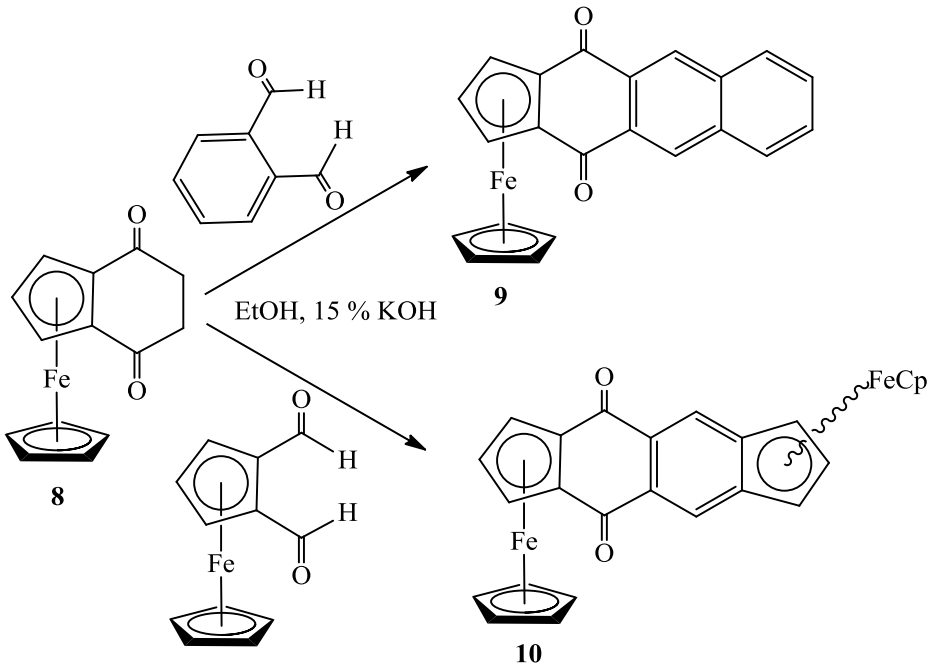

Scheme 2.4 Synthesis of ferrocene-fused α-carbonyl quinones

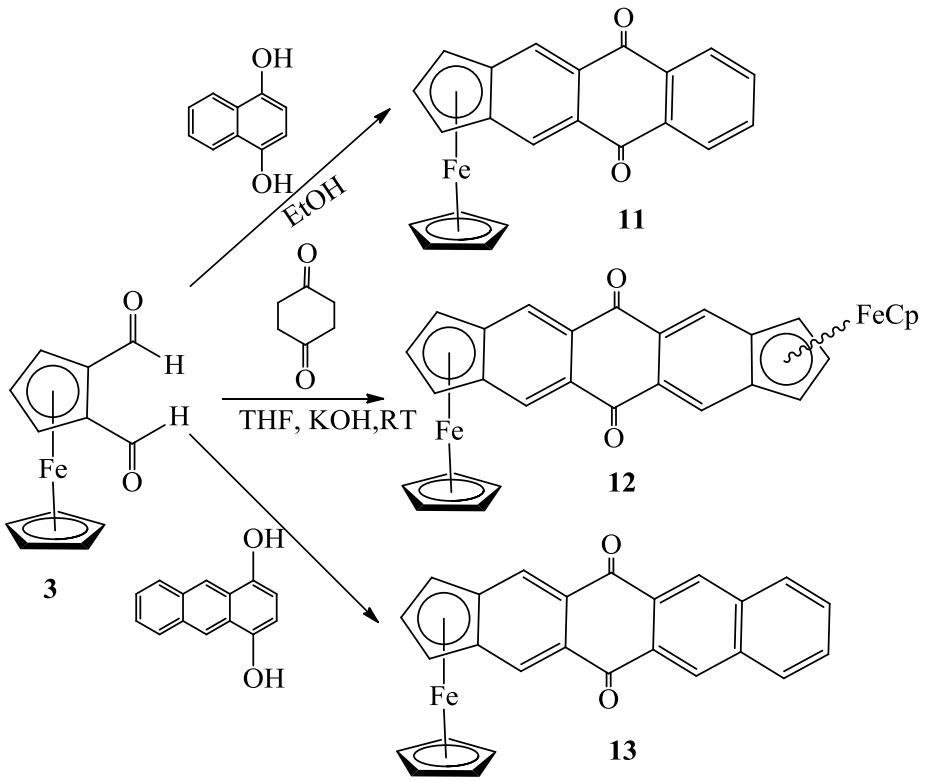

Scheme 2.5 Synthesis of ferrocene-fused quinones

Aldol condensations of 1,2-diformyl ferrocene were carried out following the literature procedure. The homologous backbone mononuclear quinones, **11** and **13** were prepared in 78.8% and 81.5% yields by reacting 1,2-diformylferocene with 1,4-dihydroxynaphthalene or with 1,4-anthracenediol in the presence of KOH. Similarly, a binuclear acenequinone, anthra-diferrocenedione, was synthesized by four-fold aldol condensation of 1,2-diformylferrocene with 1,4-cyclohexanedione in a 2:1 ratio in absolute ethanol under basic conditions, which resulted in a *syn*/*anti* isomeric mixture in 70 % combined yield. The purification of these mono- and bimetallic acenequinones involves simple frit filtration of the reaction mixture, washing the purple solid with cold ethyl ether until the filtrate is colorless, and dried under vacuum. We were unable to separate the isomers by column chromatography. ^{1}H NMR spectral integration shows a

ca. 1:1 ratio of *syn* and *anti* isomers. These deep blue, solid quinone complexes have a carbonyl group at γ-position with respect to cyclopentadienyl ring. They are stable in the solid state whereas standing in dichloromethane solution or chromatography on silica results in protolytic cleavage of the quinone ligand from the metal

The reaction of quinone complexes (**11**, **12** and **13**) with borane in THF reduced the carbonyl groups to methylenes (**14**, 45.5%; **15**, 42.4% combined yield and **16**, 40.0%). Again, we were unable to separate *syn* and *anti* isomers of **15** by column chromatography. An attempt to aromatize Cp-capped dihydroacenes (**14**, **15**, and **16**) using 2,3-dichloro-5,6-dicyano-1,4-benzoquinone (DDQ)[108] in benzene resulted in mostly decomposed products. The decomposed product was dissolved in ethyl ether. The ether layer was separated and reduced under rotary evaporation to give the yellow-green, gummy material. The purification of the gummy material on silica column chromatography eluted a yellowish green first band in 1:1 hexane: ethyl ether and evaporation of solvent gave a yellowish green viscous solid. ^{1}H NMR of that solid indicates the presence of multiple components.

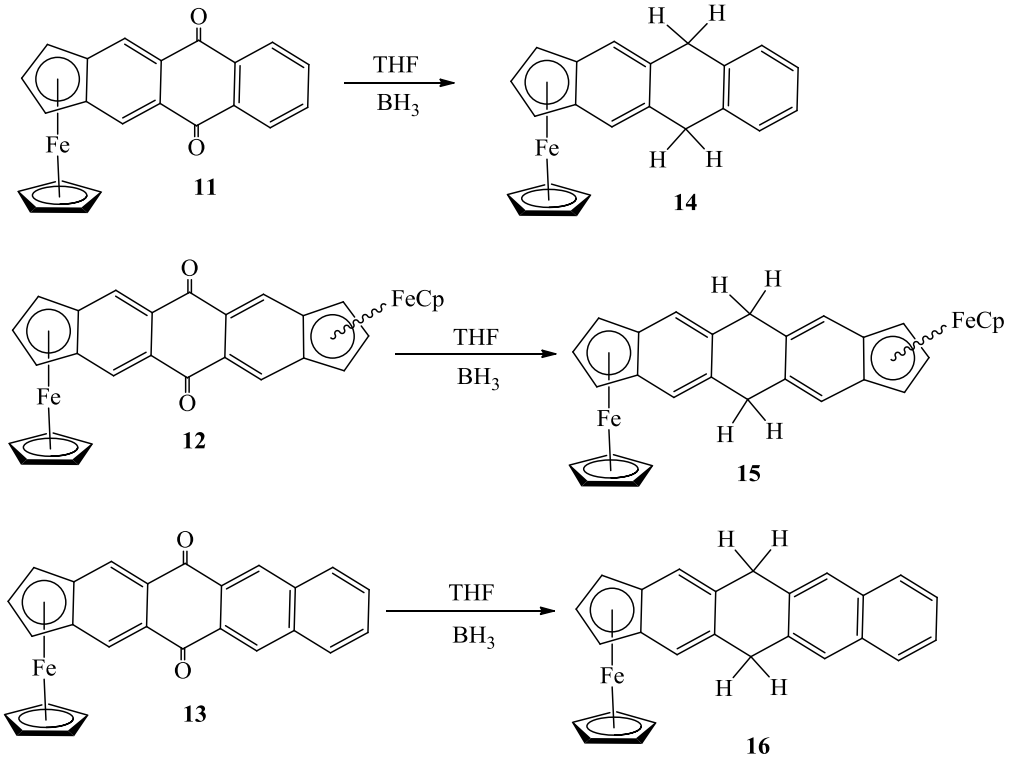

Scheme 2.6 Reduction of ferrocene-fused quinones with borane

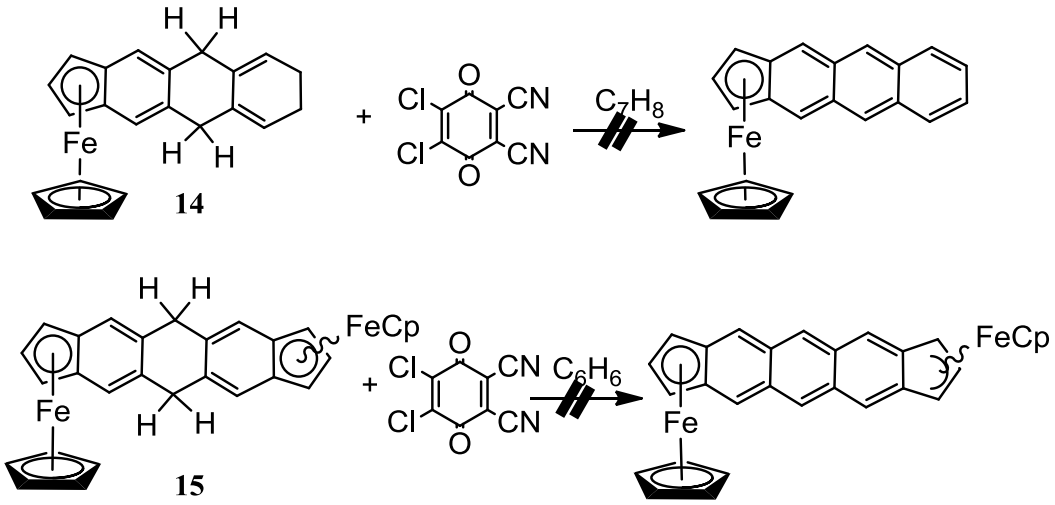

Scheme 2.7 Attempt to aromatize ferrocene-fused dihydroanthracenes

The reduction of acenequinones (**11**, **12** and **13**) using saturated aqueous solution of sodium dithionite in THF under reflux gave demetalated acenequinones in reasonably

good yield (**17**, 49.0%; **18**, 42.0% combined yield and **19**, 52.1%). Compounds **11**, **12** and **13** exhibit significant indenyl effect as a result when reducing reagent attacks on iron underwent ligand substitution reaction and resulted in demetalation to give Cp-capped acenequinones. In contrast, our attempt to demetalate compounds **9** and **10** under same reaction conditions resulted in recovery of starting material even after 55 h reaction at THF reflux temperature. We noticed the decomposition of starting material with longer reaction time. An infrared absorption around 1664 – 1672 cm^{-1} implies the presence of carbonyl groups in **17**–**19**. Attempts to improve the demetalation by treating complex **13** with aqueous potassium cyanide gave **19** in only 15% yield. Similar demetalation reactions on complex **13** by protolysis with 10% nitric acid or by reductive cleavage with zinc amalgam resulted only ~10% yield of **19**. Surprisingly, sodium dithionite is the most effective demetalation reagent.

Niebel et. al reported the synthesis of tetraketo-substituted dicyclopentanaphthalene (**2** of Chart 2.2) by the reaction of naphthalene-tetracarboxylic dianhydrides with ethyl(triphenylphosphoranylidene)acetate in high percent yield.[109] The same group synthesized dianion of octacyanotetramethylene-substituted dicyclopentanaphthalene (**3** of Chart 2.2) by refluxing tetraketo-substituted dicyclopentanaphthalene with a large excess of malononitrile in water in the presence of sodium acetate under argon atmosphere in 75 % yield, and investigation of electronic properties showed reversible redox behavior.[110] Makino and coworker have investigated some theoretical calculations to examine the aromaticity and magnetotropicity of dicyclopenta-fused polyacenes and reported that dianions of dicyclopenta-fused Polyacenes (**4** of Chart 2.2) have more aromatic character than their respective neutral

acenes.[111] Therefore, dicyclopenta-fused polyacene derivatives are valuable precursors for the synthesis of molecular and polymeric advanced materials.

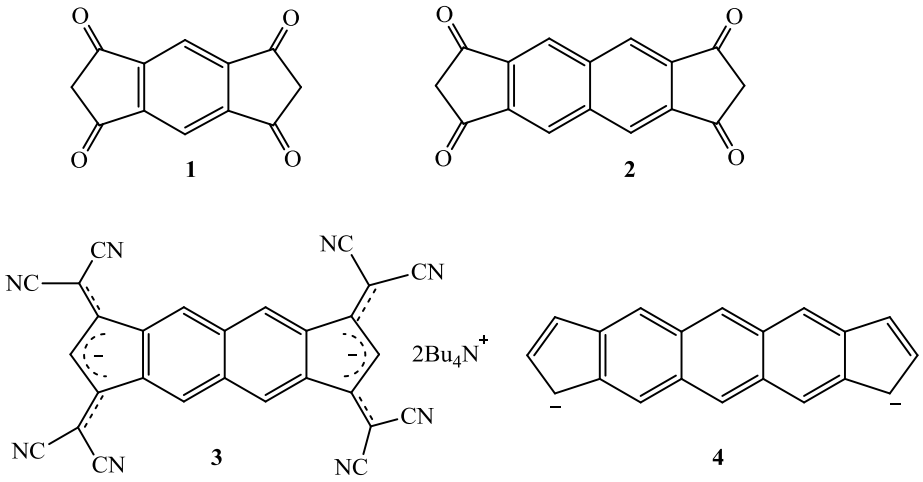

Chart 2.2 Dicyclopenta-fused Polyacene derivatives

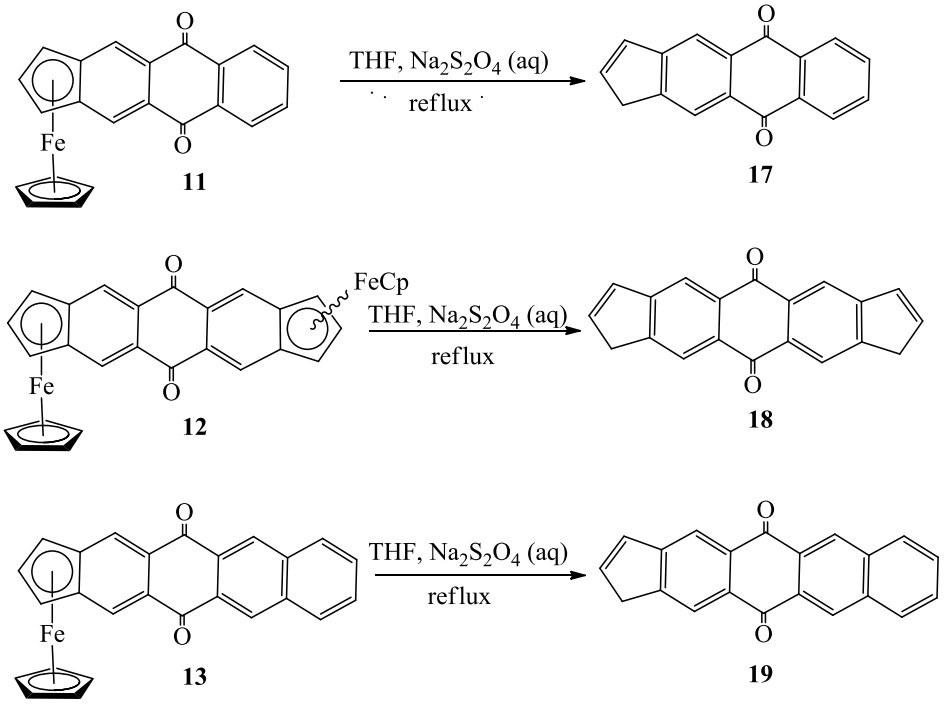

Scheme 2.8 Reduction of ferrocene-fused quinones with sodium dithionite

Since we were not able to aromatize ferrocene-fused acenequinones to ferrocene-fused polyacenes, an alternative is to aromatize the Cp-capped acenequinones. Nucleophilic addition to the quinone carbonyls followed by dehydroxylation with $SnCl_2$ in acidic conditions is a classic method of converting acenequinones to acenes.[6] Following the procedure established by Anthony's group, Cp-capped acenequinones (**17**, **18** and **19**) were reacted with triisopropylsilylacetylene/*n*-BuLi in hexane, followed by dehydroxylation with $SnCl_2$,[21] which gave Cp-capped bis(triisopropylsilylethynyl)acenes (**20**, 50%, **21**, 23% and **22**, 59%). To the best of our knowledge, we are the first to detach mono- and bis(cyclopentadiene)fused acenequinones from iron and to aromatize the free acenequinones as Cp-capped bis(triisopropylsilylethynyl)acenes. Bis(Cp-capped-triisopropylsilylethynyl)- anthracene is closely similar to Anthony's bis(triethylsilylethynyl)anthradithiophene both structurally and electronically.[6]

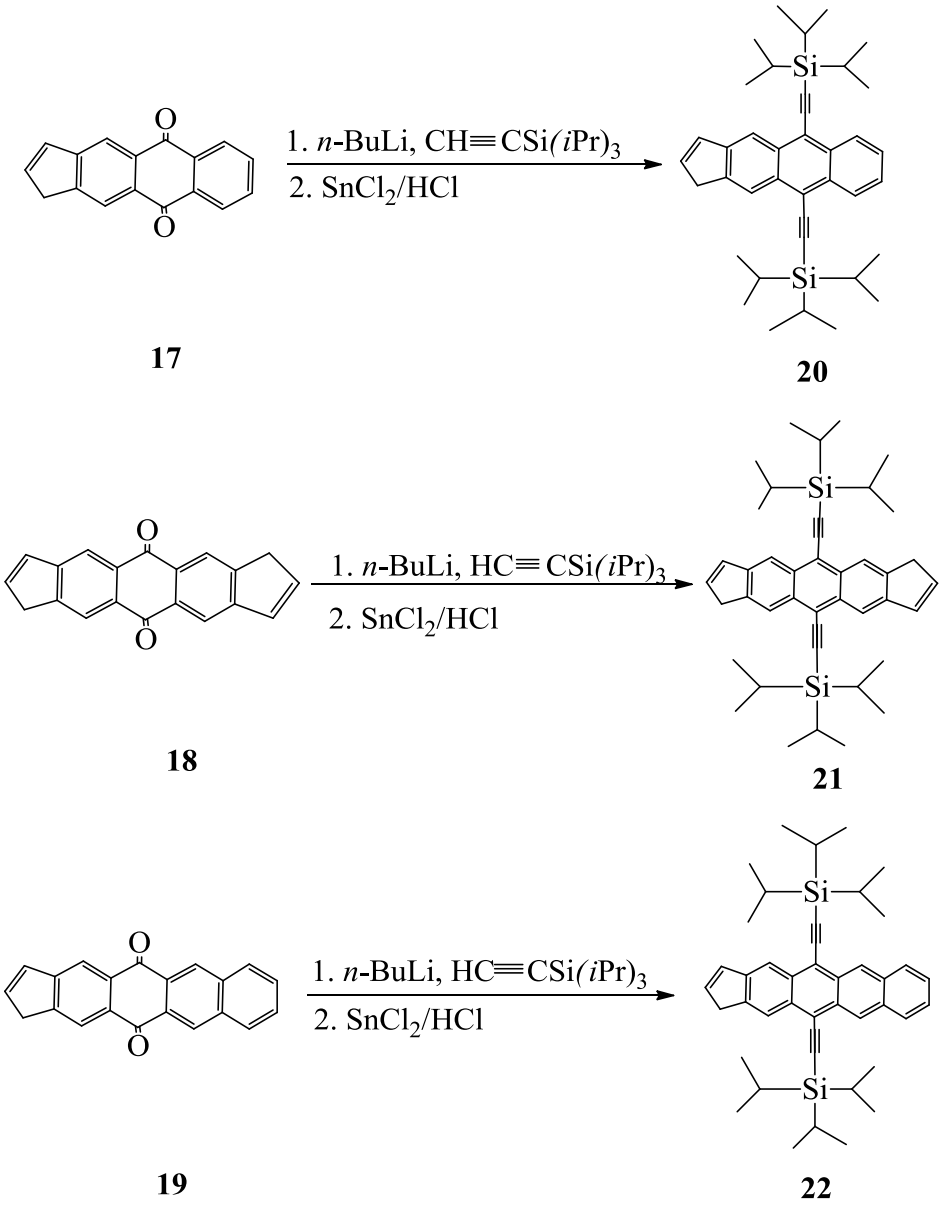

Scheme 2.9 Conversion of quinones to TIPS-acenes

2.3.2 Spectroscopy. The compounds synthesized previously were characterized by comparison of their ^{1}H NMR spectra, IR spectra and melting points with reported data. All new compounds were fully characterized by spectroscopic methods including ^{1}H and ^{13}C NMR, IR and mass spectroscopy. The ^{1}H NMR resonances of the unsubstituted cyclopentadienyl ring of **1–16** in ^{1}H NMR lie in the range of 3.69 to 4.30

ppm depending on compounds' structures with the characteristic singlet. Similarly, proton resonances of substituted cyclopentadienyls of **2–3**, and **7–16** display a characteristic doublet and triplet with an integration of a 2:1 ratio showing the symmetry of the ligand. The resonance of inner protons (CHC*H*CH) generally display in the range of 3.91 to 4.92 ppm, whereas those of outer protons (C*H*CHC*H*) lie between 4.08 to 5.43 ppm.

The ^{1}H NMR spectra of ferrocene-fused dihydroacenes (**14**, **15** and **16**) show a singlet methylene proton in the range of 3.73 to 3.98 ppm in $CDCl_3$ solvent. Similarly, the ^{1}H NMR resonances of cyclopentadiene-capped acenequinones display a characteristic singlet peak of a methylene group around 3.59–3.61 ppm. The aromatization of iron-free acenequinones to corresponding bis(triisopropylsilylethynyl) polyacenes shows the methylene proton in the range of 3.63 to 3.66 ppm in the ^{1}H NMR. The ^{13}C NMR spectra of compounds **7**–**13** and **17**–**19** show the characteristic peaks of carbonyl carbon in the range of 182 to 193 ppm. The ^{13}C NMR spectra of **10**, **11**, **12**, **13** and **14** show the upfield shift of signals for *ipso* carbons (C8, C9 in Figure 1.6) in the range of 87 to 90 ppm. Similar chemical shifts were observed by the Marder group for *ipso* carbons in the ^{13}C NMR of $[Fe(\eta\text{-}C_9H_7)_2]$ and $[Co(\eta\text{-}C_9H_7)_2]^+$, which they considered as indicative of η^5-coordination.[53]

The ^{1}H NMR of compound **12** indicates the presence of isomers with two peaks for unsubstituted cyclopentadienyl ligands (C_5H_5) at 3.90 and 3.96 ppm and arene protons at 8.92 and 8.94 ppm. Similarly, ^{1}H NMR of compound **15** also displays the two peaks for C_5H_5 at 3.65 and 3.69 ppm and arene protons at 7.35 and 7.38 ppm, which confirms the presence of isomers. Furthermore, the ^{1}H NMR of compound **18** shows presence of

arene proton peaks at 8.37 and 8.29 ppm, and compound **21** shows the evidence of isomers with a tiny splitting of the peak at 8.53 ppm. In addition, the ^{13}C NMR of **12**, **15**, **18** and **21** shows strong evidence for the presence of isomer with the significant number of carbon peaks. The IR spectra of complexes show characteristic carbonyl stretching frequencies in the region of 1650 to 1672 cm^{-1}. IR absorption frequencies of complexes are shown in Table (**2.2**). Mass spectra of all compounds show characteristic peaks corresponding to molecular ion.

Table 2.1 Selected ^{1}H data (ppm) for complexes **7**–**22**

Comp.	δ_H (ppm)				Solv.*
	C*H*CHC*H*	CHC*H*CH	C_5H_5	CCH_2CH	
7	5.09	5.37	4.30	–	a
8	4.86	5.18	4.27	–	a
9	5.12	5.52	4.17	–	a
10	4.58, 5.05	5.28, 5.45	3.89, 3.92 4.13, 4.14	–	a
11	4.65	5.36	3.93	–	a
12	4.59	5.35	3.90, 3.96	–	a
13	4.7	5.43	3.97	–	b
14	3.98	4.83	3.70		a
15	3.96	4.82	3.65, 3.69	–	a
16	3.91	4.79	3.69	–	c
17	–	–	–	3.59	a
18	–	–	–	3.59	a
19	–	–	–	3.61	a
20	–	–	–	3.63	a
21	–	–	–	3.63	a
22	–	–	–	3.66	a

* a. $CDCl_3$; b. CD_2Cl_2; c. C_6D_6

Table 2.2 Selected ^{13}C NMR data (ppm) for complexes **7**–**22**

Comp.	δ_C (ppm)				Solv.*
	C_5H_5	Ipso *CC*	C*C*H$_2$CH	*C*O	
7	74.09	70.41	–	190.59	a
8	72049	78.89	–	201	a
9	73.5	79.16	–	188.50	a
10	69.38 69.68 73.16 73.34	79.47 79.79	–	187.49 187.87	a
11	69.54	87.02		182.17	a
12	–	–	–	–	a
13	69.79	87.70	–	182.22	b
14	68.37	87.70	-	–	a
15	–	–	–	–	a
16	70.1	88.29	–	–	c
17	–	–	40.11	183.81, 183.94	a
18	–	–	40.08	192.66	a
19	–	–	40.08	183.62, 183.74	a
20	–	–	59.75	–	a
21	–	–	38.47	–	a
22	–	–	37.15	–	a

* a. $CDCl_3$; b. CD_2Cl_2; c. C_6D_6

Table 2.3 Carbonyl groups IR absorption frequencies of complexes (ATR)

Comp.	C=O(cm^{-1})
7	1650
8	1671
9	1658
10	1658
11	1669
12	1657
13	1665
17	1672
18	1664
19	1666

2.3.3 Structure. The growth of crystals was conducted at ambient temperature unless otherwise mentioned. The structures of [Fe(Cp){η^5-$C_5H_3(COCH_2)$}] (**7**), [Fe(Cp){η^5-$C_5H_3(COCH_2)_2$}] (**8**), Cis-[$Fe_2(Cp)_2${μ-(η^5:η^5)-(C_5H_3COCCH)}$_2$] (**10**), [Fe(Cp){η^5-$C_5H_3(CHCCOCCHCH)_2$}] **(11)**, Cis-[$Fe_2(Cp)_2${μ-(η^5:η^5)-($C_5H_3CHCCOCCH)_2$}] **(12)**, [Fe(Cp){η^5-$C_5H_3(CHCCOCCHCCHCH)_2$}] **(13)**, [Fe(Cp){η^5-$C_5H_3(CHCCH_2CCHCH)_2$}] **(14)**, [$C_5H_4(CHCCOCCHCH)_2$] **(17)**, [$(C_5H_4)_2(CHCCOCCH)_2$] (**18**), [$C_5H_4(CHCCOCCHCCHCH)_2$] **(19)**, [$(C_5H_4)_2(CHCCCCH)_2${C≡CSi(*i*-Pr)$_3$}$_2$] (**21**), and [(C_5H_4)($CHCCCCHCCHCH)_2$){(C≡CSi(*i*-Pr)$_3$}$_2$] (**22**) were determined by X-ray crystallography. Single crystals of 7, **13**, and **18**, were grown by slow evaporation of dichloromethane under nitrogen while crystal **19** was grown by slow evaporation of ethyl ether from its saturated solution, and **21** and **22** were grown by slow evaporation of acetone. Similarly, single crystals of **8** and **10** were grown from evaporation of dichloromethane solution in a stream of hexane-saturated N_2 through a cannula. Thermal ellipsoid plots of the molecular structures of 7, **8**, **10**, **11**, **12**, **13**, **14**, **17, 18**, **19, 21** and **22** are shown in Figures **2.3** to **2.14** with the atom numbering scheme. The crystal structure and refinement data for these compound can be found in Tables **2.3**–**2.7** as shown below.

The iron complexes **7, 8, 10, 11, 12, 13** and **14** indicate eclipsed conformation of the two cyclopentadienyl rings similar to typical ferrocene geometry. The average iron–cyclopentadienyl centroid distances (substituted, unsubstituted) are **7** [1.645(5) Å, 1.662(5) Å], **8** [1.644(2) Å, 1.658(2) Å], **10** [Fe1 1.640(3) Å, 1.653(3) Å, Fe2 1.666(3) Å, 1.659(3) Å], **11** [1.670(2) Å, 1.657(2) Å], **12** [Fe1 1.666(7) Å, 1.654(8) Å, Fe2 1.655(7)

Å, 1.649(8) Å], **13** [1.673(2) Å, 1.656(2) Å], **14** [1.669(2) Å, 1.642(3) Å]. The average bond distance between the metal center to ipso carbons and to the remaining three carbon atoms of the substituted cyclopentadienyl ring are **7** [Fe 2.034(5) Å, 2.055(5) Å, 10 [Fe1 2.018(3) Å, 2.054(3) Å, Fe2 2.088(3) Å, 2.053(3) Å], **11** [2.093(2) Å, 2.045(2) Å], **12** [Fe1 2.070(7) Å, 2.040(7) Å, Fe2 2.072(7) Å, 2.054(7) Å], **13** [2.092(2) Å, 2.055(2) Å], and **14** [2.092(5) Å, 2.045(5) Å]. The average bond distance between the iron center to *ipso* carbons (C4 and C5) in complex **7** and Fe1 to *ipso* carbons (C1 and C5) in **10** is shorter than the bond to the remaining three carbon atoms of the substituted cyclopentadienyl ring. The ring slippage parameter Δ_{Fe-C} has a value of 0.021 Å (**7**) and 0.034 Å (**10**). This shift is opposite to that found as a common feature in indenyl complexes. Similar behaviors have been observed by the Bernardivelli group in the structure of [$Cr(CO)_3(\eta^6$-5,8-naphthoquinone)] with Δ_{Cr-C} value of 0.044 Å.[112] The C–C bond distances in the substituted cyclopentadienyl ring are in the range of 1.413 to 1.447 Å.

The quinone moiety in complex **7** is slightly tilted toward the iron center. The interplanar angle between the quinone and the Cp plane is 6.22°. The bending is prominent at the carbonyl carbon, which is also supported by the torsional angle of C1–C5–C4–C9 (−174.3°) and C3–C4–C5–C6 (177.8°). The carbonyl groups in **8** are coplanar with the Cp ring; however, the structure is twisted at carbons C8 and C9 with a torsional angle (C6–C7–C8–C9) of 42.2(3)°.

The characteristic feature of indenyl complexes **11, 12, 13** and **14** is that the *ipso* carbon atoms in the substituted cyclopentadienyl ring are slightly away from the iron center, demonstrating their weaker interaction towards iron than the remaining three

carbon atoms. In contrast to ferrocene, these complexes display a gradual increase in the degree of slip-fold distortion from η^5 toward η^3 coordination, which involves slippage of the iron from *ipso* carbons. The ease of ring slippage for indenyl vs. cyclopentadienyl ligands may be due to the rehybridization of the indenyl π-system, which involves an increase in the aromatic character of the benzene ring. This results in a disruption of the aromatic character in the five-membered ring. Hence, cyclopentadienyl ligand requires a high energy process for ring slippage from η^5 to η^3 coordination[113–114]

To be a true η^3 complex, slip parameter (Δ_{M-C}) should be 0.69–0.79 Å as reported for an iridium complex $[Ir(PMe_2Ph)_3(\eta^3\text{-}C_9H_7)]$.[50] The slip parameter (Δ_{Fe-C}) is 0.048 (**11**), 0.03 Fe1, 0.018 Fe2 (**12)**, 0.037 (**13**) and 0.047 (**14**). These values correspond to bis(indenyl)ferrocene (Δ_{Fe-C} = 0.049) indicating that the Cp of these complexes have true η^5 coordination with the iron center. The true η^5 coordination of these complexes is also supported by carbon peaks of ipso carbons in the solution ^{13}C NMR, which lie in the range of 87 to 90 ppm; for η^3-complexes, ipso carbons shifts are in the range 130–160 ppm. Moreover, the slip-fold distortion of these indenyl complexes can be explained in terms of their hinge angle (HA) and fold angle (FA). The hinge angle (HA) is an angle between the planes (C5, C6, C7) and (C5, C4, C8 C7), and the fold angle (FA) is an angle between the planes (C5, C6, C7) and the rest of the plane of a complex as shown in Figure 2.6. The hinge angle represents bending at [C5, C7] and the fold angle represents bending at [C4, C8]. The calculated HA and FA is 2.29 °, 8.48 ° (**11)**, Fe1 1.67 °, 2.70 ° and Fe2 3.55 ° (**12)**, 4.68 °, 2.75 ° (**13)** and 2.16 °, 3.41 °(**14)**. The hinge angles of these complexes are close to the HA of $[Fe(\eta^5\text{-}C_9H_7)_2]$, which is 2.6 °, whereas the fold angles are slightly larger than the FA of $[Fe(\eta^5\text{-}C_9H_7)_2]$ equal to 1.6 °. Even though crystal

structures exhibit minimal indenyl effect, these values correspond to nearly undistorted η^5-coordination of a ligand, consistent with the solution ^{13}CNMR data. All C–C bonds of substituted Cp in **11**, **12**, **13** and **14** are ranging from 1.420–1.428(4) Å, 1.406–1.462(10) Å, 1.423–1.453(3) Å and 1.420–1.437(4) Å, respectively.

The mononuclear quinone complex, **13** exhibits coplanarity of quinone groups with the Cp ring. Figures 2.1 and 2.2 show the packing of ferrocene-fused and cyclopentadiene-capped quinone complexes along the *a*-axis. Ferrocene-fused-tetracenequinone (**13**) shows sandwich herringbone arrangement. The ferrocenyl groups of two molecules in **13** are oriented on the opposite face of the plane, thereby avoiding steric interactions. In both the crystal packing, the two quinone complexes are arranged in anti-parallel orientation with an intermolecular arene-arene distance of 3.36 Å (**13**) and 3.46 Å (**19**) between two of the closest molecules. The solid-state packing of **13** shows the interaction of electron-rich aromatic ring of one molecule with the electron deficient carbonyl group of neighboring molecules and **19** exhibits the interaction of allyl portion of Cp of one molecule with the quinone of another neighboring molecule.

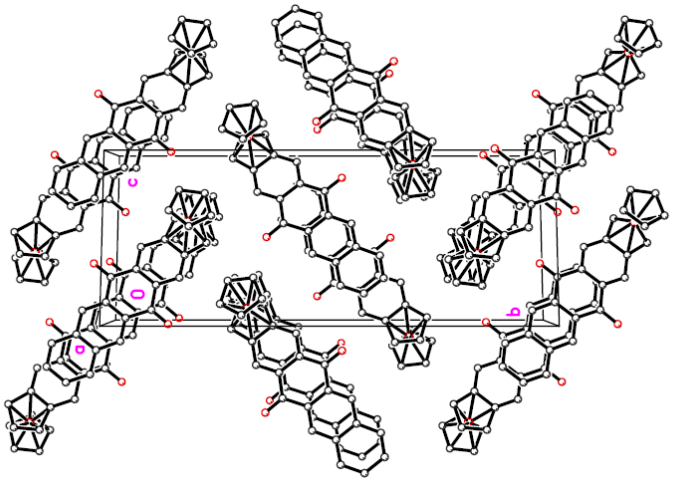

Figure 2.1 Packing of ferrocene-fused-quinone **13** on their lattice along *a*-axis

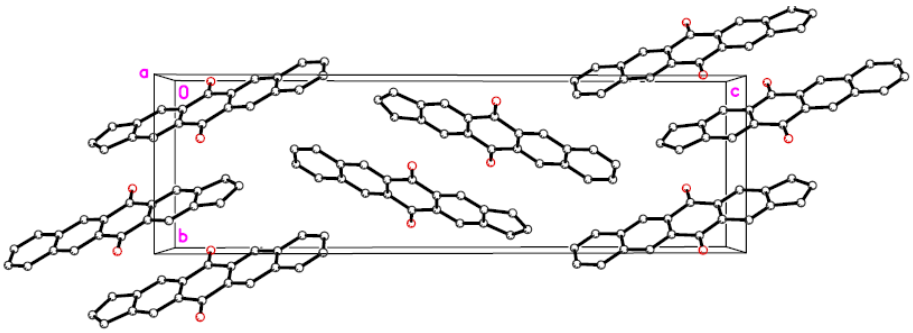

Figure 2.2 Packing of Cp-capped quinone **19** along a-axis

A crystal structure of borane-reduced ferrocene-dihydroanthracene (**14**) displays a strong folding of the dihydroacene ligand at the methylene carbon atoms with a bent angle of 44.8 ° at the reduced ring. The bond distances between carbon and oxygen lie between the range of 10 [1,228(3) Å –1.233(3) Å], **11** [1.227(3) Å–1.229(3) Å], **12** [1.219(7) Å–1.226(7) Å], **13** [1.226(3) Å–1.225(3) Å], **17** [1.2247(17) Å–1.2240(18) Å], **18** [1.230(2) Å] and **19** [1.225(2) Å]. Molecular structure of **17** is disordered crystallographically and oriented randomly. Molecular structure of **19** shows slight thermal ellipsoid elongation at C6, which might be due to slight disorder of the five-membered ring. The C=C bond length in the five-membered ring system of demetalated complexes (**17, 18** and **19**) ranges from [1.324(16) Å to 1.414 (10) Å], which lies between the C=C bond length for an alkene and benzene. The interplanar angle between the planes C12C13C14 of complex (**17)**, C6C5C4 (**18**), C4C5C6 (**19**) and C6C7C8 (**21**) and the rest of the molecules is 2.15˚, 1.11˚, 2.79˚ and 1.03˚. Cp-capped TIPS-derivatives **21** and **22** pack with significant two-dimensional π-overlap and π-face separation of 3.41 Å and 3.40 Å (vs. 3.43 Å in TIPS-pentacene).

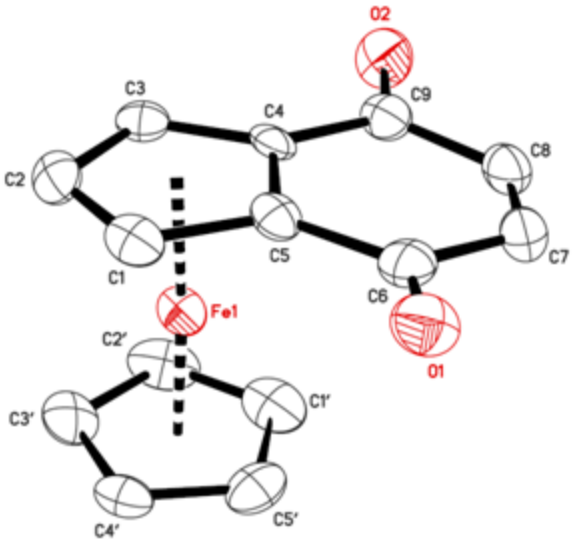

Figure 2.3 Molecular structure of [Fe(Cp){η^5-$C_5H_3(COCH_2)$}] (**7**)

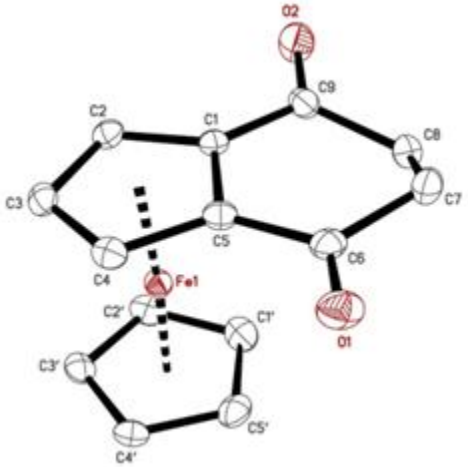

Figure 2.4 Molecular structure of [Fe(Cp){η^5-$C_5H_3(COCH_2)_2$}] (**8**)

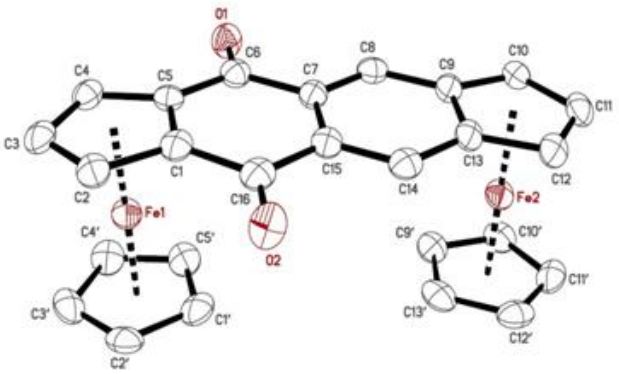

Figure 2.5 Molecular structure of Cis-[$Fe_2(Cp)_2\{\mu$-(η^5:η^5)-(C_5H_3COCCH)$\}_2$] (**10**)

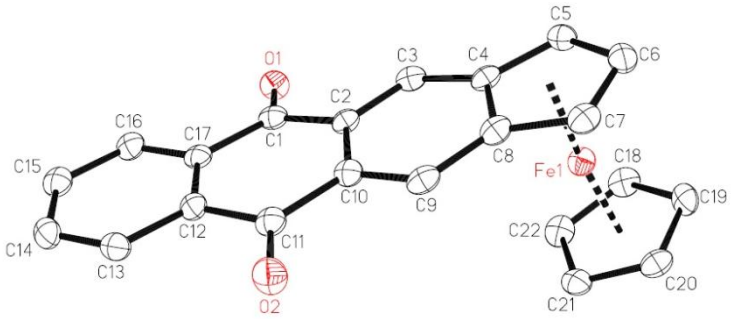

Figure 2.6 Molecular structure of [Fe(Cp)$\{\eta^5$-$C_5H_3(CHCCOCCHCH)_2\}$] (**11**)

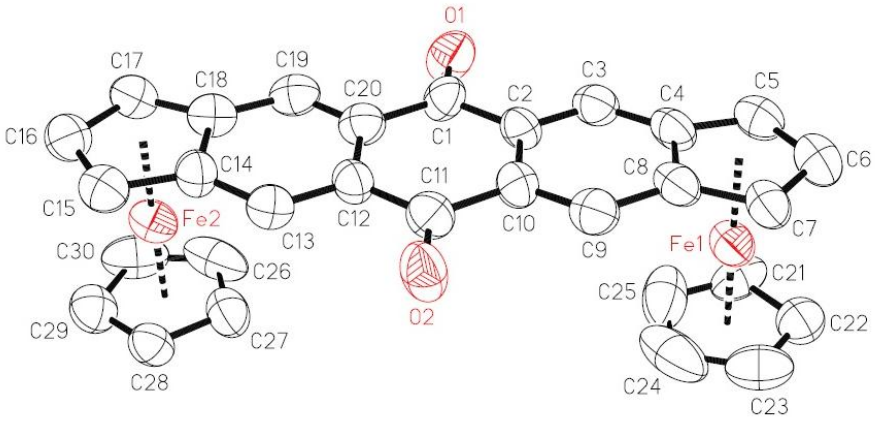

Figure 2.7 Molecular structure of Cis-[$Fe_2(Cp)_2\{\mu$-(η^5:η^5)-($C_5H_3CHCCOCCH)_2\}$]

(**12**)

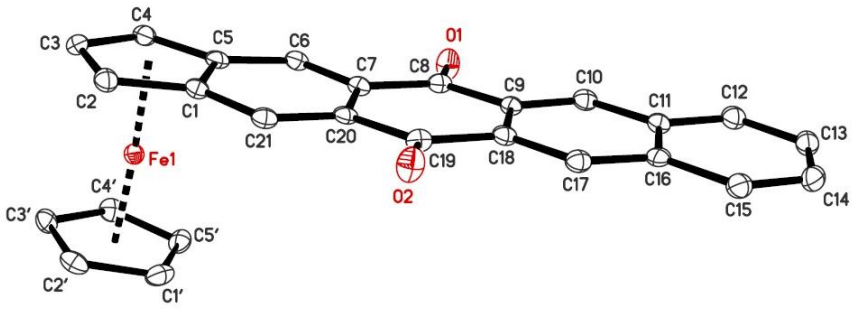

Figure 2.8 Molecular structure of [Fe(Cp){η^5-C_5H_3(CHCCOCCHCCHCH)$_2$}] (**13**)

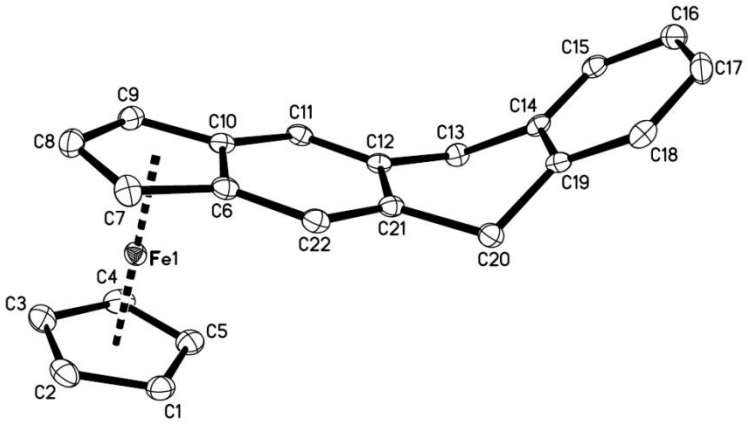

Figure 2.9 Molecular Structure of [Fe(Cp){η^5-C_5H_3(CHCCH$_2$CCHCH)$_2$}] (**14**)

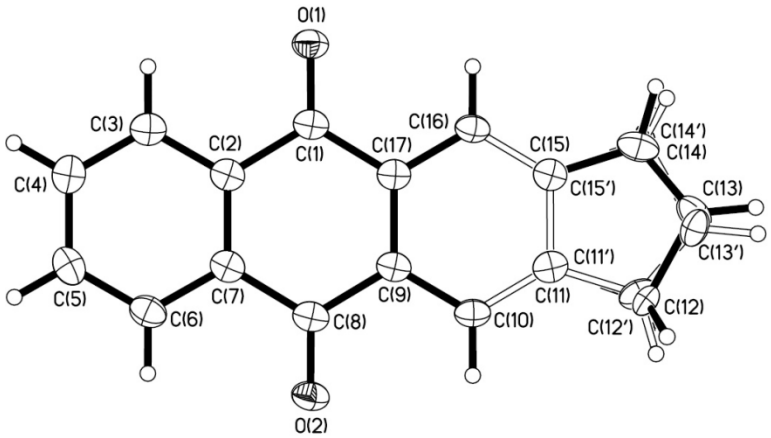

Figure 2.10 Molecular Structure of [C_5H_4(CHCCOCCHCH)$_2$] (**17**)

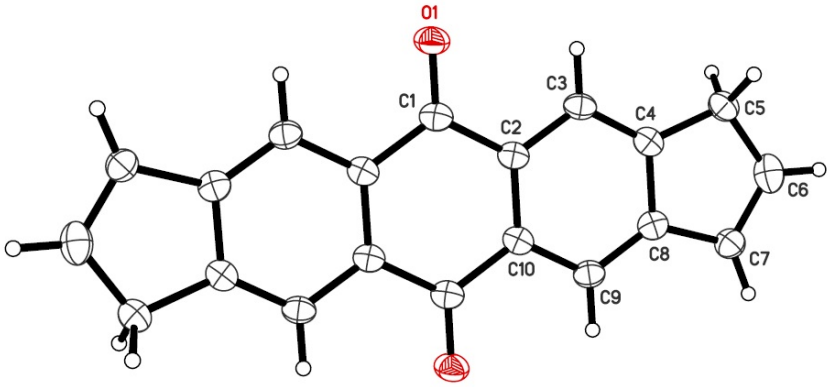

Figure 2.11 Molecular Structure of $[(C_5H_4)_2(CHCCOCCH)_2]$ (**18**)

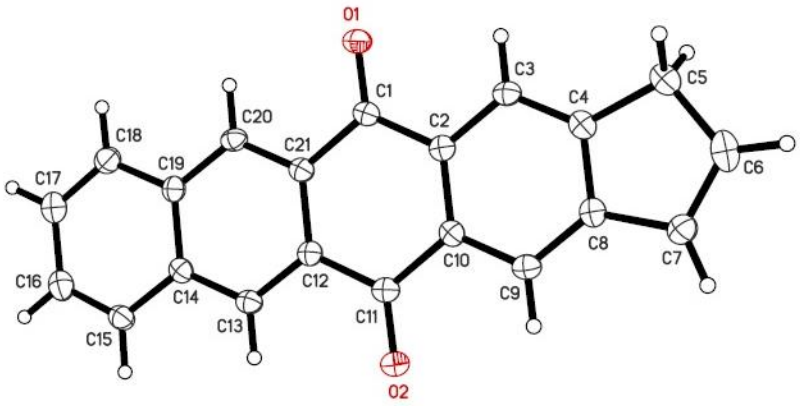

Figure 2.12 Molecular Structure of $[C_5H_4(CHCCOCCHCCHCH)_2]$ (**19**)

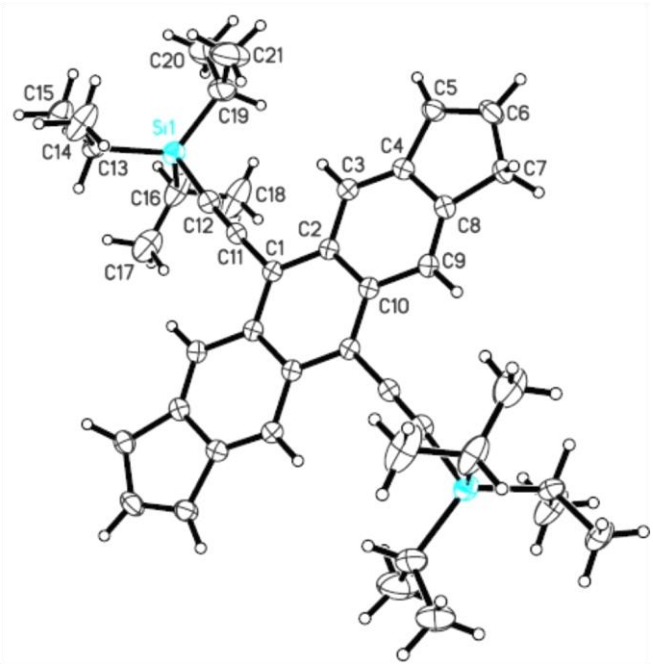

Figure 2.13 Molecular structure of $[(C_5H_4)_2(CHCCCCH)_2\{C{\equiv}CSi(i\text{-}Pr)_3\}_2]$ (**21**)

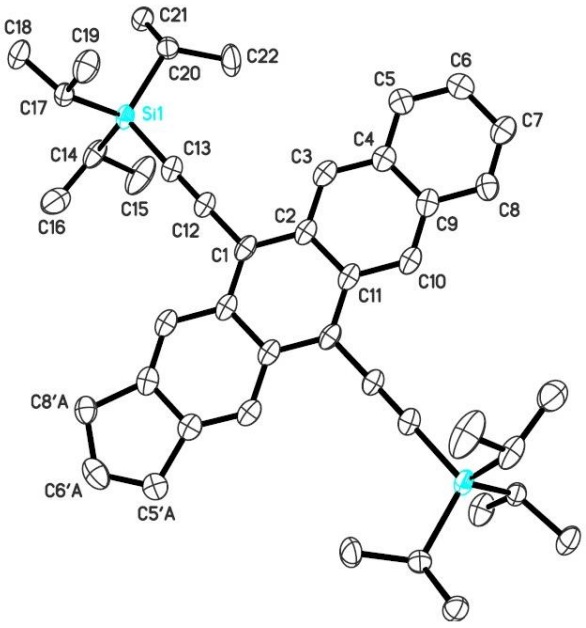

Figure 2.14 Molecular structure of $[(C_5H_4)\ (CHCCCCHCCHCH)_2)\{(C{\equiv}CSi(i\text{-}Pr)_3\}_2]$

(**22**)

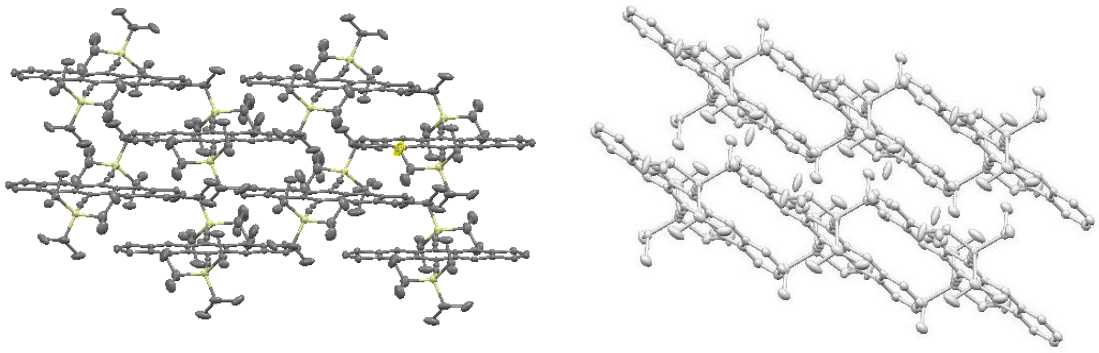

Figure 2.15 Packing arrangement of bis Cp-capped TIPS-anthracene (**21** left) and Cp-capped TIPS-tetracene (**22** right)

Table 2.4 Crystal Data and Structure Refinement for Compounds **7** and **8**

Compound	**7**	**8**
Formula	$C_{14}H_{10}FeO_2$	$C_{14}H_{12}FeO_2$
Formula wt. (amu)	266.07	268.09
T, K	90.0(2)	90.0(2)
Crystal system	Monoclinic	Monoclinic
Space group	$P2_1/c$	$P2_1/c$
Z	4	4
a, Å	10.1804(4)	10.0416(3)
b, Å	8.8224(4)	8.9648(2)
c, Å	12.1570(5)	12.2104(3)
α (deg)	90	90
β (deg)	100.456(3)	97.2458(15)
γ (deg)	90	90
V, $Å^3$	1073.76(8)	1090.41(5)
d_{calc}, Mg/m^3	1.646	1.633
F(000)	544	552
Crystal size (mm^3)	0.18 × 0.07 × 0.04	0.32 × 0.29 × 0.04
Radiation	Cu Kα (λ = 1.54178 Å)	Cu Kα (λ = 1.54178 Å)
Monochromator	Graded multilayer optics	Graded multilayer optics
Abs coefficient (mm^{-1})	11.128	1.366
Diffractometer	Bruker X8 Proteum	Bruker X8 Proteum
Range (deg)	4.42 to 68.15	2.044 to 27.494
Limiting indices	$-12 \le h \le 12$	$-13 \le h \le 13$
	$-10 \le k \le 10$	$-11 \le k \le 11$
	$-14 \le l \le 11$	$-15 \le l \le 15$
Reflections collected	12566	19592
Independent reflections	1903 [R(int) = 0.07541]	2501 [R(int) = 0.0362]
Absorption correction	Semiempirical from equivalents	Semiempirical from equivalents
Refinement method	SHELXL-97	SHELXL-97
Refinement method	Full-matrix least-squares on F^2	Full-matrix least-squares on F^2
Data/restraints/parameter	1903 / 0 / 154	2501 / 0 /154
Goodness-of-fit on F^2	1.047	1.102
Final R indices [$I > 2\sigma(I)$]	R1 = 0.0583, wR2 = 0.1337	R1 = 0.0332, wR2 = 0.0747
R indices (all data)	R1 0.0778, wR2 = 0.1512	R1 0.0436, wR2 = 0.0799
Largest diff. peak and hole	0.908 and 0.493 ($e \cdot Å^{-3}$)	0.766 and 0.517 ($e \cdot Å^{-3}$)

Table 2.5 Crystal Data and Structure Refinement for Compounds **10** and **11**

Compound	**10**	**11**
Formula	$C_{26}H_{18}Fe_2O_2$	$C_{22}H_{14}FeO_2$
Formula wt. (amu)	474.10	366.18
T, K	90.0(2)	90.0(2)
Crystal system	Monoclinic	Monoclinic
Space group	$P2_1/c$	$P2_1/c$
Z	4	4
a, Å	10.4237(2)	11.4602(6)
b, Å	12.2745(3)	11.5511(6)
c, Å	14.5526(3)	11.8446(7)
α (deg)	90	90
β (deg)	98.4296(14)	107.987(2)
γ (deg)	90	90
V, $Å^3$	1841.83(7)	1491.33(14)
d_{calc}, Mg/m^3	1.710	1.631
F(000)	968	752
Crystal size (mm^3)	0.20 × 0.16 × 0.06	0.20 × 0.18 × 0.18
Radiation	Cu Kα (λ = 1.54178 Å)	Mo Kα (λ =0.71073 Å)
Monochromator	Graded multilayer optics	Graphite
Abs coefficient (mm^{-1})	1.597	1.024
Diffractometer	Bruker X8 Proteum	Nonius KappaCCD
Range (deg)	1.975 to 27.499	1.87 to 27.50
Limiting indices	$-13 \le h \le 13$	$-14 \le h \le 14$
	$-15 \le k \le 15$	$-14 \le k \le 15$
	$-18 \le l \le 18$	$-15 \le l \le 15$
Reflections collected	41523	6519
Independent reflections	4231 [R(int) = 0.0597]	3420[R(int) = 0.0445]
Absorption correction	Semiempirical from equivalents	Semiempirical from equivalents
Refinement method	SHELXL-97	SHELXL-97
Refinement method	Full-matrix least-squares on F^2	Full-matrix least-squares on F^2
Data/restraints/parameter	4231 / 0 / 301	3420 / 0 / 226
Goodness-of-fit on F^2	1.135	1.027
Final R indices [$I > 2\sigma(I)$]	R1 = 0.0381, wR2 = 0.0710	R1 = 0.0422, wR2 = 0.0981
R indices (all data)	R1 0.0607, wR2 = 0.0837	R1 = 0.0729, wR2 = 0.1094
Largest diff. peak and hole	0.422 and 0.366 ($e \cdot Å^{-3}$)	0.651 and -0.428 ($e \cdot Å^{-3}$)

Table 2.6 Crystal Data and Structure Refinement for Compounds **14** and **17**

Compound	**14**	**17**
Formula	$C_{22}H_{18}Fe$	$C_{17}H_{10}O_2$
Formula wt. (amu)	338.21	246.25
T, K	90.0(2)	90.0(2)
Crystal system	Monoclinic	Monoclinic
Space group	$P2_1$	$P2_1/n$
Z	2	4
a, Å	6.1776(4)	5.7064(2)
b, Å	7.8391(4)	8.0655(2)
c, Å	15.2683(8)	24.3378(8)
α (deg)	90	90
β (deg)	91.127(2)	91.204(2)
γ (deg)	90	90
V, $Å^3$	739.25(7)	1119.90(6)
d_{calc}, Mg/m^3	1.519	1.461
F(000)	352	512
Crystal size (mm^3)	0.18 × 0.07 × 0.02	0.12 × 0.09 × 0.03
Radiation	Cu Kα(λ = 1.54178 Å)	Cu Kα(λ = 1.54178 Å)
Monochromator	Bruker Helios multilayer optics	Graded multilayer optics
Abs coefficient (mm^{-1})	8.113	0.765
Diffractometer	X8 Proteum	X8 Proteum
Range (deg)	2.89 to 67.94	3.63 to 67.79
Limiting indices	$-7 \le h \le 6$	$-6 \le h \le 5$
	$-9 \le k \le 9$	$-9 \le k \le 9$
	$-18 \le l \le 18$	$-29 \le l \le 29$
Reflections collected	6493	14409
Independent reflections	2064 [R(int) = 0.0304]	2002 [R(int) = 0.0528]
Absorption correction	Semiempirical from equivalents	Semiempirical from equivalents
Refinement method	SHELXL-97	SHELXL-97
Refinement method	Full-matrix least-squares on F^2	Full-matrix least-squares on F^2
Data/restraints/parameter	2064 / 1 / 209	2002 / 90 / 201
Goodness-of-fit on F^2	1.065	1.032
Final R indices [$I > 2\sigma(I)$]	R1 = 0.0285, wR2 = 0.0732	R1 = 0.0372, wR2 = 0.0916
R indices (all data)	R1 = 0.0290, wR2 = 0.0735	R1 = 0.0493, wR2 = 0.1000
Largest diff. peak and hole	0.378 and -0.398 ($e \cdot Å^{-3}$)	0.172 and -0.152 ($e \cdot Å^{-3}$)

Table 2.7 Crystal Data and Structure Refinement for Compounds **12** and **13**

Compound	**12**	**13**
Formula	$C_{34.42}H_{30.22}Cl_{.63}Fe_2O_2$	$C_{26}H_{16}FeO_2$
Formula wt. (amu)	609.94	416.24
T, K	90.0(2)	90.0(2)
Crystal system	Monoclinic	Monoclinic
Space group	*C*2/c	$P2_1/c$
Z	8	4
a, Å	a = 26.4857(8)	7.2923(1)
b, Å	10.3298(3)	24.7704(5)
c, Å	19.2096(7)	9.7670(2)
α (deg)	90	90
β (deg)	92.6509(12)	101.291(1)
γ (deg)	90	90
V, $Å^3$	5250.0(3)	1730.10(6)
d_{calc}, Mg/m^3	1.543	1.598
F(000)	2524	856
Crystal size (mm^3)	0.20 × 0.18 × 0.06	0.14 × 0.12 × 0.01
Radiation	Mo Kα (λ = 0.71073 Å)	Cu Kα (λ = 1.54178 Å)
Monochromator	Graphite	Graded multilayer optics
Absorption coefficient (mm^{-1})	1.202	7.157
Diffractometer	Nonius KappaCCD	Bruker X8 Proteum
Range (deg)	1.54 to 22.50	3.57 to 68.35
Limiting indices	$-28 \le h \le 28$	$-8 \le h \le 8$
	$0 \le k \le 11$	$-29 \le k \le 29$
	$0 \le l \le 20$	$-10 \le l \le 11$
Reflections collected	3418	23647
Independent reflections	3418 [R(int) = 0.082]	3124 [R(int) = 0.0543]
Absorption correction	Semiempirical from equivalents	Semiempirical from equivalents
Refinement method	SHELXL-97	SHELXL-97
Refinement method	Full-matrix least-squares on F^2	Full-matrix least-squares on F^2
Data/restraints/parameter	3418 / 49 / 359	3124 / 0 / 262
Goodness-of-fit on F^2	1.062	1.078
Final R indices [$I > 2\sigma(I)$]	R1 = 0.0689, wR2 = 0.1731	R1 = 0.0352, wR2 = 0.0896
R indices (all data)	R1 = 0.1287, wR2 = 0.2029	R1 = 0.0395, wR2 = 0.0922
Largest diff. peak and hole	0.827 and -0.428 ($e \cdot Å^{-3}$)	0.334 and -0.366 ($e \cdot Å^{-3}$)

Table 2.8 Crystal Data and Structure Refinement for Compounds **18** and **19**

Compound	**18**	**19**
Formula	$C_{20}H_{12}O_2$	$C_{21}H_{12}O_2$
Formula wt. (amu)	284.30	296.31
T, K	90.0(2)	90.0(2)
Crystal system	Monoclinic	Monoclinic
Space group	$P2_1/n$	$P2_1/c$
Z	2	2
a, Å	3.8243(2)	3.8556(1)
b, Å	8.81515(5)	9.3950(3)
c, Å	19.0191(13)	18.8745(7)
α (deg)	90	90
β (deg)	92.044(3)	98.502(2)
γ (deg)	90	90
V, $Å^3$	640.76(7)	676.18(4)
d_{calc}, Mg/m^3	1.474	1.455
F(000)	296	308
Crystal size (mm^3)	0.28 × 0.10 × 0.10	0.12 × 0.06 × 0.03
Radiation	Mo Kα (λ = 0.71073 Å)	Cu Kα (λ = 1.54178 Å)
Monochromator	Graphite	Graded multilayer optics
Absorption coefficient (mm^{-1})	0.094	0.741
Diffractometer	Nonius KappaCCD	Bruker X8 Proteum
Range (deg)	2.14 to 27.49	4.74 to 67.99
Limiting indices	$-4 \le h \le 4$	$-4 \le h \le 4$
	$-11 \le k \le 11$	$-11 \le k \le 11$
	$-24 \le l \le 24$	$-22 \le l \le 22$
Reflections collected	11154	8530
Independent reflections	1457 [R(int) = 0.0614]	1228 [R(int) = 0.0455]
Absorption correction	Semi-empirical from equivalents	Semiempirical from equivalents
Refinement method	SHELXL-97	SHELXL-97
Refinement method	Full-matrix least-squares on F^2	Full-matrix least-squares on F^2
Data/restraints/parameter	1457 / 0 / 100	1228 / 27 / 136
Goodness-of-fit on F^2	1.062	1.143
Final R indices [$I > 2\sigma(I)$]	R1 = 0.0609, wR2 = 0.1471	R1 = 0.0542, wR2 = 0.1588
R indices (all data)	R1 = 0.0835, wR2 = 0.1639	R1 = 0.0609, wR2 = 0.1673
Largest diff. peak and hole	0.298 and -0.366 ($e \cdot Å^{-3}$)	0.206 and 0.189 ($e \cdot Å^{-3}$)

Table 2.9 Crystal Data and Structure Refinement for Compounds **21** and **22**

Compound	**21**	**22**
Formula	$C_{42}H_{54}Si_2$	$C_{43}H_{54}Si_2$
Formula wt. (amu)	615.03	627.04
T, K	90.0(2)	90.0(2)
Crystal system	Monoclinic	Triclinic
Space group	$P2_1/c$	P -1
Z	2	1
a, Å	16.8663(3)	7.6325(2)
b, Å	14.8714(3)	7.6421(2)
c, Å	7.4434(2)	16.6663(5)
α (deg)	90	89.775(1)
β (deg)	95.7610(10)	77.623(1)
γ (deg)	90	80.906(1)
V, $Å^3$	1857.56(7)	937.14(4)
d_{calc}, Mg/m^3	1.100	1.111
F(000)	668	340
Crystal size (mm^3)	0.22 × 0.07 × 0.07	0.24 × 0.10 × 0.06
Radiation	Cu Kα (λ = 1.54178 Å)	Cu Kα (λ = 1.54178 Å)
Monochromator	Graded multilayer optics	Graded multilayer optics
Absorption coefficient (mm^{-1})	1.050	1.050
Diffractometer	Bruker X8 Proteum	Bruker X8 Proteum
Range (deg)	3.97 to 68.43	2.72 to 68.64
Limiting indices	$-20 \le h \le 19$	$-9 \le h \le 4$
	$-17 \le k \le 17$	$-9 \le k \le 9$
	$-8 \le l \le 8$	$-19 \le l \le 19$
Reflections collected	26238	12456
Independent reflections	3397 [R(int) = 0.0388]	3328 [R(int) = 0.0367]
Absorption correction	Semi-empirical from equivalents	Semi-empirical from equivalents
Refinement method	SHELXL-97	SHELXL-97
Refinement method	Full-matrix least-squares on F^2	Full-matrix least-squares on F^2
Data/restraints/parameter	3397 / 6 / 224	3328 / 17 / 239
Goodness-of-fit on F^2	1.048	1.045
Final R indices [$I > 2\sigma(I)$]	R1 = 0.0425, wR2 = 0.1116	R1 = 0.0443, wR2 = 0.1163
R indices (all data)	R1 = 0.0440, wR2 = 0.1132	R1 = 0.0495, wR2 = 0.1227
Largest diff. peak and hole	0.304 and -0.278 ($e \cdot Å^{-3}$)	0.375 and -0.292 ($e \cdot Å^{-3}$)

Table 2.10 Bond Distances (Å) and Bond Angles (°) for Compound **7**

Atoms	**Distances (Å)**
Fe1C4	2.030(5)
Fe1–C5	2.037(5)
Fe1–C2'	2.041(5)
Fe1–C3	2.046(5)
Fe1–C1'	2.048(5)
Fe1–C3'	2.050(5)
Fe1–C4'	2.053(5)
Fe1–C1	2.059(5)
Fe1–C2	2.060(5)
Fe1–C5'	2.068(5)
O1–C6	1.222(6)
O2–C9	1.222(6)
C1–C2	1.421(7)
C1–C5	1.434(7)
C2–C3	1.421(7)
C3–C4	1.431(7)
C4–C5	1.447(7)
C4–C9	1.455(7)
C5–C6	1.453(7)
C1'–C5'	1.417(8)
C1'–C2'	1.422(9)
C2'–C3'	1.418(8)
C3'–C4'	1.411(8)
C4'–C5'	1.409(8)
Atoms	**Angles (Å)**
C4–Fe1–C5	41.68(19)
C4–Fe1–C2'	118.9(2)
C5–Fe1–C2'	155.5(2)
C4–Fe1–C3	41.1(2)
C5–Fe1–C3	69.42(19)
C2'–Fe1–C3	105.7(2)
C4–Fe1–C1'	110.0(2)
C5–Fe1–C1'	122.3(2)
C2'–Fe1–C1'	40.7(3)
C3–Fe1–C1'	127.4(2)
C4–Fe1–C3'	151.8(2)
C5–Fe1–C3'	163.6(2)
C2'–Fe1–C3'	40.6(2)
C3–Fe1–C3'	116.3(2)
C1'–Fe1–C3'	67.8(3)
C4–Fe1–C4'	167.1(2)
C5–Fe1–C4'	128.1(2)
C2'–Fe1–C4'	67.8(2)
C3–Fe1–C4'	150.8(2)
C1'–Fe1–C4'	67.2(2)
C3'–Fe1–C4'	40.2(2)
C4–Fe1–C1	69.23(19)
C5–Fe1–C1	41.0(2)
C2'–Fe1–C1	161.4(2)
C3–Fe1–C1	68.63(19)
C1'–Fe1–C1	156.2(3)
C3'–Fe1–C1	124.6(2)
C4'–Fe1–C1	107.9(2)
C4–Fe1–C2	68.6(2)
C5–Fe1–C2	68.6(2)
C2'–Fe1–C2	124.1(2)
C3–Fe1–C2	40.5(2)
C1'–Fe1–C2	163.1(2)
C3'–Fe1–C2	105.1(2)
C4'–Fe1–C2	118.0(2)
C1–Fe1–C2	40.4(2)
C4–Fe1–C5'	129.7(2)
C5–Fe1–C5'	110.5(2)
C2'–Fe1–C5'	68.4(2)
C3–Fe1–C5'	166.3(2)
C1'–Fe1–C5'	40.3(2)
C3'–Fe1–C5'	67.9(2)
C4'–Fe1–C5'	40.0(2)
C1–Fe1–C5'	120.9(2)

Table 2.10 Continued

C2–Fe1–C5'	153.1(2)
C2–C1–C5	107.9(4)
C2–C1–Fe1	69.9(3)
C5–C1–Fe1	68.7(3)
C3–C2–C1	109.1(5)
C3–C2–Fe1	69.3(3)
C1–C2–Fe1	69.8(3)
C2–C3–C4	107.8(4)
C2–C3–Fe1	70.3(3)
C4–C3–Fe1	68.9(3)
C3–C4–C5	107.8(4)
C3–C4–C9	130.8(4)
C5–C4–C9	121.1(4)
C3–C4–Fe1	70.0(3)
C5–C4–Fe1	69.4(3)
C9–C4–Fe1	120.8(3)
C1–C5–C4	107.5(4)
C1–C5–C6	130.9(5)
C4–C5–C6	121.6(4)
C1–C5–Fe1	70.3(3)
C4–C5–Fe1	68.9(3)
C6–C5–Fe1	124.2(3)
O1–C6–C5	123.7(5)

O1–C6–C7	121.4(5)
C5–C6–C7	114.9(5)
C8–C7–C6	123.1(5)
C7–C8–C9	123.9(5)
O2–C9–C4	123.4(5)
O2–C9–C8	121.5(5)
C4–C9–C8	115.1(4)
C5'–C1'–C2'	108.9(5)
C5'–C1'–Fe1	70.6(3)
C2'–C1'–Fe1	69.4(3)
C3'–C2'–C1'	107.3(5)
C3'–C2'–Fe1	70.0(3)
C1'–C2'–Fe1	69.9(3)
C4'–C3'–C2'	107.7(5)
C4'–C3'–Fe1	70.0(3)
C2'–C3'–Fe1	69.4(3)
C5'–C4'–C3'	109.3(5)
C5'–C4'–Fe1	70.6(3)
C3'–C4'–Fe1	69.8(3)
C4'–C5'–C1'	106.8(5)
C4'–C5'–Fe1	69.4(3)
C1'–C5'–Fe1	69.1(3)

Table 2.11 Bond Distances (Å) and Bond Angles (°) for Compound **8**

Atoms	**Distance (Å)**
Fe1–C1	2.028(2)
Fe1–C5	2.036(2)
Fe1–C2'	2.043(2)
Fe1–C3'	2.044(2)
Fe1–C2	2.052(2)
Fe1–C3	2.052(2)
Fe1–C4'	2.053(2)
Fe1–C4	2.056(2)
Fe1–C5'	2.060(2)
Fe1–C1'	2.061(2)
O1–C6	1.223(3)
O2–C9	1.224(3)
C1–C2	1.425(3)
C1–C5	1.442(3)
C1–C9	1.465(3)
C2–C3	1.426(3)
C3–C4	1.429(3)
C4–C5	1.428(3)
C5–C6	1.464(3)
C6–C7	1.518(3)
C7–C8	1.533(3)
C8–C9	1.520(3)
C1'–C2'	1.423(3)
C1'–C5'	1.424(3)
C2'–C3'	1.419(3)
C3'–C4'	1.426(3)
C4'–C5'	1.419(3)
Atoms	**Angle (°)**
C1–Fe1–C5	41.56(8)
C1–Fe1–C2'	120.04(9)
C5–Fe1–C2'	157.41(9)
C1–Fe1–C3'	152.44(8)
C5–Fe1–C3'	161.81(8)
C2'–Fe1–C3'	40.63(8)
C1–Fe1–C2	40.88(8)
C5–Fe1–C2	69.11(8)
C2'–Fe1–C2	105.32(8)
C3'–Fe1–C2	116.06(9)
C1–Fe1–C3	68.71(8)
C5–Fe1–C3	68.61(8)
C2'–Fe1–C3	122.22(9)
C3'–Fe1–C3	103.31(8)
C2–Fe1–C3	40.67(8)
C1–Fe1–C4'	166.44(8)
C5–Fe1–C4'	127.17(8)
C2'–Fe1–C4'	68.31(9)
C3'–Fe1–C4'	40.72(8)
C2–Fe1–C4'	151.14(9)
C3–Fe1–C4'	117.31(9)
C1–Fe1–C4	69.27(8)
C5–Fe1–C4	40.84(8)
C2'–Fe1–C4	159.38(9)
C3'–Fe1–C4	122.67(8)
C2–Fe1–C4	68.83(8)
C3–Fe1–C4	40.71(8)
C4'–Fe1–C4	106.75(8)
C1–Fe1–C5'	129.89(9)
C5–Fe1–C5'	111.63(8)
C2'–Fe1–C5'	68.05(9)
C3'–Fe1–C5'	68.14(9)
C2–Fe1–C5'	165.27(9)
C3–Fe1–C5'	154.03(9)
C4'–Fe1–C5'	40.37(9)
C4–Fe1–C5'	122.01(9)
C1–Fe1–C1'	110.38(9)
C5–Fe1–C1'	124.20(9)
C2'–Fe1–C1'	40.56(9)
C3'–Fe1–C1'	68.31(9)
C2–Fe1–C1'	126.17(9)
C3–Fe1–C1'	160.99(9)
C4'–Fe1–C1'	68.18(9)
C4–Fe1–C1'	158.09(9)
C5'–Fe1–C1'	40.44(9)

Table 2.11 Continued

C2–C1–C5	107.94(17)
C2–C1–C9	129.24(18)
C5–C1–C9	122.48(18)
C2–C1–Fe1	70.43(12)
C5–C1–Fe1	69.50(11)
C9–C1–Fe1	120.34(14)
C1–C2–C3	107.75(17)
C1–C2–Fe1	68.69(11)
C3–C2–Fe1	69.67(11)
C2–C3–C4	108.82(18)
C2–C3–Fe1	69.66(11)
C4–C3–Fe1	69.81(11)
C5–C4–C3	107.51(18)
C5–C4–Fe1	68.83(11)
C3–C4–Fe1	69.49(11)
C4–C5–C1	107.97(17)
C4–C5–C6	129.77(19)
C1–C5–C6	122.26(18)
C4–C5–Fe1	70.33(12)
C1–C5–Fe1	68.94(11)
C6–C5–Fe1	126.80(14)
O1–C6–C5	122.7(2)

O1–C6–C7	121.06(19)
C5–C6–C7	116.00(18)
C6–C7–C8	116.50(18)
C9–C8–C7	114.84(17)
O2–C9–C1	122.61(19)
O2–C9–C8	122.01(19)
C1–C9–C8	115.30(17)
C2'–C1'–C5'	107.51(19)
C2'–C1'–Fe1	69.04(12)
C5'–C1'–Fe1	69.76(12)
C3'–C2'–C1'	108.41(19)
C3'–C2'–Fe1	69.73(12)
C1'–C2'–Fe1	70.40(12)
C2'–C3'–C4'	107.89(19)
C2'–C3'–Fe1	69.64(12)
C4'–C3'–Fe1	69.98(12)
C5'–C4'–C3'	107.83(19)
C5'–C4'–Fe1	70.08(12)
C3'–C4'–Fe1	69.29(12)
C4'–C5'–C1'	108.36(19)
C4'–C5'–Fe1	69.55(12)
C1'–C5'–Fe1	69.80(12)

Table 2.12 Bond Distances (Å) and Bond Angles (°) for Compound **10**

Atoms	**Distance (Å)**
Fe1–C5	2.018(2)
Fe1–C1	2.018(2)
Fe1–C4	2.039(3)
Fe1–C2'	2.040(3)
Fe1–C3'	2.044(3)
Fe1–C1'	2.045(3)
Fe1–C4'	2.045(3)
Fe1–C5'	2.052(3)
Fe1–C2	2.055(3)
Fe1–C3	2.063(3)
Fe2–C13'	2.045(3)
Fe2–C12'	2.046(3)
Fe2–C11'	2.048(3)
Fe2–C10'	2.051(3)
Fe2–C11	2.052(3)
Fe2–C10	2.052(3)
Fe2–C9'	2.053(3)
Fe2–C12	2.055(2)
Fe2–C13	2.076(3)
Fe2–C9	2.079(3)
O1–C6	1.228(3)
O2–C16	1.233(3)
C1–C2	1.431(4)
C1–C5	1.438(4)
C1–C16	1.464(4)
C2–C3	1.413(4)
C3–C4	1.416(4)
C4–C5	1.423(4)
C5–C6	1.472(4)
C6–C7	1.485(4)
C7–C8	1.370(4)
C7–C15	1.456(3)
C8–C9	1.420(4)
C9–C10	1.433(4)
C9–C13	1.444(4)
C10–C11	1.424(4)
C11–C12	1.422(4)
C12–C13	1.430(4)
C13–C14	1.423(4)
C14–C15	1.373(4)
C15–C16	1.478(4)
C1'–C5'	1.410(4)
C1'–C2'	1.411(4)
C1'–H1'	0.94(3)
C2'–C3'	1.417(4)
C2'–H2'	0.91(3)
C3'–C4'	1.417(4)
C3'–H3'	0.98(3)
C4'–C5'	1.423(4)
C4'–H4'	0.89(3)
C5'–H5'	0.93(3)
C9'–C10'	1.411(4)
C9'–C13'	1.432(4)
C9'–H9'	0.98(3)
C10'–C11'	1.403(4)
C10'–H10'	0.94(3)
C11'–C12'	1.410(4)
C11'–H11'	0.95(3)
C12'–C13'	1.406(4)
C12'–H12'	0.84(3)
C13'–H13'	0.88(3)
Atoms	**Angle (°)**
C5–Fe1–C1	41.73(10)
C5–Fe1–C4	41.07(10)
C1–Fe1–C4	69.41(10)
C5–Fe1–C2'	157.72(11)
C1–Fe1–C2'	121.50(12)
C4–Fe1–C2'	160.12(11)
C5–Fe1–C3'	160.21(12)
C1–Fe1–C3'	156.35(12)
C4–Fe1–C3'	123.09(12)
C2'–Fe1–C3'	40.60(12)

Table 2.12 Continued

C5–Fe1–C1'	122.25(11)
C1–Fe1–C1'	108.46(11)
C4–Fe1–C1'	157.32(11)
C2'–Fe1–C1'	40.42(11)
C3'–Fe1–C1'	68.09(12)
C5–Fe1–C4'	123.82(11)
C1–Fe1–C4'	161.94(11)
C4–Fe1–C4'	106.53(11)
C2'–Fe1–C4'	68.24(12)
C3'–Fe1–C4'	40.56(12)
C1'–Fe1–C4'	68.12(12)
C5–Fe1–C5'	107.87(11)
C1–Fe1–C5'	125.38(11)
C4–Fe1–C5'	121.42(11)
C2'–Fe1–C5'	67.95(12)
C3'–Fe1–C5'	68.12(12)
C1'–Fe1–C5'	40.26(11)
C4'–Fe1–C5'	40.64(11)
C5–Fe1–C2	69.23(10)
C1–Fe1–C2	41.13(10)
C4–Fe1–C2	68.39(11)
C2'–Fe1–C2	107.85(11)
C3'–Fe1–C2	120.49(11)
C1'–Fe1–C2	125.74(12)
C4'–Fe1–C2	155.26(11)
C5'–Fe1–C2	162.62(11)
C5–Fe1–C3	68.53(11)
C1–Fe1–C3	68.57(10)
C4–Fe1–C3	40.39(10)
C2'–Fe1–C3	124.33(12)
C3'–Fe1–C3	106.87(11)
C1'–Fe1–C3	161.52(12)
C4'–Fe1–C3	120.44(11)
C5'–Fe1–C3	156.22(12)

C2–Fe1–C3	40.14(10)
C13'–Fe2–C12'	40.20(12)
C13'–Fe2–C11'	67.74(12)
C12'–Fe2–C11'	40.28(12)
C13'–Fe2–C10'	68.08(11)
C12'–Fe2–C10'	67.69(12)
C11'–Fe2–C10'	40.04(11)
C13'–Fe2–C11	162.13(12)
C12'–Fe2–C11	125.68(12)
C11'–Fe2–C11	108.44(12)
C10'–Fe2–C11	121.08(11)
C13'–Fe2–C10	155.53(11)
C12'–Fe2–C10	163.29(12)
C11'–Fe2–C10	126.80(12)
C10'–Fe2–C10	109.12(11)
C11–Fe2–C10	40.61(10)
C13'–Fe2–C9'	40.92(11)
C12'–Fe2–C9'	67.95(12)
C11'–Fe2–C9'	67.57(12)
C10'–Fe2–C9'	40.22(11)
C11–Fe2–C9'	155.55(11)
C10–Fe2–C9'	121.03(11)
C13'–Fe2–C12	124.61(11)
C12'–Fe2–C12	106.22(11)
C11'–Fe2–C12	118.93(11)
C10'–Fe2–C12	153.95(11)
C11–Fe2–C12	40.52(10)
C10–Fe2–C12	69.03(11)
C9'–Fe2–C12	163.18(11)
C13'–Fe2–C13	107.64(11)
C12'–Fe2–C13	119.10(11)
C11'–Fe2–C13	153.36(11)
C10'–Fe2–C13	164.89(11)
C11–Fe2–C13	67.44(10)

Table 2.12 Continued

C10–Fe2–C13	68.37(10)
C9'–Fe2–C13	127.21(11)
C12–Fe2–C13	40.49(10)
C13'–Fe2–C9	120.60(11)
C12'–Fe2–C9	154.21(12)
C11'–Fe2–C9	164.51(12)
C10'–Fe2–C9	127.85(11)
C11–Fe2–C9	67.73(10)
C10–Fe2–C9	40.59(10)
C9'–Fe2–C9	109.27(11)
C12–Fe2–C9	68.67(10)
C13–Fe2–C9	40.67(10)
C2–C1–C5	107.5(2)
C2–C1–C16	129.0(2)
C5–C1–C16	122.8(2)
C2–C1–Fe1	70.81(14)
C5–C1–Fe1	69.11(14)
C16–C1–Fe1	118.16(18)
C3–C2–C1	107.9(2)
C3–C2–Fe1	70.23(15)
C1–C2–Fe1	68.06(14)
C2–C3–C4	108.9(2)
C2–C3–Fe1	69.63(15)
C4–C3–Fe1	68.91(15)
C3–C4–C5	108.0(2)
C3–C4–Fe1	70.70(15)
C5–C4–Fe1	68.66(14)
C4–C5–C1	107.7(2)
C4–C5–C6	129.5(2)
C1–C5–C6	122.3(2)
C4–C5–Fe1	70.28(14)
C1–C5–Fe1	69.15(14)
C6–C5–Fe1	119.83(17)
O1–C6–C5	122.1(2)

O1–C6–C7	122.2(2)
C5–C6–C7	115.7(2)
C8–C7–C15	120.5(2)
C8–C7–C6	118.3(2)
C15–C7–C6	121.3(2)
C7–C8–C9	120.3(2)
C8–C9–C10	132.9(2)
C8–C9–C13	119.5(2)
C10–C9–C13	107.5(2)
C8–C9–Fe2	124.04(18)
C10–C9–Fe2	68.71(14)
C13–C9–Fe2	69.57(14)
C11–C10–C9	107.4(2)
C11–C10–Fe2	69.68(15)
C9–C10–Fe2	70.71(14)
C12–C11–C10	109.7(2)
C12–C11–Fe2	69.86(14)
C10–C11–Fe2	69.71(14)
C11–C12–C13	106.9(2)
C11–C12–Fe2	69.61(14)
C13–C12–Fe2	70.56(14)
C14–C13–C12	132.2(2)
C14–C13–C9	119.2(2)
C12–C13–C9	108.5(2)
C14–C13–Fe2	124.14(17)
C12–C13–Fe2	68.95(14)
C9–C13–Fe2	69.75(14)
C15–C14–C13	120.4(2)
C14–C15–C7	120.1(2)
C14–C15–C16	117.6(2)
C7–C15–C16	122.3(2)
O2–C16–C1	122.4(2)
O2–C16–C15	122.2(2)
C1–C16–C15	115.5(2)

Table 2.12 Continued

C5'–C1'–C2'	108.3(3)
C5'–C1'–Fe1	70.16(16)
C2'–C1'–Fe1	69.62(16)
C5'–C1'–H1'	125.7(18)
C2'–C1'–H1'	125.9(18)
Fe1–C1'–H1'	123.9(18)
C1'–C2'–C3'	108.1(3)
C1'–C2'–Fe1	69.96(16)
C3'–C2'–Fe1	69.83(16)
C1'–C2'–H2'	128.0(19)
C3'–C2'–H2'	123.9(19)
Fe1–C2'–H2'	127.2(19)
C2'–C3'–C4'	107.9(3)
C2'–C3'–Fe1	69.57(16)
C4'–C3'–Fe1	69.78(16)
C2'–C3'–H3'	122.3(18)
C4'–C3'–H3'	129.6(17)
Fe1–C3'–H3'	130.2(18)
C3'–C4'–C5'	107.8(3)
C3'–C4'–Fe1	69.66(16)
C5'–C4'–Fe1	69.95(16)
C3'–C4'–H4'	127.7(19)
C5'–C4'–H4'	124(2)
Fe1–C4'–H4'	125.0(19)
C1'–C5'–C4'	107.9(3)
C1'–C5'–Fe1	69.58(16)
C4'–C5'–Fe1	69.41(16)
C1'–C5'–H5'	126.7(18)
C4'–C5'–H5'	125.3(18)
Fe1–C5'–H5'	125.6(18)

C10'–C9'–C13'	107.5(3)
C10'–C9'–Fe2	69.82(15)
C13'–C9'–Fe2	69.24(15)
C10'–C9'–H9'	128.2(17)
C13'–C9'–H9'	124.2(17)
Fe2–C9'–H9'	124.6(17)
C11'–C10'–C9'	108.2(3)
C11'–C10'–Fe2	69.85(16)
C9'–C10'–Fe2	69.96(15)
C11'–C10'–H10'	126.2(18)
C9'–C10'–H10'	125.5(18)
Fe2–C10'–H10'	126.0(18)
C10'–C11'–C12'	108.4(3)
C10'–C11'–Fe2	70.11(16)
C12'–C11'–Fe2	69.79(16)
C10'–C11'–H11'	125.3(18)
C12'–C11'–H11'	126.1(18)
Fe2–C11'–H11'	122.6(18)
C13'–C12'–C11'	108.2(3)
C13'–C12'–Fe2	69.85(16)
C11'–C12'–Fe2	69.92(16)
C13'–C12'–H12'	126(2)
C11'–C12'–H12'	126(2)
Fe2–C12'–H12'	123(2)
C12'–C13'–C9'	107.6(3)
C12'–C13'–Fe2	69.95(16)
C9'–C13'–Fe2	69.85(15)
C12'–C13'–H13'	125(2)
C9'–C13'–H13'	127(2)
Fe2–C13'–H13'	125(2)

Table 2.13 Bond Distances (Å) and Bond Angles (°) for Compound **11**

Atoms	**Distance (Å)**
Fe1–C19	2.032(2)
Fe1–C6	2.046(2)
Fe1–C20	2.047(2)
Fe1–C5	2.047(2)
Fe1–C18	2.057(2)
Fe1–C7	2.057(2)
Fe1–C22	2.064(2)
Fe1–C21	2.064(2)
Fe1–C8	2.092(2)
Fe1–C4	2.094(2)
O1–C1	1.227(3)
O2–C11	1.229(3)
C1–C2	1.478(3)
C1–C17	1.488(3)
C2–C3	1.368(3)
C2–C10	1.452(3)
C3–C4	1.415(3)
C4–C5	1.428(4)
C4–C8	1.462(3)
C5–C6	1.420(4)
C6–C7	1.424(4)
C7–C8	1.429(4)
C8–C9	1.416(4)
C9–C10	1.363(4)
C10–C11	1.482(3)
C11–C12	1.487(4)
C12–C13	1.394(3)
C12–C17	1.407(3)
C13–C14	1.380(4)
C14–C15	1.394(4)
C15–C16	1.377(3)
C16–C17	1.398(3)
C18–C22	1.425(4)
C18–C19	1.431(4)
C19–C20	1.425(4)
C20–C21	1.414(4)
C21–C22	1.423(3)

Atoms	**Angle (°)**
C19–Fe1–C6	102.40(11)
C19–Fe1–C20	40.89(10)
C6–Fe1–C20	117.38(11)
C19–Fe1–C5	117.54(10)
C6–Fe1–C5	40.59(10)
C20–Fe1–C5	152.62(11)
C19–Fe1–C18	40.95(10)
C6–Fe1–C18	121.00(11)
C20–Fe1–C18	68.63(10)
C5–Fe1–C18	106.24(11)
C19–Fe1–C7	119.69(11)
C6–Fe1–C7	40.60(10)
C20–Fe1–C7	104.88(10)
C5–Fe1–C7	68.75(10)
C18–Fe1–C7	156.78(11)
C19–Fe1–C22	68.29(11)
C6–Fe1–C22	159.79(10)
C20–Fe1–C22	68.01(11)
C5–Fe1–C22	126.42(10)
C18–Fe1–C22	40.46(10)
C7–Fe1–C22	159.60(11)
C19–Fe1–C21	68.18(11)
C6–Fe1–C21	154.54(11)
C20–Fe1–C21	40.24(10)
C5–Fe1–C21	164.78(10)
C18–Fe1–C21	68.14(10)
C7–Fe1–C21	122.10(10)
C22–Fe1–C21	40.34(10)
C19–Fe1–C8	158.07(10)
C6–Fe1–C8	67.72(10)
C20–Fe1–C8	124.70(10)
C5–Fe1–C8	68.46(10)
C18–Fe1–C8	160.88(11)
C7–Fe1–C8	40.28(10)
C22–Fe1–C8	127.05(11)
C21–Fe1–C8	111.94(10)

Table 2.13 Continued

C19–Fe1–C4	155.24(10)
C6–Fe1–C4	67.65(10)
C20–Fe1–C4	163.86(10)
C5–Fe1–C4	40.33(10)
C18–Fe1–C4	123.38(10)
C7–Fe1–C4	68.32(10)
C22–Fe1–C4	113.02(10)
C21–Fe1–C4	129.99(10)
C8–Fe1–C4	40.88(9)
O1–C1–C2	121.7(2)
O1–C1–C17	120.6(2)
C2–C1–C17	117.8(2)
C3–C2–C10	120.5(2)
C3–C2–C1	118.9(2)
C10–C2–C1	120.6(2)
C2–C3–C4	120.2(2)
C3–C4–C5	133.6(2)
C3–C4–C8	119.1(2)
C5–C4–C8	107.4(2)
C3–C4–Fe1	127.17(17)
C5–C4–Fe1	68.07(13)
C8–C4–Fe1	69.49(13)
C6–C5–C4	108.1(2)
C6–C5–Fe1	69.65(14)
C4–C5–Fe1	71.60(13)
C5–C6–C7	109.2(2)
C5–C6–Fe1	69.76(14)
C7–C6–Fe1	70.12(14)
C6–C7–C8	107.9(2)
C6–C7–Fe1	69.28(14)
C8–C7–Fe1	71.18(13)
C9–C8–C7	133.2(2)
C9–C8–C4	119.3(2)
C7–C8–C4	107.5(2)
C9–C8–Fe1	128.68(17)
C7–C8–Fe1	68.53(13)
C4–C8–Fe1	69.63(13)
O2–C11–C10	121.6(2)
O2–C11–C12	120.3(2)
C10–C11–C12	118.1(2)
C13–C12–C17	119.2(2)
C13–C12–C11	119.7(2)
C17–C12–C11	121.1(2)
C14–C13–C12	120.9(2)
C13–C14–C15	119.8(2)
C16–C15–C14	120.1(2)
C15–C16–C17	120.6(2)
C16–C17–C12	119.3(2)
C16–C17–C1	119.2(2)
C12–C17–C1	121.6(2)
C22–C18–C19	107.3(2)
C22–C18–Fe1	70.04(14)
C19–C18–Fe1	68.62(13)
C20–C19–C18	108.2(2)
C20–C19–Fe1	70.10(13)
C18–C19–Fe1	70.43(14)
C21–C20–C19	108.0(2)
C21–C20–Fe1	70.51(14)
C19–C20–Fe1	69.01(14)
C20–C21–C22	108.3(2)
C20–C21–Fe1	69.25(14)
C22–C21–Fe1	69.83(14)
C21–C22–C18	108.3(2)
C21–C22–Fe1	69.82(14)
C18–C22–Fe1	69.51(14)

Table 2.14 Bond Distances (Å) and Bond Angles (°) for Compound **12**

Atoms	**Distances (Å)**
Fe1–C25	2.007(9)
Fe1–C24	2.032(9)
Fe1–C23	2.032(8)
Fe1–C21	2.037(8)
Fe1–C5	2.038(7)
Fe1–C6	2.041(7)
Fe1–C7	2.042(7)
Fe1–C22	2.054(7)
Fe1–C8	2.062(7)
Fe1–C4	2.078(8)
Fe2–C27	2.031(8)
Fe2–C28	2.033(7)
Fe2–C17	2.047(7)
Fe2–C30	2.048(9)
Fe2–C15	2.053(7)
Fe2–C29	2.054(8)
Fe2–C26	2.058(8)
Fe2–C16	2.062(7)
Fe2–C14	2.069(7)
Fe2–C18	2.075(7)
O1–C1	1.219(7)
O2–C11	1.226(7)
C1–C20	1.478(10)
C1–C2	1.487(10)
C2–C3	1.355(9)
C2–C10	1.471(9)
C3–C4	1.402(10)
C4–C5	1.431(10)
C4–C8	1.462(10)
C5–C6	1.405(10)
C6–C7	1.435(10)
C7–C8	1.406(11)
C14–C18	1.452(9)
C15–C16	1.410(10)
C16–C17	1.423(10)
C17–C18	1.421(10)
C18–C19	1.416(10)
C19–C20	1.361(9)
C21–C25	1.374(13)
C21–C22	1.433(11)
C22–C23	1.387(11)
C23–C24	1.379(14)
C24–C25	1.413(15)
C26–C30	1.410(14)
C26–C27	1.419(11)
C27–C28	1.410(10)
C28–C29	1.409(10)
C29–C30	1.411(11)
Atoms	**Angles (˚)**
C25–Fe1–C24	40.9(4)
C25–Fe1–C23	67.0(4)
C24–Fe1–C23	39.7(4)
C25–Fe1–C21	39.7(4)
C24–Fe1–C21	68.0(4)
C23–Fe1–C21	67.3(3)
C25–Fe1–C5	125.5(5)
C24–Fe1–C5	163.2(6)
C23–Fe1–C5	155.4(4)
C21–Fe1–C5	107.6(3)
C25–Fe1–C6	161.3(6)
C24–Fe1–C6	155.6(6)
C23–Fe1–C6	121.2(4)
C21–Fe1–C6	124.7(4)
C5–Fe1–C6	40.3(3)
C25–Fe1–C7	156.7(5)
C24–Fe1–C7	120.6(5)
C23–Fe1–C7	108.1(3)
C21–Fe1–C7	161.8(4)
C5–Fe1–C7	68.7(3)
C6–Fe1–C7	41.1(3)
C25–Fe1–C22	67.7(4)
C24–Fe1–C22	67.7(4)
C23–Fe1–C22	39.7(3)

Table 2.14 Continued

C23–Fe1–C22	39.7(3)
C21–Fe1–C22	41.0(3)
C5–Fe1–C22	120.5(3)
C6–Fe1–C22	107.0(3)
C7–Fe1–C22	124.2(3)
C25–Fe1–C8	122.7(4)
C24–Fe1–C8	108.7(4)
C23–Fe1–C8	125.7(3)
C21–Fe1–C8	156.9(4)
C5–Fe1–C8	68.5(3)
C6–Fe1–C8	68.0(3)
C7–Fe1–C8	40.0(3)
C22–Fe1–C8	160.9(3)
C25–Fe1–C4	108.7(4)
C24–Fe1–C4	126.3(5)
C23–Fe1–C4	163.0(4)
C21–Fe1–C4	120.8(3)
C5–Fe1–C4	40.7(3)
C6–Fe1–C4	68.3(3)
C7–Fe1–C4	68.8(3)
C22–Fe1–C4	155.9(3)
C8–Fe1–C4	41.4(3)
C27–Fe2–C28	40.6(3)
C27–Fe2–C17	148.4(3)
C28–Fe2–C17	170.3(3)
C27–Fe2–C30	67.7(4)
C28–Fe2–C30	67.6(3)
C17–Fe2–C30	110.3(3)
C27–Fe2–C15	129.5(3)
C28–Fe2–C15	108.0(3)
C17–Fe2–C15	68.8(3)
C30–Fe2–C15	149.8(4)
C27–Fe2–C29	68.1(3)
C28–Fe2–C29	40.3(3)
C17–Fe2–C29	132.1(3)
C30–Fe2–C29	40.2(3)
C15–Fe2–C29	116.7(3)
C27–Fe2–C26	40.6(3)
C28–Fe2–C26	68.1(3)
C17–Fe2–C26	116.8(3)
C30–Fe2–C26	40.2(4)
C15–Fe2–C26	168.5(4)
C29–Fe2–C26	68.0(4)
C27–Fe2–C16	168.7(3)
C28–Fe2–C16	131.4(3)
C17–Fe2–C16	40.5(3)
C30–Fe2–C16	119.2(4)
C15–Fe2–C16	40.1(3)
C29–Fe2–C16	110.8(3)
C26–Fe2–C16	150.3(4)
C27–Fe2–C14	107.6(3)
C28–Fe2–C14	115.5(3)
C17–Fe2–C14	68.4(3)
C30–Fe2–C14	169.4(4)
C15–Fe2–C14	40.5(3)
C29–Fe2–C14	148.2(3)
C26–Fe2–C14	130.2(4)
C16–Fe2–C14	67.1(3)
C27–Fe2–C18	115.7(3)
C28–Fe2–C18	148.1(3)
C17–Fe2–C18	40.3(3)
C30–Fe2–C18	131.3(3)
C15–Fe2–C18	68.7(3)
C29–Fe2–C18	170.1(3)
C26–Fe2–C18	108.4(3)
C16–Fe2–C18	67.4(3)
C14–Fe2–C18	41.0(3)
O1–C1–C20	122.2(7)
O1–C1–C2	120.3(7)
C20–C1–C2	117.5(6)

Table 2.14 Continued

C2–C3–C4	121.4(7)
C3–C4–C5	133.8(7)
C3–C4–C8	120.3(7)
C5–C4–C8	105.9(7)
C3–C4–Fe1	124.9(5)
C5–C4–Fe1	68.1(4)
C8–C4–Fe1	68.7(4)
C6–C5–C4	109.2(7)
C6–C5–Fe1	70.0(4)
C4–C5–Fe1	71.2(4)
C5–C6–C7	108.4(8)
C5–C6–Fe1	69.7(4)
C7–C6–Fe1	69.5(4)
C8–C7–C6	107.9(7)
C8–C7–Fe1	70.7(4)
C6–C7–Fe1	69.4(4)
C7–C8–C9	133.9(7)
C7–C8–C4	108.6(7)
C9–C8–C4	117.3(8)
C7–C8–Fe1	69.2(4)
C9–C8–Fe1	123.4(5)
C4–C8–Fe1	69.9(4)
C10–C9–C8	121.5(7)
C9–C10–C2	120.3(7)
C9–C10–C11	119.8(7)
C2–C10–C11	119.9(7)
O2–C11–C12	120.9(7)
O2–C11–C10	120.4(7)
C12–C11–C10	118.6(6)
C13–C12–C20	118.9(7)
C13–C12–C11	119.5(6)
C20–C12–C11	121.6(7)
C12–C13–C14	121.8(7)
C13–C14–C15	133.5(7)
C13–C14–C18	118.5(8)
C15–C14–C18	108.1(7)
C13–C14–Fe2	125.1(5)
C15–C14–Fe2	69.2(4)
C18–C14–Fe2	69.7(4)
C16–C15–C14	107.3(7)
C16–C15–Fe2	70.3(4)
C14–C15–Fe2	70.4(4)
C15–C16–C17	109.6(7)
C15–C16–Fe2	69.6(4)
C17–C16–Fe2	69.1(4)
C18–C17–C16	107.7(7)
C18–C17–Fe2	70.9(4)
C16–C17–Fe2	70.3(4)
C19–C18–C17	133.8(7)
C19–C18–C14	118.9(8)
C17–C18–C14	107.2(7)
C19–C18–Fe2	124.2(5)
C17–C18–Fe2	68.8(4)
C14–C18–Fe2	69.3(4)
C25–C21–C22	107.5(9)
C25–C21–Fe1	69.0(5)
C22–C21–Fe1	70.1(4)
C23–C22–C21	106.1(9)
C23–C22–Fe1	69.3(5)
C21–C22–Fe1	68.9(4)
C24–C23–C22	110.8(9)
C24–C23–Fe1	70.2(5)
C22–C23–Fe1	71.0(4)
C23–C24–C25	106.1(10)
C23–C24–Fe1	70.2(6)
C25–C24–Fe1	68.6(6)
C21–C25–C24	109.5(11)
C21–C25–Fe1	71.3(5)
C24–C25–Fe1	70.5(6)
C30–C26–C27	107.0(8)

Table 2.14 Continued

C30–C26–Fe2	69.5(5)
C27–C26–Fe2	68.7(4)
C28–C27–C26	108.2(8)
C28–C27–Fe2	69.7(4)
C26–C27–Fe2	70.7(5)
C29–C28–C27	108.4(7)
C29–C28–Fe2	70.7(4)
C27–C28–Fe2	69.6(4)

C28–C29–C30	107.3(8)
C28–C29–Fe2	69.0(4)
C30–C29–Fe2	69.6(5)
C26–C30–C29	109.1(8)
C26–C30–Fe2	70.3(5)
C29–C30–Fe2	70.1(4)

Table 2.15 Bond Distances (Å) and Bond Angles (°) for Compound **13**

Atoms	**Distances (Å)**
Fe1–C3'	2.042(2)
Fe1–C2'	2.047(2)
Fe1–C2	2.054(2)
Fe1–C1'	2.054(2)
Fe1–C3	2.054(2)
Fe1–C4'	2.058(2)
Fe1–C4	2.058(2)
Fe1–C5'	2.061(2)
Fe1–C1	2.090(2)
Fe1–C5	2.094(2)
O1–C8	1.226(3)
O2–C19	1.225(3)
C1–C21	1.417(3)
C1–C2	1.440(3)
C1–C5	1.453(3)
C2–C3	1.423(3)
C3–C4	1.423(3)
C4–C5	1.431(3)
C5–C6	1.414(3)
C6–C7	1.371(3)
C7–C20	1.445(3)
C7–C8	1.481(3)
C8–C9	1.486(3)
C9–C10	1.372(3)
C9–C18	1.427(3)
C10–C11	1.412(3)
C11–C12	1.418(3)
C11–C16	1.430(3)
C12–C13	1.365(3)
C13–C14	1.407(3)
C14–C15	1.363(3)
C15–C16	1.419(3)
C16–C17	1.408(3)
C17–C18	1.374(3)
C18–C19	1.489(3)
C19–C20	1.480(3)
C20–C21	1.368(3)
C1'–C2'	1.421(3)
C1'–C5'	1.427(3)
C2'–C3'	1.428(3)
C3'–C4'	1.420(3)
C4'–C5'	1.426(3)
Atoms	**Angles (˚)**
C3'–Fe1–C2'	40.87(9)
C3'–Fe1–C2	119.61(9)
C2'–Fe1–C2	105.36(9)
C3'–Fe1–C1'	68.24(10)
C2'–Fe1–C1'	40.56(9)
C2–Fe1–C1'	123.26(9)
C3'–Fe1–C3	104.71(9)
C2'–Fe1–C3	120.57(9)
C2–Fe1–C3	40.55(9)
C1'–Fe1–C3	157.91(10)
C3'–Fe1–C4'	40.53(9)
C2'–Fe1–C4'	68.44(9)
C2–Fe1–C4'	155.85(9)
C1'–Fe1–C4'	68.07(9)
C3–Fe1–C4'	121.00(9)
C3'–Fe1–C4	120.76(9)
C2'–Fe1–C4	156.53(9)
C2–Fe1–C4	68.83(9)
C1'–Fe1–C4	161.12(9)
C3–Fe1–C4	40.48(9)
C4'–Fe1–C4	107.07(9)
C3'–Fe1–C5'	68.33(9)
C2'–Fe1–C5'	68.50(9)
C2–Fe1–C5'	160.94(9)
C1'–Fe1–C5'	40.58(9)

Table 2.15 Continued

C3–Fe1–C5'	158.21(10)
C4'–Fe1–C5'	40.50(9)
C4–Fe1–C5'	123.98(10)
C3'–Fe1–C1	157.09(9)
C2'–Fe1–C1	122.84(9)
C2–Fe1–C1	40.65(8)
C1'–Fe1–C1	110.22(9)
C3–Fe1–C1	67.71(9)
C4'–Fe1–C1	161.90(9)
C4–Fe1–C1	68.39(9)
C5'–Fe1–C1	126.42(9)
C3'–Fe1–C5	158.39(9)
C2'–Fe1–C5	160.55(9)
C2–Fe1–C5	68.40(9)
C1'–Fe1–C5	126.36(9)
C3–Fe1–C5	67.45(9)
C4'–Fe1–C5	124.77(9)
C4–Fe1–C5	40.31(9)
C5'–Fe1–C5	111.07(9)
C1–Fe1–C5	40.63(8)
C21–C1–C2	133.5(2)
C21–C1–C5	119.0(2)
C2–C1–C5	107.45(19)
C21–C1–Fe1	127.76(16)
C2–C1–Fe1	68.32(12)
C5–C1–Fe1	69.85(12)
C3–C2–C1	107.48(19)
C3–C2–Fe1	69.75(13)
C1–C2–Fe1	71.02(13)
C4–C3–C2	109.48(19)
C4–C3–Fe1	69.91(13)
C2–C3–Fe1	69.71(12)
C3–C4–C5	107.62(19)
C3–C4–Fe1	69.60(12)
C5–C4–Fe1	71.19(12)

C6–C5–C4	132.5(2)
C6–C5–C1	119.7(2)
C4–C5–C1	107.89(19)
C6–C5–Fe1	127.32(16)
C4–C5–Fe1	68.50(12)
C1–C5–Fe1	69.52(12)
C7–C6–C5	120.0(2)
C6–C7–C20	120.3(2)
C6–C7–C8	118.81(19)
C20–C7–C8	120.83(19)
O1–C8–C7	121.6(2)
O1–C8–C9	120.6(2)
C7–C8–C9	117.81(19)
C10–C9–C18	119.7(2)
C10–C9–C8	119.1(2)
C18–C9–C8	121.21(19)
O2–C19–C20	121.7(2)
O2–C19–C18	120.6(2)
C20–C19–C18	117.63(19)
C21–C20–C7	120.9(2)
C21–C20–C19	117.93(19)
C7–C20–C19	121.13(19)
C20–C21–C1	120.1(2)
C2'–C1'–C5'	108.5(2)
C2'–C1'–Fe1	69.45(13)
C5'–C1'–Fe1	69.98(13)
C1'–C2'–C3'	107.5(2)
C1'–C2'–Fe1	69.99(13)
C3'–C2'–Fe1	69.39(13)
C4'–C3'–C2'	108.3(2)
C4'–C3'–Fe1	70.34(13)
C2'–C3'–Fe1	69.74(13)
C3'–C4'–C5'	108.1(2)
C3'–C4'–Fe1	69.12(13)
C5'–C4'–Fe1	69.86(13)

Table 2.16 Bond Distances (Å) and Bond Angles (°) for Compound **14**

Atoms	**Distance (Å)**
Fe1–C2	2.032(3)
Fe1–C1	2.039(3)
Fe1–C8	2.040(3)
Fe1–C3	2.041(2)
Fe1–C9	2.042(2)
Fe1–C5	2.043(3)
Fe1–C4	2.047(3)
Fe1–C7	2.053(3)
Fe1–C10	2.087(2)
Fe1–C6	2.097(2)
C1–C5	1.410(4)
C1–C2	1.423(4)
C2–C3	1.419(4)
C3–C4	1.430(4)
C4–C5	1.425(4)
C6–C22	1.424(3)
C6–C7	1.432(4)
C6–C10	1.437(4)
C7–C8	1.422(4)
C8–C9	1.420(4)
C9–C10	1.427(3)
C10–C11	1.422(3)
C11–C12	1.360(3)
C12–C21	1.443(3)
C12–C13	1.500(3)
C13–C14	1.508(3)
C14–C15	1.376(4)
C14–C19	1.398(3)
C15–C16	1.388(3)
C16–C17	1.376(4)
C17–C18	1.387(3)
C18–C19	1.386(3)
C19–C20	1.506(3)
C20–C21	1.508(3)
C21–C22	1.355(4)
Atoms	**Angle (°)**

C2–Fe1–C1	40.92(11)
C2–Fe1–C8	115.72(11)
C1–Fe1–C8	148.64(11)
C2–Fe1–C3	40.79(11)
C1–Fe1–C3	68.46(10)
C8–Fe1–C3	108.15(10)
C2–Fe1–C9	147.77(10)
C1–Fe1–C9	169.93(10)
C8–Fe1–C9	40.72(10)
C3–Fe1–C9	115.45(10)
C2–Fe1–C5	68.73(11)
C1–Fe1–C5	40.42(12)
C8–Fe1–C5	169.75(12)
C3–Fe1–C5	68.67(10)
C9–Fe1–C5	130.87(11)
C2–Fe1–C4	68.87(11)
C1–Fe1–C4	68.37(11)
C8–Fe1–C4	130.59(11)
C3–Fe1–C4	40.96(11)
C9–Fe1–C4	107.99(10)
C5–Fe1–C4	40.79(11)
C2–Fe1–C7	108.27(11)
C1–Fe1–C7	116.55(11)
C8–Fe1–C7	40.66(11)
C3–Fe1–C7	130.51(10)
C9–Fe1–C7	68.72(10)
C5–Fe1–C7	148.65(11)
C4–Fe1–C7	169.56(10)
C2–Fe1–C10	170.47(10)
C1–Fe1–C10	131.73(10)
C8–Fe1–C10	67.89(10)
C3–Fe1–C10	148.13(10)
C9–Fe1–C10	40.43(10)
C5–Fe1–C10	109.30(10)
C4–Fe1–C10	116.19(10)
C7–Fe1–C10	68.23(10)
C2–Fe1–C6	131.61(10)

Table 2.16 Continued

C1–Fe1–C6	110.01(10)
C3–Fe1–C6	169.85(11)
C9–Fe1–C6	67.86(9)
C5–Fe1–C6	117.16(10)
C4–Fe1–C6	148.73(11)
C7–Fe1–C6	40.36(9)
C10–Fe1–C6	40.18(10)
C5–C1–C2	108.6(2)
C5–C1–Fe1	69.96(15)
C2–C1–Fe1	69.30(15)
C3–C2–C1	107.7(2)
C3–C2–Fe1	69.92(15)
C1–C2–Fe1	69.78(15)
C2–C3–C4	108.1(2)
C2–C3–Fe1	69.29(14)
C4–C3–Fe1	69.75(14)
C5–C4–C3	107.5(2)
C5–C4–Fe1	69.46(14)
C3–C4–Fe1	69.29(14)
C1–C5–C4	108.1(2)
C1–C5–Fe1	69.63(15)
C4–C5–Fe1	69.75(15)
C22–C6–C7	132.5(2)
C22–C6–C10	119.4(2)
C7–C6–C10	108.0(2)
C22–C6–Fe1	128.73(17)
C7–C6–Fe1	68.17(14)
C10–C6–Fe1	69.51(13)
C8–C7–C6	107.5(2)
C8–C7–Fe1	69.17(14)
C6–C7–Fe1	71.47(14)
C9–C8–C7	108.8(2)

C8–Fe1–C6	67.58(10)
C9–C8–Fe1	69.73(14)
C7–C8–Fe1	70.17(14)
C8–C9–C10	108.1(2)
C8–C9–Fe1	69.55(15)
C10–C9–Fe1	71.45(13)
C11–C10–C9	133.1(2)
C11–C10–C6	119.3(2)
C9–C10–C6	107.6(2)
C11–C10–Fe1	126.71(17)
C9–C10–Fe1	68.11(14)
C6–C10–Fe1	70.31(14)
C12–C11–C10	119.8(2)
C11–C12–C21	120.7(2)
C11–C12–C13	122.5(2)
C21–C12–C13	116.8(2)
C12–C13–C14	111.44(19)
C15–C14–C19	119.7(2)
C15–C14–C13	122.8(2)
C19–C14–C13	117.5(2)
C14–C15–C16	120.9(2)
C17–C16–C15	119.5(2)
C16–C17–C18	120.3(2)
C19–C18–C17	120.3(2)
C18–C19–C14	119.3(2)
C18–C19–C20	123.2(2)
C14–C19–C20	117.4(2)
C19–C20–C21	111.63(19)
C22–C21–C12	120.95(19)
C22–C21–C20	122.6(2)
C12–C21–C20	116.4(2)
C21–C22–C6	119.7(2)

Table 2.17 Bond Distances (Å) and Bond Angles (°) for Compound **17**

Atoms	**Distances (Å)**
C1–O1	1.2247(17)
C1–C17	1.484(2)
C1–C2	1.4926(19)
C2–C3	1.392(2)
C2–C7	1.399(2)
C3–C4	1.385(2)
C4–C5	1.392(2)
C5–C6	1.383(2)
C6–C7	1.396(2)
C7–C8	1.492(2)
C8–O2	1.2240(18)
C8–C9	1.487(2)
C9–C10	1.397(2)
C9–C17	1.409(2)
C10–C11	1.385(2)
C15–C16	1.381(2)
C15–C14	1.406(10)
C15–C11	1.407(2)
C14–C13	1.324(16)
C13–C12	1.521(16)
C12–C11	1.539(9)
C12'–C13'	1.322(18)
C13'–C14'	1.525(18)
C16–C17	1.394(2)
Atoms	**Angles (°)**
O1–C1–C17	121.47(13)
O1–C1–C2	120.62(13)
C17–C1–C2	117.90(12)
C3–C2–C7	119.84(13)
C3–C2–C1	118.99(13)
C7–C2–C1	121.11(13)
C4–C3–C2	120.11(14)
C3–C4–C5	120.12(14)
C6–C5–C4	120.19(14)
C5–C6–C7	120.10(14)
C6–C7–C2	119.62(14)
C6–C7–C8	119.28(13)
C2–C7–C8	121.08(13)
O2–C8–C9	121.48(13)
O2–C8–C7	120.72(13)
C9–C8–C7	117.79(12)
C10–C9–C17	120.32(13)
C10–C9–C8	118.65(13)
C17–C9–C8	121.02(13)
C11–C10–C9	118.92(13)
C16–C15–C14	131.7(5)
C16–C15–C11	120.86(13)
C14–C15–C11	107.5(5)
C13–C14–C15	112.4(9)
C14–C13–C12	111.0(5)
C13–C12–C11	99.5(7)
C10–C11–C15	120.56(13)
C10–C11–C12	129.9(4)
C15–C11–C12	109.6(4)
C12'–C13'–C14'	110.6(6)
C15–C16–C17	118.95(13)
C16–C17–C9	120.38(13)
C16–C17–C1	118.61(13)
C9–C17–C1	121.00(12)

Table 2.18 Bond Distances (Å) and Bond Angles (°) for Compound **18**

Atoms	**Distances (Å)**
O1–C1	1.230(2)
C1–C10#1	1.482(3)
C1–C2	1.484(3)
C2–C3	1.402(3)
C2–C10	1.409(3)
C3–C4	1.377(3)
C4–C8	1.413(3)
C4–C5	1.488(3)
C5–C6	1.453(3)
C6–C7	1.381(3)
C7–C8	1.471(3)
C8–C9	1.383(3)
C9–C10	1.396(3)
C10–C1#1	1.482(3)
Atoms	**Angles (˚)**
O1–C1–C10#1	120.88(18)
O1–C1–C2	120.71(18)
C10#1–C1–C2	118.40(16)
C3–C2–C10	120.25(18)
C3–C2–C1	119.33(17)
C10–C2–C1	120.41(18)
C4–C3–C2	119.42(17)
C3–C4–C8	120.33(18)
C3–C4–C5	130.94(18)
C8–C4–C5	108.73(17)
C6–C5–C4	103.92(18)
C7–C6–C5	112.12(19)
C6–C7–C8	106.97(18)
C9–C8–C4	120.57(18)
C9–C8–C7	131.16(18)
C4–C8–C7	108.26(18)
C8–C9–C10	119.50(18)
C9–C10–C2	119.92(19)
C9–C10–C1#1	118.92(17)
C2–C10–C1#1	121.16(17)

Table 2.19 Bond Distances (Å) and Bond Angles (°) for Compound **19**

Atoms	**Distances (Å)**
O1–C1	1.225(2)
C1–C11#1	1.476(3)
C1–C2	1.484(3)
C2–C3	1.380(3)
C2–C11	1.422(3)
C3–C4	1.399(3)
C4–C5	1.301(11)
C4–C9	1.422(3)
C5–C6	1.364(8)
C6–C7	1.408(8)
C7–C8	1.362(7)
C8–C9	1.327(8)
C9–C10	1.395(3)
C5'–C6'	1.414(10)
C6'–C7'	1.393(9)
C10–C11	1.389(3)
C11–C1#1	1.476(3)
Atoms	**Angles (Å)**
O1–C1–C11#1	121.3(2)
O1–C1–C2	120.7(2)
C11#1–C1–C2	117.95(18)
C3–C2–C11	119.9(2)
C3–C2–C1	119.37(18)
C11–C2–C1	120.7(2)
C2–C3–C4	121.16(18)
C5–C4–C3	119.7(5)
C5–C4–C9	121.3(5)
C3–C4–C9	119.0(2)
C4–C5–C6	116.9(10)
C5–C6–C7	122.0(9)
C8–C7–C6	120.7(8)
C9–C8–C7	115.8(6)
C8–C9–C10	117.2(3)
C8–C9–C4	123.2(3)
C10–C9–C4	119.6(2)
C7'–C6'–C5'	110.6(8)
C11–C10–C9	120.96(19)
C10–C11–C2	119.3(2)
C10–C11–C1#1	119.35(18)
C2–C11–C1#1	121.3(2)

Table 2.20 Bond Distances (Å) and Bond Angles (°) for Compound **21**

Atoms	**Distances (Å)**
Si1–C13'	1.836(9)
Si1–C12	1.8409(15)
Si1–C19	1.875(2)
Si1–C16	1.8810(18)
Si1–C13	1.907(2)
Si1–C19'	1.982(10)
C1–C10#1	1.4135(19)
C1–C2	1.4159(19)
C1–C11	1.4359(19)
C2–C3	1.4247(19)
C2–C10	1.4390(19)
C3–C4	1.361(2)
C4–C8	1.435(2)
C4–C5	1.474(2)
C5–C6	1.381(2)
C6–C7	1.456(2)
C7–C8	1.494(2)
C8–C9	1.360(2)
C9–C10	1.4275(19)
C10–C1#1	1.4135(19)
C11–C12	1.208(2)
C13–C14	1.525(5)
C13–C15	1.546(3)
C13'–C14'	1.449(12)
C13'–C15'	1.553(17)
C16–C17	1.529(3)
C16–C18	1.532(3)
C19–C21	1.524(4)
C19–C20	1.536(5)
C19'–C20'	1.534(14)
C19'–C21'	1.558(18)
Atoms	Angles (˚)
C13'–Si1–C12	115.1(3)
C13'–Si1–C19	103.7(3)
C12–Si1–C19	104.42(9)
C13'–Si1–C16	118.0(3)
C12–Si1–C16	106.79(7)
C19–Si1–C16	107.80(11)
C13'–Si1–C13	19.6(3)
C12–Si1–C13	106.58(8)
C19–Si1–C13	123.35(13)
C16–Si1–C13	106.90(9)
C13'–Si1–C19'	81.1(5)
C12–Si1–C19'	112.2(3)
C19–Si1–C19'	22.8(3)
C16–Si1–C19'	122.4(3)
C13–Si1–C19'	100.7(4)
C10#1–C1–C2	121.36(12)
C10#1–C1–C11	120.04(12)
C2–C1–C11	118.59(12)
C1–C2–C3	121.51(12)
C1–C2–C10	119.34(13)
C3–C2–C10	119.14(13)
C4–C3–C2	119.89(13)
C3–C4–C8	121.02(13)
C3–C4–C5	131.13(13)
C8–C4–C5	107.86(12)
C6–C5–C4	107.53(13)
C5–C6–C7	112.07(13)
C6–C7–C8	104.37(12)
C9–C8–C4	120.76(13)
C9–C8–C7	131.07(13)
C4–C8–C7	108.17(12)
C8–C9–C10	119.86(13)
C1#1–C10–C9	121.39(12)
C1#1–C10–C2	119.29(13)
C9–C10–C2	119.32(13)
C12–C11–C1	177.78(15)
C11–C12–Si1	174.90(13)
C14–C13–C15	109.4(3)
C14–C13–Si1	113.3(3)
C15–C13–Si1	112.39(16)

Table 2.20 Continued

C14'–C13'–C15'	114.3(13)
C14'–C13'–Si1	117.7(7)
C15'–C13'–Si1	112.6(11)
C17–C16–C18	110.19(18)
C17–C16–Si1	110.91(13)
C18–C16–Si1	112.14(14)
C21–C19–C20	111.1(4)
C21–C19–Si1	114.1(2)
C20–C19–Si1	112.4(4)
C20'–C19'–C21'	108.3(14)
C20'–C19'–Si1	110.0(7)
C21'–C19'–Si1	110.7(16)

Table 2.21 Bond Distances (Å) and Bond Angles (°) for Compound **22**

Atoms	**Distances (Å)**
Si1–C20'	1.777(8)
Si1–C13	1.8380(18)
Si1–C17	1.8825(17)
Si1–C14	1.883(2)
Si1–C20	1.954(3)
C1–C2	1.413(2)
C1–C11#1	1.414(3)
C1–C12	1.435(2)
C2–C3	1.413(3)
C2–C11	1.445(2)
C3–C4	1.372(3)
C4–C5	1.38(2)
C4–C9	1.438(2)
C4–C5'	1.53(2)
C5–C6	1.381(11)
C6–C7	1.426(7)
C7–C8	1.348(13)
C8–C9	1.38(2)
C5'–C6'	1.378(12)
C6'–C8'	1.455(14)
C8'–C9	1.54(2)
C9–C10	1.373(3)
C10–C11	1.416(2)
C11–C1#1	1.414(3)
C12–C13	1.210(2)
C14–C16	1.524(3)
C14–C15	1.545(3)
C17–C19	1.530(3)
C17–C18	1.533(2)
C20–C21	1.524(5)
C20–C22	1.544(4)
C20'–C22'	1.506(11)
C20'–C21'	1.522(12)
Atoms	Angles (˚)
C20'–Si1–C13	103.8(3)
C20'–Si1–C17	124.8(3)
C13–Si1–C17	106.96(8)
C20'–Si1–C14	102.6(3)
C13–Si1–C14	107.81(8)
C17–Si1–C14	109.79(8)
C20'–Si1–C20	18.1(2)
C13–Si1–C20	109.82(10)
C17–Si1–C20	106.95(11)
C14–Si1–C20	115.22(12)
C2–C1–C11#1	121.35(15)
C2–C1–C12	119.09(16)
C11#1–C1–C12	119.52(16)
C1–C2–C3	121.75(15)
C1–C2–C11	119.46(16)
C3–C2–C11	118.77(16)
C4–C3–C2	121.25(16)
C3–C4–C5	120.0(5)
C3–C4–C9	119.92(17)
C5–C4–C9	120.1(5)
C3–C4–C5'	133.1(5)
C5–C4–C5'	13.1(9)
C9–C4–C5'	107.0(5)
C6–C5–C4	119.9(12)
C5–C6–C7	118.8(9)
C8–C7–C6	121.9(10)
C7–C8–C9	120.0(13)
C6'–C5'–C4	107.7(13)
C5'–C6'–C8'	112.9(13)
C6'–C8'–C9	104.3(12)
C10–C9–C8	120.6(6)
C10–C9–C4	120.11(16)
C8–C9–C4	119.2(6)
C10–C9–C8'	131.8(5)
C8–C9–C8'	11.4(11)
C4–C9–C8'	108.1(5)
C9–C10–C11	120.94(16)
C1#1–C11–C10	121.81(15)
C1#1–C11–C2	119.18(16)
C10–C11–C2	119.00(16)
C13–C12–C1	177.44(18)

Table 2.21 Continued

C12–C13–Si1	176.54(15)
C16–C14–C15	110.73(19)
C16–C14–Si1	111.33(14)
C15–C14–Si1	111.78(15)
C19–C17–C18	110.95(15)
C19–C17–Si1	112.66(12)
C18–C17–Si1	113.37(12)
C21–C20–C22	110.1(3)
C21–C20–Si1	111.7(3)
C22–C20–Si1	112.9(2)
C22'–C20'–C21'	113.6(8)
C22'–C20'–Si1	114.8(6)
C21'–C20'–Si1	114.3(8)

2.4 Electrochemistry. Cyclic voltammetry was used to ascertain the HOMO and LUMO energy levels of the new Cp-capped acenes. This technique involves application of forward and reverse linear potential scans to a working electrode immersed in a solution of the redox-active analyte and a supporting electrolyte. If the material has accessible oxidation, an anodic wave develops in the forward positive scan, and a corresponding cathodic wave can observed in the reverse scan.

The voltammetric instrument consists of a three-electrode electrochemical cell. At a platinum button working electrode, potential is varied linearly with time. A platinum wire counter electrode conducts current via the electrolyte solution to the working electrode. A silver wire serves as a pseudoreference electrode. Ferrocene/ferrocenium (Fc/Fc^+), a stable redox couple that is soluble in common organic solvents and whose potential is independent of the solvent,[115] is used as an internal standard. Fc/Fc^+ is estimated to be around 4.8 eV against vacuum.[116] HOMO and LUMO energies of compounds are determined by using their first oxidation and first reduction potentials with respect to Fc/Fc^+.

Cyclic voltammetry measures how current (mA) changes as the potential (V) of the working electrode is varied in a supporting electrolyte solution. In a redox reaction, the oxidation potential (E_{oxd}) is a measurement of the ionization potential or HOMO of a compound, and reduction potential (E_{red}) is a measurement of the electron affinity or LUMO of a compound.

Cyclic voltammetry of bis(Cp-capped) TIPS-anthracene (**21**) and Cp-capped TIPS-tetracene (**22**) was run in 0.1 M Bu_4NPF_6/CH_2Cl_2 under nitrogen at scan rate of 100 $mV \cdot sec^{-1}$. The half-wave potentials of each oxidation ($E^0_{1/2,ox}$) and reduction ($E^0_{1/2,red}$)

wave were calculated by averaging the corresponding anodic (E_{pa}) and cathodic (E_{pc}) peak potentials. The cyclic voltammograms for compounds (**20**), (**21**) and (**22**) are shown in Figure (2.16–2.20). The electrochemical data are summarized in Table 2.20.

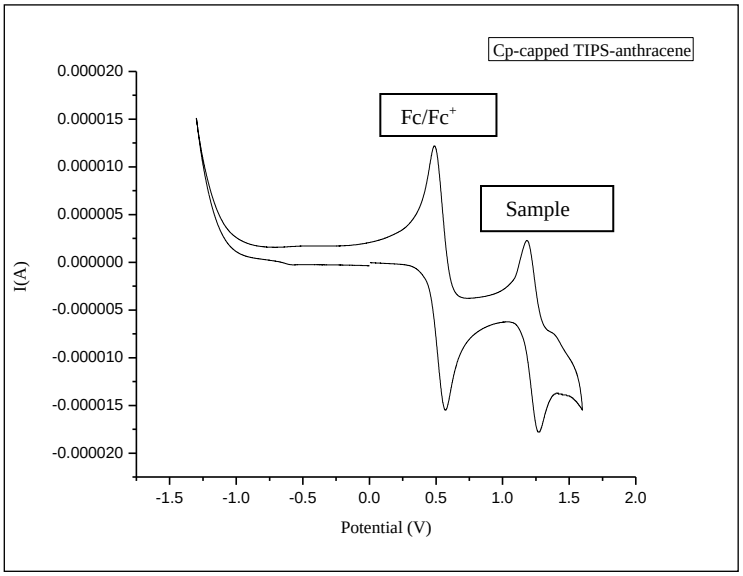

Figure 2.16 Cyclic voltammogram of **20** showing oxidation vs. Fc/Fc^+ in 0.1 M Bu_4NPF_6/CH_2Cl_2 at scan rate 100 $mV \cdot sec^{-1}$

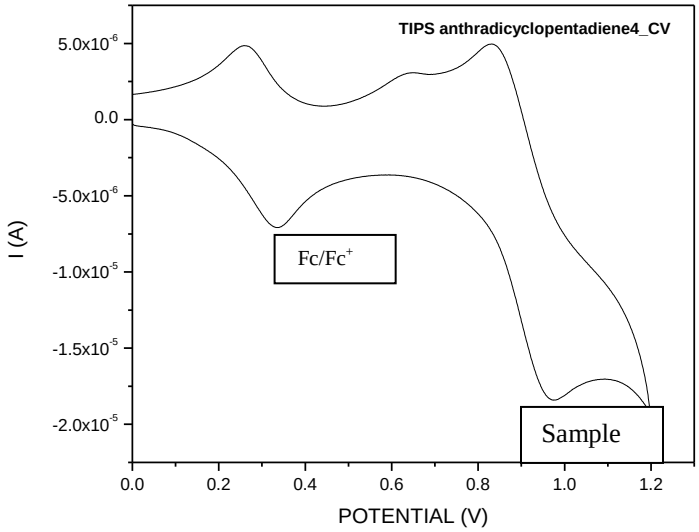

Figure 2.17 Cyclic voltammogram of **21** showing oxidation vs. Fc/Fc^+ in 0.1 M Bu_4NPF_6/CH_2Cl_2 at scan rate 100 $mV \cdot sec^{-1}$

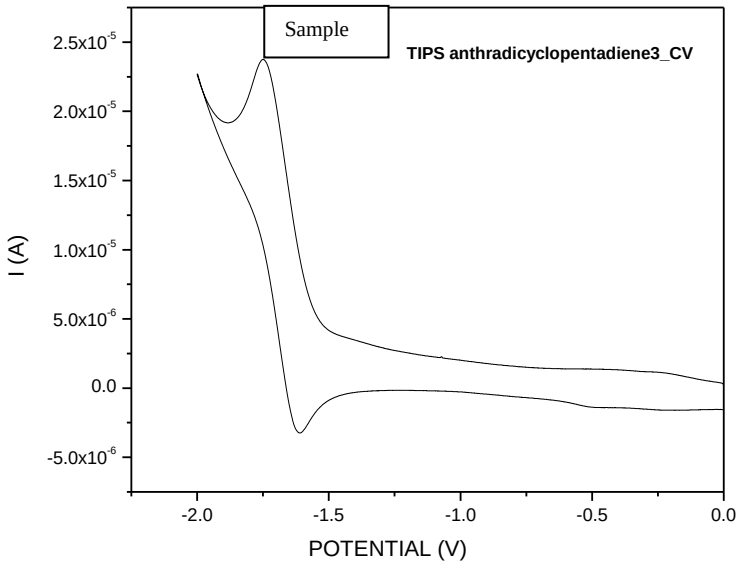

Figure 2.18 Cyclic voltammogram of **21** showing reduction vs. Fc^{+}/Fc in 0.1M Bu_4NPF_6/CH_2Cl_2 at scan rate 100 $mV \cdot sec^{-1}$

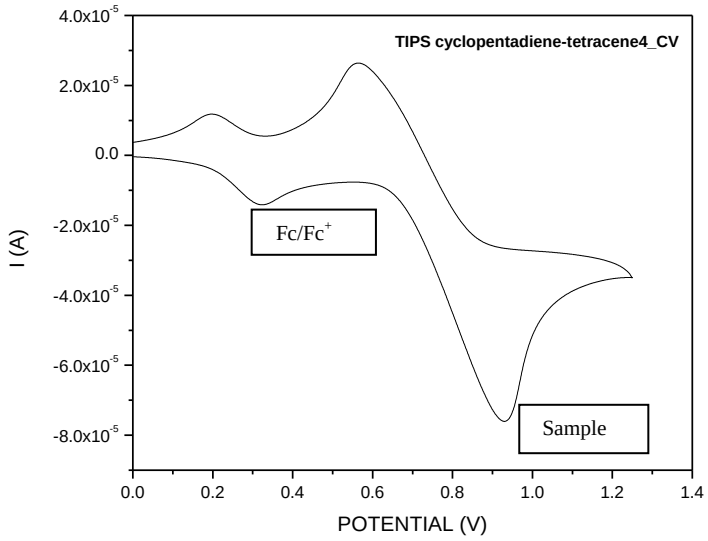

Figure 2.19 Cyclic voltammogram showing oxidation of **22** vs. Fc/Fc^{+} in 0.1 M Bu_4NPF_6/CH_2Cl_2 at scan rate 100 $mV \cdot sec^{-1}$

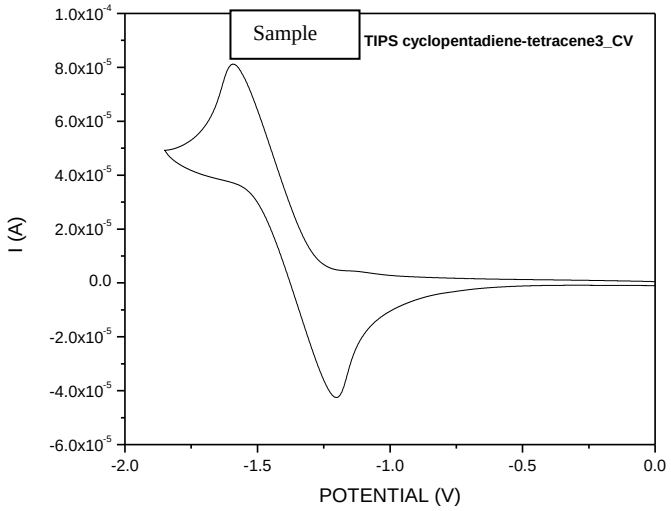

Figure 2.20 Cyclic voltammogram of **22** showing reduction vs. Fc^{+}/Fc in 0.1 M Bu_4NPF_6/CH_2Cl_2 at scan rate 100 $mV \cdot sec^{-1}$

Table 2.22 Electrochemical data of compound **20**, **21** and **22** showing oxidation and reduction

Compd.	Oxidation (mV)				Reduction (mV)			
	E_{pa}	E_{pc}	$E_{1/2}$	ΔE	E_{pa}	E_{pc}	$E_{1/2}$	ΔE
20	1254	1180	1217	74	–	–	–	–
Fc/Fc^{+}	558	508	533	50	–	–	–	–
21	975	833	904	142	–1611	–1749	–1680	138
Fc/Fc^{+}	333	259	296	74	–	–	–	–
22	929	564	746.5	365	–1202	–1592	–1397	–390
Fc/Fc^{+}	324	197	260.5	127	–	–	–	–

0.1 M Bu_4NPF_6 solution was prepared in CH_2Cl_2, Cyclic voltammetry was run under N_2 atmosphere

Table 2.23 Electrochemical and spectroscopic data for compounds **21** and **22**

Compound	E_{HOMO}[a]	E_{LUMO}[b]	$E_{g,EC}$	λ_{max}abs	$E_{g,opt}$[e]
20	-5.48	–	–	468	2.65
21	–5.41	–2.82	2.58	494	2.51
22	–0.29	–3.14	2.15	599	2.07

[a]HOMO = –[4.8–(E_{ox}–Fc/Fc$^+$)], E_{ox} calculated using cyclic voltammetry (oxidation).
[b]LUMO = –[4.8–(E_{red}–Fc/Fc$^+$)], E_{red} calculated using cyclic voltammetry (reduction).
[C]E_g^{ec} Electrochemical band gap obtained from difference between LUMO and HOMO values.
[d]π_{max} obtained from the absorption edges of film (prepared by drop cast using 2 % by weight solution of compound in chlorobenzene).
[e]E_g^{opt} Optical band gap estimated from the absorption edge of the film.

UV-vis absorption spectra for compounds **20**, **21** and **22** were recorded in dichloromethane solution and as a solid film prepared by solution-casting 2 % by weight solution in chlorobenzene (**21** and **22**). Absorption spectra are plotted as wavelength vs. absorbance in Figure 2.21.

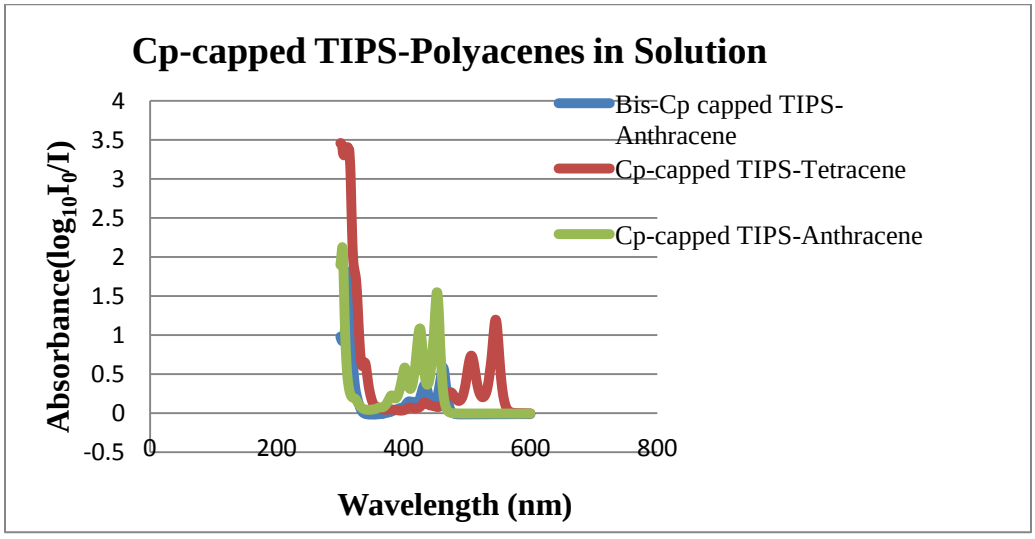

Figure 2.21 UV-vis absorbance spectra of **20** (green), **21** (blue) and **22** (red) in dichloromethane

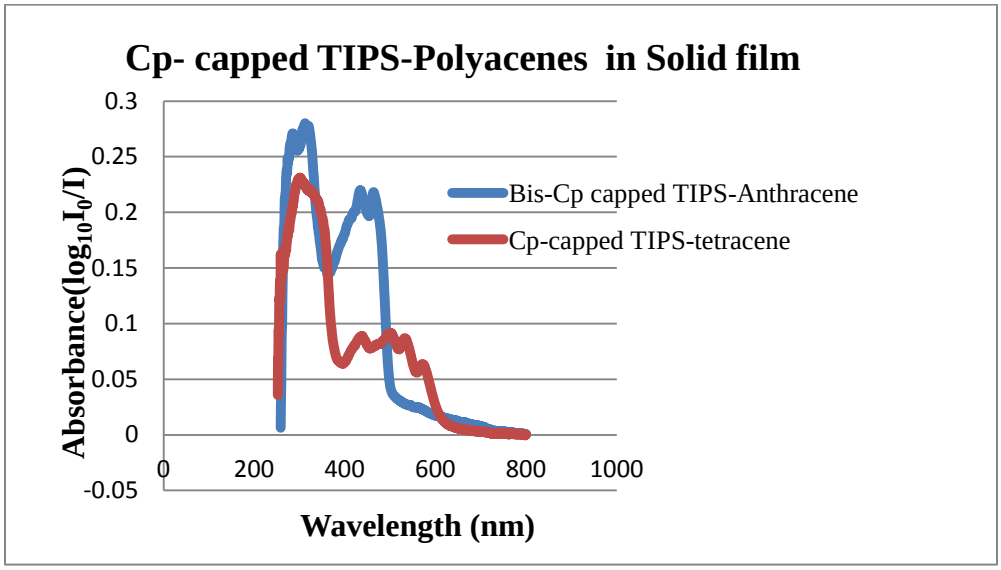

Figure 2.22 UV-vis absorbance spectrum of **21** (blue) and **22** (red) in solid

The UV-vis spectra of **21** and **22** show a blue shift in absorption compared to TIPS-pentacene (644 nm), TIPS-anthradithiophene (555 nm)[21] and 5,12-bis(triisopropylsilylethynyl)tetraceno[2,3-*b*]thiophene (~600 nm in THF)[35] indicating that an extended π conjugation system contributes a vital role in absorbance. The oxidation (0.61 V vs. Fc/Fc^+) and reduction (–1.98 V vs. Fc^+/Fc) of **21** reveals an electrochemical HOMO-LUMO gap (2.58 eV) that complements the gap obtained from the absorption edge of the optical spectrum [2.51 eV (494 nm)]. Similarly, the oxidation (0.49 V vs. Fc/Fc^+) and reduction (–1.66 V) of **22** reveal an electrochemical HOMO-LUMO gap (2.15 eV) that complements the gap derived from the absorption edge of the optical spectrum [2.07 eV (599 nm)]. The absorption spectra of **21** and **22** show that the fusion of an additional aromatic ring leads to a further ~100 nm red shift in absorption, which is similar to the absorption spectra data reported by Payne *et al.* for higher acenes (hexacene

and heptacene).[117] We calculated the optical energy gap for compounds **21** and **22** in solution as 2.62 eV (473 nm) and 2.23 eV (557 nm).

Table 2.24 Ionization potential of **21** and **22**

Compound	1[a]	2[a]	3[a]	Average	STDEV
21 (3 %)	5.40	5.41	5.41	5.41	0.006
(5 %)	5.38	5.40	5.40	5.39	0.01
(6 %)	5.41	5.41	5.39	5.40	0.01
22 (1 %)	5.47	5.45	5.55	5.49	0.05
(2 %)	5.44	5.56	5.58	5.53	0.08
(3 %)	5.53	5.46	5.56	5.52	0.05

[a]In chlorobenzene. Thin films of sample were prepared by solution-casting using different concentration by weight and slow evaporation of solvent in air. Samples were stored under nitrogen before measurement.

The ionization potentials (IP) of **21** and **22** were studied in three different locations of thin film. The IP for compound **21** matches well with the HOMO energy (5.41 eV) obtained from cyclic voltammetry, whereas the IP of compound **22** is slightly larger than the HOMO energy level (5.29 eV) obtained from cyclic voltammetry. The large IP variation observed for compound **22** in the different location is possibly due to inhomogeneity of crystalline films or instability in air.

2.5 Cyclopentadiene-capped TIPS-Acenes Device Study

The main target of this entire research is to study charge-carrier mobility of the synthesized compounds. After the structural and electrochemical properties were studied, device performance of the reported Cp-capped TIPS-acenes was investigated by Aram Amassian and Muhammad Rizwan Khan Niazi of King Abdullah University of Science and Technology, Saudi Arabia. They used bottom-contact, bottom-gate (BCBG) device architecture to obtain OTFT device performance, with gold source and drain electrodes and SiO_2 as a dielectric layer. Bottom contacts (Au electrodes) were deposited by thermal evaporation using shadow masks with channel length of 50 μm and channel width of 1000 μm (*W*/*L* 20). The images shown in the Figure 2.5.1 show the thermal deposition of thin film by blade coating at 70 °C with a shearing speed of 1.5 mm/sec. The films of organic semiconductor materials are deposited with blade coating at different blade speeds to optimize the processing condition as shown in Figure 2.23.

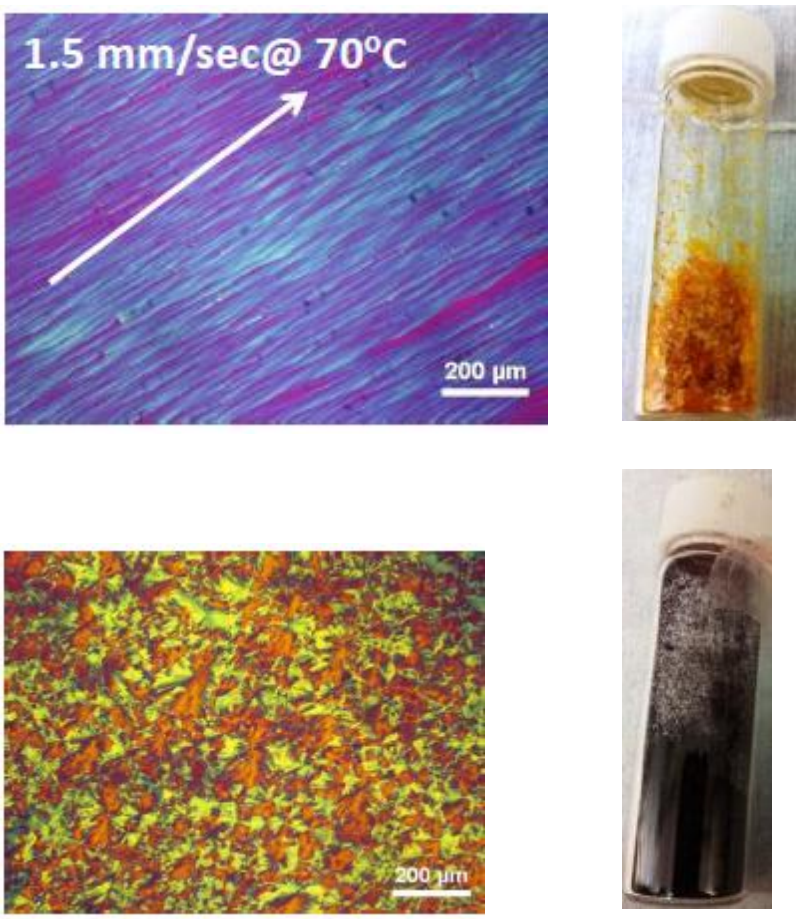

Figure 2.23 Images of thin films deposited by thermal deposition at 70 °C with a shearing speed 1.5 mm/sec top [bis(Cp-capped) TIPS-anthracene] and bottom [Cp-capped TIPS-tetracene]

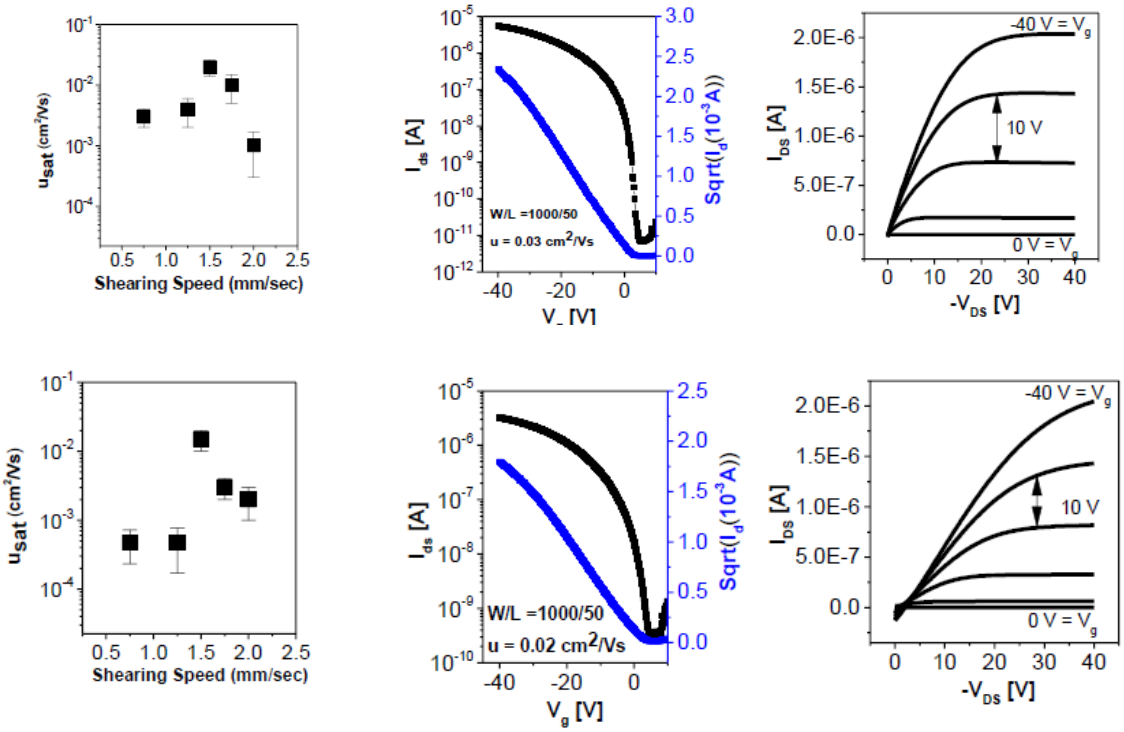

Figure 2.24 Different shearing speed to optimize the processing condition (left), $\sqrt{I}$ and log$I$ vs. gate voltage (middle) and output of device study (right)

Figure 2.24 shows that the thin films of compounds **21** and **22** show better device performance at 1.5 mm/sec blade speed. These films gave a mobility of 0.03 $cm^2/(V\ s)$ (**21**) and 0.02 $cm^2/(V\ s)$ (**22**) with I_{on}/I_{off} of 10^6 and 10^4, respectively. Compounds **21** and **22** have moderate mobility from solution-deposited film. These mobilities are not good enough to consider **21** and **22** as potential candidates for device applications. In order to be useful for commercial application, a material should have mobility greater than 0.5 $cm^2/(V\ s)$ and *on*/*off* current ratio greater than 10^5. TES-ADT, analogous to **21**, shows mobility as high as of 1.0 $cm^2/(V\ s)$ and on/off current ratio of 10^7 from drop-cast films.[6] Similarly, TIPS-tetraceno[2,3-*b*]thiophene exhibits a mobility as high as 1.25 $cm^2/(V\ s)$ from vacuum-deposited film.[37] The performance of these materials is likely due to the

close π-stacked interaction in the crystal. Moreover, the ability to form high-quality films is essential for better device performance.

2.6 Summary

1,2-Diformylferrocene is the key precursor for the synthesis of mononuclear and binuclear quinone complexes of iron with carbonyl groups either at α or γ position with respect to cyclopentadienyl ring. 1,2-Diformylferrocene was prepared in moderate yield (50.4%).[89,90] Following the idea supported by the work of Rinehart group, ferrocene was reacted with succinic anhydride in the presence of anhydrous $AlCl_3$ in CH_2Cl_2, reduction of carbonyl group under Clemmensen reduction conditions and cyclized in the presence of trifluoroacetic anhydride to give **6** (92.1%). Oxidation of **6** with activated manganese dioxide gave **7** (44%). Ferrocenebenzoquinone (**7**) was reduced to ferrocene-fused-1,4-cyclohexanedione (**8**, 41%) with sodium dithionite. A series of ferroceneacenequinones was synthesized by aldol condensation. Aldol condensation between **8** and phthalaldehyde gave **9** (62.5%) and condensation between 1,2-diformylferrocene and naphthalene-1,2-diol or anthracene-1,2-diol gave **11** (78.8%) and **13** (81.5%).The carbonyl groups in **9** and **11** are located at the α and γ position respectively with respect to the Cp ring.

Similarly, aldol condensation between 1,2-diformylferrocene and ferrocene-fused-1,4-cyclohexanedione (**8**) or 1,4-cyclohexanedione resulted in an inseparable isomer mixture (syn/anti) of binuclear quinone complexes (**10,** 79.5% and **12**, 69.6% combined). These quinones appear at very close R_f values by TLC in various combinations of hexane, ethyl ether and dichloromethane and could not be separated by chromatography. The ferrocene-fused quinones are deep blue and stable in the solid state at room temperature. However, solutions of complexes **11**, **12** and **13** change from blue to yellow

on contact with silica, and the characterization of yellow compounds indicate the detachment of iron from the organic quinone ligand. This might be due to the indenyl effect, which is also supported by their single X-ray crystal data.

Organometallic acenequinones are not the final product of our research. Therefore, the carbonyl groups of quinones **11**, **12** (mixture), and **13** were reduced to methylenes with borane in THF (excess), leading to light pink dihydroacenes. Attempts to dehydrogenate the dihydroacenes with DDQ resulted in decomposition. Using saturated aqueous sodium dithionite is the next logical step to reduce acenequinones to hydroquinones. Attempted reduction of organometallic acenequinones (**11, 12** and **13**) to organometallic hydroquinones by using aqueous sodium dithionite gave the demetalated acenequinones as the main product (**17**, 49%, **18**, 42% combined and **19**, 52%). Nucleophilic addition of triisopropylsilylethynyllithium to the quinone carbonyls followed by dehydroxylation with aqueous $SnCl_2$ gave the desired Cp- and bis(Cp)-capped triisopropylsilylethynylacenes (**20,** 50%**, 21** 23% combined and **22,** 59%) . After purification of compounds by chromatography, **21** and **22** were recrystallized from acetone to yield orange and dark purple needles, respectively, which are suitable for single X-ray diffraction. Analysis revealed that these molecules packing with two-dimensional π–stacking similar to the packing nature of TIPS-pentacene and TES-anthracene. The interplanar arene-arene distances are 3.41 Å (**21**) and 3.40 Å (**22**). Both compounds are highly soluble in common organic solvents and thus easily processible.

The electrochemistry of Cp-capped acenes **21** and **22** was investigated. Cyclic voltammetry shows oxidation and reduction potentials for **21** and **22** at 0.61 V, –1.98 V and 0.49 V, –1.66 V, respectively, versus Fc/Fc^+, corresponding to estimated HOMO and

LUMO energy levels of −5.41 eV, –2.82 eV, –5.29 eV and –3.14 eV, respectively. The electrochemical HOMO level energy of –5.41 eV for compound **21** agrees well with the IP determined from Photoelectron Spectroscopy in Air (PESA). UV-vis absorption spectra of compound **21** and **22** were recorded in dichloromethane solution and in a solid film deposited from dichlorobenzene solution. The UV absorption maxima in dichloromethane solution of **21** and **22** are 462 nm 545 nm respectively. A greater 90–100 nm bathochromic shift in absorption of TES-ADT and TIPS-pentacene as compared to Cp-capped TIPS-acenes is attributed to the extended π–conjugation. The electrochemical HOMO-LUMO gaps of **21** and **22** are 2.58 eV and 2.15 eV, respectively, which are close to the optically determined HOMO-LUMO gaps in solid films of **21** (2.51 eV at 494 nm) and **22** (2.07 eV at 599 nm). The OTFT study using bottom-contact-bottom gate (BCBG) device architecture from solution-deposited film shows relatively poor device performance with the hole mobility of 0.03 $cm^2/(V\ s)$, I_{on}/I_{off} of 10^6 for **21** and 0.02 $cm^2/(V\ s)$, I_{on}/I_{off} of 10^4 for **22**.

In general, we made a series of mononuclear and binuclear organometallic acenequinones with carbonyl groups positioned at either α or γ position with respect to cyclopentadienyl ring using aldol condensation. Organometallic acenequinones are potential precursors for organometallic acenes. Ferrocene-fused acenequinones (**11**, **12** and **13**) exhibit a significant indenyl effect, which makes it possible to release the cyclopentadiene-capped acenequinones from the metal centers. The Cp-capped acenequinones were aromatized by the nucleophilic addition of lithium triisopropylsilylethynyl to carbonyl, followed by dehydroxylation with $SnCl_2$ in acidic conditions. The resultant Cp-capped TIPS acenes are highly soluble in common organic

solvents. The electrochemical and optical properties of Cp-capped TIPS acenes that are essential for organic semiconductor candidate were measured using cyclic voltammetry and UV-vis spectroscopy. The OFET performance of **21** and **22** shows hole mobilities of 0.03 $cm^2/(V\ s)$ and 0.02 $cm^2/(V\ s)$ respectively using a blade coating. These mobilities are comparable to the hole mobilities of thiophene analogues, TIPS anthracenedithiophene (0.05 $cm^2/(V\ s)$ solution deposited)[6] and TIPS tetracene[2,3-*b*]thiophene (average 0.028 $cm^2/(V\ s)$ solution deposited)[37].

Chapter 3 Synthesis and Characterization of Ferrocene-Fused Tropones, Thiotropones and Oxime Derivatives

3.1 Introduction

The first nonlinear optical phenomenon was observed in inorganic crystalline materials, lithium niobate, gallium arsenide (GaAs), indium antimonide (InSb) and potassium dihydrogen phosphate (KDP), whose refractive index changed with an applied electric field. The study of nonlinear effects increased after the invention of lasers in 1960, followed by the observation of second-harmonic generation (SHG) in quartz by Franken et al.[118,119, 120] 3,4-Benzopyrene is the first organic material in which SHG was observed in 1965.[121] Further, SHG was explored in another organic crystal (hexamethylenetetramine) by Heilmer et al. in the same year.[122] Organic and polymeric nonlinear optical (NLO) materials have been a subject of intense investigation over the last three decades due to potential applications in electro-optic devices for telecommunication, optical computing and optical information processing.[3]

NLO materials possess high first-order hyperpolarizabilities and give rise to large second-order effects.[123] The basic requirements for a molecule to exhibit nonlinear optical properties are polarizability, asymmetric charge distribution and acentric crystal packing. Inorganic materials have a high dielectric constant, which can perturb the incoming electric field in optoelectronic applications.[2] Organic materials have a number of advantages over inorganic materials for NLO application. The distribution of π-electrons plays the dominant role in defining dielectric constant and refractive indexes. Organic materials have fast response time and the ease of modification of organic structures makes it possible to synthesize appropriate molecules and to tune the properties for

electro-optic applications.[124] Molecules with π–donor and π–acceptor interactions are promising candidates to fulfill the requirement of NLO materials.[125] Push–pull compounds where donor and acceptor end groups interact through a π–conjugated system can give large quadratic hyperpolarizabilities. Many recently reported NLO materials utilize new heterocyclic chromophores, such as tricyanofuran, as acceptor moieties.[126]

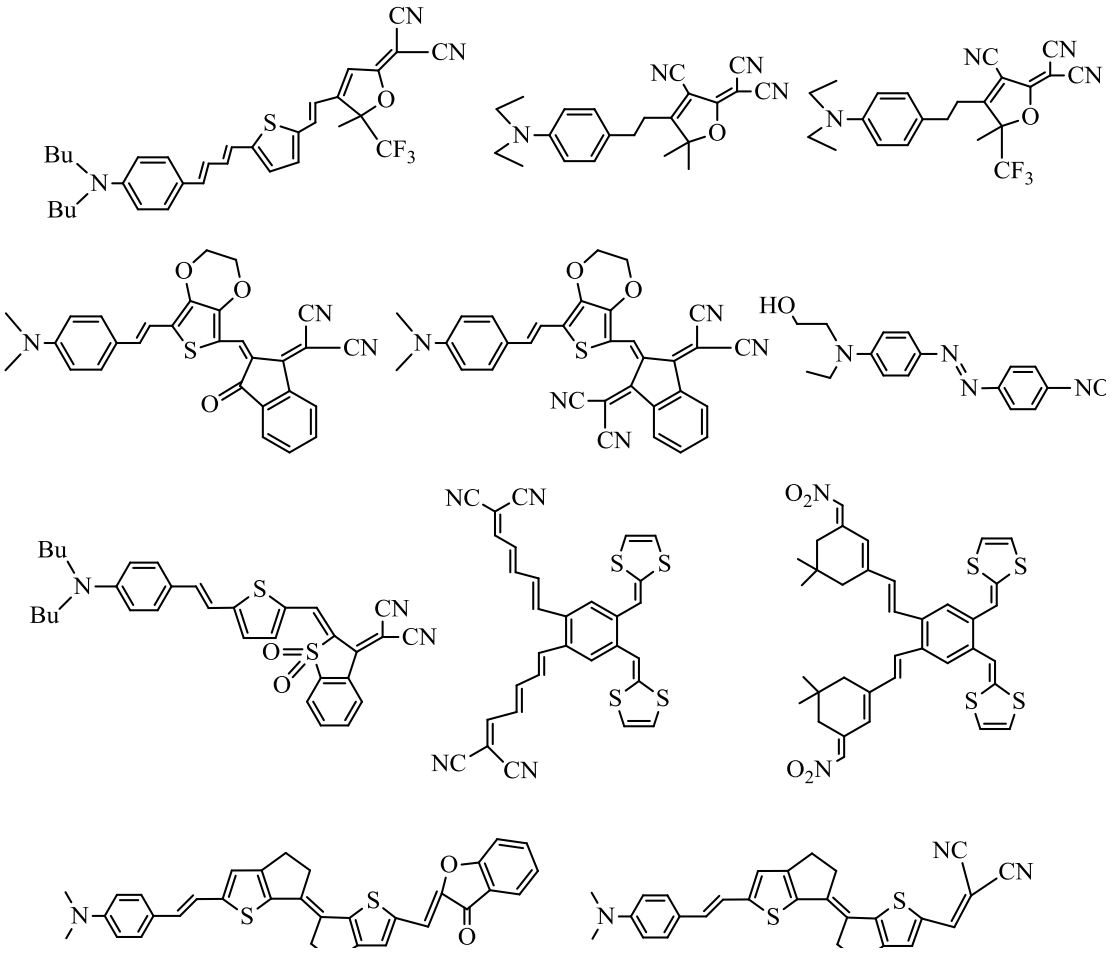

Chart 3.1 Nonlinear optical organic materials

Metallocenes are similar to organic molecules in that they can possess large NLO responses, a fast response time and ease of synthesis and fabrication. Organometallic

complexes allow greater flexibility for the design of nonlinear optical polarizabilities. The oxidation state of transition metals can be changed, which changes the number of *d* electrons involved and allows for the study of the differences between diamagnetic and paramagnetic complexes, ligand environment and a geometrical pattern of complexes.[124] These properties eventually allow tuning of NLO responses.

Organometallic and coordination compounds allow exploration of new variables for the engineering of nonlinear optical hyperpolarizabilities. These compounds can have metal-to-ligand and ligand-to-metal charge transfer bands in the UV-visible region. One can change the transition-metal element, oxidation state and the number of *d* electrons to examine the difference between diamagnetic and paramagnetic complexes and the effect of new coordination pattern. Complexes containing metal chromophores are intensely colored and the strength of the optical absorption band is also associated with large optical nonlinearities. Ligand environments and oxidation states can be adjusted to make the metal center of an organometallic complex electron rich or electron poor. Hence, the metal center may act as a strong donor or a strong acceptor.[127]

Green et al. reported that (*Z*)-[1-ferrocenyl-2-(4-nitrophenyl)ethylene] shows SHG efficiency 62 times that of urea.[128] A salt of the form (*E*)-[1-ferrocenyl-2-(N-methylpyridinium-4-yl)ethylene] iodide has the largest efficiency, roughly 220 times that of urea, and the related nitrate salt has a SHG efficiency of 110 times that of urea.[129] Moreover, series of push–pull ferrocene and ruthenocene polyenic derivatives have been synthesized by Alain et al. in order to achieve enhanced quadratic optical nonlinearity.[130]

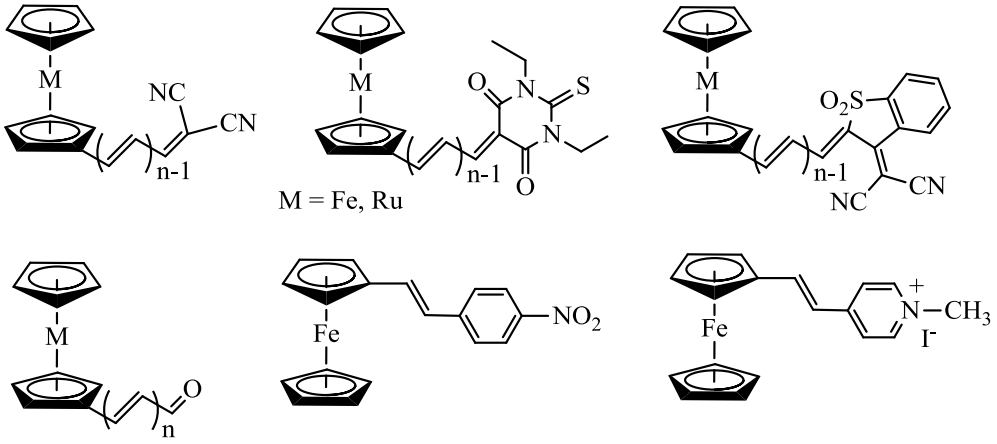

Chart 3.2 Organometallic NLO materials

Fulvenes (**1**) and heptafulvenes (**2**) (shown in Chart 3.3) are nonalternate, conjugated cyclic hydrocarbons with a strong double-bond fixation. The specific conjugated structure and the nonbenzenoid aromatic character of the seven-membered ring systems results in interesting excited-state structures. Unlike other systems of similar size, these compounds are colored.[131] For example, azulene, (**3** of Chart 3.3), a nonbenzenoid aromatic compound, is blue, whereas naphthalene, an isomer of azulene, is colorless.[132] Seven-membered nonbenzenoid aromatic compounds (heptafulvenes) have a low energy electronic transition (π–π*). Large changes of the dipole moment upon excitation enhance the electronic properties of these compounds as compared to typical aromatic systems.[13] The extension of the π–electron conjugation or the substitution of sulfur for the exocyclic oxygen atom may significantly decrease the optical gap of these compounds without increasing the overall size of the molecule.[133,134] 8,8-Dicyanophenylheptafulvene derivatives (**4** of Chart 3.3) are highly colored and have attracted attention as chromophores for pigmentary and electronic applications.[135]

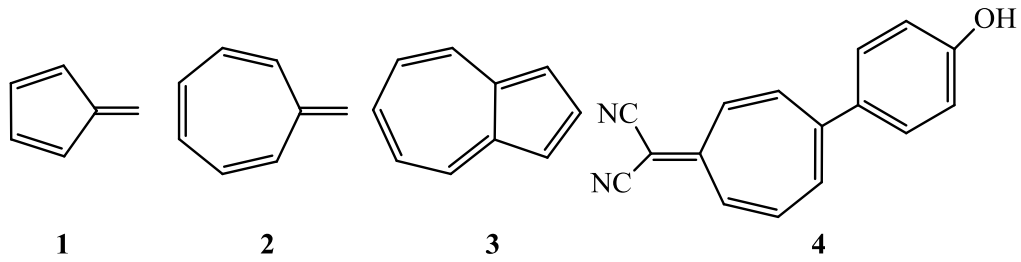

Chart 3.3 Fulvene and heptafulvene derivatives

Cycloheptatrienones, also known as tropones, are stable non-benzenoid aromatic compounds characterized by large dipole moments. Tropone might be represented as a hybrid between **1a** and **1b** as shown in Figure **3.1**. Tropone's high dipole moment (4.3 D) and carbonyl stretch at 1582 cm^{-1} support the importance of the dipolar form.[136,137,138] The most notable contribution of **1b** to the chemical properties of tropone is the reduced reactivity of the carbonyl group toward common carbonyl reagents such as 2,4-dinitrophenylhydrazine, hydroxylamine, hydrazine etc.[139]

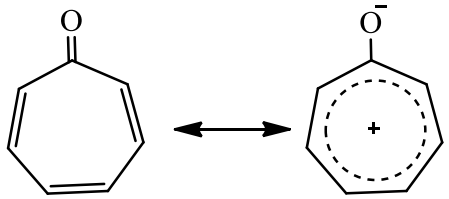

Figure 3.1 Resonance structure of tropone

Small molecules with π–electron delocalization along the main chain are candidates for optoelectronic applications such as transistors, light-emitting diodes and organic photovoltaics. The changing morphology of connecting aromatic rings significantly affects the electronic and optical properties of compounds.[6]

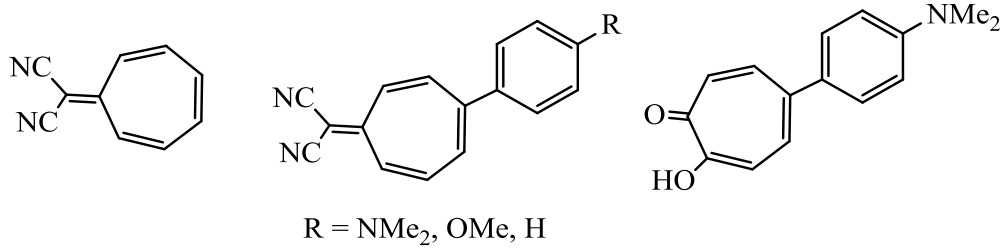

Chart 3.4 Nonlinear optical materials

Several studies have been carried out by the Yuki group on conjugated oligomers and polymers containing benzotropone in the main chain for their potential application in optoelectronic devices. The introduction of benzotropone into the poly(p–phenylenevinylene) (PPV) backbone improved the heat resistance of the material.[140,141,142] The Swager group reported the synthesis of tropone-containing polythiophenes (Chart 3.5), which can gain aromaticity by protonation of carbonyl oxygen. Switching the tropone moiety between nonaromatic and aromatic forms in the conjugated polymer backbones may affect electronic delocalization of the conjugated polymer by conformational change. These phenomena may enable the tuning of desired properties of conjugated polymers for their optoelectronic properties.[143]

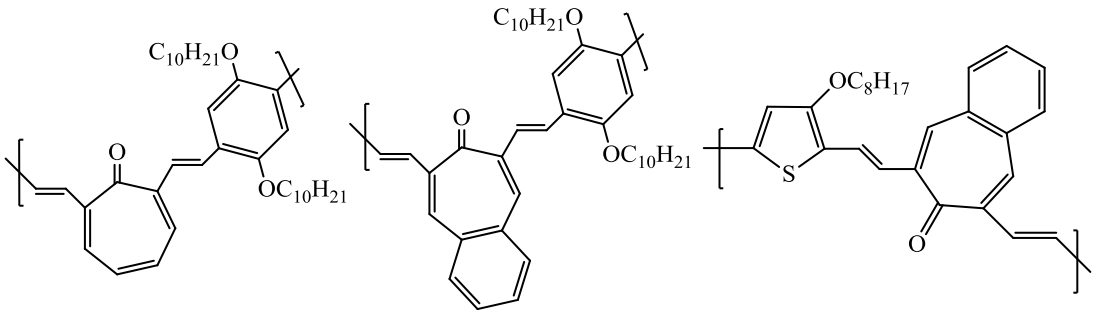

Chart 3.5 Tropone-containing polymers

The introduction of π–donor and π–acceptor substituents on opposite sides of π–conjugated systems such as benzene[123,144,145] and thiophene[126,26] promotes high second–

order hyperpolarizabilities. Similarly, when one end of nonbenzenoid chromophore of tropone is fused with a metallocene donor and the other end is functionalized with a strong acceptor group, the resultant compound demonstrates an unsymmetrical charge distribution. This is one of the most characteristic features of NLO materials. The strength of the donor and acceptor moieties can directly affect the ground and excited state dipole moments and the transition dipole moment. These properties not only change the physical properties of materials but also tune their optical properties and induce a large bathochromic shift.[137, 26] Chart **3.6** shows some of the reported tropone metal complexes.

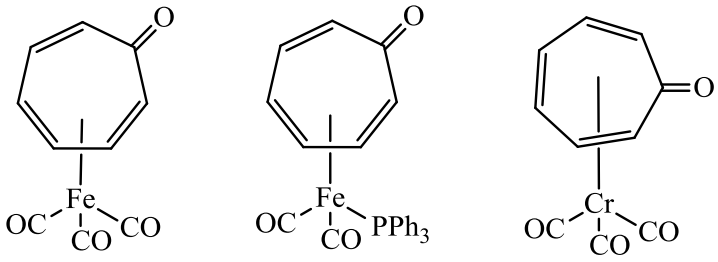

Chart 3.6 Metal tropone complexes[146,147]

For a long period, our group has been exploring metallocene chemistry of 5,5-fused[148] and 5,6-fused[149,150] ring systems. The presence of a metal can allow for control of physical properties, electronic properties, optical properties and redox potential. Therefore, we are interested in potential applications of metallocene-fused tropones (5,7-fused ring system) and their derivatives as organic electronic materials.

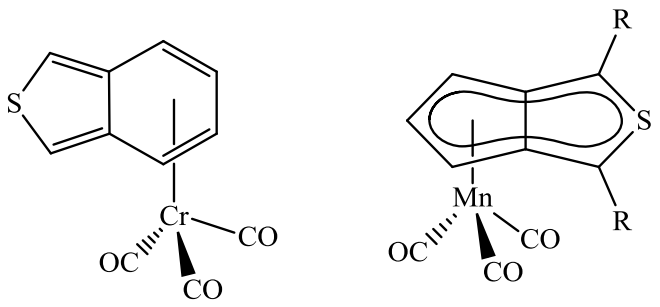

Figure 3.2 5,5– and 5,6–fused complexes synthesized in our group

3.2 Experimental

All reactions were carried out using standard Schlenk techniques under nitrogen atmosphere unless otherwise noted. Solvents (Pharmco Aaper) were dried and distilled under nitrogen before use, including ethyl ether, toluene, and benzene over sodium benzophenone ketyl. Dichloromethane and acetonitrile were dried and distilled over calcium hydride. Acetone (Sigma-Aldrich) was dried in molecular selves for overnight and distilled. Chloroform was dried and distilled over P_2O_5. $CDCl_3$, and CD_2Cl_2 were purchased from Cambridge Isotopes and used without purification. Lawesson's reagent, hydroxylamine (50% aqueous solution) (Sigma-Aldrich), butyllithium (2.5 M), N,N-dimethylformamide, activated manganese dioxide (Acros), anhydrous magnesium sulfate, sodium hydroxide (Fisher), potassium hydroxide (EMD), 1,3-diphenylacetone (Alfa Aesar), and were used without further purification. N,N,N',N-Tetramethylmethylenediamine, N,N-dimethylaminomethylferrocene, N,N-dimethylaminomethyl-2-formylferrocene, and 1,2-diformylferrocene were prepared using the procedure developed by Lednicer and Hauser,[119] Goetgheluck et al.[116] and Malfait et al.[117] Organic phases were dried over anhydrous magnesium sulfate. Flash chromatography was carried out with silica gel (60 Å pore size, 230–400 mesh) from Sorbent Technologies.

^1H and ^{13}C NMR spectra were recorded on a Varian Gemini–400 NMR spectrometer unless otherwise mentioned. Infrared spectra were recorded on an ATI–Mattson Galaxy^{TM} Series 5000 FTIR spectrometer. Electron ionization (EI) mass spectra were collected at 70 eV on a Thermo Finnigan Polaris Q (quadrupole ion trap) at the University of Kentucky Mass Spectrometry Center. Melting points were recorded

(uncorrected) on an Electrothermal Mel-Temp melting point apparatus. X-ray diffraction data were collected at 90 K on either a Nonius KappaCCD diffractometer or a Bruker-Nonius X8 Proteum diffractometer. The structures were solved and refined by using SHELXL-97. UV-visible spectral analyses was performed on an Agilent 8453 Diode Array Spectrophotometer and electrochemistry was performed on a CH Instruments Model 600D Series.

Synthesis of ferrocene-fused tropone (23). 1,2-Diformylferrocene (200 mg, 0.83 mmol) and 3 mL of ethanol were added to an oven-dried 25 mL round bottom flask equipped with a stir bar and cooled under N_2. Acetone (91 µL, 0.80 mmol) was added, followed by 15% KOH (0.03 mL). The solution was stirred at room temperature for 3 h. A dark red solution was obtained. Silica was added into a solution then evaporated the solvent and a slurry was poured onto a column of silica, and then eluted with hexane:ethyl ether (1:1). The solvent was removed under reduced pressure to yield 218 mg (83.0%) of product, and recrystallized by slow diffusion of hexane-saturated N_2 into its ethyl ether solution resulting in red needles. **^{1}H NMR (400 MHz, $CDCl_3$, ppm):** δ 4.09 (s, 5 H, H7), 4.38 (t, 1 H, ^3J = 2.4 Hz, H6), 4.78 (d, 2 H, ^3J = 2.4 Hz, H5), 6.37 (AB, 2 H, J_{AB} = 12 Hz, H2), 7.31 (AB, 2 H, J_{AB} = 12 Hz, H3). **^{13}C{^{1}H} NMR (100 MHz, $CDCl_3$, ppm):** 70.62 (C7), 71.45 (C6), 73.65 (C5), 81.77 (C4), 129.43 (C2, C9), 141.75 (C3), 190.36 (C1). **IR (ATR, cm^{-1}):** 1618 (C=O). **MS (EI):** m/z 264 (M^+). **Mp:** 139 ˚C–140 ˚C.

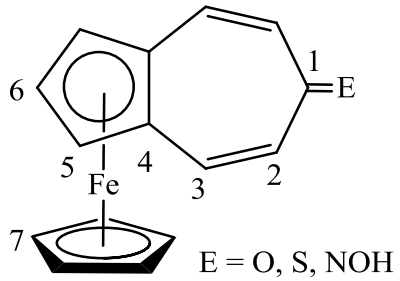

Figure 3.3 Numbering scheme in ferrocene-fused tropone

Synthesis of ferrocene-fused 5,7-diphenyltropone (24a). 1,2-Diformylferrocene (100 mg, 0.41 mmol) and 2 mL of ethanol were added to an oven-dried 25 mL round bottom flask equipped with a stir bar and cooled under N_2. 1,3-Diphenylacetone (86.9 mg, 0.41 mmol) was added, followed by 15% KOH (0.05 mL). The solution was stirred at room temperature overnight. A dark red solution was obtained. Silica was added, the solvent was vacuum-evaporated and the powder was poured onto a column of silica, then eluted with hexane:ethyl ether (7:3). Solvent was removed under reduced pressure to yield 61 mg (**24a**, 36%) of product and recrystallized from ethyl ether and hexane. Further, the second red band was eluted with hexane:ethyl ether (1:1) and evaporation of solvent under reduced pressure yielded a dark red solid (**24b**, 30%). **24b** was characterized by single X-ray crystal structure. **24a: ^{1}H NMR (400 MHz, $CDCl_3$, ppm):** δ 4.11 (s, 5 H, C7), 4.35 (t, 1 H, ^{3}J = 2.4 Hz, C2), 4.79 (d, 2 H, ^{3}J = 2.4 Hz, C1), 7.07–7.39 (m, 5 H, Ph), 7.44 (s, 2 H, C4). **^{13}C{^{1}H} NMR (100 MHz, $CDCl_3$, ppm):** 70.49 (C7), 71.47 (C2), 72.98 (C1), 81.26 (C3a), 127.17, 128.73, 139.15, 139.15 (Ph), 140.38 (C5), 141.61 (C4), 189.98 (C6). **IR (ATR, cm^{-1}):** 1622 (C=O). **MS (EI):** m/z 416 (M^+). **Mp:** 166 ˚C. **24b: ^{1}H NMR (400 MHz, $CDCl_3$, ppm):** δ 3.64–3.65 (m, 1 H, Cp), 4.00 (s, 5 H, C11), 3.94

(H_AH_B, 1 H, $^2J_{AB}$ = 14.8 Hz, H10), 4.17 (H_AH_B, 1 H, $^2J_{AB}$ = 14.4 Hz, H10), 4.47 (t, 1 H, ^3J = 2.4 Hz, Cp), 4.82 (m, 1 H, Cp), 7.05–7.08 (m, 2 H, Ph), 7.30–7.40 (m, 8 H, Ph), 8.31 (s, 1 H, C7) , 10.11 (s, 1 H, H1). **$^{13}C\{^1H\}$ NMR (100 MHz, $CDCl_3$, ppm):** 46.67 (C10), 71.58 (C11), 74.47 (Cp), 74.51 (Cp), 74.73 (Cp), 79.23 (Cp), 79.73 (Cp), 126.97, 128.07, 128.94, 129.44, 129.70, 135.70, 137.27 (Ph), 138.94 (C7), 139.06 (C8), 193.72 (C1), 198.02 (C9).70.49 (C7), 71.47 (C6), 72.98 (C5), 81.26 (C4), 127.17, 128.73, 139.15, 139.15 (Ph), 140.38 (C2), 141.61 (C3), 189.98 (C1). **IR (ATR, cm^{-1}):** 1674, 1650 (C=O).

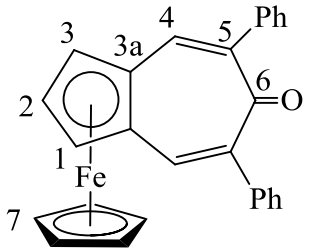

24a

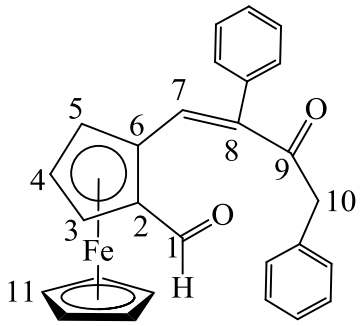

24b

Synthesis of ferrocene-fused 5,7-diphenyl-8-piperidinyl-4-cyclohepten-6-one (25). 1,2-Diformylferrocene (0.05 g, 0.21 mmol), benzene (5 mL) and 1,3-diphenylacetone (69.6 mg 0.33 mmol) were added to an oven-dried 125 mL Schlenk flask cooled under N_2. After stirring, 1 drop of piperidine was added, and the reaction mixture was refluxed with a Dean-Stark trap for 5 h. The reaction mixture was cooled to room temperature and the volume of the solution was reduced by half under a vacuum. The remaining solution was loaded on a silica column and eluted using hexane:ethyl ether (95:5). The first red fraction was evaporated to yield a gummy product (30 mg, 35%). The product was triturated with pentane under liquid N_2 to

yield a red solid (13 mg, 15%). Recrystallization by slow diffusion of hexane-saturated N_2 into its ethyl ether solution resulted in red needles. **^{1}H NMR (400 MHz, acetone-d_6, ppm):** δ 1.12–1.15 (m, 4 H, CH_2 piperidine), 1.70–1.72 (m, 2 H, CH_2 piperidine), 2.46–2.49 (m, 4 H, CH_2 piperidine), 3.60 (d, 1 H, ^3J = 2.4 Hz, H8), 4.03 (s, 5 H, H9), 4.23 (ABC, 1 H, Cp), 4.27 (ABC, 1 H, Cp), 4.35 (ABC, 1 H, Cp), 4.96 (d, 1 H, ^3J = 2.4 Hz, H7), 6.84–7.04 (m, 10 H, Ph), 7.57 (d, 1H, H4),. **^{13}C{^{1}H} NMR (100 MHz, acetone-d_6, ppm):** δ 24.97(*C*H_2 piperidine), 27.22 (*C*H_2 piperidine), 53.30 (*C*H_2 piperidine), 62.65, (C8), 70.20 (Cp), 71.34 (C9), 72.43 (Cp), 74.38 (Cp), 78.01 (Cp), 80.44 (Cp), 86.76 (C7), 127.59, 127.76, 128.40, 128.75, 129.52, 131.22, 138.36, 139.85 (Ph), 141.41 (C4), 200.01 (C6). **IR (ATR, cm^{-1}):** 1670 (CO). **MS (EI)** m/z 501 (M^+). **Mp:** 195 ˚C–206 ˚C (dec). The compound was fully characterized by a single X-ray crystal structure.

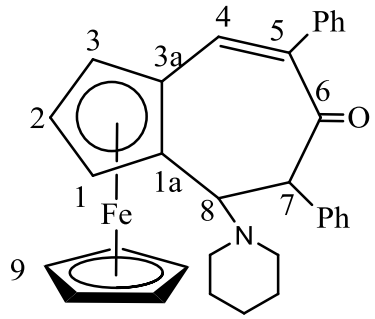

25

Synthesis of ferrocene-fused thiotropone (26). In an oven-dried 100 mL Schlenk equipped with a magnetic stir bar, ferrocene-fused tropone (**23**, 30.0 mg, 0.11 mmol) and dried benzene (10 mL) were added and stirred at room temperature under N_2 to dissolve. Lawesson's reagent (230 mg, 0.57 mmol) was added to the solution. The solution was stirred at room temperature for 7 h. The dark green solution was

loaded onto a column of neutral alumina, then eluted with hexane:dichloromethane (3:7). The first, dark green band was collected. The solvent was evaporated under reduced pressure to yield 20.0 mg (63.0%) of product. The product was recrystallized by dissolving in hot heptanes followed by cooling to −10 °C. **^{1}H NMR (400 MHz, $CDCl_3$, ppm):** δ 4.16 (s, 5 H, H7), 4.43 (t, 1 H, ^{3}J = 2.4 Hz, H6), 4.84 (d, 2 H, ^{3}J = 2.4 Hz, H5), 7.10 (AB, 2 H, $^{3}J_{AB}$ = 11.6 Hz H2), 7.33 (AB, 2 H, $^{3}J_{AB}$ = 11.6 Hz, H3). **^{13}C{^{1}H} NMR (100 MHz, $CDCl_3$, ppm):** 70.79 (C7), 73.02 (C5), 73.67 (C6), 84.36 (C4), 136.64 (C2), 138.98 (C3), 217.62 (C1). **IR (ATR, cm^{-1}):** 1078 (C=S) **MS (EI):** m/z 280 (m^{+}). **Mp:** 265–370˚C (dec).

Synthesis of ferrocene-fused tropone oxime (27). In an oven-dried 100 mL Schlenk equipped with a magnetic stir bar, ferrocene-fused thiotropone (**26**, 62.0 mg, 0.22 mmol) and dried, N_2-purged chloroform (5 mL) were added and cooled to 0 ˚C. A solution of hydroxylamine (0.66 mmol, 20.0 μL) in 1 mL ethanol was added. The reaction solution was stirred at 0 ˚C for 5 h. A dark red solution was evaporated under reduced pressure to obtain a red solid. The solid was triturated with pentane under liquid N_2 and dried under vacuum to give 52.6 mg (83.0%) as a dark red solid. Red needles were obtained by slow diffusion of hexane-saturated N_2 into an ethyl ether solution. The compound was fully characterized by X-ray diffraction. **^{1}H NMR (400 MHz, $CDCl_3$, ppm):** δ 4.09 (s, 5 H, H11), 4.27(ABC, 1 H, Cp), 4.46 (ABC, 1 H, Cp), 4.47 (ABC, 1 H, Cp), 6.09–6.12 (dd, 1 H, J_{dd} = 12 Hz, H2), 6.53 (d, 1 H, ^{3}J = 12.4 Hz, H3), 6.67(d, 1H, ^{3}J = 12 Hz, H9), 6.79–6.83(dd, 1 H, J_{dd} = 12 Hz, H10). **^{13}C{^{1}H} NMR (100 MHz, $CDCl_3$, ppm):** 70.95 (C11), 71.03 (Cp), 72.46 (Cp), 72.79 (Cp), 80.11 (Cp), 81.79 (Cp), 113.59 (C2), 123.73 (C3), 131.86 (C9), 135.98 (C10), 156.28

(C1). **IR (ATR, cm^{-1}):** 1634(C=N), 2936.15–3208.44 (OH). **MS (EI):** m/z 279 (M^+). **Mp:** 150–175 ˚C (dec).

5,7-Diphenylazulenethiol (28). 5,7-Diphenylferrocene-fused tropone (**24a**, 0.03 g , 0.07 mmol), and Lawesson's reagent (206 mg, 0.50 mmol) were added to the dried N_2-purged benzene (10 ml). The reaction mixture was refluxed for 8 h until starting material was consumed (TLC). The reaction solution was poured onto a short column of silica and eluted with hexane:ethyl ether (9:1). The first blue band was collected and removal of the solvent under reduced pressure yielded 13.0 mg (58.0%) as a dark blue solid. The product was recrystallized by slow evaporation of diethyl ether and further characterized by X-ray crystallography. **^{1}H NMR (400 MHz, $CDCl_3$, ppm):** δ 3.88 (s, 1 H, S*H*), 7.20 (d, 2 H, ^3J = 3.6 Hz H5), 7.37–7.47 (m, Ph), 7.75 (t, 1 H, ^3J = 3.6 Hz H6,), 8.18 (s, 2 H, H3). **^{13}C{^{1}H} NMR (100 MHz, $CDCl_3$, ppm):** 119.12 (C2,), 127.76 (C4), 129.48 (C6), 134.10 (C5), 128.92, 135.89, 136.59, 136.69 (Ph), 146.02 (C3), 147.42 (C1). **IR (ATR, cm^{-1}):** 2573.26 (SH). **MS (EI):** m/z 312 (M^+). **Mp:** 130.5–132 ˚C.

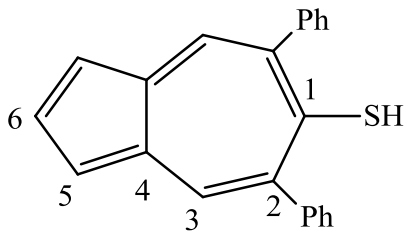

28

3.3 Results and Discussion

3.3.1 Synthesis. Double aldol condensation of 1,2-diformylferrocene with acetone in the presence of base catalyst (KOH) gave the ferrocene-fused tropone (**23**) in 83% yield as dark red needles. The appearance of AB patterns at δ 6.37 (H2) and 7.31 (H3) ppm with a coupling constant (J_{AB} = 12 Hz) in its ^{1}H NMR and a peak at 1618 cm^{-1} in its IR suggest the formation of ferrocene-fused tropone (**23**). The carbonyl stretch of tropone appears at 1582 cm^{-1} in its infrared spectrum, which signifies the high polarizability between carbon and oxygen. Ferrocene-fused tropone was previously reported by Tirouflet but characterized only by the melting point.[151] We characterized the compound **23** with spectroscopic, electronic and optical analysis.

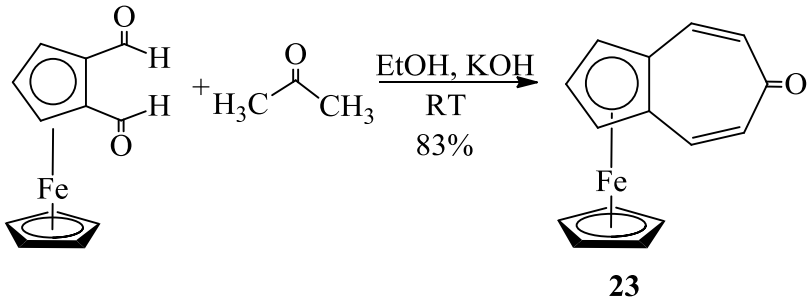

23

Scheme 3.1 Synthesis of ferrocene-fused tropone

Condensation of 1,2-diformylferrocene with 1,3-diphenylacetone in the presence of KOH leads to the aldol condensation product (**24a**) and the mono-aldol product (**24b**) in a 1:1 ratio. Compound **24a** and its methyl derivative were previously reported by Tirouflet but characterized only by melting point. We characterized both compounds by X-ray crystallography. In the presence of piperidine, the condensation of 1,2-diformylferrocene and 1,3-diphenylacetone gave the Michael addition of piperidine to the

tropone (**25**, 15%). The proposed mechanism of the formation of the Michael addition of piperidine to α, β-unsaturated ketone is shown in Scheme 3.4.

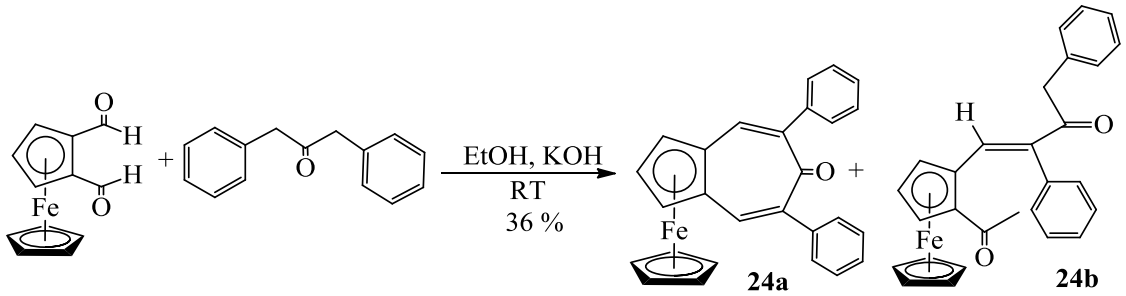

Scheme 3.2 Synthesis of ferrocene-fused–5,7-diphenyltropone

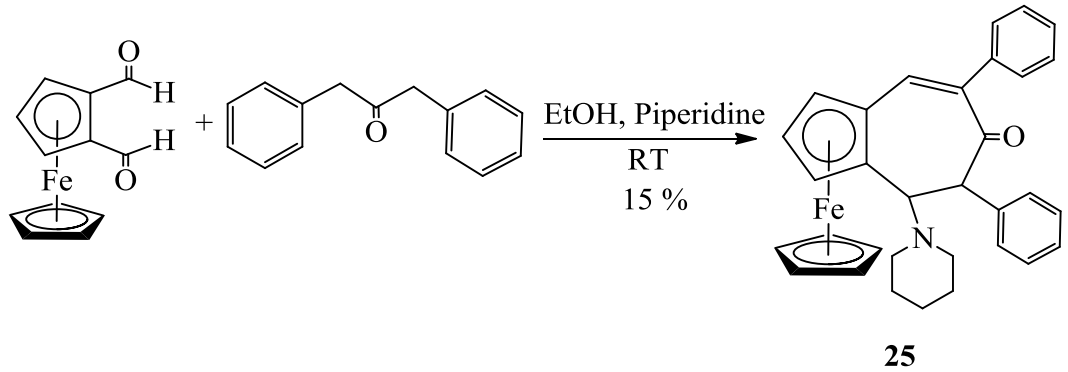

Scheme 3.3 Synthesis of a piperidine adduct of tropone **24a**

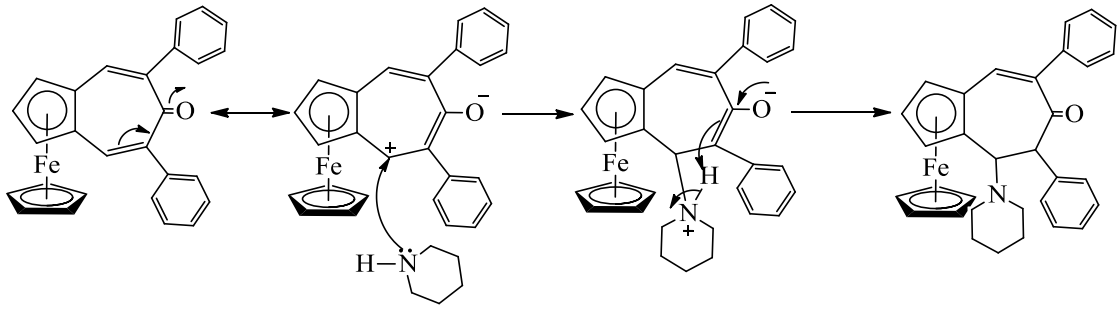

Scheme 3.4 Proposed mechanism for Michael addition of piperidine to tropone **24a**

Several attempts to convert ferrocene-fused tropones **23** and **24a** directly to oximes by reaction with hydroxylamine or hydroxylamine hydrochloride failed. Conditions ranged from $CHCl_3$ at room temperature (no reaction) to refluxing ethanol (decomposition). These results are consistent with the low reactivity of tropone carbonyls with hydroxylamine reported by Machiguhi et al. Tropone **23** was smoothly converted to thiotropone **26** in 63% yield by reaction with Lawesson's reagent in anhydrous benzene at room temperature for 7 h.[152] Thiotropone **26,** dark green in solution and dark blue as a solid, was characterized by spectroscopic analysis and single X-ray crystal analysis. The C=S group of **26** showed an IR absorption at 1078 cm^{-1} and a ^{13}C NMR signal at 217.62 ppm.

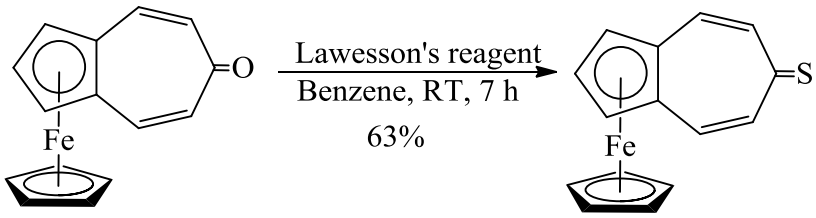

23 **26**

Scheme 3.5 Synthesis of ferrocene-fused thiotropone

In contrast to tropone **23,** thiotropone **26** was readily converted to tropone oxime by using hydroxylamine in anhydrous chloroform at 0 °C.[153] The reaction was apparent from the change of solution color from dark green to deep red over 5 h. A standard, non-chromatographic workup gave **27** as a dark red solid in 83% yield. Single crystals were obtained by slow diffusion of hexane-saturated N_2 through a cannula into an ethyl ether solution.

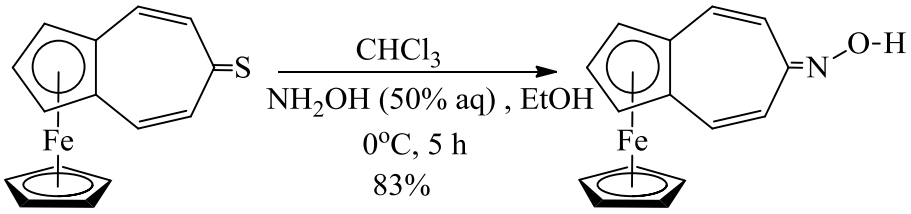

26 **27**

Scheme 3.6 Synthesis of ferrocene-fused tropone oxime

The formation of ferrocene-fused oxime from ferrocene-fused thiotropone shows that nucleophilic attack on ferrocene-fused thiotropone takes place at the carbon center of a thiocarbonyl (C=S) group. Machiguchi et al. rationalized the C–2 attack on tropone and the C–1 attack on thiotropone in terms of frontier–orbital theory. They reported that LUMO in tropone is the pπ component of C–2 or C–7 and whereas the LUMO of thiotropone is π* C=S character. Therefore, nucleophiles attack at the C–2 or C–7 of tropone and C–1 of thiotropone.[154]

Thiation of ferrocene-fused tropone **24a** gave a different result. Tropone **24a** did not react with Lawesson's reagent at temperatures up to 50 °C. At 60 to 80 °C in benzene, **24a** was converted to **28.** The detachment of the thiated ligand from the metal may be due to harsher reaction conditions. Chromatographic workup gave **28** as a purple-blue solid in 45% yield. The ^{1}H NMR reveals a SH peak at δ 3.88 ppm.

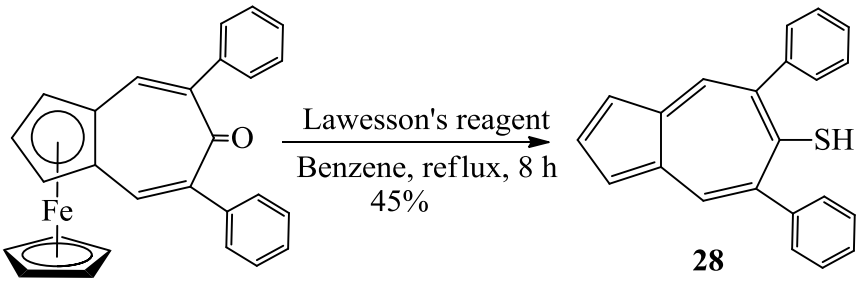

Scheme 3.7 Synthesis of 5,7–diphenylazulenethiol

3.3.2 Spectroscopy. All new complexes were characterized with ^{1}H NMR, ^{13}C NMR, IR and mass spectroscopy. ^{1}H NMR spectra of symmetrically disubstituted **23**, **24a** and **26** display the disubstituted Cp ring as a doublet at 4.78–4.84 ppm for the 2, 4-protons and a triplet at 4.35–4.43 ppm for the 3-proton, confirming a plane of symmetry. The ^{1}H NMR spectra of the unsymmetrically disubstituted Cp ring of **24b**, **25** and **27** exhibit three pseudo-triplets. The unsubstituted Cp resonances in the ^{1}H NMR spectra of **23**–**27** display singlet between 4.03–4.11. ^{13}C NMR spectra of these complexes show a characteristic peak ranging from 156.03 to 217.35 ppm. ^{1}H NMR spectrum of **28** displays disubstituted Cp ring as a doublet at 7.20 ppm for the 1, 3-protons and a triplet at 7.75 ppm for the 2-proton and a characteristic singlet peak for a SH proton at 3.88 ppm. A strong IR stretching of carbonyl groups ranges from 1618 cm^{-1} to 1670 cm^{-1}. The selected spectroscopic data of complexes **23**–**28** are shown in table **3.1**

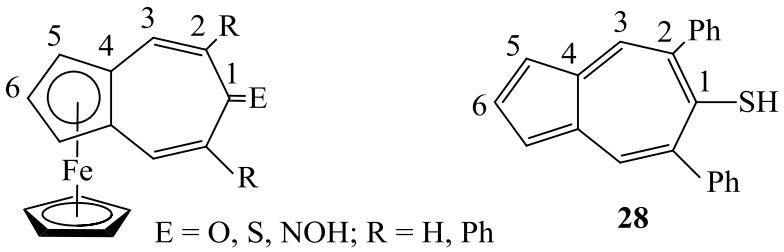

Table 3.1 Selected NMR (ppm, $CDCl_3$) and IR (ATR, cm^{-1}) data of **23**–**28**

	23		**26**		**27**		**24a**		**28**	
	R	E	R	E	R	E	R	E	R	E
	H	O	H	S	H	NOH	Ph	O	Ph	S
H5	4.78		4.84		4.46		4.79		7.24	
H6	4.38		4.43		4.27		4.38		7.75	
H3	7.32		7.33		6.79, 6.53		7.44		8.18	
H2	6.37		7.10		6.81, 6.10		–		–	
C3	142.16		138.75		135.73, 131.61		141.61		146.02	
C2	129.58		136.41		123.00, 113.34		133.99		119.08	
C1	190.67		217.35		156.03		189.98		147.42	
ν(CO)	1618		–		–		1622		–	
ν(CS)	–		1078		–		–		–	
ν(CN)	–		–		1634		–		–	

3.3.3 Structure. The structures of ferrocene-fused tropone and its derivatives [Fe(Cp){η^5-C_5H_3(CHCH)$_2$CO}] **23**, [Fe(Cp){η^5-C_5H_3(CHCPh)$_2$CO}] **24a**, [Fe(Cp){η^5-C_5H_3(CHCHCOCH$_2$PhCHO)}] **24b**, [Fe(Cp){η^5-C_5H_3(CHCPhCOCHPhCHC_5H_{11}N)}] **25**, [Fe(Cp){η^5-C_5H_3(CHCH)$_2$CS}] **26**, [Fe(Cp){η^5-C_5H_3(CHCH)$_2$NOH}] **27** and [C_5H_3(CHCC_6H_5)$_2$CSH] **28** were determined by X–ray crystallographic methods. All the crystals except **26** and **28** were grown by slow evaporation of a concentrated diethyl ether solution in a stream of hexane-saturated N_2 at room temperature, while **26** was grown from its saturated solution in hot heptanes by cooling to –10 °C, and **28** was grown by slow evaporation of a concentrated diethyl ether solution at room temperature. Hydrogen

atoms were placed in geometrically calculated positions. Thermal ellipsoid plots with numbering schemes are shown in figures **3.8**–**3.14**. The crystal structure and refinement data for compounds **23**, **24a**, **24b**, **25**, **26**, **27** and **28** can be found in Tables **3.2**–**3.5**. Bond distances and angles for **23**, **24a**, **24b**, **25**, **26**, **27** and **28** can be found in Tables **3.6**–**3.12**.

The angles between the centroids of two Cp and Fe in **23**, **24a**, **25**, **26** and **27** are 177.99 °, 176.46 °, 176.38 °, 178.03 ° and 178.25 °, which are nearly linear. The average bond distances of iron to the centroids of substituted Cp and unsubstituted Cp are **23** [1.657(16) Å, 1.656(16) Å], **24a** [1.652(3) Å, 1.657(3) Å], **25** [1.642(16) Å, 1.652(16) Å], **26** [1.661(3) Å, 1.655(3) Å] and **27** [1.646(16) Å, 1.648(16) Å]. The average bond distances of iron to the substituted Cp and unsubstituted Cp are **23** [2.055(16) Å, 2.052(16) Å], **24a** [2.051(3) Å, 2.051(3) Å], **25** [2.044(16) Å, 2.057(16) Å], **26** [2.058(3) Å, 2.051(3) Å] and **27** [2.047(16) Å, 2.046(16) Å]. These calculated values demonstrate that the iron center is coordinated evenly between substituted and unsubstituted cyclopentadienyl ligands. The average bond distances of iron to the substituted and unsubstituted Cp ligands of ferrocene–fused tropone derivatives are close to the calculated average bond distances of iron to two Cp ligands of ferrocene, which are 2.048 Å and 2.045 Å.[155]

The interplanar angles between C1–C2–C3-C4-C5-C6-C10 and C7-C8-C9 of the molecules **23**, **24a** and **27** are 20.95 °, 21.94 ° and 7.42 °. The planarity of the cyclopentadienyl ring and seven-membered thiotropone ring in **26** is also supported by the chemical shift of H3 (7.33 ppm) and H2 (7.10 ppm) in the ^{1}H NMR. Moreover, it is also proved by a strong UV absorption at 408 nm [ϵ = 14933 ($M^{-1}cm^{-1}$)] as compared to other ferrocene–fused tropone derivatives. The C8–O1 bond length in **23** and **24a** is

1.238(2) Å and 1.230(4) Å respectively, which is comparatively close to the C–O bond length [1.232(2) Å] reported for 4,5-benzotropone, and in contrast to that in furo[3,4-*d*]tropone [1.242(3) Å]. These values suggest that although all the tropone rings are nearly planar in tropone annulated aromatic compounds, they are deformed into a slightly boat-shaped conformation. The boat conformation in furo[3,4-*d*]tropone is slightly shallower[156] than 4,5-benzotropone, which results in slightly longer C–O bond length. [157] The C8–S1 bond length in **26** is 1.675(3) Å, close to that in thiotropone (1.676(5) Å) which has been reported as indicating the major contribution of polar resonance structure, and in contrast to those in 2,4,6-tri-*t*-butylthiobenzaldehyde (1.596 Å) and in cyclopentadienethione (1.633 Å) whose C=S is not conjugated with the benzene ring.[158,156] Similarly the C8–N1 and N1–O1 bond lengths in ferrocene–fused tropone oxime are 1.309(2) Å and 1.461(2) Å, respectively.

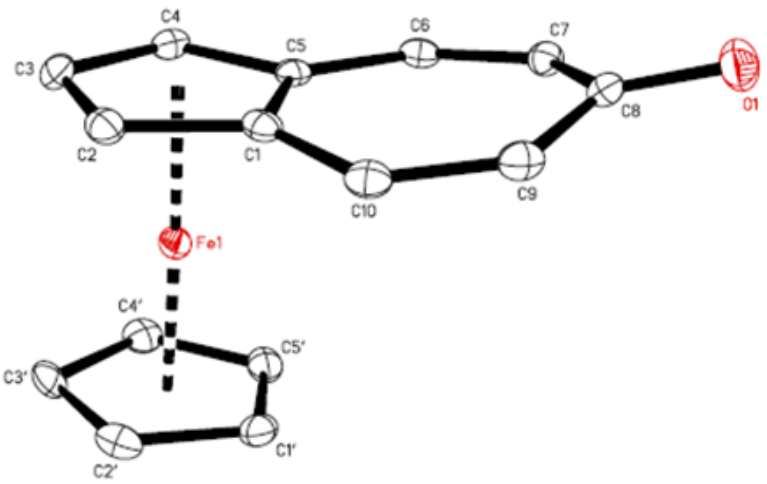

Figure 3.4 Molecular structure of [Fe(Cp){η^5-$C_5H_3(CHCH)_2CO$}] (**23**)

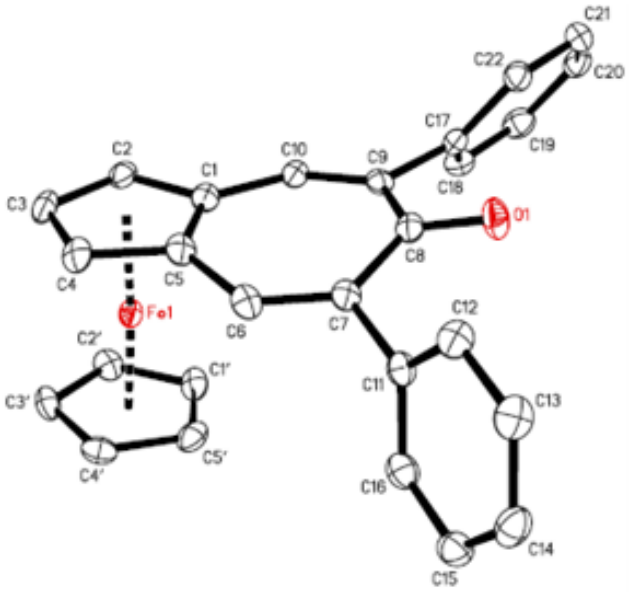

Figure 3.5 Molecular structure of [Fe(Cp){η^5-$C_5H_3(CHCC_6H_5)_2CO$}] (**24a**)

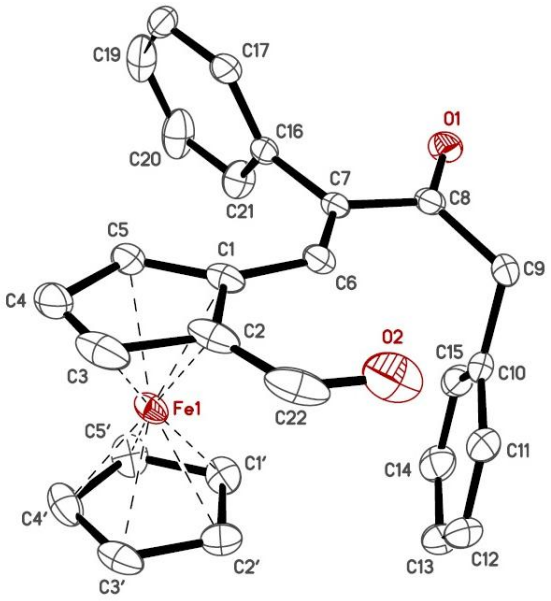

Figure 3.6 Molecular structure of [Fe(Cp){η^5-$C_5H_3(CHCHCOCH_2PhCHO)$}] (**24b**)

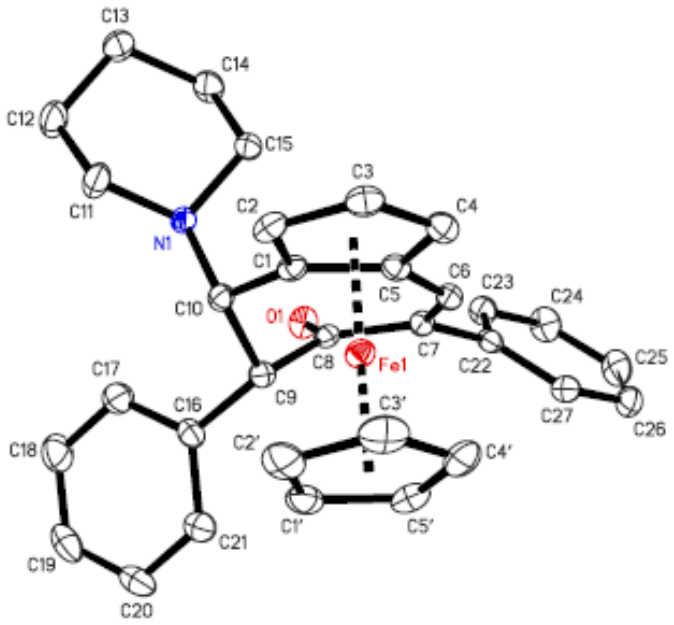

Figure 3.7 Molecular structure of $[Fe(Cp)\{\eta^5C_5H_3(CHCC_6H_5COCHC_6H_5CHC_5H_{10}N)\}$ (**25**)

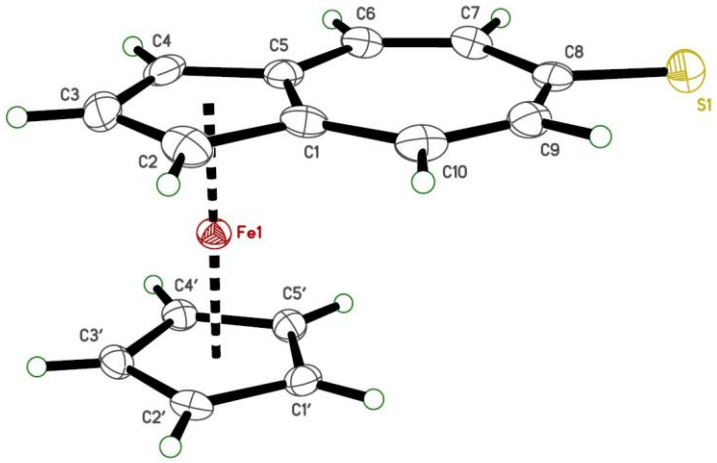

Figure 3.8 Molecular structure of $[Fe(Cp)\{\eta^5\text{-}C_5H_3(CHCH)_2CS\}]$ (**26**)

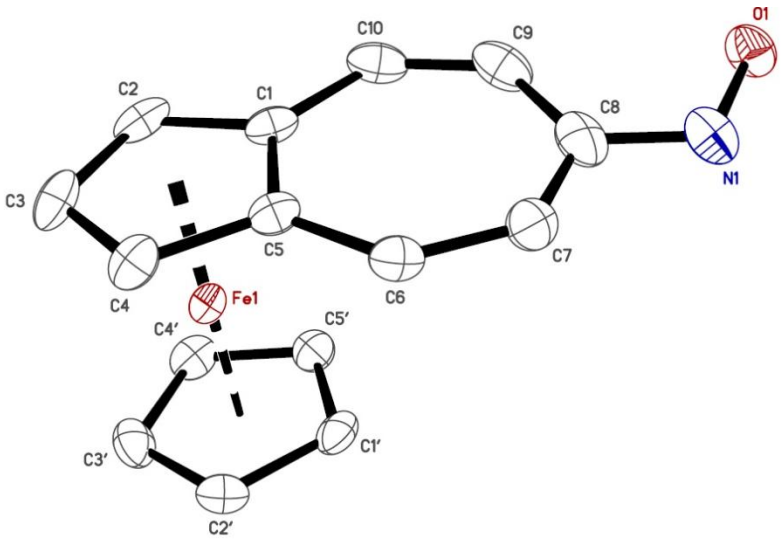

Figure 3.9 Molecular structure of [Fe(Cp){η^5-$C_5H_3(CHCH)_2NOH$}] (**27**)

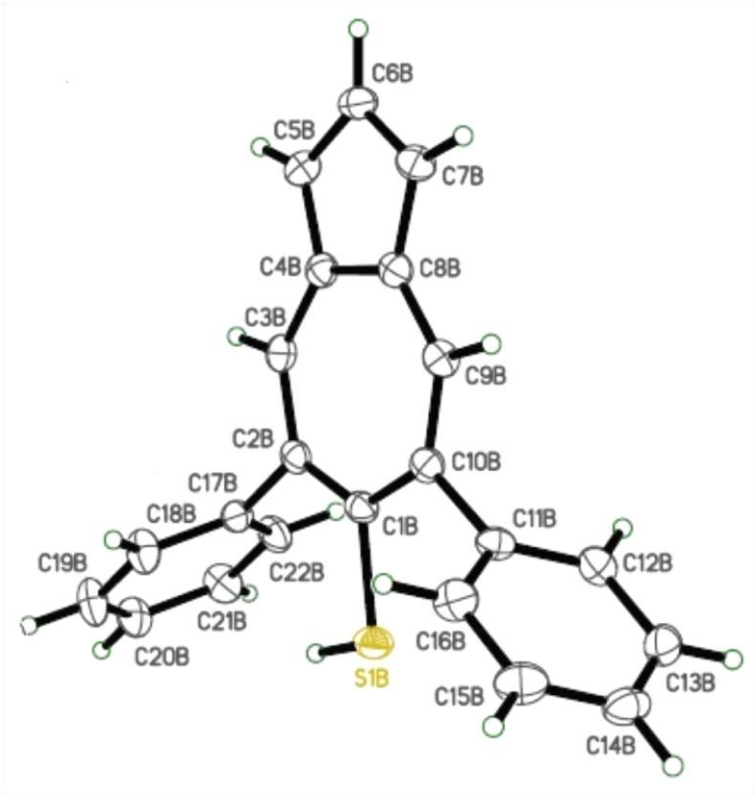

Figure 3.10 Molecular structure of [$C_5H_3(CHCC_6H_5)_2CSH$] (**28**)

Table 3.2 Crystal Data and Structure Refinement for Compounds **23** and **24a**

Compound	**23**	**24a**
Formula	$C_{15}H_{12}FeO$	$C_{27}H_{20}FeO$
Formula wt. (amu)	264.10	416.28
T, K	90.0(2)	90.0(2)
Crystal system	Orthorhombic	Orthorhombic
Space group	P 21	Pbca
Z	4	8
a, Å	6.2602(1)	9.5928(2)
b, Å	7.7079(1)	19.7551(5)
c, Å	22.2233(4)	19.8786(5)
α (deg)	90	90
β (deg)	90	90
γ (deg)	90	90
V, $Å^3$	1072.34(3)	3767.13(16)
d_{calc}, Mg/m^3	1.636	1.468
F(000)	544	1728
Crystal size (mm^3)	0.26 × 0.22 × 0.20	0.22 × 0.10 × 0.01
Radiation	Mo Kα (λ = 0.71073 Å)	Cu Kα (λ = 1.54178 Å)
Monochromator	Graphite	Graded multilayer optics
Absorption coefficient (mm^{-1})	1.381	6.529
Diffractometer	Nonius KappaCCD	Bruker X8 Proteum
Range (deg)	1.83 to 27.50	4.45 to 68.51
Limiting indices	$-8 \le h \le 8$	$-9 \le h \le 11$
	$-9 \le k \le 10$	$-23 \le k \le 23$
	$-28 \le l \le 28$	$-23 \le l \le 23$
Reflections collected	15348	46454
Independent reflections	2445 [R(int) = 0.0380]	3425 [R(int) = 0.0998]
Absorption correction	Semi-empirical from equivalents	Semi-empirical from equivalents
Refinement method	SHELXL-97	SHELXL-97
Refinement method	Full-matrix least-squares on F^2	Full-matrix least-squares on F^2
Data/restraints/parameter	2445 / 0 / 154	3425 / 0 / 262
Goodness-of-fit on F^2	1.130	1.025
Final R indices [$I > 2\sigma(I)$]	R1 = 0.0251, wR2 = 0.0504	R1 = 0.0450, wR2 = 0.1009
R indices (all data)	R1 = 0.0231, wR2 = 0.0513	R1 = 0.391, wR2 = 0.1100
Largest diff. peak and hole	0.360 and -0.321 ($e \cdot Å^{-3}$)	0.391 and -0.475 ($e \cdot Å^{-3}$)

Table 3.3 Crystal Data and Structure Refinement for Compounds **24b** and **25**

Compound	**24b**	**25**
Formula	$C_{27}H_{22}FeO_2$	$C_{32}H_{31}FeNO$
Formula wt. (amu)	434.29	501.43
T, K	90.0(2)	90.0(2)
Crystal system	Monoclinic	Orthorhombic
Space group	P2 (1)/n	Pbca
Z	4	8
a, Å	11.0086(3)	11.3767(1)
b, Å	10.1171(3)	17.2315(2)
c, Å	18.4300(5)	25.3074(4)
α (deg)	90	90
β (deg)	90.153(1)	90
γ (deg)	90	90
V, $Å^3$	2026.51(10)	4961.20(11)
d_{calc}, Mg/m^3	1.423	1.343
F(000)	904	2112
Crystal size (mm^3)	0.110 × 0.080 × 0.075	0.28 × 0.25 × 0.22
Radiation	Cu Kα (λ = 1.54178 Å)	Mo Kα (λ = 0.71073 Å)
Monochromator	Graded multilayer optics	Graphite
Absorption coefficient (mm^{-1})	6.129	0.634
Diffractometer	Bruker X8 Proteum	Nonius KappaCCD
Range (deg)	4.394 to 68.231	2.29 to 27.48
Limiting indices	$-13 \le h \le 12$	$-14 \le h \le 14$
	$-12 \le k \le 12$	$-22 \le k \le 22$
	$-22 \le l \le 13$	$-32 \le l \le 32$
Reflections collected	26789	101012
Independent reflections	3673 [R(int) = 0.0460]	5686 [R(int) = 0.0430]
Absorption correction	Semi-empirical from equivalents	Semi-empirical from equivalents
Refinement method	SHELXL-97	SHELXL-97
Refinement method	Full-matrix least-squares on F^2	Full-matrix least-squares on F^2
Data/restraints/parameter	3673 / 0 / 271	5686 / 0 / 316
Goodness-of-fit on F^2	1.059	1.072
Final R indices [$I > 2\sigma(I)$]	R1 = 0.0323, wR2 = 0.0891	R1 = 0.0361, wR2 = 0.0922
R indices (all data)	R1 = 0.0330, wR2 = 0.0897	R1 = 0.0455, wR2 = 0.0978
Largest diff. peak and hole	0.300 and -0.418 ($e \cdot Å^{-3}$)	0.626 and -0.416 ($e \cdot Å^{-3}$)

Table 3.4 Crystal Data and Structure Refinement for Compounds **26** and **27**

Compound	**26**	**27**
Formula	$C_{15}H_{12}FeS$	$C_{15}H_{13}FeNO$
Formula wt. (amu)	280.16	279.11
T, K	90.0(2)	90.0(2)
Crystal system	Monoclinic	Monoclinic
Space group	*P* 21/c	*P* 21/c
Z	4	4
a, Å	7.5644(1)	12.9022(2)
b, Å	15.3150(3)	7.6993(1)
c, Å	10.3756(2)	12.0275(2)
α (deg)	90	90
β (deg)	108.373(1)	100.0684(6)
γ (deg)	90	90
V, $Å^3$	1140.73(4)	1176.39(3)
d_{calc}, Mg/m^3	1.631	1.576
F(000)	576	576
Crystal size (mm^3)	0.200 ×0.080 × 0.020	0.300 × 0.200 × 0.130
Radiation	Cu Kα (λ = 1.54178 Å)	Cu Kα (λ = 1.54178 Å)
Monochromator	Graded multilayer optics	Graded multilayer optics
Absorption coefficient (mm^{-1})	1.202	1.266
Diffractometer	Bruker X8 Proteum	Bruker X8 Proteum
Range (deg)	5.341 to 67.892	1.603 to 27.492
Limiting indices	$-7 \leq h \leq 9$	$-16 \leq h \leq 16$
	$-18 \leq k \leq 12$	$-9 \leq k \leq 10$
	$-12 \leq l \leq 12$	$-15 \leq l \leq 15$
Reflections collected	13325	23080
Independent reflections	2053 [R(int) = 0.0456]	2692 [R(int) = 0.0407]
Absorption correction	Semi-empirical from equivalents	Semi-empirical from equivalents
Refinement method	SHELXL-97	SHELXL-97
Refinement method	Full-matrix least-squares on F^2	Full-matrix least-squares on F^2
Data/restraints/parameter	2053 / 0 / 154	2692 / 0 / 199
Goodness-of-fit on F^2	1.036	1.052
Final R indices [$I > 2\sigma(I)$]	R1 = 0.0336, wR2 = 0.0816	R1 = 0.0260, wR2 = 0.0608
R indices (all data)	R1 = 0.0386, wR2 = 0.0853	R1 = 0.0341, wR2 = 0.0635
Largest diff. peak and hole	0.580 and -0.361($e \cdot Å^{-3}$)	0.338 and -0.365 ($e \cdot Å^{-3}$)

Table 3.5 Crystal Data and Structure Refinement for Compound **28**

Compound	**28**
Formula	$C_{22}H_{16}S$
Formula wt. (amu)	312.41
T, K	90.0(2)
Crystal system	Monoclinic
Space group	*P* 21/n
Z	8
a, Å	16.4756(4)
b, Å	9.5813(2)
c, Å	21.5374(5)
α (deg)	90
β (deg)	104.617(1)
γ (deg)	90
V, Å^3	3289.80(13)
d_{calc}, Mg/m^3	1.262
F(000)	1312
Crystal size (mm^3)	0.200 × 0.180 × 0.030
Radiation	Cu Kα (λ = 1.54178 Å)
Monochromator	Graded multilayer optics
Absorption coefficient (mm^{-1})	1.692
Diffractometer	Bruker X8 Proteum
Range (deg)	3.035 to 67.994
Limiting indices	$-19 \leq h \leq 19$
	$-11 \leq k \leq 4$
	$-25 \leq l \leq 25$
Reflections collected	39708
Independent reflections	5705 [R(int) = 0.0386]
Absorption correction	Semi-empirical from equivalents
Refinement method	SHELXL-97
Refinement method	Full-matrix least-squares on F^2
Data/restraints/parameter	5705 / 0 / 421
Goodness-of-fit on F^2	1.073
Final R indices [$I > 2\sigma(I)$]	R1 = 0.0390, wR2 = 0.0984
R indices (all data)	R1 = 0.0451, wR2 = 0.1036
Largest diff. peak and hole	0.292 and -0.274 (e·Å^{-3})

Table 3.6 Bond Distances (Å) and Bond Angles (°) for Compound **23**

Atoms	**Distances (Å)**
Fe1–C2	2.0418(17)
Fe1–C2'	2.0440(18)
Fe1–C1'	2.0498(17)
Fe1–C3'	2.0508(16)
Fe1–C1	2.0521(16)
Fe1–C4'	2.0537(17)
Fe1–C4	2.0575(17)
Fe1–C3	2.0582(16)
Fe1–C5'	2.0606(18)
Fe1–C5	2.0662(17)
O1–C8	1.238(2)
C1–C5	1.441(2)
C1–C2	1.442(2)
C1–C10	1.442(2)
C2–C3	1.416(2)
C3–C4	1.416(2)
C4–C5	1.433(2)
C5–C6	1.440(2)
C6–C7	1.348(2)
C7–C8	1.468(2)
C8–C9	1.468(2)
C9–C10	1.350(2)
C1'–C2'	1.415(3)
C1'–C5'	1.424(3)
C2'–C3'	1.430(3)
C3'–C4'	1.425(3)
C4'–C5'	1.424(2)
Atoms	**Angle (°)**
C2–Fe1–C2'	105.86(7)
C2–Fe1–C1'	126.38(7)
C2'–Fe1–C1'	40.45(7)
C2–Fe1–C3'	116.82(7)
C2'–Fe1–C3'	40.88(7)
C1'–Fe1–C3'	68.32(7)
C2–Fe1–C1	41.24(7)
C2'–Fe1–C1	118.25(7)
C1'–Fe1–C1	108.33(7)
C3'–Fe1–C1	151.99(7)
C2–Fe1–C4'	151.61(7)
C2'–Fe1–C4'	68.50(8)
C1'–Fe1–C4'	68.27(8)
C3'–Fe1–C4'	40.64(7)
C1–Fe1–C4'	166.20(7)
C2–Fe1–C4	68.49(7)
C2'–Fe1–C4	163.14(7)
C1'–Fe1–C4	155.39(7)
C3'–Fe1–C4	126.10(7)
C1–Fe1–C4	68.70(7)
C4'–Fe1–C4	108.45(7)
C2–Fe1–C3	40.40(7)
C2'–Fe1–C3	125.44(8)
C1'–Fe1–C3	163.32(7)
C3'–Fe1–C3	106.50(7)
C1–Fe1–C3	68.32(7)
C4'–Fe1–C3	118.87(8)
C4–Fe1–C3	40.24(7)
C2–Fe1–C5'	165.23(7)
C2'–Fe1–C5'	68.21(8)
C1'–Fe1–C5'	40.54(8)
C3'–Fe1–C5'	68.22(7)
C1–Fe1–C5'	128.39(7)
C4'–Fe1–C5'	40.50(7)
C4–Fe1–C5'	121.01(8)
C3–Fe1–C5'	153.99(7)
C2–Fe1–C5	68.91(7)
C2'–Fe1–C5	153.88(7)
C1'–Fe1–C5	120.97(7)
C3'–Fe1–C5	164.73(7)
C1–Fe1–C5	40.95(7)

Table 3.6 Continued

C4'–Fe1–C5	128.26(7)
C4–Fe1–C5	40.68(7)
C3–Fe1–C5	67.99(7)
C5'–Fe1–C5	110.07(7)
C5–C1–C2	107.49(15)
C5–C1–C10	127.50(16)
C2–C1–C10	125.00(16)
C5–C1–Fe1	70.05(9)
C2–C1–Fe1	69.00(9)
C10–C1–Fe1	125.31(13)
C3–C2–C1	107.73(15)
C3–C2–Fe1	70.42(10)
C1–C2–Fe1	69.76(10)
C2–C3–C4	109.10(15)
C2–C3–Fe1	69.18(10)
C4–C3–Fe1	69.85(10)
C3–C4–C5	108.07(15)
C3–C4–Fe1	69.91(10)
C5–C4–Fe1	69.99(10)
C4–C5–C6	124.99(16)
C4–C5–C1	107.58(15)
C6–C5–C1	127.42(15)
C4–C5–Fe1	69.33(10)
C6–C5–Fe1	127.86(12)

C1–C5–Fe1	69.00(9)
C7–C6–C5	129.09(16)
C6–C7–C8	130.22(16)
O1–C8–C7	117.75(16)
O1–C8–C9	118.26(16)
C7–C8–C9	123.91(15)
C10–C9–C8	130.20(16)
C9–C10–C1	128.79(16)
C2'–C1'–C5'	108.31(16)
C2'–C1'–Fe1	69.56(10)
C5'–C1'–Fe1	70.14(10)
C1'–C2'–C3'	108.04(17)
C1'–C2'–Fe1	70.00(10)
C3'–C2'–Fe1	69.81(10)
C4'–C3'–C2'	107.73(16)
C4'–C3'–Fe1	69.79(9)
C2'–C3'–Fe1	69.30(9)
C5'–C4'–C3'	108.02(17)
C5'–C4'–Fe1	70.01(10)
C3'–C4'–Fe1	69.57(9)
C4'–C5'–C1'	107.89(16)
C4'–C5'–Fe1	69.49(10)
C1'–C5'–Fe1	69.32(10)

Table 3.7 Bond Distances (Å) and Bond Angles (°) for Compound **24a**

Atoms	**Distances (Å)**
Fe1–C4	2.040(3)
Fe1–C3'	2.043(3)
Fe1–C4'	2.047(3)
Fe1–C3	2.047(3)
Fe1–C5	2.049(3)
Fe1–C2	2.049(3)
Fe1–C5'	2.049(3)
Fe1–C2'	2.053(3)
Fe1–C1'	2.061(3)
Fe1–C1	2.069(3)
O1–C8	1.230(4)
C1'–C2'	1.418(4)
C1'–C5'	1.419(5)
C1–C2	1.429(4)
C1–C5	1.440(4)
C1–C10	1.441(4)
C2'–C3'	1.420(4)
C2–C3	1.417(4)
C3'–C4'	1.430(4)
C3–C4	1.423(4)
C4–C5	1.434(4)
C4'–C5'	1.420(4)
C5–C6	1.431(4)
C6–C7	1.350(4)
C7–C8	1.484(4)
C7–C11	1.495(4)
C8–C9	1.495(4)
C9–C10	1.352(4)
C9–C17	1.496(4)
C11–C16	1.387(4)
C11–C12	1.400(4)
C12–C13	1.385(4)
C13–C14	1.390(5)
C14–C15	1.378(4)
C15–C16	1.386(4)
C17–C18	1.393(4)
C17–C22	1.403(4)
C18–C19	1.389(4)
C19–C20	1.378(5)
C20–C21	1.385(5)
C21–C22	1.384(4)
Atoms	**Angle (°)**
C4–Fe1–C3'	114.42(12)
C4–Fe1–C4'	105.05(13)
C3'–Fe1–C4'	40.92(12)
C4–Fe1–C3	40.76(12)
C3'–Fe1–C3	104.81(12)
C4'–Fe1–C3	125.15(13)
C4–Fe1–C5	41.05(12)
C3'–Fe1–C5	149.25(12)
C4'–Fe1–C5	116.87(13)
C3–Fe1–C5	68.78(12)
C4–Fe1–C2	68.49(13)
C3'–Fe1–C2	126.69(12)
C4'–Fe1–C2	163.73(12)
C3–Fe1–C2	40.46(12)
C5–Fe1–C2	68.75(12)
C4–Fe1–C5'	127.48(13)
C3'–Fe1–C5'	68.46(12)
C4'–Fe1–C5'	40.58(13)
C3–Fe1–C5'	164.13(13)
C5–Fe1–C5'	109.18(12)
C2–Fe1–C5'	154.81(13)
C4–Fe1–C2'	148.99(12)
C3'–Fe1–C2'	40.55(12)
C4'–Fe1–C2'	68.25(13)
C3–Fe1–C2'	116.92(12)
C5–Fe1–C2'	169.27(12)

Table 3.7 Continued

C2–Fe1–C2'	109.11(13)
C5'–Fe1–C2'	67.98(13)
C4–Fe1–C1'	167.07(13)
C3'–Fe1–C1'	68.22(12)
C4'–Fe1–C1'	68.13(13)
C3–Fe1–C1'	152.15(13)
C5–Fe1–C1'	130.97(12)
C2–Fe1–C1'	121.00(13)
C5'–Fe1–C1'	40.38(13)
C2'–Fe1–C1'	40.32(12)
C4–Fe1–C1	68.66(12)
C3'–Fe1–C1	166.32(13)
C4'–Fe1–C1	152.69(12)
C3–Fe1–C1	68.28(12)
C5–Fe1–C1	40.94(12)
C2–Fe1–C1	40.60(11)
C5'–Fe1–C1	121.22(12)
C2'–Fe1–C1	130.78(12)
C1'–Fe1–C1	112.00(12)
C2'–C1'–C5'	107.9(3)
C2'–C1'–Fe1	69.55(17)
C5'–C1'–Fe1	69.38(17)
C2–C1–C5	107.5(3)
C2–C1–C10	125.6(3)
C5–C1–C10	126.9(3)
C2–C1–Fe1	68.95(16)
C5–C1–Fe1	68.77(16)
C10–C1–Fe1	128.2(2)
C1'–C2'–C3'	108.4(3)
C1'–C2'–Fe1	70.13(17)
C3'–C2'–Fe1	69.35(17)
C3–C2–C1	108.6(3)
C3–C2–Fe1	69.69(17)
C1–C2–Fe1	70.45(17)
C2'–C3'–C4'	107.6(3)

C2'–C3'–Fe1	70.09(17)
C4'–C3'–Fe1	69.66(17)
C2–C3–C4	108.3(3)
C2–C3–Fe1	69.85(17)
C4–C3–Fe1	69.35(17)
C3–C4–C5	108.2(3)
C3–C4–Fe1	69.89(17)
C5–C4–Fe1	69.80(16)
C5'–C4'–C3'	107.8(3)
C5'–C4'–Fe1	69.82(18)
C3'–C4'–Fe1	69.42(18)
C6–C5–C4	124.9(3)
C6–C5–C1	127.2(3)
C4–C5–C1	107.5(3)
C6–C5–Fe1	119.8(2)
C4–C5–Fe1	69.15(16)
C1–C5–Fe1	70.29(16)
C1'–C5'–C4'	108.3(3)
C1'–C5'–Fe1	70.24(18)
C4'–C5'–Fe1	69.60(18)
C7–C6–C5	130.1(3)
C6–C7–C8	128.4(3)
C6–C7–C11	116.9(3)
C8–C7–C11	114.7(2)
O1–C8–C7	117.0(3)
O1–C8–C9	118.5(3)
C7–C8–C9	124.3(3)
C10–C9–C8	128.1(3)
C10–C9–C17	117.0(3)
C8–C9–C17	114.9(2)
C9–C10–C1	130.6(3)
C16–C11–C12	118.4(3)
C16–C11–C7	119.2(3)
C12–C11–C7	122.4(3)
C13–C12–C11	120.6(3)

Table 3.7 Continued

C12–C13–C14	120.0(3)
C15–C14–C13	119.7(3)
C14–C15–C16	120.2(3)
C15–C16–C11	121.0(3)
C18–C17–C22	118.1(3)
C18–C17–C9	120.4(3)
C22–C17–C9	121.2(3)
C19–C18–C17	120.8(3)
C20–C19–C18	120.6(3)
C19–C20–C21	119.2(3)
C22–C21–C20	120.8(3)
C21–C22–C17	120.5(3)

Table 3.8 Bond Distances (Å) and Bond Angles (°) for Compound **24b**

Atoms	**Distances (Å)**
Fe1–C2	2.0246(18)
Fe1–C3	2.0312(19)
Fe1–C5'	2.0413(18)
Fe1–C1	2.0450(16)
Fe1–C4'	2.0471(17)
Fe1–C3'	2.0537(17)
Fe1–C5	2.0540(18)
Fe1–C1'	2.0548(18)
Fe1–C4	2.0573(19)
Fe1–C2'	2.0595(18)
O1–C8	1.222(2)
O2–C22	1.213(3)
C1–C5	1.434(3)
C1–C6	1.454(2)
C1–C2	1.457(2)
C2–C3	1.435(3)
C2–C22	1.451(3)
C3–C4	1.411(3)
C4–C5	1.426(3)
C6–C7	1.346(2)
C7–C16	1.488(2)
C7–C8	1.491(2)
C8–C9	1.519(2)
C9–C10	1.515(2)
C10–C15	1.391(3)
C10–C11	1.393(2)
C11–C12	1.382(3)
C12–C13	1.382(3)
C13–C14	1.386(3)
C14–C15	1.389(3)
C16–C21	1.386(3)
C16–C17	1.390(2)
C17–C18	1.404(3)
C18–C19	1.381(3)
C19–C20	1.358(3)
C20–C21	1.390(3)
C1'–C5'	1.420(3)
C1'–C2'	1.425(3)
C2'–C3'	1.420(3)
C3'–C4'	1.414(3)
C4'–C5'	1.425(3)
Atoms	**Angle (°)**
C2–Fe1–C3	41.43(8)
C2–Fe1–C5'	162.65(8)
C3–Fe1–C5'	153.70(9)
C2–Fe1–C1	41.96(7)
C3–Fe1–C1	69.97(7)
C5'–Fe1–C1	123.46(7)
C2–Fe1–C4'	155.95(7)
C3–Fe1–C4'	119.15(8)
C5'–Fe1–C4'	40.80(7)
C1–Fe1–C4'	159.75(8)
C2–Fe1–C3'	122.22(7)
C3–Fe1–C3'	107.59(8)
C5'–Fe1–C3'	68.33(8)
C1–Fe1–C3'	158.63(8)
C4'–Fe1–C3'	40.35(8)
C2–Fe1–C5	69.24(8)
C3–Fe1–C5	68.70(8)
C5'–Fe1–C5	105.57(8)
C1–Fe1–C5	40.95(7)
C4'–Fe1–C5	122.40(8)
C3'–Fe1–C5	159.46(8)
C2–Fe1–C1'	126.75(8)
C3–Fe1–C1'	164.21(9)
C5'–Fe1–C1'	40.57(7)
C1–Fe1–C1'	107.97(7)
C4'–Fe1–C1'	68.31(7)
C3'–Fe1–C1'	68.30(7)
C5–Fe1–C1'	120.64(8)
C2–Fe1–C4	68.80(9)
C3–Fe1–C4	40.38(10)
C5'–Fe1–C4	118.71(9)

Table 3.8 Continued

C1–Fe1–C4	69.00(7)
C4'–Fe1–C4	105.41(8)
C3'–Fe1–C4	123.66(8)
C5–Fe1–C4	40.59(7)
C1'–Fe1–C4	154.70(9)
C2–Fe1–C2'	110.01(8)
C3–Fe1–C2'	126.65(9)
C5'–Fe1–C2'	68.07(8)
C1–Fe1–C2'	123.15(7)
C4'–Fe1–C2'	67.84(8)
C3'–Fe1–C2'	40.39(8)
C5–Fe1–C2'	157.40(7)
C1'–Fe1–C2'	40.53(7)
C4–Fe1–C2'	161.73(8)
C5–C1–C6	129.94(16)
C5–C1–C2	106.55(15)
C6–C1–C2	123.25(16)
C5–C1–Fe1	69.86(9)
C6–C1–Fe1	122.07(12)
C2–C1–Fe1	68.27(9)
C3–C2–C22	123.65(18)
C3–C2–C1	107.83(17)
C22–C2–C1	128.19(18)
C3–C2–Fe1	69.53(11)
C22–C2–Fe1	121.11(13)
C1–C2–Fe1	69.77(9)
C4–C3–C2	108.26(16)
C4–C3–Fe1	70.81(11)
C2–C3–Fe1	69.04(10)
C3–C4–C5	108.67(18)
C3–C4–Fe1	68.81(11)
C5–C4–Fe1	69.58(11)
C4–C5–C1	108.68(17)
C4–C5–Fe1	69.83(11)
C1–C5–Fe1	69.19(10)

C7–C6–C1	128.84(16)
C6–C7–C16	124.55(15)
C6–C7–C8	119.61(15)
C16–C7–C8	115.84(14)
O1–C8–C7	120.47(15)
O1–C8–C9	119.81(15)
C7–C8–C9	119.68(14)
C10–C9–C8	112.42(13)
C15–C10–C11	118.53(16)
C15–C10–C9	120.73(15)
C11–C10–C9	120.73(17)
C12–C11–C10	120.72(18)
C11–C12–C13	120.49(18)
C12–C13–C14	119.43(18)
C13–C14–C15	120.22(19)
C14–C15–C10	120.59(17)
C21–C16–C17	119.04(17)
C21–C16–C7	119.48(15)
C17–C16–C7	121.48(16)
C16–C17–C18	119.39(19)
C19–C18–C17	120.23(19)
C20–C19–C18	120.45(18)
C19–C20–C21	120.0(2)
C16–C21–C20	120.92(19)
O2–C22–C2	127.06(18)
C5'–C1'–C2'	107.55(16)
C5'–C1'–Fe1	69.2(1)
C2'–C1'–Fe1	69.91(10)
C3'–C2'–C1'	108.32(16)
C3'–C2'–Fe1	69.58(11)
C1'–C2'–Fe1	69.56(10)
C4'–C3'–C2'	107.91(16)
C4'–C3'–Fe1	69.58(10)
C2'–C3'–Fe1	70.02(10)
C3'–C4'–C5'	108.16(16)

Table 3.8 Continued

C3'–C4'–Fe1	70.07(10)
C5'–C4'–Fe1	69.38(10)
C1'–C5'–C4'	108.06(17)
C1'–C5'–Fe1	70.23(10)
C4'–C5'–Fe1	69.82(10)

Table 3.9 Bond Distances (Å) and Bond Angles (°) for Compound **25**

Atoms	**Distances (Å)**
Fe1–C4	2.0355(16)
Fe1–C4'	2.0388(17)
Fe1–C3'	2.0429(17)
Fe1–C3	2.0438(16)
Fe1–C2	2.0449(16)
Fe1–C2'	2.0462(17)
Fe1–C1	2.0476(15)
Fe1–C5	2.0494(15)
Fe1–C5'	2.0526(17)
Fe1–C1'	2.0572(17)
N1–C11	1.463(2)
N1–C15	1.4701(19)
N1–C10	1.481(2)
O1–C8	1.2156(19)
C1–C2	1.428(2)
C1–C5	1.449(2)
C1–C10	1.496(2)
C2–C3	1.424(2)
C3–C4	1.419(2)
C4–C5	1.440(2)
C5–C6	1.451(2)
C1'–C5'	1.417(2)
C1'–C2'	1.422(2)
C2'–C3'	1.423(3)
C3'–C4'	1.424(3)
C4'–C5'	1.425(3)
C6–C7	1.356(2)
C7–C22	1.491(2)
C7–C8	1.501(2)
C8–C9	1.529(2)
C9–C16	1.516(2)
C9–C10	1.560(2)
C11–C12	1.524(2)
C12–C13	1.520(2)
C13–C14	1.521(2)
C14–C15	1.527(2)
C16–C17	1.393(2)
C16–C21	1.394(2)
C17–C18	1.394(2)
C18–C19	1.387(3)
C19–C20	1.384(3)
C20–C21	1.393(2)
C22–C23	1.399(2)
C22–C27	1.400(2)
C23–C24	1.392(2)
C24–C25	1.388(3)
C25–C26	1.388(3)
C26–C27	1.389(2)
Atoms	**Angle (°)**
C4–Fe1–C4'	105.69(7)
C4–Fe1–C3'	118.86(7)
C4'–Fe1–C3'	40.85(8)
C4–Fe1–C3	40.72(6)
C4'–Fe1–C3	120.33(7)
C3'–Fe1–C3	103.42(7)
C4–Fe1–C2	68.61(6)
C4'–Fe1–C2	156.75(7)
C3'–Fe1–C2	120.62(7)
C3–Fe1–C2	40.77(6)
C4–Fe1–C2'	154.77(7)
C4'–Fe1–C2'	68.48(8)
C3'–Fe1–C2'	40.71(7)
C3–Fe1–C2'	119.46(7)
C2–Fe1–C2'	106.56(7)
C4–Fe1–C1	69.44(6)
C4'–Fe1–C1	160.34(7)
C3'–Fe1–C1	158.40(7)
C3–Fe1–C1	69.13(6)
C2–Fe1–C1	40.83(6)
C2'–Fe1–C1	124.06(7)
C4–Fe1–C5	41.27(6)
C4'–Fe1–C5	122.55(7)
C3'–Fe1–C5	156.61(7)

Table 3.9 Continued

C3–Fe1–C5	69.10(6)
C2–Fe1–C5	68.92(6)
C2'–Fe1–C5	162.20(7)
C1–Fe1–C5	41.42(6)
C4–Fe1–C5'	124.36(7)
C4'–Fe1–C5'	40.77(7)
C3'–Fe1–C5'	68.50(7)
C3–Fe1–C5'	158.51(7)
C2–Fe1–C5'	160.44(7)
C2'–Fe1–C5'	68.15(7)
C1–Fe1–C5'	125.36(7)
C5–Fe1–C5'	110.02(7)
C4–Fe1–C1'	162.11(7)
C4'–Fe1–C1'	68.34(7)
C3'–Fe1–C1'	68.41(7)
C3–Fe1–C1'	156.99(7)
C2–Fe1–C1'	123.56(7)
C2'–Fe1–C1'	40.55(7)
C1–Fe1–C1'	110.18(7)
C5–Fe1–C1'	126.60(7)
C5'–Fe1–C1'	40.33(7)
C11–N1–C15	109.70(13)
C11–N1–C10	112.33(12)
C15–N1–C10	114.94(12)
C2–C1–C5	107.28(14)
C2–C1–C10	125.77(14)
C5–C1–C10	126.86(13)
C2–C1–Fe1	69.48(9)
C5–C1–Fe1	69.36(8)
C10–C1–Fe1	129.01(11)
C3–C2–C1	108.97(14)
C3–C2–Fe1	69.57(9)
C1–C2–Fe1	69.68(9)
C4–C3–C2	107.94(14)
C4–C3–Fe1	69.33(9)

C2–C3–Fe1	69.66(9)
C3–C4–C5	108.57(14)
C3–C4–Fe1	69.95(9)
C5–C4–Fe1	69.88(9)
C4–C5–C1	107.23(13)
C4–C5–C6	122.63(14)
C1–C5–C6	130.13(14)
C4–C5–Fe1	68.85(9)
C1–C5–Fe1	69.22(8)
C6–C5–Fe1	126.94(11)
C5'–C1'–C2'	107.98(16)
C5'–C1'–Fe1	69.66(10)
C2'–C1'–Fe1	69.31(10)
C1'–C2'–C3'	108.25(16)
C1'–C2'–Fe1	70.14(10)
C3'–C2'–Fe1	69.52(10)
C2'–C3'–C4'	107.68(16)
C2'–C3'–Fe1	69.77(10)
C4'–C3'–Fe1	69.42(10)
C3'–C4'–C5'	107.99(16)
C3'–C4'–Fe1	69.73(10)
C5'–C4'–Fe1	70.14(10)
C1'–C5'–C4'	108.10(16)
C1'–C5'–Fe1	70.01(10)
C4'–C5'–Fe1	69.10(10)
C7–C6–C5	131.89(15)
C6–C7–C22	118.47(14)
C6–C7–C8	122.71(14)
C22–C7–C8	118.80(13)
O1–C8–C7	122.37(14)
O1–C8–C9	121.75(13)
C7–C8–C9	115.78(13)
C16–C9–C8	112.61(13)
C16–C9–C10	113.46(13)
C8–C9–C10	112.18(12)

Table 3.9 Continued

N1–C10–C1	114.47(13)
N1–C10–C9	112.75(13)
C1–C10–C9	110.37(12)
N1–C11–C12	110.48(14)
C13–C12–C11	111.20(14)
C12–C13–C14	110.56(14)
C13–C14–C15	111.25(14)
N1–C15–C14	110.02(13)
C17–C16–C21	118.36(15)
C17–C16–C9	123.07(15)
C21–C16–C9	118.56(14)
C16–C17–C18	120.65(17)
C19–C18–C17	120.31(18)
C20–C19–C18	119.67(16)
C19–C20–C21	119.96(17)
C20–C21–C16	121.05(17)
C23–C22–C27	118.33(14)
C23–C22–C7	123.13(14)
C27–C22–C7	118.51(14)
C24–C23–C22	120.34(16)
C25–C24–C23	120.62(16)
C24–C25–C26	119.61(16)
C25–C26–C27	119.91(16)
C26–C27–C22	121.16(15)

Table 3.10 Bond Distances (Å) and Bond Angles (°) for Compound **26**

Atoms	**Distances (Å)**
Fe1–C2	2.045(3)
Fe1–C2'	2.046(2)
Fe1–C1'	2.050(3)
Fe1–C3'	2.051(2)
Fe1–C4'	2.052(3)
Fe1–C5'	2.053(2)
Fe1–C4	2.055(3)
Fe1–C1	2.061(3)
Fe1–C3	2.063(3)
Fe1–C5	2.065(3)
S1–C8	1.675(3)
C1–C2	1.436(4)
C1–C10	1.437(4)
C1–C5	1.439(4)
C2–C3	1.413(4)
C3–C4	1.420(4)
C4–C5	1.435(4)
C5–C6	1.428(4)
C6–C7	1.355(4)
C7–C8	1.440(4)
C8–C9	1.449(4)
C9–C10	1.352(4)
C1'–C2'	1.419(4)
C1'–C5'	1.429(4)
C2'–C3'	1.428(4)
C3'–C4'	1.418(4)
C4'–C5'	1.423(4)
Atoms	**Angle (°)**
C2–Fe1–C2'	105.85(11)
C2–Fe1–C1'	120.84(11)
C2'–Fe1–C1'	40.54(10)
C2–Fe1–C3'	122.40(11)
C2'–Fe1–C3'	40.80(10)
C1'–Fe1–C3'	68.42(10)
C2–Fe1–C4'	159.27(11)
C2'–Fe1–C4'	68.43(10)
C1'–Fe1–C4'	68.59(10)
C3'–Fe1–C4'	40.43(10)
C2–Fe1–C5'	157.70(11)
C2'–Fe1–C5'	68.20(10)
C1'–Fe1–C5'	40.76(11)
C3'–Fe1–C5'	68.02(10)
C4'–Fe1–C5'	40.56(10)
C2–Fe1–C4	68.03(11)
C2'–Fe1–C4	155.94(11)
C1'–Fe1–C4	162.61(11)
C3'–Fe1–C4	121.35(11)
C4'–Fe1–C4	108.60(11)
C5'–Fe1–C4	126.07(11)
C2–Fe1–C1	40.94(11)
C2'–Fe1–C1	122.92(11)
C1'–Fe1–C1	107.40(11)
C3'–Fe1–C1	159.30(11)
C4'–Fe1–C1	158.82(11)
C5'–Fe1–C1	122.92(10)
C4–Fe1–C1	68.65(11)
C2–Fe1–C3	40.24(12)
C2'–Fe1–C3	120.07(11)
C1'–Fe1–C3	155.61(12)
C3'–Fe1–C3	106.54(10)
C4'–Fe1–C3	123.98(11)
C5'–Fe1–C3	161.49(12)
C4–Fe1–C3	40.34(12)
C1–Fe1–C3	68.43(11)
C2–Fe1–C5	68.39(11)
C2'–Fe1–C5	160.76(10)
C1'–Fe1–C5	125.35(10)
C3'–Fe1–C5	157.81(11)
C4'–Fe1–C5	123.37(10)
C5'–Fe1–C5	109.76(10)
C4–Fe1–C5	40.75(10)
C1–Fe1–C5	40.83(10)
C3–Fe1–C5	68.17(11)

Table 3.10 Continued

C2–C1–C10	125.7(3)
C2–C1–C5	106.9(2)
C10–C1–C5	127.4(3)
C2–C1–Fe1	68.95(15)
C10–C1–Fe1	126.62(19)
C5–C1–Fe1	69.75(14)
C3–C2–C1	108.9(2)
C3–C2–Fe1	70.58(15)
C1–C2–Fe1	70.11(15)
C2–C3–C4	108.1(2)
C2–C3–Fe1	69.18(15)
C4–C3–Fe1	69.53(15)
C3–C4–C5	108.3(2)
C3–C4–Fe1	70.14(16)
C5–C4–Fe1	69.99(15)
C6–C5–C4	124.8(3)
C6–C5–C1	127.4(2)
C4–C5–C1	107.7(2)
C6–C5–Fe1	125.69(18)
C4–C5–Fe1	69.26(15)
C1–C5–Fe1	69.41(14)
C7–C6–C5	129.7(3)

C6–C7–C8	130.5(3)
C7–C8–C9	125.0(3)
C7–C8–S1	116.6(2)
C9–C8–S1	118.4(2)
C10–C9–C8	130.8(3)
C9–C10–C1	129.1(3)
C2'–C1'–C5'	107.6(2)
C2'–C1'–Fe1	69.61(14)
C5'–C1'–Fe1	69.76(14)
C1'–C2'–C3'	108.1(2)
C1'–C2'–Fe1	69.85(14)
C3'–C2'–Fe1	69.77(14)
C4'–C3'–C2'	108.1(2)
C4'–C3'–Fe1	69.81(14)
C2'–C3'–Fe1	69.42(14)
C3'–C4'–C5'	107.9(2)
C3'–C4'–Fe1	69.76(14)
C5'–C4'–Fe1	69.78(14)
C4'–C5'–C1'	108.3(2)
C4'–C5'–Fe1	69.67(14)
C1'–C5'–Fe1	69.48(14)

Table 3.11 Bond Distances (Å) and Bond Angles (°) for Compound **27**

Atoms	**Distances (Å)**
Fe1–C1'	2.0338(16)
Fe1–C2'	2.0367(17)
Fe1–C4	2.0423(16)
Fe1–C3	2.0432(16)
Fe1–C5'	2.0449(17)
Fe1–C2	2.0450(16)
Fe1–C3'	2.0506(17)
Fe1–C5	2.0509(16)
Fe1–C1	2.0526(15)
Fe1–C4'	2.0556(17)
C1–C2	1.434(2)
C1–C5	1.444(2)
C1–C10	1.447(2)
C2–C3	1.417(3)
C2–H2	0.93(2)
C3–C4	1.418(2)
C3–H3	0.94(2)
C4–C5	1.435(2)
C4–H4	0.989(19)
C5–C6	1.442(2)
C6–C7	1.344(2)
C7–C8	1.455(3)
C8–N1	1.309(2)
C8–C9	1.457(3)
C9–C10	1.336(3)
C1'–C2'	1.420(2)
C1'–C5'	1.420(2)
C1'–H1'	0.959(19)
C2'–C3'	1.424(2)
C2'–H2'	0.94(2)
C3'–C4'	1.421(3)
C3'–H3'	0.97(2)
C4'–C5'	1.424(2)
C4'–H4'	0.95(2)
C5'–H5'	0.95(2)
N1–O1	1.461(2)
N1–O1'	1.497(3)
Atoms	**Angle (°)**
C1'–Fe1–C2'	40.82(7)
C1'–Fe1–C4	125.06(7)
C2'–Fe1–C4	106.66(7)
C1'–Fe1–C3	163.27(7)
C2'–Fe1–C3	126.52(8)
C4–Fe1–C3	40.62(7)
C1'–Fe1–C5'	40.74(7)
C2'–Fe1–C5'	68.58(7)
C4–Fe1–C5'	162.82(7)
C3–Fe1–C5'	155.18(7)
C1'–Fe1–C2	153.78(7)
C2'–Fe1–C2	164.80(7)
C4–Fe1–C2	68.37(7)
C3–Fe1–C2	40.57(7)
C5'–Fe1–C2	120.38(7)
C1'–Fe1–C3'	68.46(7)
C2'–Fe1–C3'	40.79(7)
C4–Fe1–C3'	119.67(7)
C3–Fe1–C3'	108.99(7)
C5'–Fe1–C3'	68.26(7)
C2–Fe1–C3'	128.00(7)
C1'–Fe1–C5	105.49(7)
C2'–Fe1–C5	117.49(7)
C4–Fe1–C5	41.04(7)
C3–Fe1–C5	68.89(7)
C5'–Fe1–C5	125.17(7)
C2–Fe1–C5	68.88(7)
C3'–Fe1–C5	153.09(7)
C1'–Fe1–C1	117.95(7)
C2'–Fe1–C1	152.34(7)
C4–Fe1–C1	69.01(7)

Table 3.11 Continued

C3–Fe1–C1	68.89(7)
C5'–Fe1–C1	107.10(7)
C5–Fe1–C1	41.20(6)
C1'–Fe1–C4'	68.53(7)
C2'–Fe1–C4'	68.57(7)
C4–Fe1–C4'	154.69(7)
C3–Fe1–C4'	121.05(7)
C5'–Fe1–C4'	40.65(7)
C2–Fe1–C4'	109.38(7)
C3'–Fe1–C4'	40.51(7)
C5–Fe1–C4'	163.71(7)
C1–Fe1–C4'	126.93(7)
C2–C1–C5	107.22(14)
C2–C1–C10	125.40(15)
C5–C1–C10	127.36(15)
C2–C1–Fe1	69.23(9)
C5–C1–Fe1	69.33(9)
C10–C1–Fe1	125.44(12)
C3–C2–C1	108.70(15)
C3–C2–Fe1	69.65(10)
C1–C2–Fe1	69.80(9)
C3–C2–H2	126.6(12)
C1–C2–H2	124.7(12)
Fe1–C2–H2	125.8(12)
C2–C3–C4	108.19(15)
C2–C3–Fe1	69.78(9)
C4–C3–Fe1	69.65(9)
C2–C3–H3	125.6(12)
C4–C3–H3	126.2(12)
Fe1–C3–H3	124.6(12)
C3–C4–C5	108.53(15)
C3–C4–Fe1	69.73(9)
C5–C4–Fe1	69.80(9)
C2–Fe1–C1	40.97(7)
C3'–Fe1–C1	165.09(7)
C3–C4–H4	125.0(11)
C5–C4–H4	126.4(11)
Fe1–C4–H4	122.9(11)
C4–C5–C6	124.74(15)
C4–C5–C1	107.37(14)
C6–C5–C1	127.86(15)
C4–C5–Fe1	69.16(9)
C6–C5–Fe1	125.02(11)
C1–C5–Fe1	69.46(9)
C7–C6–C5	129.16(16)
C6–C7–C8	129.66(16)
N1–C8–C7	114.63(16)
N1–C8–C9	118.84(16)
C7–C8–C9	126.52(16)
C10–C9–C8	129.73(17)
C9–C10–C1	129.42(16)
C2'–C1'–C5'	108.18(15)
C2'–C1'–Fe1	69.70(9)
C5'–C1'–Fe1	70.05(9)
C2'–C1'–H1'	125.5(12)
C5'–C1'–H1'	126.2(12)
Fe1–C1'–H1'	123.8(12)
C1'–C2'–C3'	107.80(16)
C1'–C2'–Fe1	69.48(9)
C3'–C2'–Fe1	70.13(10)
C1'–C2'–H2'	126.2(12)
C3'–C2'–H2'	125.9(12)
Fe1–C2'–H2'	123.3(12)
C4'–C3'–C2'	108.21(15)
C4'–C3'–Fe1	69.93(10)
C2'–C3'–Fe1	69.08(10)
C4'–C3'–H3'	124.7(12)
C2'–C3'–H3'	127.0(12)
Fe1–C3'–H3'	124.0(12)
C3'–C4'–C5'	107.70(15)

Table 3.11 Continued

C3'–C4'–Fe1	69.56(10)
C5'–C4'–Fe1	69.27(9)
C3'–C4'–H4'	128.1(12)
C5'–C4'–H4'	124.2(12)
Fe1–C4'–H4'	124.4(12)
C1'–C5'–C4'	108.11(15)
C1'–C5'–Fe1	69.21(9)
C4'–C5'–Fe1	70.08(9)
C1'–C5'–H5'	127.9(11)
C4'–C5'–H5'	123.9(11)
Fe1–C5'–H5'	123.0(12)
C8–N1–O1	114.59(16)
C8–N1–O1'	114.64(18)

Table 3.12 Bond Distances (Å) and Bond Angles (°) for Compound **28**

Atoms	**Distances (Å)**
S1A–C1A	1.7767(19)
S1A–H1A	1.19(2)
C1A–C2A	1.416(3)
C1A–C10A	1.422(3)
C2A–C3A	1.397(3)
C2A–C17A	1.503(3)
C3A–C4A	1.388(3)
C4A–C5A	1.406(3)
C4A–C8A	1.479(3)
C5A–C6A	1.394(3)
C6A–C7A	1.398(3)
C7A–C8A	1.404(3)
C8A–C9A	1.388(3)
C9A–C10A	1.396(3)
C10A–C11A	1.506(3)
C11A–C12A	1.389(3)
C11A–C16A	1.392(3)
C12A–C13A	1.390(3)
C13A–C14A	1.379(3)
C14A–C15A	1.385(3)
C15A–C16A	1.385(3)
C17A–C18A	1.388(3)
C17A–C22A	1.393(3)
C18A–C19A	1.393(3)
C19A–C20A	1.378(4)
C20A–C21A	1.374(3)
C21A–C22A	1.385(3)
S1B–C1B	1.7754(18)
S1B–H1B	1.22(2)
C1B–C2B	1.417(3)
C1B–C10B	1.418(3)
C2B–C3B	1.396(3)
C2B–C17B	1.507(3)
C3B–C4B	1.389(3)
C4B–C5B	1.402(3)
C4B–C8B	1.475(3)
C5B–C6B	1.396(3)
C6B–C7B	1.395(3)
C7B–C8B	1.401(3)
C8B–C9B	1.390(3)
C9B–C10B	1.392(3)
C10B–C11B	1.502(3)
C11B–C12B	1.386(3)
C11B–C16B	1.392(3)
C12B–C13B	1.385(3)
C13B–C14B	1.382(3)
C14B–C15B	1.383(3)
C15B–C16B	1.386(3)
C17B–C18B	1.386(3)
C17B–C22B	1.391(3)
C18B–C19B	1.386(3)
C19B–C20B	1.381(3)
C20B–C21B	1.384(3)
C21B–C22B	1.382(3)
Atoms	**Angle (°)**
C1A–S1A–H1A	99.2(12)
C2A–C1A–C10A	128.90(17)
C2A–C1A–S1A	112.14(14)
C10A–C1A–S1A	118.96(14)
C3A–C2A–C1A	127.93(18)
C3A–C2A–C17A	114.97(16)
C1A–C2A–C17A	117.08(16)
C4A–C3A–C2A	130.81(18)
C3A–C4A–C5A	126.56(19)
C3A–C4A–C8A	126.81(17)
C5A–C4A–C8A	106.63(17)
C6A–C5A–C4A	108.41(18)
C5A–C6A–C7A	109.91(18)
C6A–C7A–C8A	108.34(18)
C9A–C8A–C7A	126.55(19)
C9A–C8A–C4A	126.69(18)
C7A–C8A–C4A	106.71(17)
C8A–C9A–C10A	131.62(18)

Table 3.12 Continued

C9A–C10A–C1A	126.87(17)
C9A–C10A–C11A	113.49(16)
C1A–C10A–C11A	119.64(16)
C12A–C11A–C16A	118.88(17)
C12A–C11A–C10A	121.31(16)
C16A–C11A–C10A	119.73(16)
C11A–C12A–C13A	120.45(18)
C14A–C13A–C12A	120.11(18)
C13A–C14A–C15A	119.98(18)
C14A–C15A–C16A	120.00(18)
C15A–C16A–C11A	120.58(17)
C18A–C17A–C22A	118.68(19)
C18A–C17A–C2A	121.95(18)
C22A–C17A–C2A	119.37(17)
C17A–C18A–C19A	120.1(2)
C20A–C19A–C18A	120.5(2)
C21A–C20A–C19A	119.8(2)
C20A–C21A–C22A	120.2(2)
C21A–C22A–C17A	120.74(19)
C1B–S1B–H1B	98.4(11)
C2B–C1B–C10B	129.23(17)
C2B–C1B–S1B	118.85(13)
C10B–C1B–S1B	111.91(14)
C3B–C2B–C1B	126.86(17)
C3B–C2B–C17B	113.62(16)
C1B–C2B–C17B	119.51(16)
C4B–C3B–C2B	131.00(18)
C3B–C4B–C5B	125.80(18)

C3B–C4B–C8B	127.48(17)
C5B–C4B–C8B	106.72(16)
C6B–C5B–C4B	108.44(17)
C7B–C6B–C5B	109.64(17)
C6B–C7B–C8B	108.50(17)
C9B–C8B–C7B	126.56(18)
C9B–C8B–C4B	126.73(17)
C7B–C8B–C4B	106.69(16)
C8B–C9B–C10B	130.28(18)
C9B–C10B–C1B	128.34(17)
C9B–C10B–C11B	115.05(16)
C1B–C10B–C11B	116.60(16)
C12B–C11B–C16B	119.31(18)
C12B–C11B–C10B	119.92(16)
C16B–C11B–C10B	120.73(17)
C13B–C12B–C11B	120.49(18)
C14B–C13B–C12B	120.00(19)
C13B–C14B–C15B	119.87(19)
C14B–C15B–C16B	120.31(19)
C15B–C16B–C11B	119.99(19)
C18B–C17B–C22B	118.85(18)
C18B–C17B–C2B	120.59(16)
C22B–C17B–C2B	120.55(16)
C19B–C18B–C17B	120.49(18)
C20B–C19B–C18B	120.31(18)
C19B–C20B–C21B	119.55(18)
C22B–C21B–C20B	120.23(18)
C21B–C22B–C17B	120.57(17)

3.3.4 Electrochemistry. The three-electrode electrochemical cell consists of a glassy carbon button working electrode, a carbon rod counter electrode and an Ag/AgCl reference electrode. All electrodes were connected to a potentiostat. Ferrocene/ferrocenium (Fc/Fc^+), a stable redox couple that is soluble in common organic solvents and whose potential is independent of the solvent, is used as an internal standard. Fc/Fc^+ is estimated to be around 4.8 eV against vacuum. HOMO and LUMO energies of compounds are determined by using their first oxidation and first reduction potentials with respect to Fc/Fc^+.

Cyclic voltammetry of ferrocene-fused tropone (**23**), ferrocene-fused-5,7-diphenyltropone (**24a**) and ferrocene–fused thiotropone (**26**) was carried out at room temperature at scan rate 100 $mV \cdot sec^{-1}$ in a 0.1 M (Bu_4NPF_6/CH_2Cl_2) solution as the supporting electrolyte. The half-wave potentials of each oxidation ($E^0_{1/2,ox}$) and reduction ($E^0_{1/2,red}$) wave were calculated by averaging the corresponding anodic (E_{pa}) and cathodic (E_{pc}) peak potentials. The cyclic voltammograms for complexes **23**, **24a** and **26** are shown in Figures **3.11**–**3.13**. The electrochemical data are summarized in Table **3.13**.

The electrochemical data reveal that complex **23** gave a pseudo-reversible oxidation potential ($E_{1/2}$ = 0.26 V vs. Fc/Fc^+), indicated by the i_{pa}/i_{pc} ratio of 1.15. Similarly, the complex **24a** exhibited a reversible oxidation potential ($E_{1/2}$ = 0.19 V vs. Fc/Fc^+), indicated by i_{pa}/i_{pc} of 0.95. The peak-to-peak separation ($E_p = E_{pa} - E_{pc}$) is equal to 78 mV and 86 mV for complexes **23** and **24a** respectively. These oxidation potentials correspond to an electrochemical HOMO energy gap of –5.06 eV (**23**) and –4.99 eV (**24a**).

Figure 3.13 shows one to fifteen scans of cyclic voltammograms of ferrocene–fused thiotropone (**26**). The cyclic voltammogram curve on the top left is after five scans, the top right is after ten scans and the bottom is after fifteen scans. The observed electrochemical behavior shows a disappearance of the first oxidative peak at about 0.72 V and the increasing of the intensity of another oxidative peak at about 0.55 V and one reductive peak at about 0.45 V. The non-reversible feature in the cyclic voltammetry of ferrocene-fused thiotropone suggests that the oxidation of the compound is followed by a chemical reaction. A similar electrochemical behavior was reported by Blankespoor et al. in the study of electrochemical oxidation of thiourea derivatives, thioketones and 1,3-dithiolan-2-thione in anhydrous acetonitrile solution containing tetra-*n*-butylammonium perchlorate as the supporting electrolyte. They also observed two oxidative peaks and one reductive peak due to the reduction of an oxidation product in the cyclic voltammogram curve. They justified those electrochemical behaviors by the oxidative electron transfer mechanism, which involved the stepwise electron transfer oxidation of thiocarbonyl compounds to their corresponding radical cations, followed by addition to a neutral thiocarbonyl compound and one-electron oxidation of the resultant dimer radical cation.[159] Based upon the reported electrochemical data of thioketone compounds, we may be observing similar types of chemical reactions as shown in Scheme 3.8.

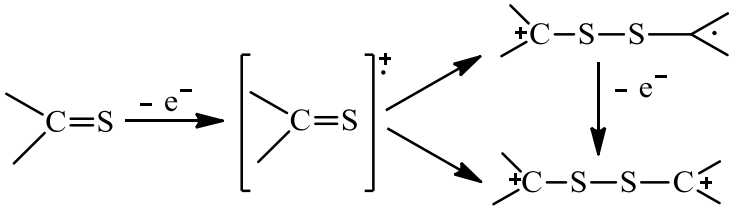

Scheme 3.8 Oxidative electron-transfer mechanism in thiocarbonyl compound

Mouanga and Bercot have also reported the electrochemistry of thiourea in acetonitrile solution containing lithium perchlorate as the supporting electrolytes with platinum as a working electrode. They observed two reductive waves (C_I and C_{II}) and one oxidative wave in the voltammogram. They noticed the peak C_I about –250 mV vs. SCE only after the scan towards the oxidative potential. Furthermore, they mentioned that during a scan towards the anodic potential, the thiourea oxidized to its oxidized product formamidine disulfide [$(H_2N)_2(H_2N)_2C_2S_2$] and the resultant oxidized product reduced at reductive potential about –250 mV vs. SCE. Therefore they believed the peak C_I at around –250 mV does not correspond to the reaction due to the reduction of thiourea; rather a reduction of the compound produced by an oxidation of thiourea.[160]

Table 3.13 Electrochemical data of compounds **23** and **24a**

Compounds	$\Delta E = Ep_a - Ep_c$ (mV)	$E_{1/2}$ vs. Fc/Fc^+ (V)	i_{pa}/i_{pc}	*E*HOMO (eV)
23	78	0.26	1.15	–5.06
24a	86	0.19	0.95	– 4.99

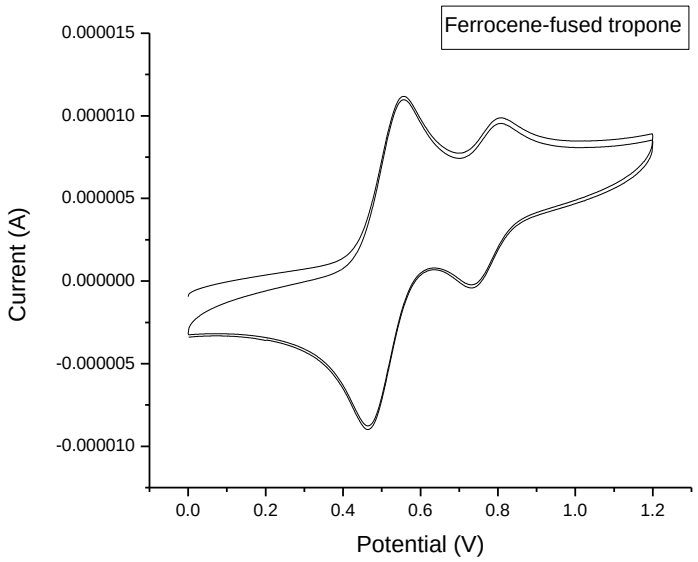

Figure 3.11 Cyclic voltammetry of **23** vs. Ag/AgCl in 0.1 M Bu_4NPF_6/CH_2Cl_2 at scan rate 100 $mV \cdot sec^{-1}$ with a Fc/Fc^+ reference

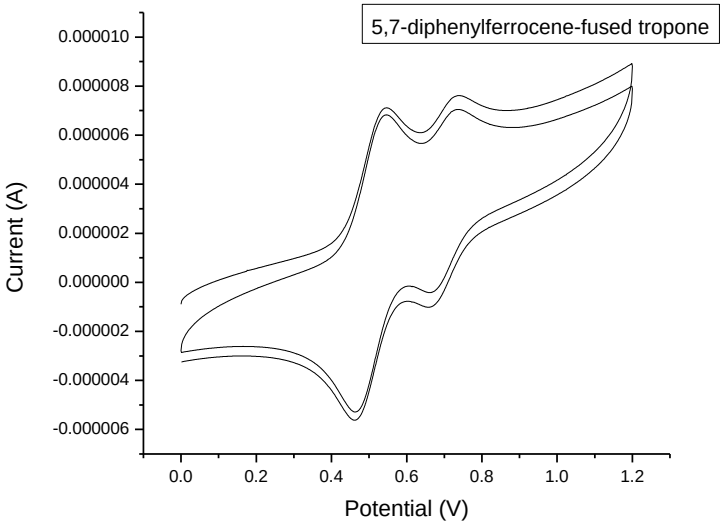

Figure 3.12 Cyclic voltammetry of **24a** vs. Ag/AgCl in 0.1 M Bu_4NPF_6/CH_2Cl_2 at scan rate 100 $mV \cdot sec^{-1}$ with Fc/Fc^+ reference

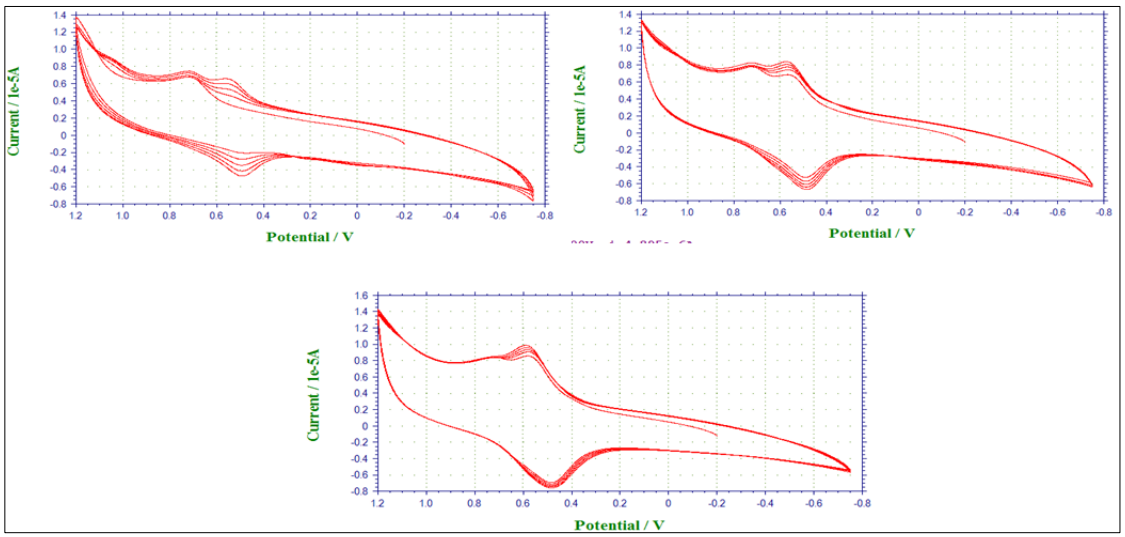

Figure 3.13 Cyclic voltammetry of **26** vs. Ag/AgCl in 0.1 M Bu_4NPF_6/CH_2Cl_2 at scan rate 100 $mV \cdot sec^{-1}$ without a Fc. (1-15 cycles)

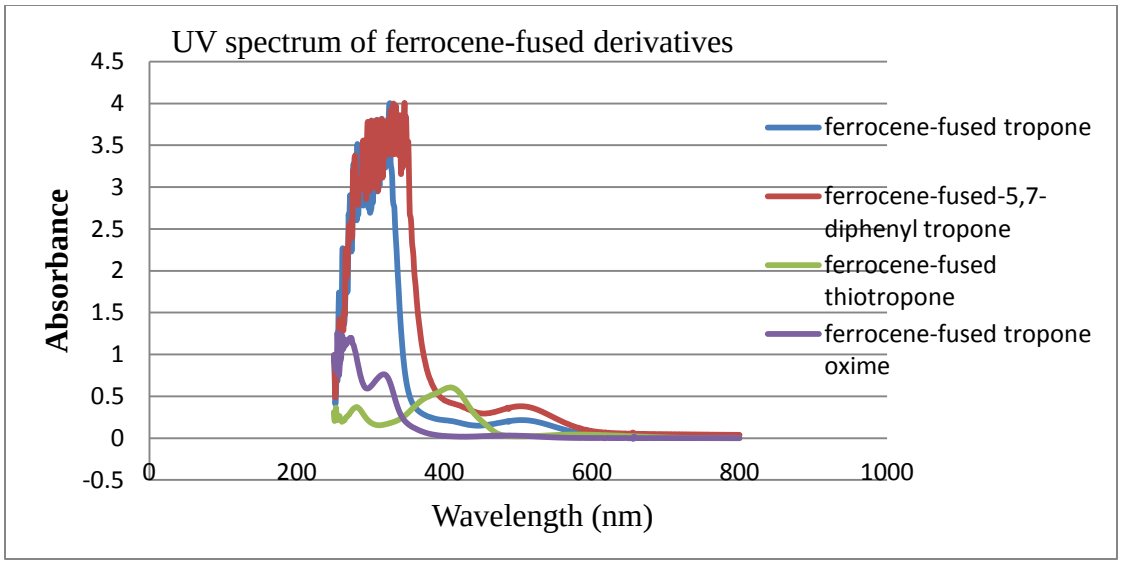

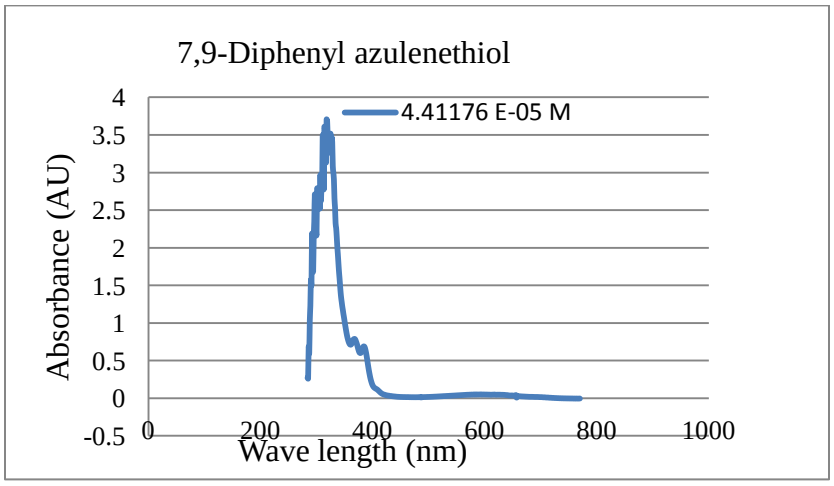

Figure 3.14 UV Spectra of ferrocene-fused tropone derivatives (combined) and diphenylazulenethiol

The figure 3.14 shows the UV of spectra of ferrocene-fused tropone derivatives and 5,7-diphenylazulenethiol (**23, 24a**, **25**, **26**, **27** and **28**). The electronic spectrum of ferrocene-fused tropone (**23**) is characterized with three bands at 520 nm (2.39 eV), 319 nm (3.89 eV) and 274 nm (4.53 eV). Serrano-Andres *et al.* have computed the absorption spectra of a series of cyclic conjugated ketones and thioketones including tropone and

thiotropone. The computational study for tropone shows the n-π* transitions lie at 3.86 and 3.94 eV while the π-π* transitions appear at 4.22 eV and 4.26 eV.[158] The calculated data suggested that the transitions observed at 3.89 eV and 4.53 eV in **23** may be due to *n*-π* and π-π* respectively. Tropone shows two characteristic bands in the UV spectrum at 230 mμ and 300 mμ.[161,162] The absorption band at 520 nm is due to *d-d* transition of metal, since ferrocene has a strong absorption at 535 nm.[163] The absorption spectrum of ferrocene-fused 5,7-diphenyltropone (**24a**) shows bands at 503 nm (2.47 eV), 330 nm (3.76 eV) and 287 nm (4.32 eV) similar to **23**.

The UV spectrum of ferrocene-fused thiotropone (**26**) displays three transitions at 585 nm (2.12 eV), 408 nm (3.04 eV) and 281 nm (4.42 eV). Among those three transitions, the most intense band is located at 3.04 eV with an extinction coefficient of 14933 $M^{-1}cm^{-1}$. Similar behavior was observed by Serrano-Andres et al. in the theoretical study of the electronic excited state for thiotropone. The computed π-π* transition at 3.34 eV is the strongest band in hexane with an extinction coefficient of 151351 $M^{-1}cm^{-1}$. They also have reported two weak bands at 1.82 eV and 2.03 eV, and those transitions are computed as n-π*. Therefore, the absorption band at 585 nm (2.12 eV) in **26** may be the combined transitions of metal *d-d* and *n*-π*. The low energy electronic transition of ferrocene–fused thiotropone (3.04 eV) as compared to ferrocene–fused tropone (3.89 eV) may be due to the larger size of the sulfur atom and longer C=S bond in thiotropone. Ferrocene–fused oxime tropone exhibits three electronic transitions at 482 nm (2.57 eV), 318 nm (3.92 eV) and 272 nm (4.56 eV). 7,9-Diphenylazulenethiol shows the strongest π-π* transition at 320 nm (3.88 eV) with an extinction coefficient of 32383 $M^{-1}cm^{-1}$.

3.4 Summary

1,2-Diformylferrocene is the starting material for the synthesis of unsubstituted and substituted ferrocene–fused tropones. The starting material was prepared following the literature reported protocol.[116,117,119] The reaction of 1,2-diformylferrocene with acetone at room temperature in absolute ethanol under N_2 in presence of KOH gave ferrocene-fused tropone (**23**) in good yield (83%). Further, the reaction of 1,2-diformylferrocene with 1,3-diphenylacetone under similar reaction conditions overnight yielded a 1:1 ratio of the desired compound (**24a**) and mono-aldol condensed product (**24b**). The presence of an aldehyde peak in the ^{1}H NMR confirmed the compound **24b**. Finally, compound **24b** was verified by an X-ray crystal analysis. To improve the reaction yield, we attempted the reaction of 1,2-diformylferrocene with 1,3-diphenylacetone in piperidine gave **25**, a piperidine adduct of tropone **24a** in poor yield (15%).

Attempts to convert ferrocene-fused tropones **23** and **24a** directly to oximes by reaction with hydroxylamine or hydroxylamine hydrochloride in $CHCl_3$ at room temperature and in ethanol at refluxing temperature resulted in decomposition. The reaction of ferrocene-fused tropone with Lawesson's reagent in dry benzene at room temperature for 7 h gave a moderate yield of a dark blue ferrocene–fused thiotropone (63%). The ferrocene-fused tropone oxime (**27**) was prepared by reacting **26** with hydroxylamine in chloroform at 0 °C for 5 h gave in good yield (83%). Refluxing the ferrocene–fused 5,7-diphenyltropone with Lawesson's reagent in dried benzene for 7 h gave a blue, demetalated product, 7,9-diphenylazulenethiol (45%).

All the complexes were characterized by X-ray crystallography. The interplanar angle between C1–C2–C3–C4–C5–C6–C10 and C7–C8–C9 of the ferrocene-fused thiotropone is 2.14 °, which shows almost planar, and the planarity of the molecule is also supported by the ^{1}H NMR data and UV absorption. Cyclic voltammetry of **23** and **24a** shows an oxidation potentials at 0.26 V and 0.19 V respectively, versus Fc/Fc^{+}, corresponding to estimated HOMO and LUMO energy levels of –5.06 eV, –4.99 eV respectively. UV-vis absorption spectra for compounds **23, 24a, 26, 27** and **28** were recorded in the dichloromethane solution, and the UV absorption spectrum reveals that ferrocene-fused thiotropone shifts about 80 nm more towards the visible region as compared to other derivatives. The most intense absorption observed in the ferrocene–fused thiotropone lies at 3.34 eV (409 nm) with an extinction coefficient of 14933 Mol^{-1} cm^{-1}. The planarity of compound **26** was supported by the downfield shift of signals H6 (7.33 ppm) and H7 (7.10 ppm), and a strong UV absorption at blue region as compared to other tropone derivatives (**23** and **27**).

In summary, we have synthesized unsubstituted and phenyl substituted ferrocene-fused tropone using aldol condensation. The reaction of **23** and **24a** with Lawesson's reagent resulted in ferrocene-fused thiotropone and 5,7-diphenylazulenethiol. Furthermore, the reaction of **26** with hydroxylamine gave the corresponding oxime. Compound **26** has an interesting color in solid form as compared to the other derivatives. All the ferrocene-fused tropone derivatives were characterized by a single X-ray crystal structure. The oxidation potential of **23** and **24a** were measured by cyclic voltammetry. The UV-vis spectrum of ferrocene-fused tropone derivatives was recorded. Among those derivatives, **26** showed an interesting absorption towards the visible region (λ_{max} 409 nm)

and exhibits a high dipole moment. This result suggested that **26** has extended conjugations, which is also supported by the downfield shift of protons at C2 and C3 (shown in Figure 3.3). Therefore, compound **26** may be considered as a potential candidate for optoelectronic application.

Chapter 4 Synthesis and Characterization of Ferrocene-Fused Thiepin Derivatives

4.1 Conducting polymers

Conducting polymers are extended, π-conjugated polymers, also known as synthetic metals, which possess electronic (conductive, magnetic, optical) properties of metals and acquire high conductivity due to incorporation of a small concentration of dopants into the matrix of the initial extended π-conjugated polymer.[164] The new era of conducting polymers began with the discovery in 1977 by Heeger et al. that polyacetylene exhibits a 12-fold increase in its conductivity upon oxidative doping (I_2, Br_2 and Cl_2).[165] The light weight, easy processability, low fabrication costs and corrosion resistance of organic polymers have led to the replacement of inorganic materials in electronic applications.[166] This class of materials has attracted great attention and rapidly become a subject of considerable interest for both materials chemists and industrial researchers.[167]

The potential applications of conducting polymers in chemical and biological sensors are another reason for the intensive development of these materials.[168] Conducting polymers offer a wide range of applications including field-effect transistors, light-emitting diodes, photovoltaics, nonlinear optic devices and batteries.[169] Polyacetylene and other linear-backbone polymers (polypyrrole, polyaniline) may display favorable electronic properties. However, these materials have limited use practically due to poor environmental stability.[170]

One important class of organic conducting polymers is polyheterocycles. Polythiophenes and polypyrroles have been the most extensively studied due to their possibilities of structural modification, ease of formation by either chemical or

electrochemical polymerization techniques[171] and their stability in air and moisture greater than polyacetylenes. The heteroatoms (sulfur and nitrogen) tend to stabilize the positive charges in the *p*-doped state. Heterocyclic conducting polymers, in particular polythiophenes, are stable to oxygen and moisture in both their doped and undoped states at ambient temperature.[172,173]

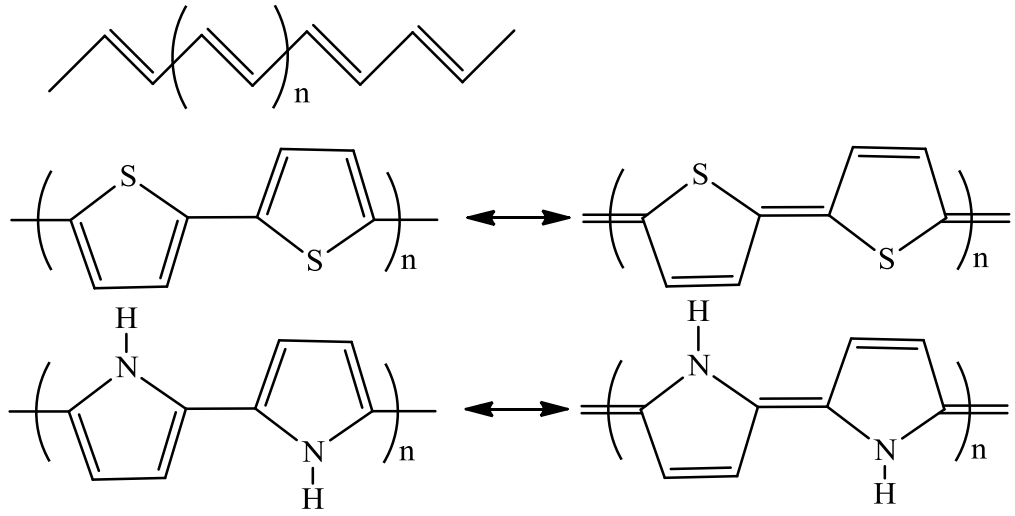

Figure 4.1 Conjugated conductive polymers

Polythiophene is synthesized by anodic or chemical polymerization of pure thiophene or oligothiophene, and by metal-catalyzed cross-coupling of the thienyl Grignard reagent shown in **2** of Figure 4.2. Electrochemically synthesized polythiophene (**1** of Figure 4.2) is a tough, blue-black film, whereas chemically synthesized polythiophene is crystalline with definite number-average molecular weight. Their poor solubility in organic solvents makes chemically synthesized polythiophene difficult to purify and process into films. [174,175] However, these issues can be circumvented by introducing alkyl chains or other solubilizing organic groups.

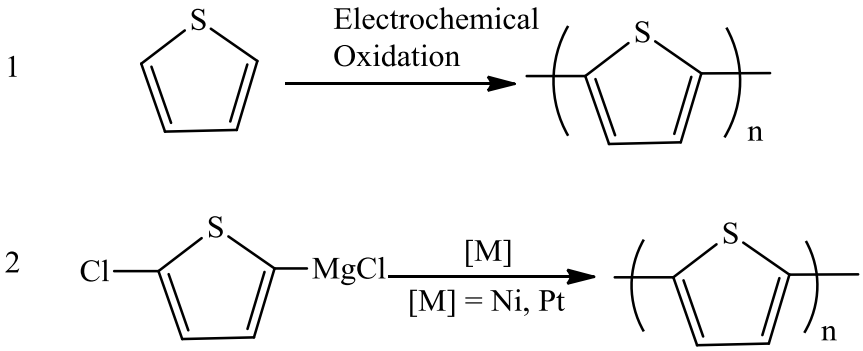

Figure 4.2 Synthesis of polythiophene. 1. Electrochemical polymerization.

2. Chemical polymerization to polythiophene

3-Substituted thiophenes are asymmetric monomers, which results in three possible couplings when two monomers are linked at 2- and 5- positions (Figure 4.3); i.e., 2,2' (head-to-head, HH), 2,5' (head-to-tail, HT) and 5,5' (tail-to-tail, TT). Regioregular functionalized polythiophene exhibits more highly ordered polymer, thereby decreasing band gap and increasing the conductivity as compared to regiorandom analogous.[176]

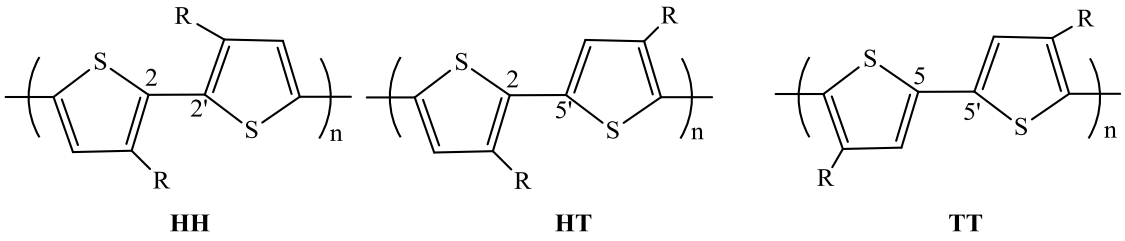

Figure 4.3 Regioisomeric coupling patterns in poly(alkylthiophene)s

Another goal of chemists is to prepare polymers with small band gaps and intrinsic high conductivities. Considering these parameters, Wudl and coworkers prepared poly(benzo[3,4-*c*]thiophene), also known as poly(isothianaphthene) or PITN, which exhibits a band gap approximately 1 eV lower than polythiophene (~2 eV). The

increased conductivity of PITN may be due to the resonance contribution from the quinoid canonical form (**b** of Figure 4.4), which increases the aromaticity of phenyl ring.[174] Analogous organometallic heterocycles could potentially add a new dimension to the optoelectronic polymers. Brédas and coworkers reported that for conjugated polymers based on aromatic rings, the band gap decreases as the quinoidal character of the backbone increases, possibly due to the nearly equal bond lengths along the polyene backbone.[177]

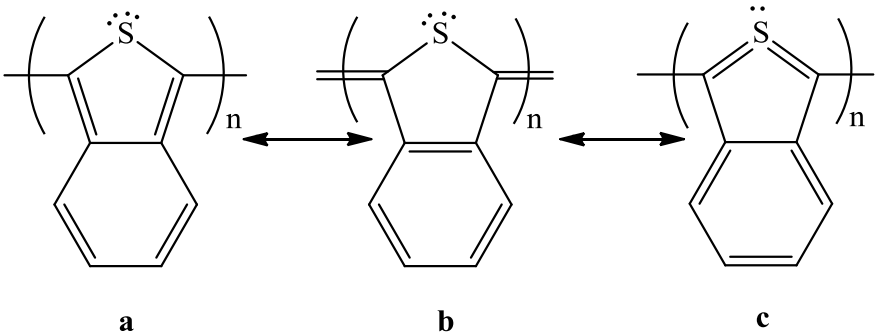

Figure 4.4 Resonance forms of PITN

PITN shows some non-classical thiophene character (**c** of Figure 4.4), with a tetravalent sulfur.[174] Thieno[3,4-*c*]thiophene is a typical non-classical thiophene. The first stable non-classical thiophene was tetraphenylthieno[3,4-*c*]thiophene (**1** of Chart 4.1), synthesized by Cava and Husbands.[178] Other stable derivatives of nonclassical thiophene have been synthesized as shown below in Chart 4.1 (**2** and **3**).[179,180] The stability of non-classical thiophenes is enhanced by introducing bulky and electron-accepting substituents. Chart 4.1 shows a few examples of stable non-classical thiophenes.

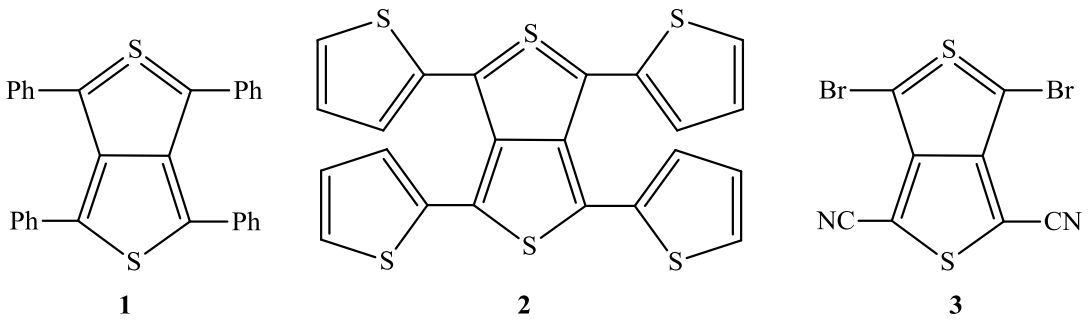

Chart 4.1 Few examples of non-classical thiophenes

The discovery of PITN has attracted researchers to prepare polymers incorporating a fused ring with a wide variety of structural variation. Chart 4.2 shows some examples of fused-ring polythiophenes.[175,176,181]

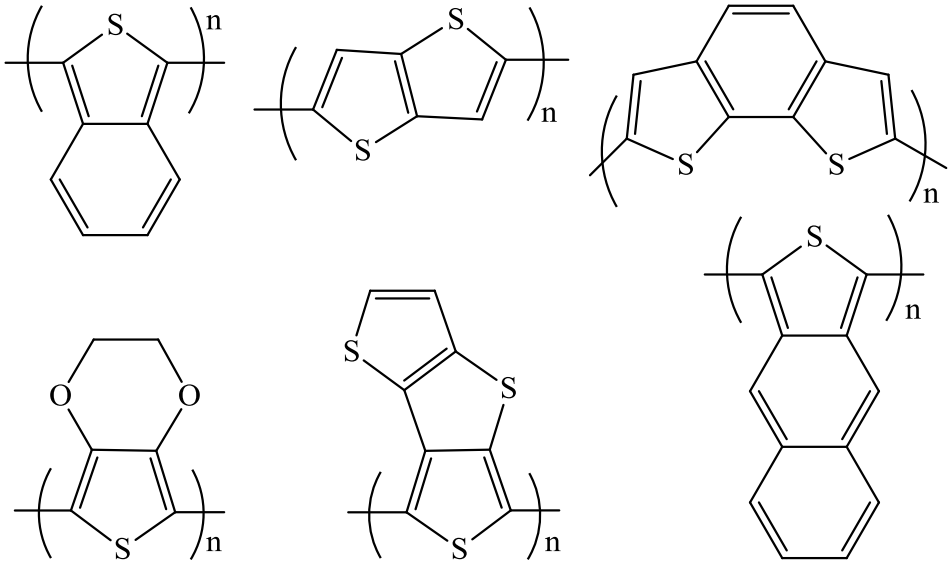

Chart 4.2 Fused-ring polythiophenes

Kim and coworkers prepared thieno[3,2-*b*]thiophene-substituted benzo[1,2-*b*:4,5-*b'*]dithiophene (**1** of Figure 4.5), which has an optical band gap of 1.55 eV, as a promising building block for semiconducting polymers in high-performance organic solar cells.[182] Similarly, Zhou et al. synthesized D-A copolymer (PBTT-TBDTT) **2** of Figure 4.5, which has a narrow optical band gap around 1.45 eV and shows broader absorption

range from 300–850 nm. Designing materials with the combination of an electron-rich donor (D) unit and an electron-deficient acceptor (A) unit is a powerful strategy in the preparation of small-band-gap π-conjugated polymers.[183]

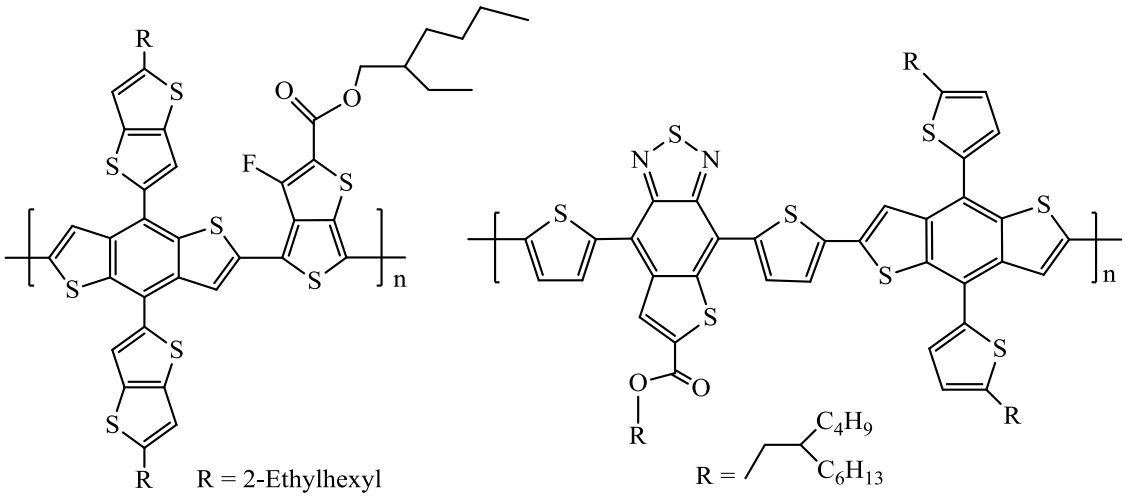

Figure 4.5 Thienyl group substituted donor-acceptor copolymer

Incorporating transition metals into conducting polymers may add several advantages including environmental stability, solubility in organic solvents and unique redox properties.[41] There are several other examples of organometallic π-complexes with thiophene ligands. In 1958, E.O Fisher prepared tricarbonyl[(2,3,4,5-η)-thiophene-κS]chromium (**1** of Chart 4.3).[184] Further, E.O Fisher et al. utilized benzo[*b*]thiophene as a ligand for tricarbonylchromium complex where the chromium is bonded to six-membered ring (**2** of Figure 4.8).[185] In 1992, Loft and coworkers synthesized trialkylsilyl substituted thiophenetricarbonylchromium(0) (**3** of Chart 4.3).[186]

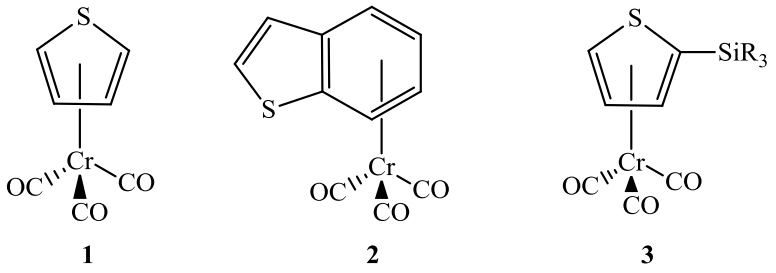

Chart 4.3 Thiophene-based chromium complexes

The Selegue group has a long-term interest in the structural and electronic properties of materials based on η^5-cyclopentadienyl-fused heterocycles (Chart 4.4). Selegue and Swarat synthesized [Cr(benzo[3,4-*c*]thiophene)$(CO)_3$] (**1**) from the reaction of benzo[3,4-*c*]thiophene with photolytically generated [Cr(thf)$(CO)_5$] at room temperature. A crystal structure showed that tricarbonylchromium is η^6-bonded to the arene ring of the ligand.[149] Selegue and Wallace prepared the pyridazine complexes of ruthenium (**2**) via two methodologies. One method involves the reaction of [Ru{η^5-$C_5H_3(CO_2Ph)_2$}(Cp*)] with hydrazine monohydrate; and the second method involves the generation of thallium pyridazine salt by deprotonation of cyclopenta[*d*]pyridazine with thallium ethoxide followed by treatment with [Ru(μ_3-Cl)$(Cp^*)]_4$ to prepare pyridazine complexes.[150]

Moreover, several other derivatives of cyclopentadienyl-fused heterocycles have been synthesized in Selegue's group. Selegue and coworkers prepared η^5-cyclopenta[*c*]thienyl complexes of manganese via two methodologies. The first method involves the lithiation of 1,3-disubstituted-cyclopent[*c*]thiophene followed by treatment with Me_3SnCl, which in turn reacts with [$MnBr(CO)_5$] to give **3** of Chart 4.4. The second method involves the complexation of 1,2-diacylcyclopentadienyl ligand, followed by ring closure using either Lawesson's reagent or $P_4S_{10}/NaHCO_3$ in CS_2.[148] Further, Tice

expanded the work to synthesize a number of halogen-substituted derivatives of cyclopenta[*c*]thienyl complexes of manganese employing the appropriate acid chlorides.[152]

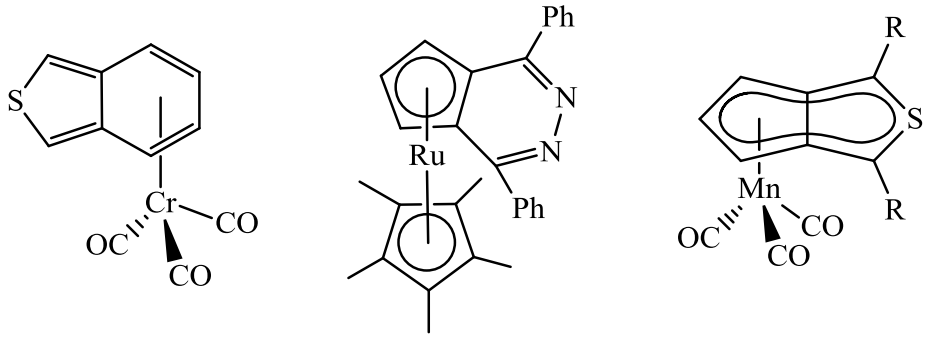

Chart 4.4 Some organometallic complexes prepared by Selegue group

1. η^6-Benzo[3,4-c]thiophene complex of chromium(0); 2. Sandwich pyridazine complex of ruthenium(II); 3. η^5-cyclopenta[c]thienyl complexes of manganese(I)

Thiepins, conjugated seven-membered ring system with a thioether group, are another important class of heterocycles. Including one lone pair of electrons from the sulfur atom, a thiepin can be considered an 8π-electron heteroannulene, antiaromatic according to Hückel's rule.[187] Parent thiepin is thermally unstable, possibly due to the valence isomerization of thiepin to the corresponding benzene sulfide followed by irreversible loss of sulfur to form benzene.[188] However, bulky substituents at both the 2 and 7 positions of thiepins increase their stability because steric repulsion disfavors formation of the thianorcaradiene intermediate (Figure 4.6).[187]

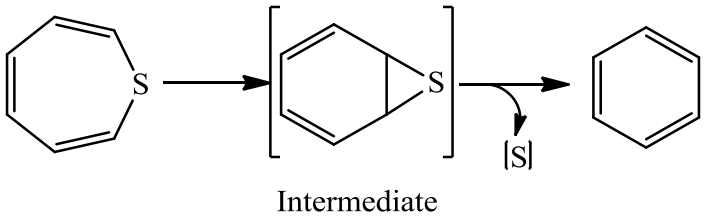

Figure 4.6 Sulfur extrusion from thiepin

There are several reported examples of benzannulated thiepins. Traynelis et al. prepared thermally unstable benzo[*b*]thiepin from the reaction of 2,4-dichloro-2,3-dihydro-1-benzothiepin with potassium *tert*-butoxide[189],[190] The same group reported mono- and di-halo substituted benzo[*b*]thiepin, which are more stable than parent benzo[*b*]thiepin.[189] Further, Traynelis and Love prepared the seven-membered heterocycle, benzo[*b*]thiepin 1,1-dioxide.[191] Benzo[*b*]thiepin (**1** of Chart 4.5, X = S) and benzo[*b*]thiepin 1,1-dioxide (**1** of Chart 4.5, X = SO_2) are well characterized by single X-ray crystal analysis by Yasuoka et al.[192,193] Benzo[*b*]thiepin 1-oxide (**1** of Chart 4.5, X = SO) has not been prepared. However, a highly substituted benzo[*b*]thiepin 1-oxide (**6** of Chart 4.5, X = SO) has been synthesized. These molecules are thermally less stable than the corresponding benzo[*b*]thiepin.[194] Recently, Swager and Song synthesized thiophene-annulated thiepins (**7** of Chart 4.5), which can be polymerized electrochemically to give thiepin-containing electroactive polymers.[187]

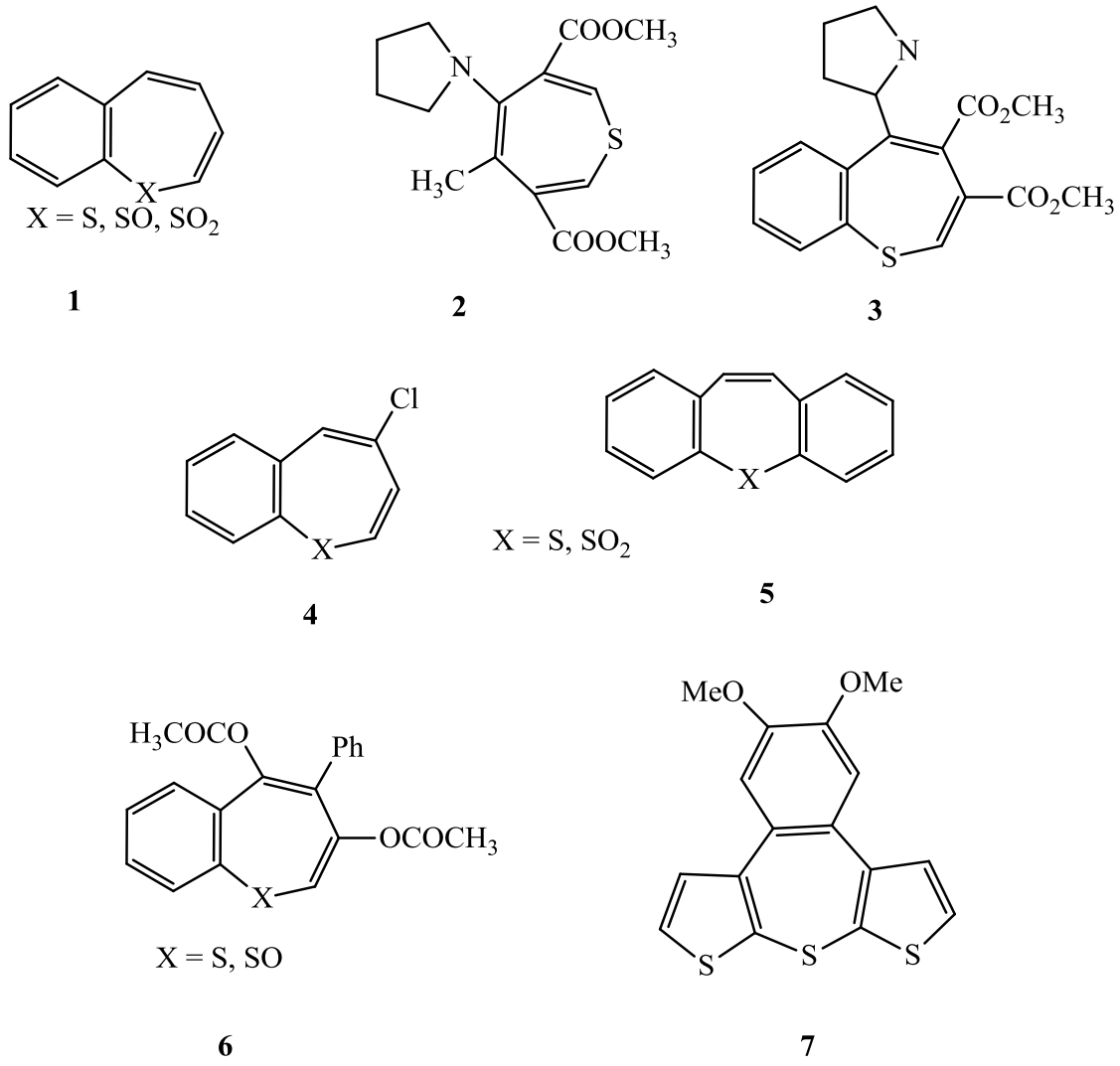

Chart 4.5 Derivatives of thiepins and benzannulated thiepins

Benzo[*d*]thiepin diacid (**1a** of Figure 4.7) undergoes extrusion of sulfur much more readily than its naphthalene homologue (**2a** of Figure 4.7). This may be due to the extra energy required to convert two benzene rings into quinoid form in naphthalene thiepin diacid (**2b** of Figure 4.7) during sulfur extrusion, while in benzo[*d*]thiepin, sulfur extrusion requires conversion of a benzene ring into quinoid form as shown in Figure 4.7 (**1b**). This result suggests that if there is a sufficiently great energy difference between the

ground state of the heterocycle and the benzene sulfide, it might be easier to prepare a simple thiepin.[195,196]

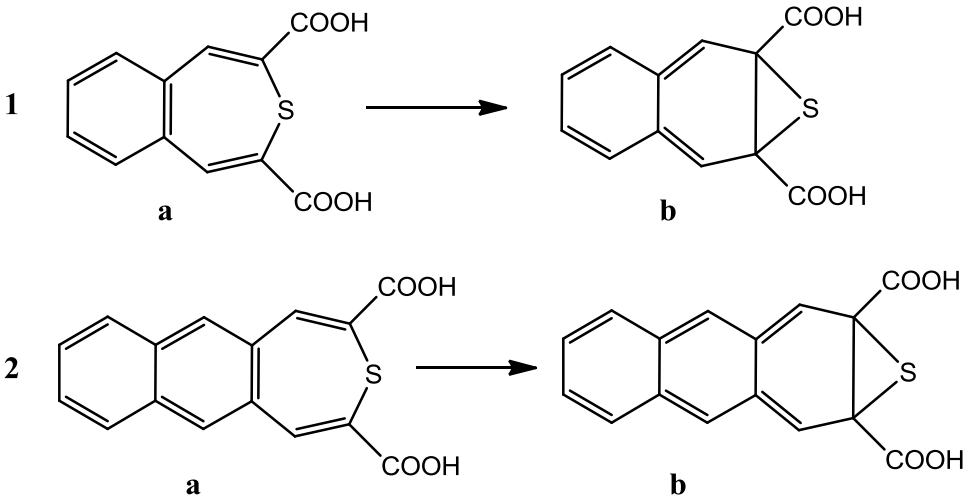

Figure 4.7 Benzo[*d*]thiepin-diacid and corresponding benzene sulfur

Considering these parameters, Schlessinger and Ponticello prepared a thermally stable, unsubstituted thieno[3,4-*d*]thiepin. The great stability of thieno[3,4-*d*]thiepin may be due to charge-separated species **b** and **c** of Figure 4.8. They have also reported that sulfur extrusion might require a high-energy process due to the tetravalent sulfur atom present in the quinoid position of the benzene sulfide intermediate **d** of Figure 4.8.[197]

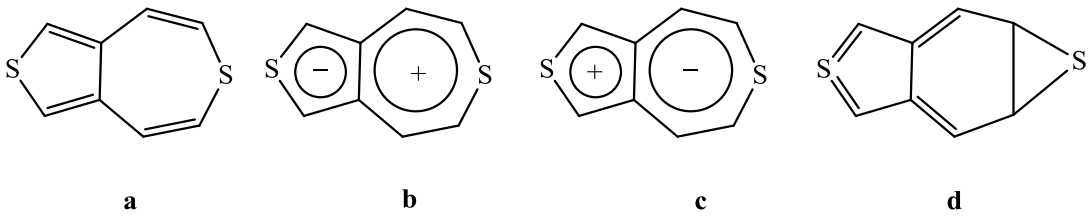

Figure 4.8 Structure of unsubstituted and charge separated thieno[3,4-*d*]thiepins and corresponding benzene sulfide intermediate

Recently Cai et al. prepared new π-conjugated molecules with thiepin-fused heteroacenes for the development of high-performance p-type optoelectronic materials

and found that thin films of those molecules possess relatively high hole-carrier mobility.[198] Thiepin-containing derivatives have not only potential application in optoelectronic devices but also display potent biological activities (prostaglandin antagonist, antiestrogenic effect). Therefore Shirani and Janosik synthesized dibenzothiophene[*b*,*f*]thiepins.[199]

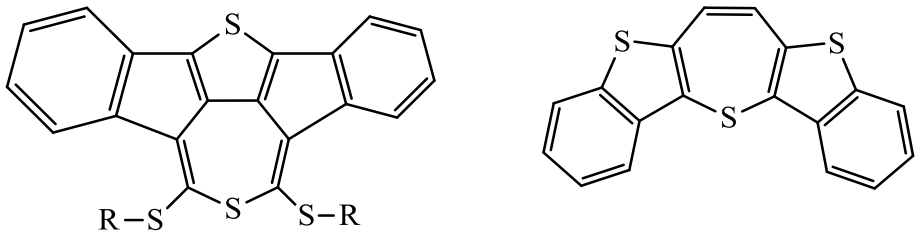

R = CH_3, C_6H_{13}

Figure 4.9 π-conjugated thiepin-fused heteroacenes

Labile thiepins cannot only be stabilized by the addition of benz- or thiophene-annulations and steric effects but also by transition-metal complexation. The ability of transition metals to stabilize reactive species allowed researchers to isolate kinetically unstable conjugated molecules such as cyclobutadiene,[200,201,202] pentalene,[203] and norcaradiene.[204] Similarly, Nishino et al. took the advantage of a transition-metal complexation strategy to stabilize a thermally labile parent thiepin and prepared the iron tricarbonyl thiepin. This is the first transition metal complex of a thiepin (Chart 4.6).[205,188] Herein, we are preparing ferrocene-fused thiepins, which may allow us to design new organometallic conducting polymers.

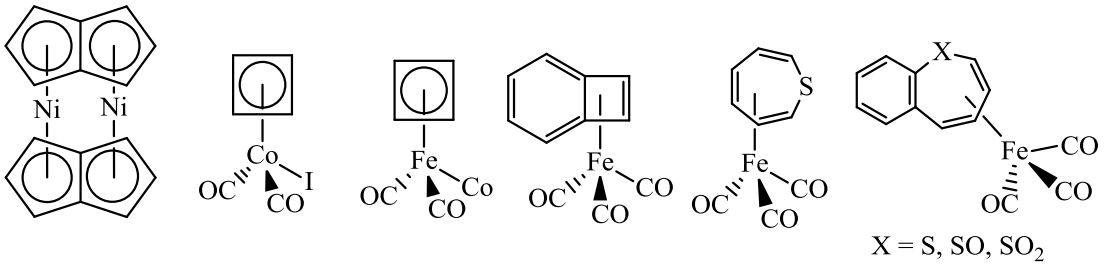

Chart 4.6 Examples of transition metal complexes

Borepins are unsaturated seven-membered heterocyclic compounds with six carbon atoms and one boron atom as a heteroatom. Tovar and coworkers have been synthesized new boron-containing polyacenes for the past few years. The incorporation of boron atoms into π-conjugated polycyclic materials has emerged a useful strategy to develop new optoelectronic materials with unique optical properties that result from vacant p-orbital of the boron center.[206,207] Borepin derivatives show well-behaved cathodic electrochemistry at the boron centers. Thus these materials are useful for n-type materials.[208] The Tovar group has been utilized the strong Lewis acidity of tricoordinate boron to enhance the electronic delocalization along the π-conjugated system relative to benzo-fused analogues.[209] Recently same group has prepared air- and moisture-stable dithienoborepins (**2** and **3** of Chart 4.7).[210]

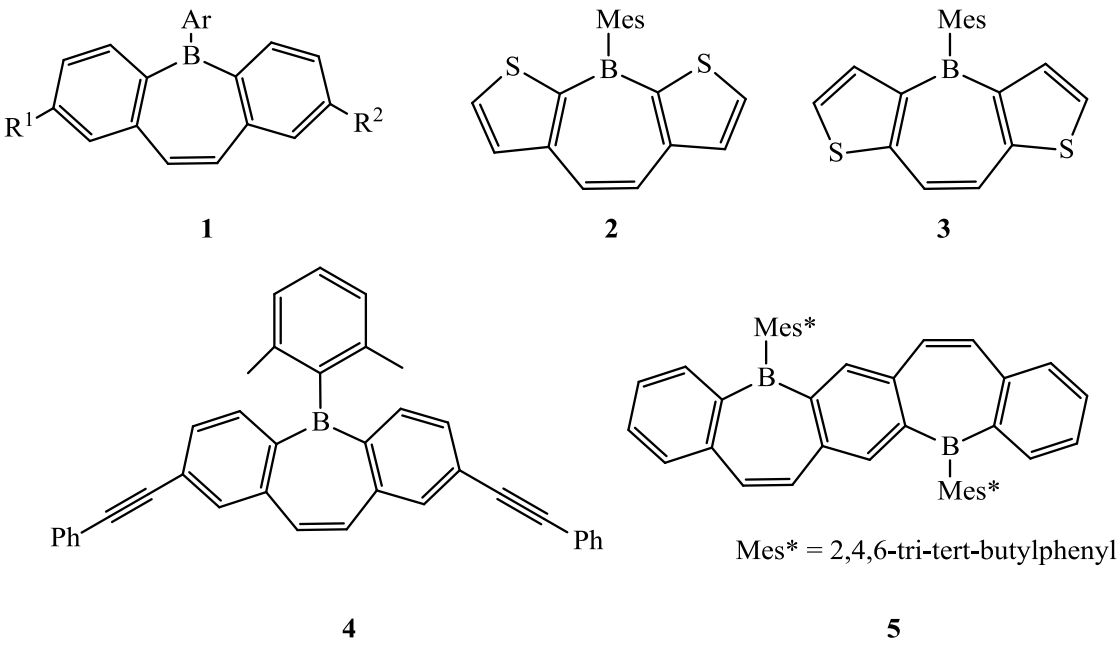

1 **2** **3** **4** **5**

Chart 4.7 Few examples of boron-containing polyacenes

4.2 Experimental

Chapter 2 lists the general condition for all experiments. Thiodiglycolic acid, *m*-chloroperoxybenzoic acid, oxalyl chloride, 4-dimethylaminopyridine, quinoline, silver carbonate, Pyridine, triethylamine (Aldrich), copper powder (Fisher), 2-chloro-1,3,2-benzodioxaphosphole and 1-Hydroxypyridine-2(1*H*)-thione sodium salt (Alfa Aesar), pyridine and triethylamine were freshly distilled before used. 1-Hydroxypyridine-2(1*H*)-thione sodium salt was received as a 40 % solution in water. The water was removed under reduced pressure, the resulting yellow solid was dissolved in ethanol and hexane was added slowly to give a white powder.[211] Dimethylthiodiglycoate was prepared from esterification of thiodiglycolic acid in MeOH under acidic conditions (conc. H_2SO_4). Dimethylthiodiglycolate sulfoxide[212] ($(CH_3OCOCH_2)_2SO$) and copper phthalocyanine[213] were prepared according to the literature procedures.

Synthesis of $C_{18}H_{16}FeO_5S$ (29a) and $C_{18}H_{18}FeO_6S$ (29b). To an oven-dried 125 mL Schlenk flask cooled under N_2, 5 mL dried methanol, dimethylthiodiglycolate sulfoxide (0.19 g, 0.99 mmol), then 0.1 mL of freshly distilled Et_3N were added. After stirring at room temperature for 90 min, a solution of 1,2-diformylferrocene (200 mg, 0.83 mmol) in 3 mL methanol was added dropwise, and the reaction mixture was stirred for 16 h. Then the original volume of reaction mixture was reduced by half under vacuum and poured into a column of silica. The column was flushed with hexane:ethyl ether (1:1). Pure ethyl ether eluted a purple band containing **29b**, then ethyl ether:dichloromethane (3:1) eluted a dark red band containing **29a**. The evaporation of the solvent from both collected fractions gave gummy solids, which were triturated with pentane and dried under vacuum to yield red (**29a**) and purple (**29b**) solids in a ratio of

2:1 (**29a** 40 % and **29b** 22 %). **29a: ^{1}H NMR (400 MHz, $CDCl_3$, ppm):** δ 3.89 (s, 6 H, H9), 4.29 (s, 5 H, H7), 4.84 (t, 1 H, ^{3}J = 2.8 Hz, H6), 5.20 (d, 2 H, ^{3}J = 2.4 Hz, H5), 8.30 (s, 2 H, H3). **^{13}C{^{1}H} NMR (100 MHz, $CDCl_3$, ppm):** 53.08 (C9), 72.13 (C7), 76.64 (C6), 78.25 (C5), 78.96 (C4), 147.20 (C3), 164.50 (C8). **IR (ATR, cm^{-1}):** 1704 (C=O), 1032 (S=O). **29b: ^{1}H NMR (400 MHz, $CDCl_3$, ppm):** δ 2.64 (d, 1 H, H2), 3.79 (s, 1 H, OH), 3.85 (s, 3 H, CH_3), 3.90 (s, 3 H, CH_3), 4.36 (s, 5 H, H15), 4.66 (s, 1 H, H3), 4.68 (ABC, 1 H, Cp), 4.93 (ABC, 1 H, Cp), 5.21 (ABC, 1 H, Cp), 8.03 (s, 1 H, H9). **^{13}C{^{1}H} NMR (100 MHz, $CDCl_3$, ppm):** 53.11 (*C*H_3), 53.48 (*C*H_3), 62.92 (C2), 66.53 (C3), 70.84 (C11), 72.77 (Cp), 72.92 (Cp), 74.22 (Cp), 78.36 (Cp), 92.36 (Cp), 129.29 (C10), 151.84 (C9), 164.54 (*C*O), 169.32 (*C*O) . **IR (ATR, cm^{-1}):** 1054 (S=O), 1720 (CO), 1744 (CO), 3373 (OH).

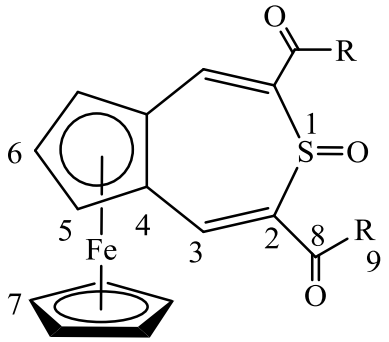

R = OCH_3 (**29a**), OH (**31**)

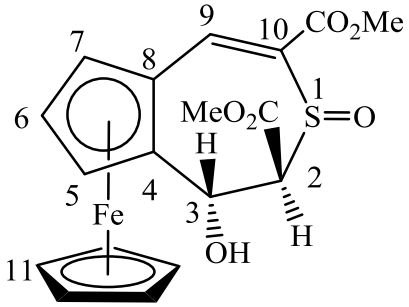

29b

Figure 4.10 Ferrocene-fused dimethyl ester thiepin S-oxide with numbering

Synthesis of $C_{18}H_{16}FeO_4S$ (30). Compound **29a** (0.10 g, 0.25 mmol) and pyridine (0.30 mmol, 22 μL) were dissolved in dry benzene (5 mL) in a 100 mL Schlenk flask purged with N_2. The resulting solution was cooled in an ice bath. To the stirring reaction mixture, 2-chloro-1,3,2-benzodioxaphospole (0.11 g, 0.62 mmol) was added

slowly. The reaction mixture was warmed to room temperature and stirred for 3 h. Aqueous sodium hydroxide (2 M, 3 mL) was added and the benzene layer was washed again with sodium hydroxide (2 M, 5 mL) solution, followed by one water wash. The benzene layer was dried with anhydrous magnesium sulfate; and the solvent was removed to yield the crude product. The product was dissolved in a minimum amount of dichloromethane, loaded onto a silica gel column and eluted using ethyl ether:hexane (1:1). The first red band was collected, and the solvent was removed to yield a dark red solid (78 mg, 81 %) that was recrystallized by slow diffusion of hexane-saturated N_2 into its ethyl ether solution through a cannula. **^{1}H NMR (400 MHz, $CDCl_3$, ppm):** δ 3.79 (s, 6 H, H9), 4.28 (s, 5 H, H7), 4.66 (t, 1 H, ^{3}J = 2.4 Hz, H6), 4.70 (d, 2 H, ^{3}J = 2.4 Hz, H5), 7.72 (s, 2 H, H3). **^{13}C{^{1}H} NMR (100 MHz, $CDCl_3$, ppm):** 53.22 (C9), 72.19 (C7), 74.17 (C6), 78.05 (C5), 78.05 (C4), 119.40 (C2), 143.09 (C3), 165.45 (C8). **IR (ATR, cm^{-1}):** 1700 (C=O).

Synthesis of $C_{16}H_{12}FeO_5S$ (31). In a 100 mL Schlenk flask, KOH (84 mg, 1.5 mmol) was added to a stirred solution of **29a** (200 mg, 0.50 mmol) in 3 mL methanol under N_2. The reaction mixture was refluxed for 3 h, cooled to room temperature and quenched with water (4 mL). The layers were separated and the aqueous layer was washed with ethyl ether (3 × 5 mL) and acidified to pH 2 with conc. HCl. The aqueous layer was extracted with dichloromethane (4 × 10 mL), the solvent was removed and the residue was triturated with ethyl ether to give a red solid (88 mg, 47 %). **^{1}H NMR (400 MHz, acetone-d_6, ppm):** δ 4.41 (s, 5 H, H7), 4.97 (t, 1 H, ^{3}J = 2.4 Hz, H6), 5.41 (d, 2 H, ^{3}J = 2.4 Hz, H5), 8.37 (s, 2 H, H3). **^{13}C{^{1}H} NMR (100 MHz, acetone-d_6, ppm):** 72.86

(C7), 77.06 (C6), 78.76 (C5), 80.21 (C4), 131.34(C2), 147.52 (C3), 165.29 (C8). **IR (ATR, cm^{-1}):** 1151 (S=O), 1700 (C=O), 2856–3106 (COOH).

Synthesis of $C_{16}H_{12}FeO_4S$ (32). In a 100 mL Schlenk flask, NaOH (23 mg, 0.60 mmol) in 1 mL methanol was added to a stirred solution of **30** (50 mg, 0.10 mmol) in 5 ml dichloromethane and allowed to reflux for 12 h under N_2. The reaction mixture was cooled to room temperature and quenched with water (4 mL). The layers were separated and the aqueous layer was washed with ethyl ether (3 × 5 mL) and acidified to pH 2 with 6 M HCl. The dark red precipitate was collected on a medium-porosity glass frit, washed with water (20 mL) and hexane (10 mL), and dried in a vacuum overnight to give dark red powder **32** (30 mg, 65%). **^{1}H NMR (400 MHz, acetone-d_6, ppm):** δ 4.38 (s, 5 H, H7), 4.85 (s, 3 H, H5 and H6 merge), 7.72 (s, 2 H, H3). **^{13}C{^{1}H} NMR (100 MHz, acetone-d_6, ppm):** 72.84 (C7), 74.86 (C6), 77.85 (C5), 78.62 (C4), 120.77 (C2), 142.52 (C3), 165.90 (C8). **IR (ATR, cm^{-1}):** 1700 (C=O), 2947–3100 (COOH).

Synthesis of $C_{16}H_{10}Cl_2FeO_2S$ (33). In a 100 mL Schlenk flask, oxalyl chloride (48 μL 0.60 mmol,) and anhydrous DMF (5 μL) were added to a stirred suspension of **32** (50 mg, 0.1 mmol) in anhydrous benzene (10 mL) under N_2. The reaction mixture was stirred at room temperature for 5 h. The solvent was removed to yield **33** (42 mg, 75 %). An analytical sample was obtained by slow diffusion of hexane-saturated N_2 into its ethyl ether solution through a cannula. **^{1}H NMR (400 MHz, $CDCl_3$, ppm):** δ 4.41 (s, 5 H, H7), 5.06 (s, 1 H, H6), 5.07 (s, 2 H, H5), 8.29 (s, 2 H, H3). **^{13}C{^{1}H} NMR (100 MHz, $CDCl_3$, ppm):** 73.14 (C7), 76.93 (C6), 77.55 (C5), 79.35 (C4), 120.71 (C2), 153.17 (C3), 164.59 (C8). **IR (ATR, cm^{-1}):** 1700 (C=O).

4.3 Results and Discussion

4.3.1 Synthesis. The two-fold Knoevenagel reaction of 1,2-diformylferrocene and dimethylthioglycolate sulfoxide in the presence of freshly distilled triethylamine, by slight modification of the procedure developed by Borai et al.,[214] gave mono- and di-dehydrated products **29b** and **29a** in a ratio of 1:2. In order to eliminate mono-dehydrated product **29b**, the reaction was carried out with 16 h stirring at room temperature followed by 6 h at 60 °C. The progress of the reaction was monitored by TLC until there was no change in the reaction mixture. The compounds **29a** and **29b** were typically obtained in pure form by column chromatography on silica, followed by recrystallization by slow diffusion of hexane-saturated N_2 into their dichloromethane solutions through a cannula. Compound **29a** was a dark red solid, whereas **29b** was a dark purple solid. Byproduct **29b** was characterized by ^{1}H NMR, which shows an unsymmetrical pattern of substituted Cp protons in a ratio of 1:1:1. Further, the compound was characterized by IR, which shows the presence of an –OH group at 3378 cm^{-1} along with two carbonyl stretches at 1720 and 1743 cm^{-1}. This also proves that **29b** is an asymmetric compound.

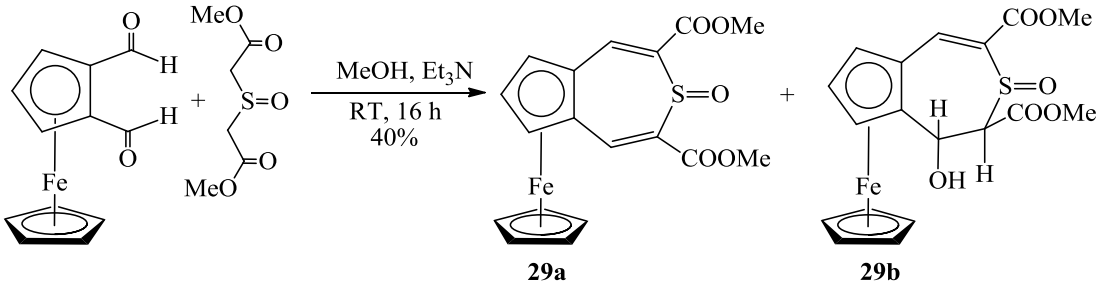

29a **29b**

Scheme 4.1 Synthesis of ferrocene-fused 5,7-dimethylester thiepin S-oxide

Following the procedure for the deoxygenation of 1,3-dibenzalthiophthalan 2-oxide,[215] ferrocene-fused 5,7-dimethylester thiepin S-oxide (**29a**) was reacted with 2-

chloro-1,3,2-benzodioxaphosphole to form ferrocene-fused 5,7-dimethylester thiepin (**30**) in good yield (81%). The absence of an S=O peak in its IR spectrum indicates the formation of deoxygenated product (**30**). An analytically pure compound was obtained by slow diffusion of hexane-saturated N_2 into its ethyl ether solution.

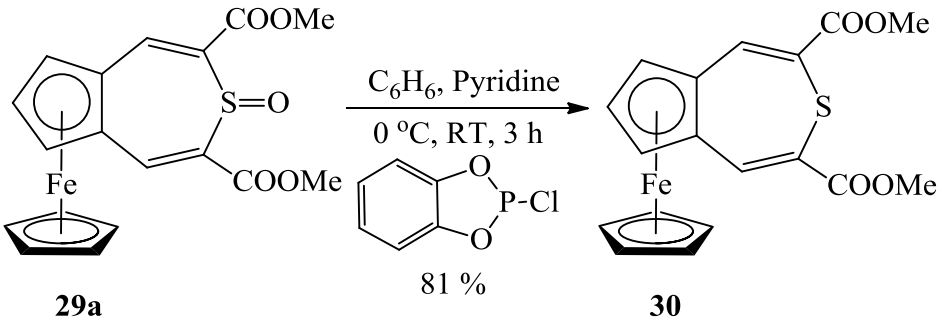

Scheme 4.2 Synthesis of ferrocene-fused 5,7-dimethylester thiepin

The saponification of **29a** was carried out by using KOH in refluxing methanol for 3 h to give thiepin S-oxide diacid **31** (47 %).[107] The saponification of **30** was accomplished by using NaOH in refluxing dichloromethane/methanol for 12 h to yield thiepin diacid **32** (65 %).[107] The conversion of esters to carboxylic acids was confirmed by IR spectra, which displayed a broad COOH stretch from 2626 to 3106 cm^{-1}.

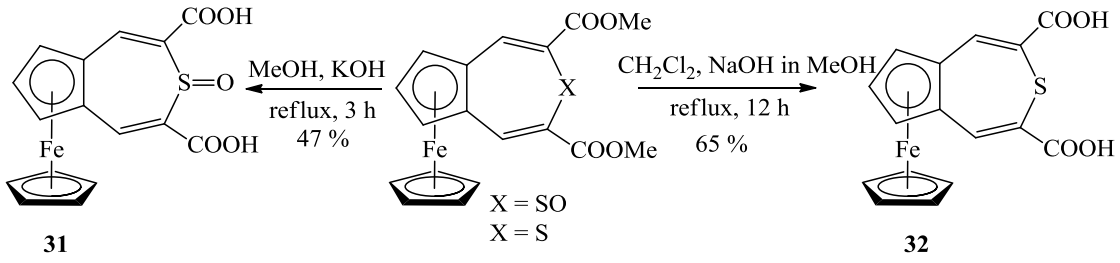

Scheme 4.3 Saponification of diesters

.

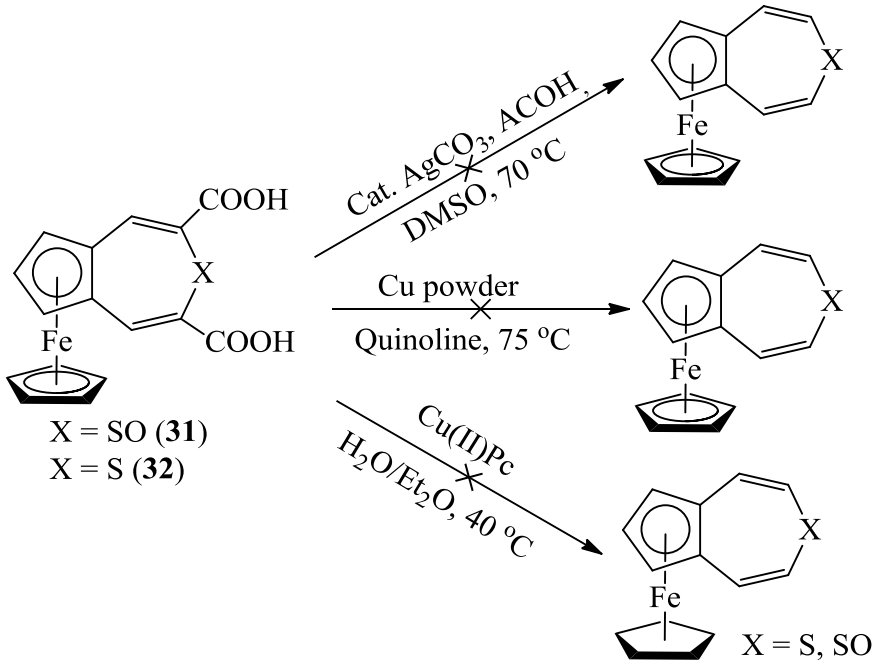

Scheme 4.4 Attempted decarboxylation of **31** and **32**

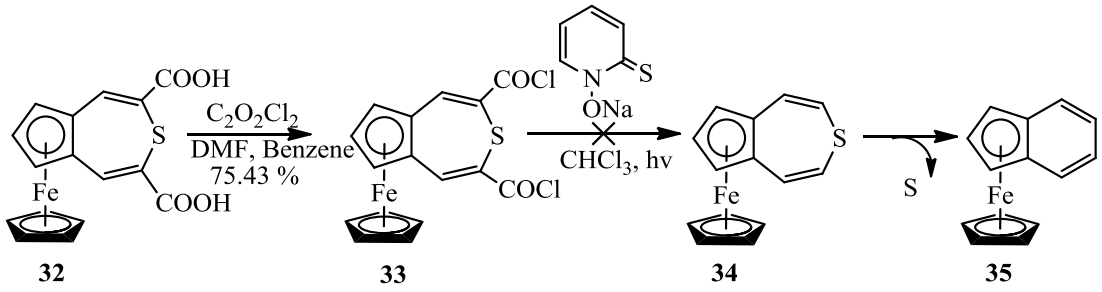

Scheme 4.5 Attempted synthesis of ferrocene-fused thiepin (**34**)

Multiple attempts to decarboxylate diacids **31** and **32** ended in failure. Reactions with silver acetate/acetic acid in DMSO according to Larrosa,[216] with copper powder in quinoline at 75 °C[217] and with copper(II) phthalocyanine in H_2O/ethyl ether at 40 °C[218] all resulted in decomposition.

The Barton reductive decarboxylation is a powerful method for converting difficult carboxylic acids to alkanes. We attempted to decarboxylate diacid **32** by employing the procedure of Eun et al.[211] Thiepin diacid (**32**) reacted with oxalyl chloride in the presence of catalytic DMF to give thiepin diacyl chloride (**33**) in good yield (75%). Subsequent reaction of **33** with 1-hydroxypyridine-2(1*H*)-thione sodium salt in chloroform also resulted in decomposition. Based upon literature reports,[189,190] benzannulated thiepins are thermally labile and readily undergo extrusion of sulfur to give naphthalenes. We may be observing similar chemical behavior in our system, with extrusion of sulfur from the unsubstituted ferrocene-fused thiepin **34** resulting in formation of (η^5-cyclopentadienyl)(η^5-indenyl)iron (**35**), which decomposed under the reaction conditions. It may be possible to trap compound **35** *in situ*, but we made no attempt to do so.

4.3.2 Spectroscopy. New compounds were fully characterized by spectroscopic methods, including ^{1}H and ^{13}C NMR, and IR. The substituted cyclopentadienyl (Cp) resonances in the ^{1}H NMR spectra of ferrocene-fused thiepin derivatives **29a** and **30**–**33** display a characteristic doublet and triplet with an integration of a 2:1 ratio. The resonances for the outer protons (H5 in Figure 4.10) range from 4.70 to 5.20 ppm. The resonances for the inner protons (H6 in Figure 4.10) generally range from 4.66 to 5.06 ppm. The ^{1}H NMR singlet of unsubstituted cyclopentadienyl (H7 in Figure 4.10) lies between 4.28 and 4.41 ppm. The formation of byproduct **29b** was indicated in the ^{1}H NMR by the ABC pattern from 4.68 to 5.21 ppm for the substituted Cp (H4, H5 and H6 in Figure 4.10), indicating the unsymmetrical nature of the ligand. The proton peak at 3.79 ppm in ^{1}H NMR and an OH stretch at 3373 cm^{-1} in IR indicate the presence of a

hydroxyl group in **29b**, a mono-dehydrated product of a double Knoevenagel reaction. The methyl ester protons for compounds **29a**, **29b** and **30**–**33** range between 3.79 and 3.89 ppm.

The ^{13}C NMR of **29b** shows a resonance of unsubstituted Cp carbon at 70.84 ppm, whereas for the complexes **29a** and **30**–**33** it ranges between 72.13 to 73.14 ppm. The Cp carbon resonances for the ferrocene-fused thiepin derivatives **29a** and **30**–**33** consist of a set of three resonances attributed to the inner position (74.86–77.06 ppm, C6), the outer positions (77.55 to 78.76 ppm, C5) and the *ipso* positions (78.62 to 80.21 ppm, C4) as shown in Figure 4.10. The ester carbonyl carbon resonances of **29a**, **29b**, **30**, and carboxylic acid carbonyl carbon resonances of **31** and **32** display between 164.50 and 169.32 ppm, typical of organic carbonyls. The IR spectra of **29a**, **30** and **33** display carbonyl stretching between 1700 and 1720 cm^{-1} typical of α, β unsaturated organic ester compounds, and the IR spectra of **31** and **32** exhibit very broad COOH absorbances from 2856 to 3106 cm^{-1}. Table 4.1 shows some selected ^{1}H and ^{13}C NMR and IR data for compounds **29a**, **29b** and **30**–**33**.

Table 4.1 Selected NMR and IR (ATR, cm^{-1}) data of **29a** and **30**–**33**

Compd.	H6 δ_H	H5 δ_H	H4 δ_H	C6 δ_C	C5 δ_C	C4 δ_C	C=O δ_C	S=O (cm^{-1})	C=O (cm^{-1})	Sol vent
29a	4.84	5.20	8.30	76.64	78.25	78.96	164.50	1032	1704	a
30	4.66	4.70	7.72	74.17	78.05	78.05	165.45	–	1700	a
31	4.97	5.41	8.37	77.06	78.76	80.21	165.29	1151	1700	b
32	4.85	4.85	7.72	74.86	77.85	78.62	165.90	–	1700	b
33	5.06	5.07	8.29	76.93	77.55	79.35	164.59	–	1700	a

Solvent: a = $CDCl_3$, b = acetone-d_6

4.3.3 Structure. Single crystals of **29a**, **29b** and **33** were grown by slow evaporation of dichloromethane solutions with a stream of hexane-saturated N_2 through a cannula; a single crystal of **30** was grown by slow evaporation of ethyl ether solution by the diffusion of hexane-saturated N_2 through a cannula. The structures of [Fe(Cp){η^5-$C_5H_3(CHCCOOMe)_2SO$}] (**29a**), [Fe{(Cp)η^5-$C_5H_3(CHCCOOMeCHOHCHCOOMeSO)$}] (**29b**), [Fe(Cp){$\eta^5$-$C_5H_3(CHCCOOMe)_2S$}] (**30**), [Fe(Cp){$\eta^5$-$C_5H_3(CHCCOCl)_2S$}] (**33**) were determined by X-ray crystallographic methods. Thermal ellipsoid plots with numbering schemes are shown in Figures 4.11 to 4.14**.** The crystal structure and refinement data for compounds **29a**, **29b**, **30** and **33** can be found in Tables 4.2 to 4.3**.** Bond distances and angles for **29a, 29b, 30 and 33** can be found in Tables 4.4 to 4.7.

The ferrocene complexes **29a**, **29b**, **30** and **33** show the typical ferrocene geometry. The average bond distances of metal to substituted Cp are 2.048(3) Å for **29a**, 2.048(2) Å for **29b**, 2.046(3) Å for **30** and 2.046(3) Å for **33**. Similarly, the average bond distances of metal to unsubstituted Cp are 2.050(3) Å for **29a**, 2.052(3) Å for **29b**, 2.056(3) Å for **30** and 2.060 (3) Å for **33**. The average bond distances of iron to the centroids of substituted Cp and unsubstituted Cp are **29a** [1.646(3) Å, 1.657(3) Å], **29b** [1.646(2) Å, 1.655(2) Å], **30** [1.644(3) Å, 1.664(3) Å], and **33** [1.718 (3) Å, 1.667(3) Å].

The SO groups of complexes **29a** and **29b** are *exo* with respect to the iron center. The ester groups are positioned in the least-squares plane of Cp and the seven-membered ring. The molecular structure of **29b** shows that the ester on C7 is *exo* and the hydroxy on C8 is *endo* to the iron center. The *endo* orientation of the hydroxy group and the mutually cis orientation of the hydrogen atom on C7 may explain the failure of the C7–C8 bond to

dehydrate under basic (*E*2) conditions.. The interplanar angle between C4–C3–C2–C1–C5–C9 and C12–C8–S1 of complex **30** is 7.12°. The sulfur-oxygen bond distances of **29a** and **29b** are 1.495(2) Å and 1.5008(19) Å, which are close to the S=O bond distance [(1.431(3) Å and 1.436(3) Å] in benzo[*b*]thiepin 1,1-dioxide.[193]

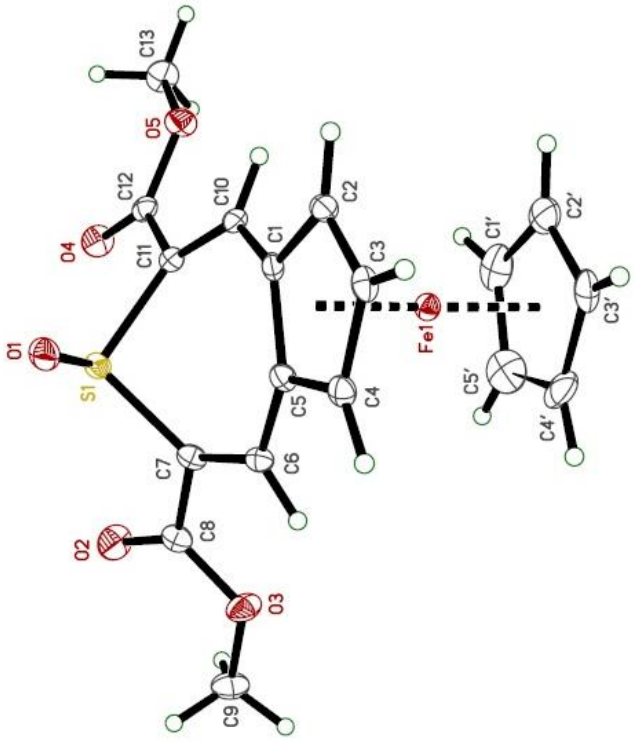

Figure 4.11 Molecular structure of [Fe(Cp){η^5-$C_5H_3(CHCCOOMe)_2SO$}] (**29a**)

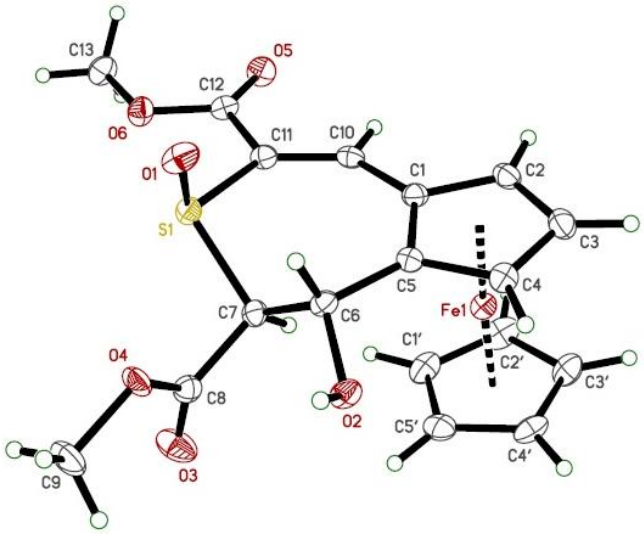

Figure 4.12 Molecular structure of [Fe(Cp){η^5-C_5H_3(CHCCOOMeCHOHCHCOOMe-SO)}] (**29b**)

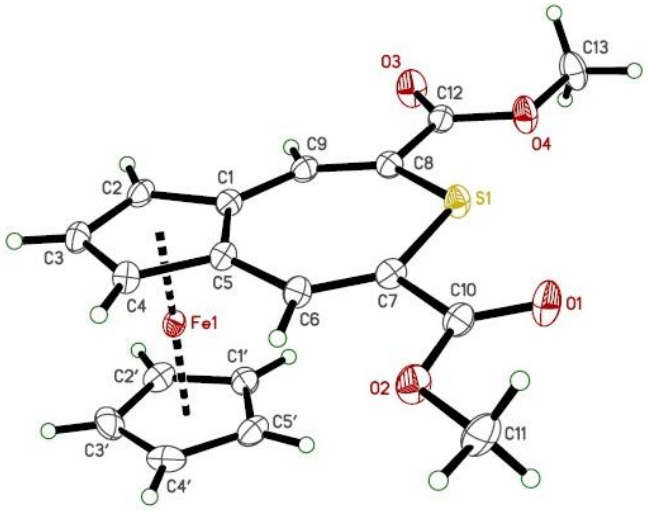

Figure 4.3 Molecular structure of [Fe(Cp){η^5-C_5H_3(CHCCOOMe)$_2$S}] (**30**)

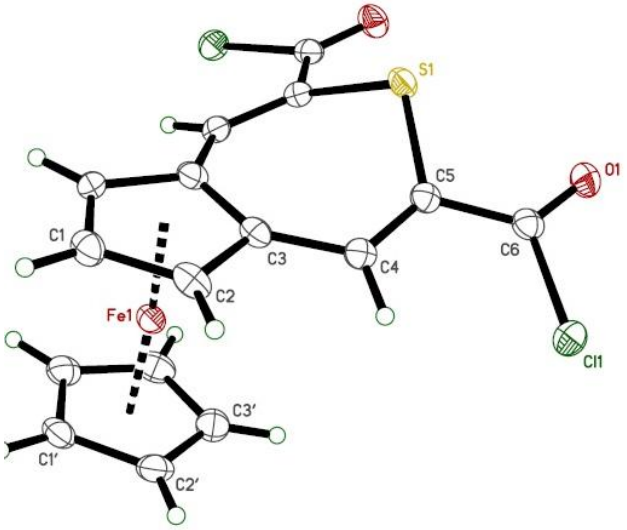

Figure 4.4 Molecular structure of [Fe(Cp){η^5-$C_5H_3(CHCCOCl)_2S$}] (**33**)

Table 4.2 Crystal Data and Structure Refinement for Compounds **29a** and **29b**

Compound	**29a**	**29b**
Formula	$C_{18}H_{16}FeO_5S$	$C_{18}H_{18}FeO_6S$
Formula wt. (amu)	400.22	418.23
T, K	90.02)	90.0(2)
Crystal system	Tetragonal	Monoclinic
Space group	P4 (3)2(1)2	P2(1)/2
Z	8	4
a, Å	10.9279(2)	7.4534(2)
b, Å	10.9279(2)	17.3952(4)
c, Å	27.4104(5)	13.0244(3)
α (deg)	90	90
β (deg)	90	95.3810(13)
γ (deg)	90	90
V, $Å^3$	3273.32(13)	1681.22(7)
d_{calc}, Mg/m^3	1.624	1.652
F(000)	1648	864
Crystal size (mm^3)	0.100 × 0.100 × 0.030	0.420 × 0.260 × 0.160
Radiation	Cu Kα (λ = 1.54178 Å)	Cu Kα (λ = 1.54178 Å)
Monochromator	Graded multilayer optics	Graded multilayer optics
Absorption coefficient (mm^{-1})	8.827	1.055
Diffractometer	Bruker X8 Proteum	Bruker X8 Proteum
Range (deg)	4.355 to 68.308	1.959 to 27.491
Limiting indices	$-13 \le h \le 13$	$-9 \le h \le 9$
	$-5 \le k \le 12$	$-22 \le k \le 22$
	$-33 \le l \le 33$	$-16 \le l \le 16$
Reflections collected	37471	29727
Independent reflections	2867 [R(int) = 0.0512]	3869[R(int) = 0.0448]
Absorption correction	Semi-empirical from equivalents	Semi-empirical from equivalents
Refinement method	SHELXL-97	SHELXL-97
Refinement method	Full-matrix least-squares on F^2	Full-matrix least-squares on F^2
Data/restraints/parameter	2867 / 0 / 252	3869 / 0 / 238
Goodness-of-fit on F^2	1.054	1.148
Final R indices [$I > 2\sigma(I)$]	R1 = 0.0248, wR2 = 0.0654	R1 = 0.0411, wR2 = 0.0989
R indices (all data)	R1 = 0.0252, wR2 = 0.0657	R1 = 0.0577, wR2 = 0.1077
Largest diff. peak and hole	0.270 and -0.238 ($e \cdot Å^{-3}$)	0.761 and -0.466 ($e \cdot Å^{-3}$)

Table 4.3 Crystal Data and Structure Refinement for Compounds **30** and **33**

Compound	**30**	**33**
Formula	$C_{18}H_{16}FeO_4S$	$C_{16}H_{10}Cl_2FeO_2S$
Formula wt. (amu)	384.22	393.05
T, K	90.0(2)	90.0(2)
Crystal system	Monoclinic	Monoclinic
Space group	P2(1)/c	P2(1)/m
Z	4	2
a, Å	10.9690(7)	7.0751(3)
b, Å	16.2019(11)	11.4732(6)
c, Å	9.5500(6)	9.0779(4)
α (deg)	90	90
β (deg)	112.739(4)	105.677(3)
γ (deg)	90	90
V, $Å^3$	1565.30(18)	709.48(6)
d_{calc}, Mg/m^3	1.630	1.840
F(000)	792	396
Crystal size (mm^3)	0.220 × 0.050 × 0.030	0.260 × 0.150 × 0.140
Radiation	Cu Kα (λ = 1.54178 Å)	Cu Kα (λ = 1.54178 Å)
Monochromator	Graded multilayer optics	Graded multilayer optics
Absorption coefficient (mm^{-1})	9.152	1.588
Diffractometer	Bruker X8 Proteum	Bruker X8 Proteum
Range (deg)	4.370 to 68.551	2.330 to 27.495
Limiting indices	$-12 \le h \le 13$	$-9 \le h \le 9$
	$-19 \le k \le 19$	$-14 \le k \le 14$
	$-11 \le l \le 4$	$-11 \le l \le 11$
Reflections collected	19870	9641
Independent reflections	2811 [R(int) = 0.0636]	1706 [R(int) = 0.0320]
Absorption correction	Semi-empirical from equivalents	Semi-empirical from equivalents
Refinement method	SHELXL-97	SHELXL-97
Refinement method	Full-matrix least-squares on F^2	Full-matrix least-squares on F^2
Data/restraints/parameter	2811 / 0 / 219	1706 / 36 / 146
Goodness-of-fit on F^2	1.092	1.119
Final R indices [$I > 2\sigma(I)$]	R1 = 0.0405, wR2 = 0.1072	R1 = 0.0340, wR2 = 0.0819
R indices (all data)	R1 = 0.0481, wR2 = 0.1126	R1 = 0.0428, wR2 = 0.0849
Largest diff. peak and hole	0.410 and -0.894 ($e \cdot Å^{-3}$)	0.476 and -0.456 ($e \cdot Å^{-3}$)

Table 4.4 Bond Distances (Å) and Bond Angles (°) for Compound **29a**

Atoms	**Distances (Å)**
Fe1–C2	2.030(3)
Fe1–C4	2.037(2)
Fe1–C3'	2.042(3)
Fe1–C2'	2.045(3)
Fe1–C1'	2.049(3)
Fe1–C3	2.051(3)
Fe1 –C4'	2.056(3)
Fe1–C1	2.057(2)
Fe1–C5'	2.059(3)
Fe1–C5	2.063(3)
S1–O1	1.495(2)
S1–C11	1.796(3)
S1–C7	1.798(3)
O2–C8	1.204(3)
O3–C8	1.349(3)
O3–C9	1.444(3)
O4–C12	1.214(3)
O5–C12	1.345(3)
O5–C13	1.445(3)
C1–C10	1.435(4)
C1–C2	1.435(4)
C1–C5	1.452(4)
C2–C3	1.414(4)
C2–H2	0.94(3)
C3–C4	1.417(4)
C3–H3	0.89(3)
C4–C5	1.438(4)
C4–H4	0.97(3)
C5–C6	1.437(4)
C6–C7	1.347(4)
C7–C8	1.477(4)
C10–C11	1.349(4)
C11–C12	1.475(4)
C1'–C2'	1.409(5)
C1'–C5'	1.431(5)
C1'–H1'	0.95(4)
C2'–C3'	1.425(4)
C2'–H2'	0.94(4)
C3'–C4'	1.419(5)
C3'–H3'	0.95(4)
C4'–C5'	1.410(5)
C4'–H4'	0.94(4)
C5'–H5'	0.89(4)
Atoms	**Angles (°)**
C2–Fe1–C4	69.10(11)
C2–Fe1–C3'	120.25(12)
C4–Fe1–C3'	118.01(12)
C2–Fe1–C2'	105.86(12)
C4–Fe1–C2'	153.80(13)
C3'–Fe1–C2'	40.80(12)
C2–Fe1–C1'	123.00(12)
C4–Fe1–C1'	163.10(13)
C3'–Fe1–C1'	68.14(13)
C2'–Fe1–C1'	40.27(14)
C2–Fe1–C3	40.54(11)
C4–Fe1–C3	40.56(11)
C3'–Fe1–C3	103.54(12)
C2'–Fe1–C3	119.10(13)
C1'–Fe1–C3	156.24(13)
C2–Fe1–C4'	156.50(12)
C4–Fe1–C4'	105.59(12)
C3'–Fe1–C4'	40.53(13)
C2'–Fe1–C4'	68.29(13)
C1'–Fe1–C4'	68.13(13)
C3–Fe1–C4'	120.81(13)
C2–Fe1–C1	41.10(11)
C4–Fe1–C1	69.21(11)
C3'–Fe1–C1	158.89(12)
C2'–Fe1–C1	124.78(12)
C1'–Fe1–C1	111.11(12)
C3–Fe1–C1	68.3(1)
C4'–Fe1–C1	160.33(12)
C2–Fe1–C5'	160.82(13)
C4–Fe1–C5'	124.55(13)
C3'–Fe1–C5'	67.86(14)

Table 4.4 Continued

C2'–Fe1–C5'	68.06(14)
C1'–Fe1–C5'	40.76(14)
C3–Fe1–C5'	158.52(13)
C4'–Fe1–C5'	40.09(14)
C1–Fe1–C5'	126.37(13)
C2–Fe1–C5	69.33(11)
C4–Fe1–C5	41.07(10)
C3'–Fe1–C5	155.66(12)
C2'–Fe1–C5	163.22(12)
C1'–Fe1–C5	127.99(13)
C3–Fe1–C5	68.36(11)
C4'–Fe1–C5	122.55(12)
C1–Fe1–C5	41.28(10)
C5'–Fe1–C5	110.95(13)
O1–S1–C11	106.35(12)
O1–S1–C7	106.14(12)
C11–S1–C7	100.36(12)
C8–O3–C9	115.3(2)
C12–O5–C13	115.9(2)
C10–C1–C2	123.6(2)
C10–C1–C5	128.6(2)
C2–C1–C5	107.5(2)
C10–C1–Fe1	121.72(18)
C2–C1–Fe1	68.44(14)
C5–C1–Fe1	69.56(14)
C3–C2–C1	108.1(2)
C3–C2–Fe1	70.50(15)
C1–C2–Fe1	70.46(15)
C3–C2–H2	128.4(19)
C1–C2–H2	123.6(19)
Fe1–C2–H2	124(2)
C2–C3–C4	109.2(2)
C2–C3–Fe1	68.96(15)
C4–C3–Fe1	69.22(15)
C2–C3–H3	127(2)
C4–C3–H3	124(2)
Fe1–C3–H3	125(2)
C3–C4–C5	108.1(2)
C3–C4–Fe1	70.23(15)
C5–C4–Fe1	70.41(14)
C3–C4–H4	128.9(19)
C5–C4–H4	123.0(19)
Fe1–C4–H4	123.5(19)
C6–C5–C4	123.7(3)
C6–C5–C1	128.5(2)
C4–C5–C1	107.1(2)
C6–C5–Fe1	120.28(19)
C4–C5–Fe1	68.52(14)
C1–C5–Fe1	69.17(14)
C7–C6–C5	126.9(3)
C6–C7–C8	122.7(3)
C6–C7–S1	123.1(2)
C8–C7–S1	112.8(2)
O2–C8–O3	122.7(3)
O2–C8–C7	125.0(3)
O3–C8–C7	112.4(2)
C11–C10–C1	127.2(2)
C10–C11–C12	122.3(2)
C10–C11–S1	123.3(2)
C12–C11–S1	113.30(19)
O4–C12–O5	123.1(3)
O4–C12–C11	124.7(2)
O5–C12–C11	112.3(2)
C2'–C1'–C5'	107.9(3)
C2'–C1'–Fe1	69.72(17)
C5'–C1'–Fe1	69.97(17)
C2'–C1'–H1'	124(2)
C5'–C1'–H1'	128(2)
Fe1–C1'–H1'	122(2)
C1'–C2'–C3'	107.9(3)

Table 4.4 Continued

C1'–C2'–Fe1	70.02(17)
C3'–C2'–Fe1	69.46(16)
C1'–C2'–H2'	127(2)
C3'–C2'–H2'	125(2)
Fe1–C2'–H2'	122(2)
C4'–C3'–C2'	108.1(3)
C4'–C3'–Fe1	70.27(17)
C2'–C3'–Fe1	69.75(17)
C4'–C3'–H3'	126(2)
C2'–C3'–H3'	125(2)
Fe1–C3'–H3'	119(2)
C5'–C4'–C3'	108.0(3)
C5'–C4'–Fe1	70.07(18)
C3'–C4'–Fe1	69.20(17)
C5'–C4'–H4'	125(2)
C3'–C4'–H4'	127(2)
Fe1–C4'–H4'	122(2)
C4'–C5'–C1'	108.1(3)
C4'–C5'–Fe1	69.84(18)
C1'–C5'–Fe1	69.27(18)
C4'–C5'–H5'	127(3)
C1'–C5'–H5'	125(3)
Fe1–C5'–H5'	125(3)

Table 4.5 Bond distances (Å) and Bond Angles (°) for Compound **29b**

Atoms	**Distances (Å)**
Fe1–C2	2.036(2)
Fe1–C3'	2.042(2)
Fe1–C4'	2.045(2)
Fe1–C4	2.048(2)
Fe1–C2'	2.051(3)
Fe1–C1	2.051(2)
Fe1–C5	2.052(2)
Fe1–C3	2.054(3)
Fe1–C5'	2.059(3)
Fe1–C1'	2.061(3)
S1–O1	1.5008(19)
S1–C11	1.781(2)
S1–C7	1.847(2)
O2–C6	1.420(3)
O3–C8	1.197(3)
O4–C8	1.332(3)
O4–C9	1.450(3)
O5–C12	1.206(3)
O6–C12	1.347(3)
O6–C13	1.446(3)
C1–C10	1.442(3)
C1–C2	1.443(3)
C1–C5	1.452(3)
C2–C3	1.415(4)
C3–C4	1.426(3)
C4–C5	1.431(3)
C5–C6	1.497(3)
C1'–C5'	1.417(4)
C1'–C2'	1.424(4)
C2'–C3'	1.439(4)
C3'–C4'	1.420(4)
C4'–C5'	1.422(4)
C6–C7	1.534(3)
C7–C8	1.505(3)
C10–C11	1.352(3)
C11–C12	1.485(3)
Atoms	**Angle (°)**
C2–Fe1–C3'	116.98(11)
C2–Fe1–C4'	149.08(11)
C3'–Fe1–C4'	40.66(10)
C2–Fe1–C4	68.56(10)
C3'–Fe1–C4	124.32(11)
C4'–Fe1–C4	104.51(10)
C2–Fe1–C2'	109.42(11)
C3'–Fe1–C2'	41.18(11)
C4'–Fe1–C2'	68.59(11)
C4–Fe1–C2'	163.89(11)
C2–Fe1–C1	41.34(9)
C3'–Fe1–C1	153.06(10)
C4'–Fe1–C1	166.17(10)
C4–Fe1–C1	68.89(10)
C2'–Fe1–C1	120.91(11)
C2–Fe1–C5	69.52(9)
C3'–Fe1–C5	162.78(10)
C4'–Fe1–C5	125.82(10)
C4–Fe1–C5	40.85(10)
C2'–Fe1–C5	154.80(11)
C1–Fe1–C5	41.44(9)
C2–Fe1–C3	40.47(10)
C3'–Fe1–C3	104.94(11)
C4'–Fe1–C3	114.65(11)
C4–Fe1–C3	40.69(10)
C2'–Fe1–C3	127.52(11)
C1–Fe1–C3	68.83(10)
C5–Fe1–C3	68.98(10)
C2–Fe1–C5'	169.71(11)
C3'–Fe1–C5'	68.50(11)
C4'–Fe1–C5'	40.54(11)
C4–Fe1–C5'	116.47(10)
C2'–Fe1–C5'	68.40(11)
C1–Fe1–C5'	130.34(10)
C5–Fe1–C5'	107.91(10)
C3–Fe1–C5'	148.92(11)
C2–Fe1–C1'	131.78(11)
C3'–Fe1–C1'	68.38(11)

Table 4.5 Continued

C4'–Fe1–C1'	67.86(11)
C4–Fe1–C1'	151.96(11)
C2'–Fe1–C1'	40.53(11)
C1–Fe1–C1'	111.92(10)
C5–Fe1–C1'	120.52(10)
C3–Fe1–C1'	167.33(11)
C5'–Fe1–C1'	40.22(11)
O1–S1–C11	108.54(11)
O1–S1–C7	106.95(11)
C11–S1–C7	98.96(11)
C8–O4–C9	116.4(2)
C12–O6–C13	115.03(19)
C10–C1–C2	120.2(2)
C10–C1–C5	132.5(2)
C2–C1–C5	107.3(2)
C10–C1–Fe1	125.34(17)
C2–C1–Fe1	68.78(14)
C5–C1–Fe1	69.33(13)
C3–C2–C1	108.6(2)
C3–C2–Fe1	70.45(14)
C1–C2–Fe1	69.88(13)
C2–C3–C4	108.1(2)
C2–C3–Fe1	69.08(14)
C4–C3–Fe1	69.41(14)
C3–C4–C5	108.9(2)
C3–C4–Fe1	69.90(14)
C5–C4–Fe1	69.74(13)
C4–C5–C1	107.1(2)
C4–C5–C6	125.3(2)
C1–C5–C6	127.7(2)
C4–C5–Fe1	69.40(13)
C1–C5–Fe1	69.23(13)

C6–C5–Fe1	126.77(16)
C5'–C1'–C2'	108.8(2)
C5'–C1'–Fe1	69.82(14)
C2'–C1'–Fe1	69.33(15)
C1'–C2'–C3'	107.3(2)
C1'–C2'–Fe1	70.13(15)
C3'–C2'–Fe1	69.10(14)
C4'–C3'–C2'	107.6(2)
C4'–C3'–Fe1	69.77(14)
C2'–C3'–Fe1	69.72(15)
C3'–C4'–C5'	108.6(2)
C3'–C4'–Fe1	69.57(14)
C5'–C4'–Fe1	70.27(14)
C1'–C5'–C4'	107.7(2)
C1'–C5'–Fe1	69.96(15)
C4'–C5'–Fe1	69.19(14)
O2–C6–C5	109.68(19)
O2–C6–C7	110.76(19)
C5–C6–C7	110.74(19)
C8–C7–C6	112.88(19)
C8–C7–S1	106.45(16)
C6–C7–S1	111.61(16)
O3–C8–O4	124.5(2)
O3–C8–C7	124.3(2)
O4–C8–C7	111.1(2)
C11–C10–C1	132.8(2)
C10–C11–C12	117.4(2)
C10–C11–S1	127.20(19)
C12–C11–S1	115.32(18)
O5–C12–O6	123.5(2)
O5–C12–C11	125.0(2)
O6–C12–C11	111.5(2)

Table 4.6 Bond distances (Å) and Bond Angles (°) for Compound **30**

Atoms	**Distances (Å)**
Fe1–C5	2.032(3)
Fe1–C4	2.040(3)
Fe1–C1	2.045(3)
Fe1–C3'	2.046(3)
Fe1–C4'	2.046(3)
Fe1–C5'	2.052(3)
Fe1–C2	2.053(3)
Fe1–C3	2.060(3)
Fe1–C2'	2.064(3)
Fe1–C1'	2.072(3)
S1–C8	1.767(3)
S1–C7	1.768(3)
O1–C10	1.208(4)
O2–C10	1.346(4)
O2–C11	1.444(4)
O3–C12	1.210(4)
O4–C12	1.337(3)
O4–C13	1.453(4)
C1–C5	1.438(4)
C1–C2	1.445(4)
C1–C9	1.445(4)
C2–C3	1.423(4)
C3–C4	1.420(4)
C4–C5	1.434(4)
C5–C6	1.445(4)
C6–C7	1.344(4)
C7–C10	1.484(4)
C8–C9	1.334(4)
C8–C12	1.498(4)
C1'–C2'	1.415(4)
C1'–C5'	1.426(4)
C2'–C3'	1.413(5)
C3'–C4'	1.418(5)
C4'–C5'	1.421(5)
Atoms	**Angles (°)**
C5–Fe1–C4	41.23(11)
C5–Fe1–C1	41.31(11)
C4–Fe1–C1	69.02(12)
C5–Fe1–C3'	151.89(13)
C4–Fe1–C3'	117.60(13)
C1–Fe1–C3'	165.26(13)
C5–Fe1–C4'	117.20(13)
C4–Fe1–C4'	104.95(13)
C1–Fe1–C4'	153.53(13)
C3'–Fe1–C4'	40.56(14)
C5–Fe1–C5'	106.60(12)
C4–Fe1–C5'	124.63(12)
C1–Fe1–C5'	120.50(12)
C3'–Fe1–C5'	67.95(13)
C4'–Fe1–C5'	40.57(13)
C5–Fe1–C2	69.35(11)
C4–Fe1–C2	68.37(12)
C1–Fe1–C2	41.28(11)
C3'–Fe1–C2	126.58(13)
C4'–Fe1–C2	162.27(12)
C5'–Fe1–C2	156.56(13)
C5–Fe1–C3	69.13(11)
C4–Fe1–C3	40.52(11)
C1–Fe1–C3	68.94(11)
C3'–Fe1–C3	106.86(12)
C4'–Fe1–C3	124.04(13)
C5'–Fe1–C3	161.49(13)
C2–Fe1–C3	40.47(12)
C5–Fe1–C2'	165.33(12)
C4–Fe1–C2'	153.18(12)
C1–Fe1–C2'	128.73(12)
C3'–Fe1–C2'	40.23(13)
C4'–Fe1–C2'	67.94(13)
C5'–Fe1–C2'	67.68(12)
C2–Fe1–C2'	110.17(12)
C3–Fe1–C2'	120.66(12)
C5–Fe1–C1'	127.06(12)
C4–Fe1–C1'	163.32(12)
C1–Fe1–C1'	110.04(12)
C3'–Fe1–C1'	67.67(12)

Table 4.6 Continued

C4'–Fe1–C1'	68.08(12)
C5'–Fe1–C1'	40.44(12)
C2–Fe1–C1'	122.67(12)
C3–Fe1–C1'	155.88(13)
C2'–Fe1–C1'	40.01(12)
C8–S1–C7	109.99(14)
C10–O2–C11	115.3(2)
C12–O4–C13	115.0(2)
C5–C1–C2	107.5(3)
C5–C1–C9	129.7(2)
C2–C1–C9	122.8(3)
C5–C1–Fe1	68.85(16)
C2–C1–Fe1	69.67(16)
C9–C1–Fe1	124.6(2)
C3–C2–C1	108.2(3)
C3–C2–Fe1	70.01(16)
C1–C2–Fe1	69.06(16)
C4–C3–C2	108.0(2)
C4–C3–Fe1	68.99(16)
C2–C3–Fe1	69.52(16)
C3–C4–C5	108.9(3)
C3–C4–Fe1	70.49(17)
C5–C4–Fe1	69.08(16)
C4–C5–C1	107.4(2)
C4–C5–C6	122.3(3)
C1–C5–C6	130.3(3)
C4–C5–Fe1	69.69(17)
C1–C5–Fe1	69.84(16)
C6–C5–Fe1	123.4(2)

C7–C6–C5	130.8(3)
C6–C7–C10	119.3(3)
C6–C7–S1	133.1(2)
C10–C7–S1	107.6(2)
C9–C8–C12	114.7(3)
C9–C8–S1	133.3(2)
C12–C8–S1	111.9(2)
C8–C9–C1	131.2(3)
O1–C10–O2	122.7(3)
O1–C10–C7	124.2(3)
O2–C10–C7	113.1(2)
O3–C12–O4	122.6(3)
O3–C12–C8	124.8(3)
O4–C12–C8	112.6(2)
C2'–C1'–C5'	107.6(3)
C2'–C1'–Fe1	69.67(17)
C5'–C1'–Fe1	69.03(17)
C3'–C2'–C1'	108.3(3)
C3'–C2'–Fe1	69.20(17)
C1'–C2'–Fe1	70.32(17)
C2'–C3'–C4'	108.4(3)
C2'–C3'–Fe1	70.57(18)
C4'–C3'–Fe1	69.73(17)
C3'–C4'–C5'	107.5(3)
C3'–C4'–Fe1	69.71(17)
C5'–C4'–Fe1	69.96(18)
C4'–C5'–C1'	108.2(3)
C4'–C5'–Fe1	69.47(17)
C1'–C5'–Fe1	70.53(17)

Table 4.7 Bond distances (Å) and Bond Angles (°) for Compound **33**

Atoms (33)	**Distances (Å)**
Fe1–C2#1	2.037(2)
Fe1–C2	2.037(2)
Fe1–C1'	2.038(3)
Fe1–C3#1	2.050(3)
Fe1–C3	2.050(3)
Fe1–C1	2.053(4)
Fe1–C2'#1	2.054(2)
Fe1–C2'	2.054(2)
Fe1–C3'	2.077(3)
Fe1–C3'#1	2.077(3)
S1–C5	1.770(2)
S1–C5#1	1.770(2)
O1–C6	1.194(3)
Cl1–C6	1.801(2)
C1–C2#1	1.423(3)
C1–C2	1.424(3)
C2–C3	1.440(3)
C3–C4	1.440(3)
C3–C3#1	1.444(5)
C4–C5	1.353(3)
C5–C6	1.468(3)
C1'–C2'	1.425(3)
C1'–C2'#1	1.425(3)
C2'–C3'	1.419(4)
C3'–C3'#1	1.427(6)
Fe1A–C2A	2.034(10)
Fe1A–C2A#1	2.034(10)
Fe1A–C1'A	2.038(10)
Fe1A–C1A	2.049(10)
Fe1A–C3A#1	2.05(1)
Fe1A–C3A	2.05(1)
Fe1A–C2'A	2.053(10)
Fe1A–C2'A#1	2.053(10)
Fe1A–C3'A#1	2.077(10)
Fe1A–C3'A	2.077(10)
S1A–C5A	1.766(10)
S1A–C5A#1	1.766(10)
O1A–C6A	1.195(11)
Cl1A–C6A	1.80(1)
C1A–C2A	1.423(10)
C1A–C2A#1	1.423(10)
C2A–C3A	1.442(10)
C3A–C4A	1.437(10)
C3A–C3A#1	1.44(6)
C4A–C5A	1.350(11)
C5A–C6A	1.477(10)
C1'A–C2'A	1.425(10)
C1'A–C2'A#1	1.425(10)
C2'A–C3'A	1.419(11)
C3'A–C3'A#1	1.39(8)
Atoms	**Angles (°)**
C2#1–Fe1–C2	69.18(15)
C2#1–Fe1–C1'	118.15(11)
C2–Fe1–C1'	118.16(11)
C2#1–Fe1–C3#1	41.25(9)
C2–Fe1–C3#1	69.4(1)
C1'–Fe1–C3#1	156.84(9)
C2#1–Fe1–C3	69.4(1)
C2–Fe1–C3	41.25(9)
C1'–Fe1–C3	156.84(9)
C3#1–Fe1–C3	41.26(14)
C2#1–Fe1–C1	40.74(8)
C2–Fe1–C1	40.74(8)
C1'–Fe1–C1	101.96(14)
C3#1–Fe1–C1	68.80(11)
C3–Fe1–C1	68.80(11)
C2#1–Fe1–C2'#1	105.38(10)
C2–Fe1–C2'#1	154.36(10)
C1'–Fe1–C2'#1	40.76(9)
C3#1–Fe1–C2'#1	123.88(10)
C3–Fe1–C2'#1	162.26(10)
C1–Fe1–C2'#1	118.99(11)
C2#1–Fe1–C2'	154.36(10)
C2–Fe1–C2'	105.38(10)
C1'–Fe1–C2'	40.76(9)

Table 4.7 Continued

C3#1–Fe1–C2'	162.26(10)
C3–Fe1–C2'	123.88(10)
C1–Fe1–C2'	118.99(11)
C2'#1–Fe1–C2'	68.17(14)
C2#1–Fe1–C3'	162.29(11)
C2–Fe1–C3'	124.22(11)
C1'–Fe1–C3'	68.06(12)
C3#1–Fe1–C3'	127.98(10)
C3–Fe1–C3'	111.91(10)
C1–Fe1–C3'	156.97(10)
C2'#1–Fe1–C3'	67.73(11)
C2'–Fe1–C3'	40.16(10)
C2#1–Fe1–C3'#1	124.22(11)
C2–Fe1–C3'#1	162.29(11)
C1'–Fe1–C3'#1	68.06(12)
C3#1–Fe1–C3'#1	111.91(10)
C3–Fe1–C3'#1	127.98(10)
C1–Fe1–C3'#1	156.97(10)
C2'#1–Fe1–C3'#1	40.16(10)
C2'–Fe1–C3'#1	67.73(11)
C3'–Fe1–C3'#1	40.20(17)
C5–S1–C5#1	106.9(2)
C2#1–C1–C2	108.6(3)
C2#1–C1–Fe1	69.03(16)
C2–C1–Fe1	69.03(16)
C1–C2–C3	108.1(2)
C1–C2–Fe1	70.23(17)
C3–C2–Fe1	69.86(14)
C2–C3–C4	122.8(2)
C2–C3–C3#1	107.55(14)
C4–C3–C3#1	129.26(14)
C2–C3–Fe1	68.89(14)
C4–C3–Fe1	121.77(18)
C3#1–C3–Fe1	69.37(7)
C5–C4–C3	127.4(2)

C4–C5–C6	123.0(2)
C4–C5–S1	125.48(19)
C6–C5–S1	111.13(17)
O1–C6–C5	127.0(2)
O1–C6–Cl1	117.5(2)
C5–C6–Cl1	115.37(17)
C2'–C1'–C2'#1	107.7(3)
C2'–C1'–Fe1	70.22(16)
C2'#1–C1'–Fe1	70.22(16)
C3'–C2'–C1'	108.2(2)
C3'–C2'–Fe1	70.79(15)
C1'–C2'–Fe1	69.02(16)
C2'–C3'–C3'#1	107.96(15)
C2'–C3'–Fe1	69.05(15)
C3'#1–C3'–Fe1	69.90(8)
C2A–Fe1A–C2A#1	69.0(12)
C2A–Fe1A–C1'A	118.7(9)
C2A#1–Fe1A–C1'A	118.7(9)
C2A–Fe1A–C1A	40.8(3)
C2A#1–Fe1A–C1A	40.8(3)
C1'A–Fe1A–C1A	102.4(8)
C2A–Fe1A–C3A#1	69.3(13)
C2A#1–Fe1A–C3A#1	41.4(3)
C1'A–Fe1A–C3A#1	157.2(10)
C1A–Fe1A–C3A#1	69.1(6)
C2A–Fe1A–C3A	41.4(3)
C2A#1–Fe1A–C3A	69.3(13)
C1'A–Fe1A–C3A	157.2(10)
C1A–Fe1A–C3A	69.1(6)
C3A#1–Fe1A–C3A	41.0(18)
C2A–Fe1A–C2'A	105.9(8)
C2A#1–Fe1A–C2'A	155.0(9)
C1'A–Fe1A–C2'A	40.8(3)
C1A–Fe1A–C2'A	119.6(10)

Table 4.7 Continued

C3A#1–Fe1A–C2'A	161.7(11)
C3A–Fe1A–C2'A	123.9(9)
C2A–Fe1A–C2'A#1	155.0(9)
C2A#1–Fe1A–C2'A#1	105.9(8)
C1'A–Fe1A–C2'A#1	40.8(3)
C1A–Fe1A–C2'A#1	119.6(10)
C3A#1–Fe1A–C2'A#1	123.9(9)
C3A–Fe1A–C2'A#1	161.7(11)
C2'A–Fe1A–C2'A#1	67.9(12)
C2A–Fe1A–C3'A#1	161.6(13)
C2A#1–Fe1A–C3'A#1	124.6(11)
C1'A–Fe1A–C3'A#1	68.0(6)
C1A–Fe1A–C3'A#1	157.6(12)
C3A#1–Fe1A–C3'A#1	111.7(8)
C3A–Fe1A–C3'A#1	127.2(9)
C2'A–Fe1A–C3'A#1	67.1(16)
C2'A#1–Fe1A–C3'A#1	40.2(3)
C2A–Fe1A–C3'A	124.6(11)
C2A#1–Fe1A–C3'A	161.6(13)
C1'A–Fe1A–C3'A	68.0(6)
C1A–Fe1A–C3'A	157.6(12)
C3A#1–Fe1A–C3'A	127.2(9)
C3A–Fe1A–C3'A	111.7(8)
C2'A–Fe1A–C3'A	40.2(3)
C2'A#1–Fe1A–C3'A	67.1(16)
C3'A#1–Fe1A–C3'A	39(2)
C5A–S1A–C5A#1	107(4)
C2A–C1A–C2A#1	108(2)

C2A–C1A–Fe1A	69.0(5)
C2A#1–C1A–Fe1A	69.0(5)
C1A–C2A–C3A	108.4(13)
C1A–C2A–Fe1A	70.2(5)
C3A–C2A–Fe1A	69.9(5)
C4A–C3A–C3A#1	130.1(12)
C4A–C3A–C2A	122.1(16)
C3A#1–C3A–C2A	107.5(10)
C4A–C3A–Fe1A	121.9(17)
C3A#1–C3A–Fe1A	69.5(9)
C2A–C3A–Fe1A	68.7(5)
C5A–C4A–C3A	130(2)
C4A–C5A–C6A	121.1(16)
C4A–C5A–S1A	126.9(19)
C6A–C5A–S1A	109.4(13)
O1A–C6A–C5A	126(2)
O1A–C6A–Cl1A	117.6(18)
C5A–C6A–Cl1A	113.2(13)
C2'A–C1'A–C2'A#1	107(2)
C2'A–C1'A–Fe1A	70.2(5)
C2'A#1–C1'A–Fe1A	70.2(5)
C3'A–C2'A–C1'A	108.0(14)
C3'A–C2'A–Fe1A	70.8(5)
C1'A–C2'A–Fe1A	69.0(5)
C3'A#1–C3'A–C2'A	108.4(14)
C3'A#1–C3'A–Fe1A	70.4(12)
C2'A–C3'A–Fe1A	69.0(5)

4.4 Summary

Two-fold Knoevenagel reaction of 1,2-diformylferrocene with dimethylthioglycolate sulfoxide in the presence of triethylamine resulted in ferrocene-fused 5,7-dimethylester thiepin S-oxide along with the mono-dehydrated byproduct **29b** with a ratio of 2:1. The formation of mono-dehydrated product **29b** was indicated by the ABC pattern of substituted Cp in ^{1}H NMR. **29b** was fully characterized with a single X-ray crystal structure. The analysis of the molecular structure of **29b** showed that the hydroxyl and hydrogen groups were oriented *endo* with respect to the iron center. The molecular structure of **29a** and **29b** displayed that the SO groups were directed *exo* with respect to the iron center.

To study the reactivity of ferrocene-fused thiepin S-oxide and ferrocene-fused thiepin in the further reaction steps, ferrocene-fused 5,7-dimethylester thiepin (**30**, 81%) was synthesized via deoxygenation of ferrocene-fused 5,7-dimethylester thiepin S-oxide with 2-chloro-1,3,2-benzodioxaphosphole in the presence of pyridine. Saponification of the resulting ferrocene-fused 5,7-dimethylester thiepin was carried out by using a methanolic solution of NaOH in dichloromethane at reflux temperature of dichloromethane for 12 h to yield ferrocene-fused 5,7-dicarboxylic acid thiepin (**32**). The diester complex of ferrocene-fused thiepin S-oxide (**29a**) was hydrolyzed to the corresponding dicarboxylic acid (47%) using KOH in methanol for 3 h at reflux temperature.

Attempts to decarboxylate complexes **31** and **32** using copper powder in quinoline, $AgCO_3$/AcOH in DMSO and copper(II) phthalocyanine in H_2O/ethyl ether

resulted in decomposition. The Barton reductive decarboxylation of **32** by conversion to its acid chloride followed by reaction with 1-hydroxypyridine-2(1*H*)-thione sodium salt also resulted in decomposition. We have been unable to find suitable reaction conditions for the decarboxylation of **31** or **32**.

In summary, ferrocene-fused 5,7-dimethylester thiepin S-oxide was synthesized using a two-fold Knoevenagel reaction. Deoxygenation of **29a** with 2-chloro-1,3,2-benzodioxaphosphole resulted in corresponding thiepin (**30**). The saponification of **29a** and **30** resulted in diacids **31** and **32**. Attempts to decarboxylate **31** and **32** under different reaction conditions were unsuccessful. Ferrocene-fused 5,7-disubstituted thiepin derivatives are dark red solid. Organometallic thiepins are not common in chemistry literature. The first transition metal complex of thiepin, benzo[*b*]thiepin(tricarbonyl)iron was reported by Nishino et.al in 1988.[205] Organometallic thiepin **29a** is more stable than the heavily substituted benzo[*b*]thiepin S-oxide (**6** of Chart 4.5). We can explore the electrochemical polymerization of **30** and the resultant compound may be a potential candidate for organometallic semiconducting material.

Chapter 5 Conclusions and Future Directions

Chapter 2 focused upon the synthesis of mononuclear and binuclear organometallic acenequinones by using a classic organic reaction that has served well for making organic acenes (aldol condensation). The key precursor in the preparation of organometallic acenes is 1,2-diformylferrocene, which was prepared by using a well-optimized literature procedure. Cp-capped acenequinones were synthesized from organometallic acenequinones by demetalation with saturated, aqueous sodium dithionite in THF. The resultant acenequinones were aromatized into corresponding TIPS acenes using a classic method of converting acenequinones to useful acenes. We have studied their structural and physical properties, including oxidation and reduction processes. Cp-capped TIPS acenes (**21** and **22**) exhibit a 2-D brickwork structure in single crystals. The HOMO energy level and the important HOMO-LUMO gap of Cp-capped TIPS acenes were measured using cyclic voltammetry. The optical energy gap of Cp-capped TIPS acenes was calculated from UV-vis spectra. Finally, we have investigated the OFET performance of **21** and **22** and observed hole mobilities of 0.03 $cm^2/(V\ s)$ and 0.02 $cm^2/(V\ s)$, respectively.Continuing research will further explore synthetic approaches to prepare extended benzannulated organometallic acenequinones and corresponding organometallic acenes, and investigate their structural and physical properties including important parameters for organometallic semiconducting materials.

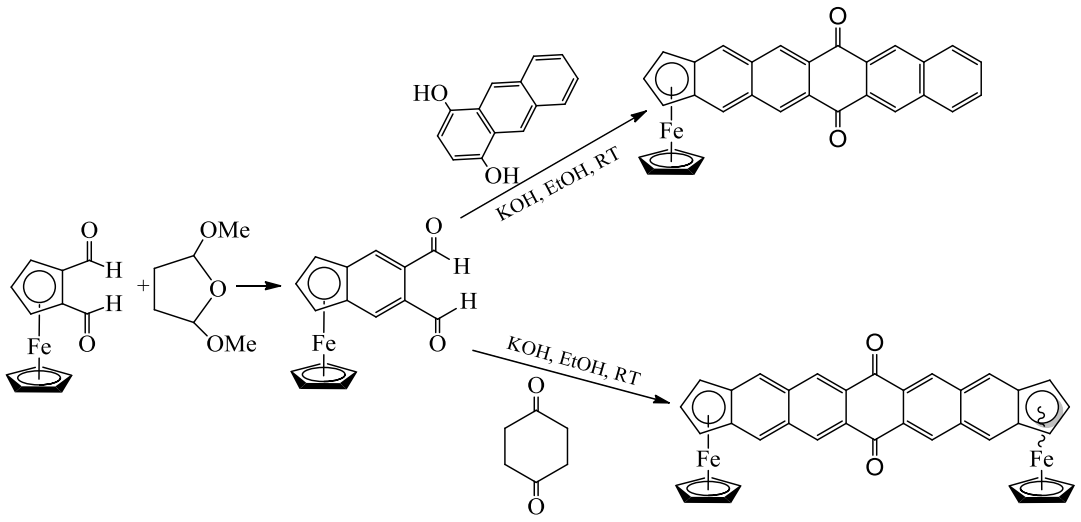

Scheme 5.1 Synthesis of extended π-conjugated organometallic acenequinones

Chapter 3 demonstrated the synthetic approaches to prepare unsubstituted and phenyl-substituted ferrocene-fused tropones by using two-fold aldol condensation. We have synthesized ferrocene-fused thiotropone and a detached 5,7-diphenylazulenethiol by reacting **23** and **24a** with Lawesson's reagent. Furthermore, the reaction of **26** with hydroxylamine resulted in ferrocene-fused tropone oxime. Tropones **23** and **24a** have HOMO energy levels of –5.06 eV and – 4.99 eV measured by cyclic voltammetry. The UV-vis spectra of all the tropone derivatives were recorded. Among those derivatives, ferrocene-fused thiotropone has unique physical (color) and optical properties (visible region absorption). Continuing research will study the electrochemical properties of ferrocene-fused thiotropones and investigate synthetic routes to prepare ferrocene-fused dicyanoheptafulvene.

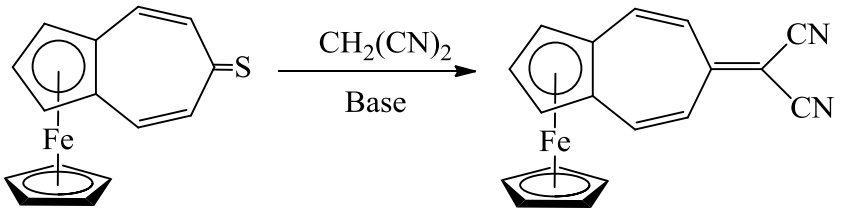

Scheme 5.2 Synthesis of ferrocene-fused dicyanoheptafulvene

Chapter 4 focused on the synthesis of ferrocene-fused 5,7-disubstituted thiepins and thiepin S-oxides. We have been unable to find suitable reaction conditions for the decarboxylation of **31** or **32** to prepare an unsubstituted ferrocene-fused thiepin or thiepin S-oxide. Future research will examine the physical properties, including oxidation processes and UV absorption of the synthesized ferrocene-fused 5,7-disubstituted thiepin and thiepin S-oxide derivatives. Moreover, the electrochemical polymerization of ferrocene-fused 5,7-dimethylester thiepin may be explored in continuing research. In addition, synthetic approaches to ferrocene-fused 5,7-diphenylthiepin and ferrocene-fused 5,7-dicyanothiepin will be examined.

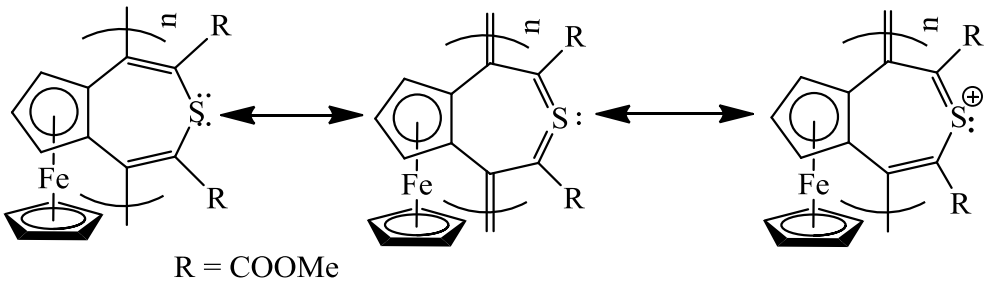

Scheme 5.3 Electrochemical polymerization of ferrocene-fused 5,7-dimethylester thiepin

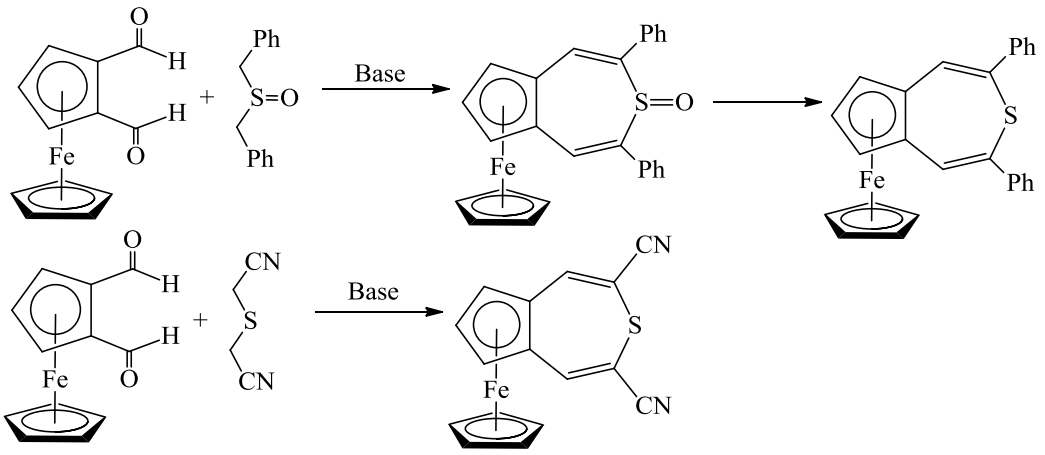

Scheme 5.4 Synthesis of ferrocene-fused thiepin derivatives

Appendix

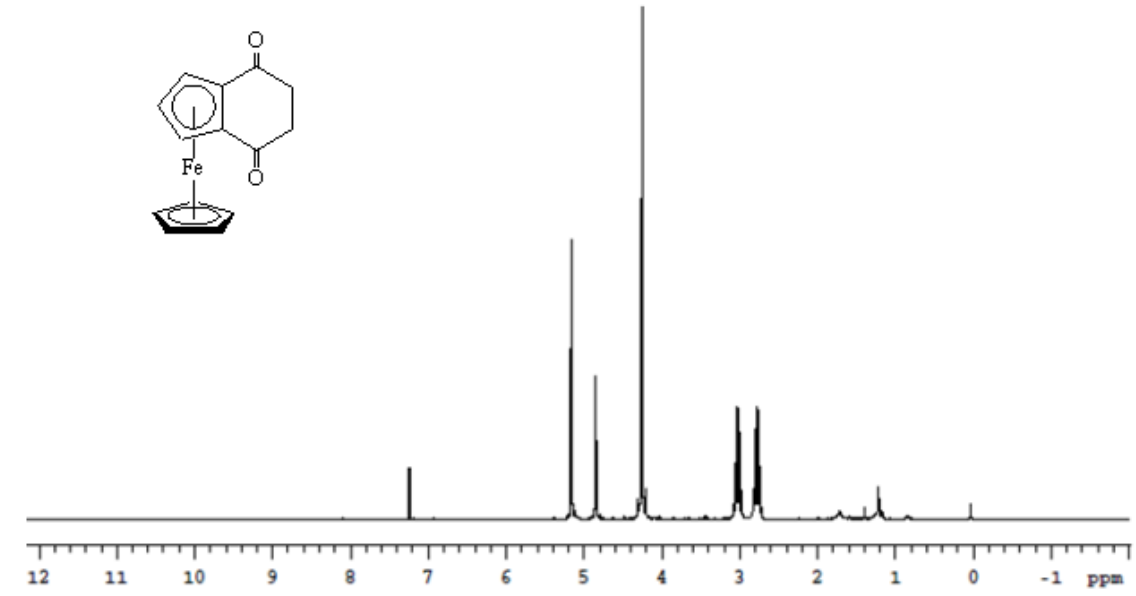
O
Fe
O
12
11
10
9
8
7
6
5
4
3
2
1
0
-1
ppm

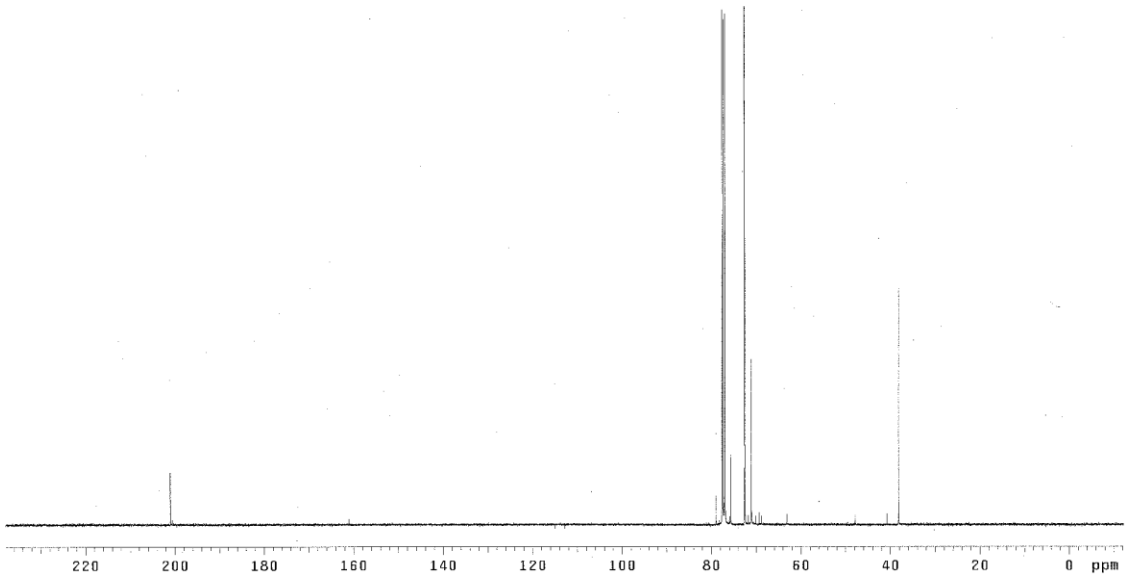
220
200
180
160
140
120
100
80
60
40
20
0
ppm

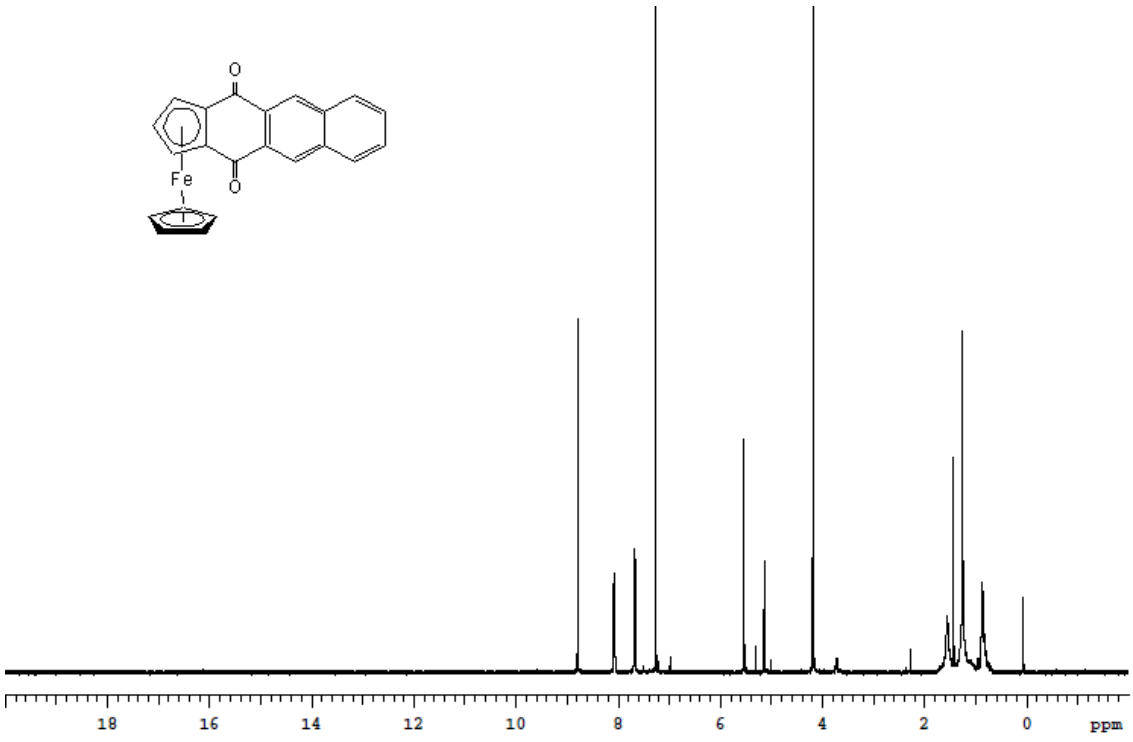
O
Fe
O
18
16
14
12
10
8
6
4
2
0
ppm

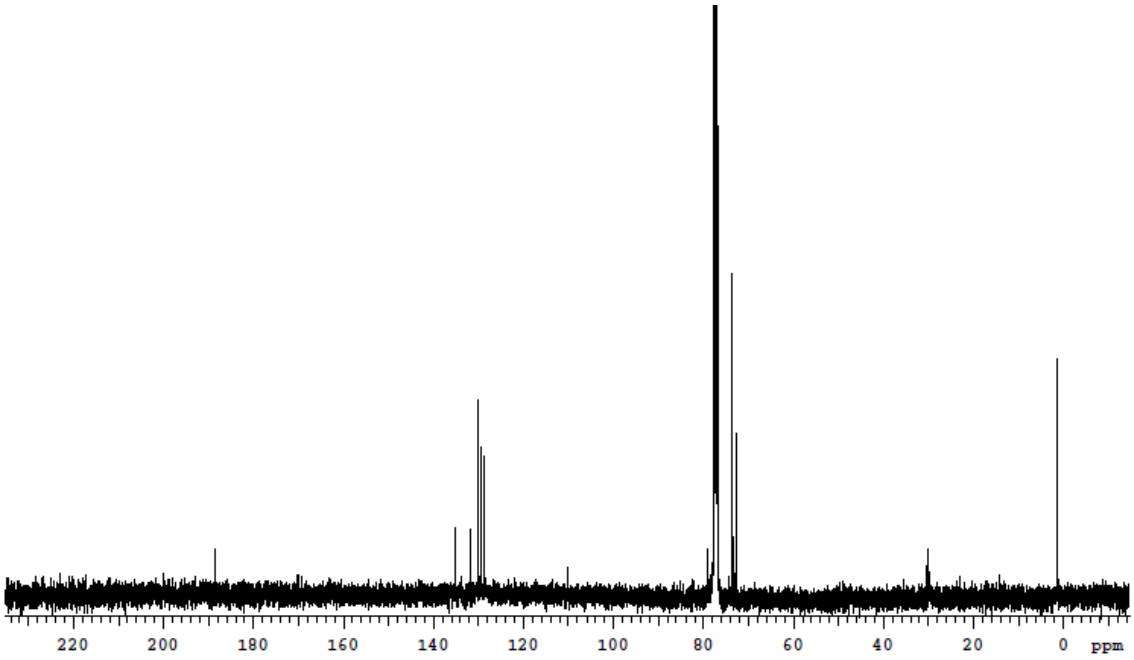
220
200
180
160
140
120
100
80
60
40
20
0
ppm

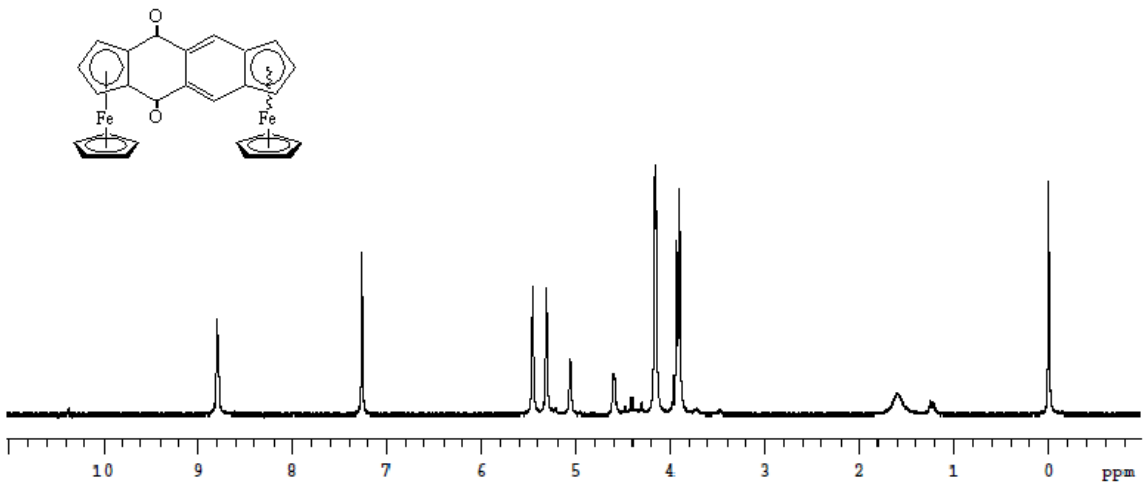
O
Fe
O
Fe
10
9
8
7
6
5
4
3
2
1
0
ppm

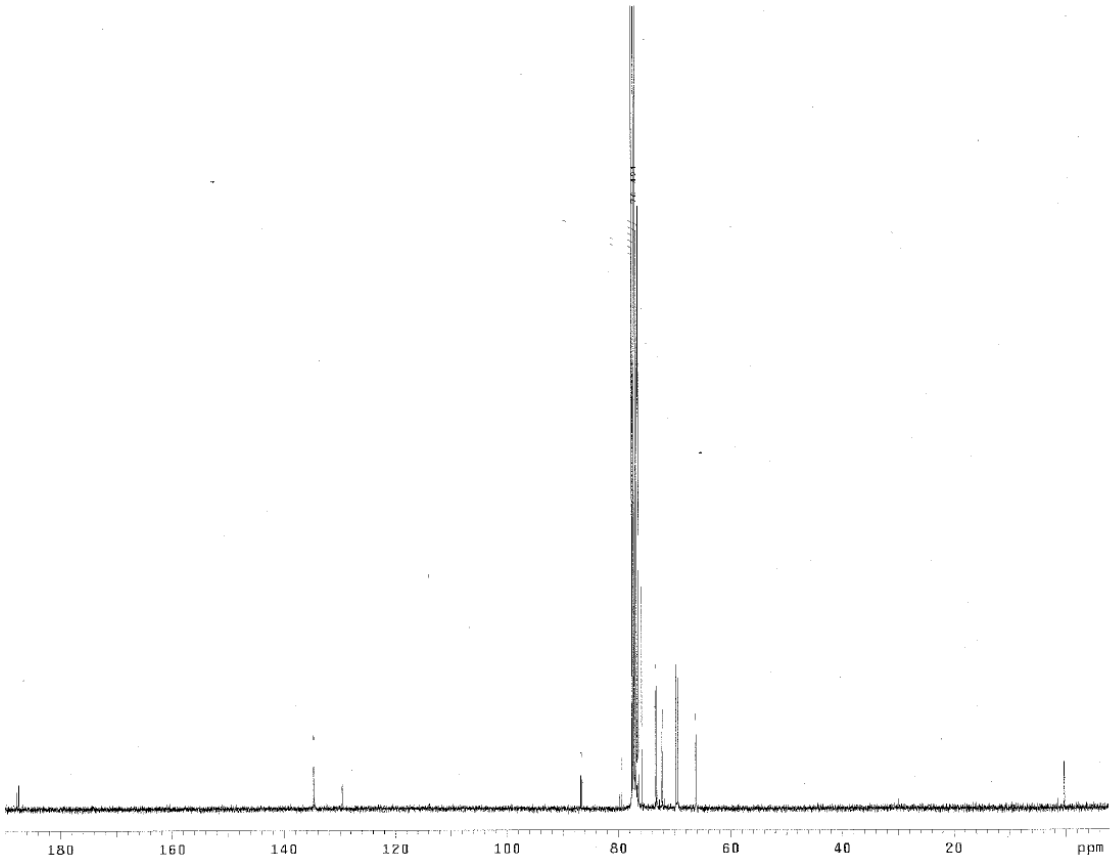
180
160
140
120
100
80
60
40
20
ppm

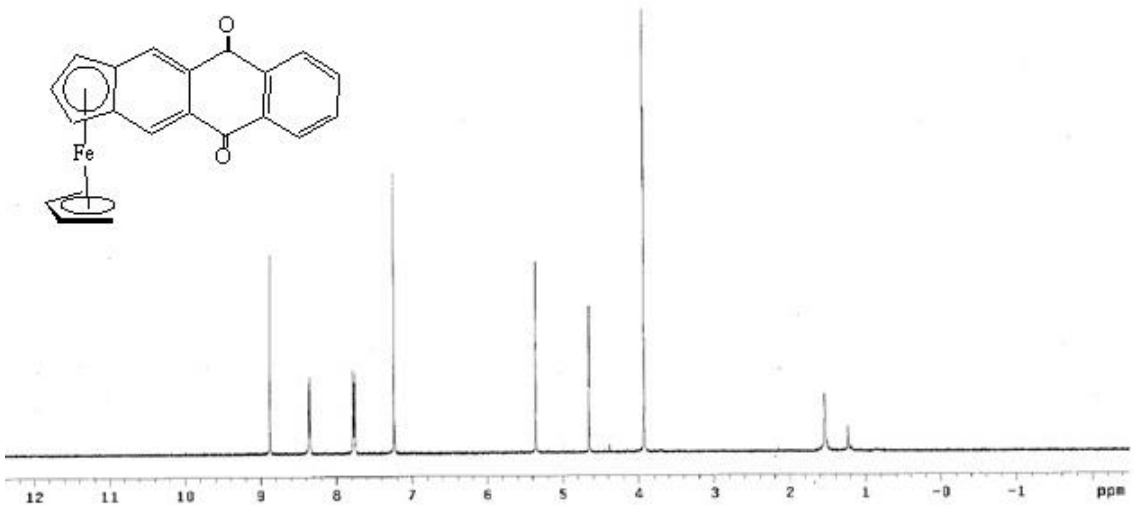
O
Fe
O
12
11
10
9
8
7
6
5
4
3
2
1
-0
-1
ppm

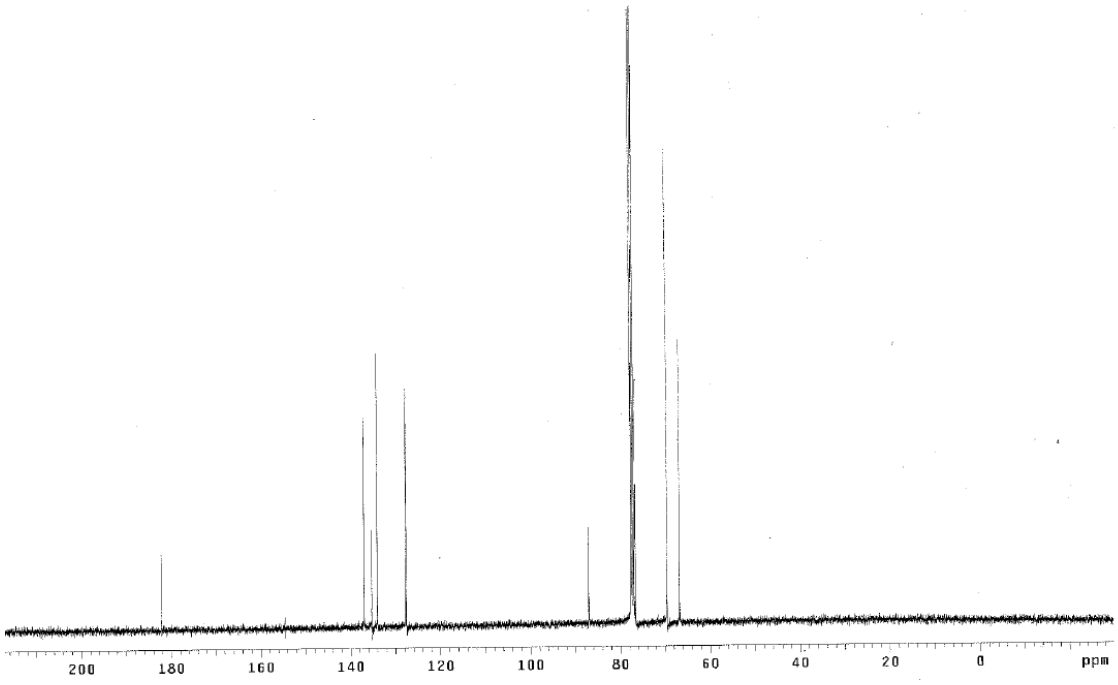
200
180
160
140
120
100
80
60
40
20
0
ppm

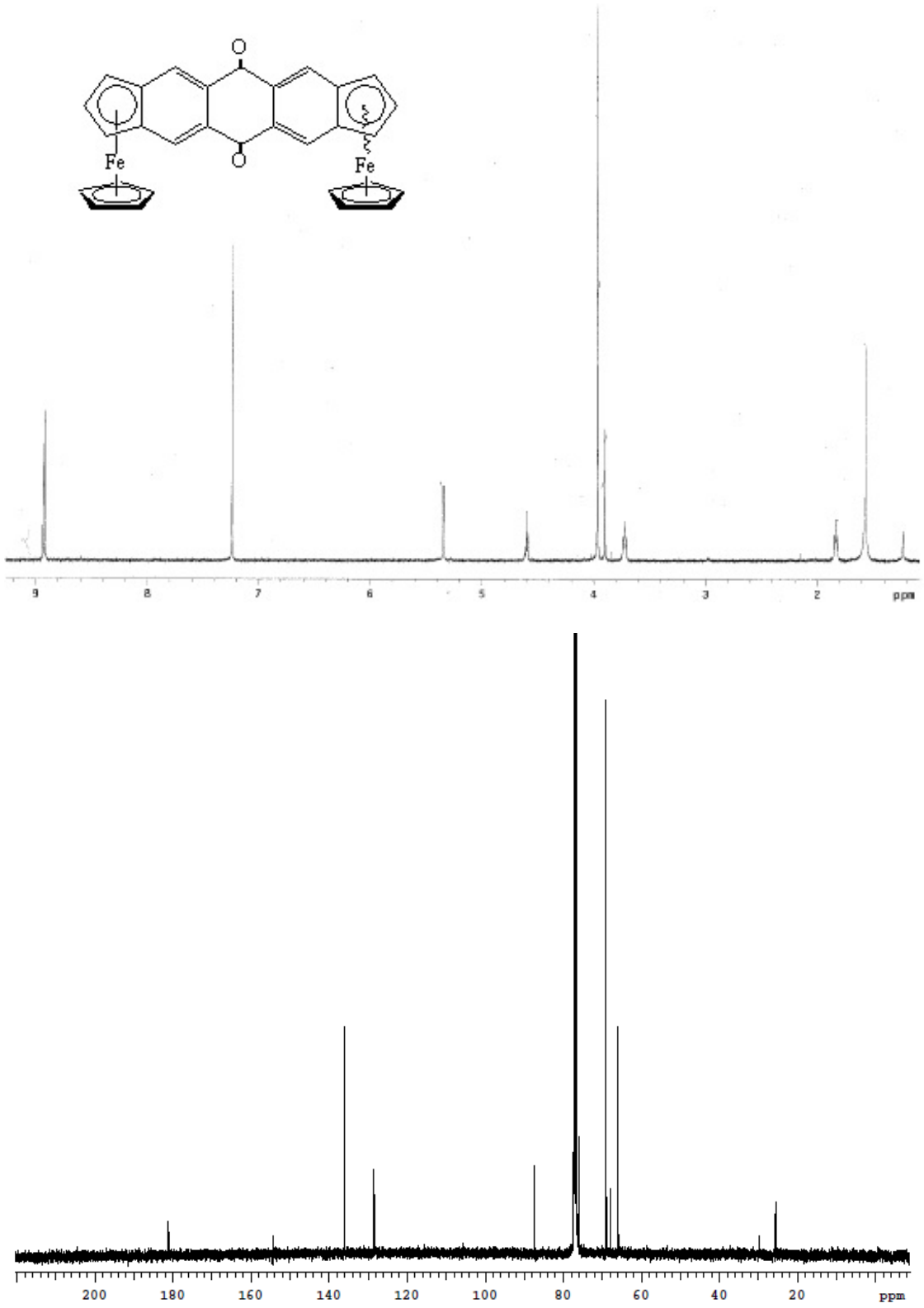
O
O
Fe
Fe
9
8
7
6
5
4
3
2
ppm
200
180
160
140
120
100
80
60
40
20
ppm

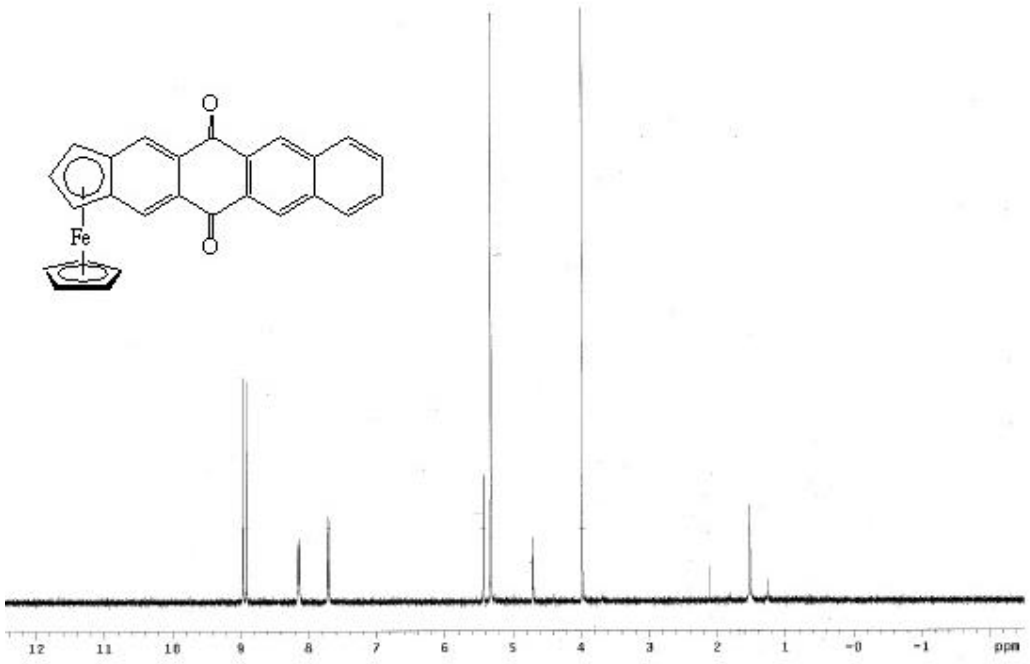
O
O
Fe
12
11
10
9
8
7
6
5
4
3
2
1
-0
-1
ppm

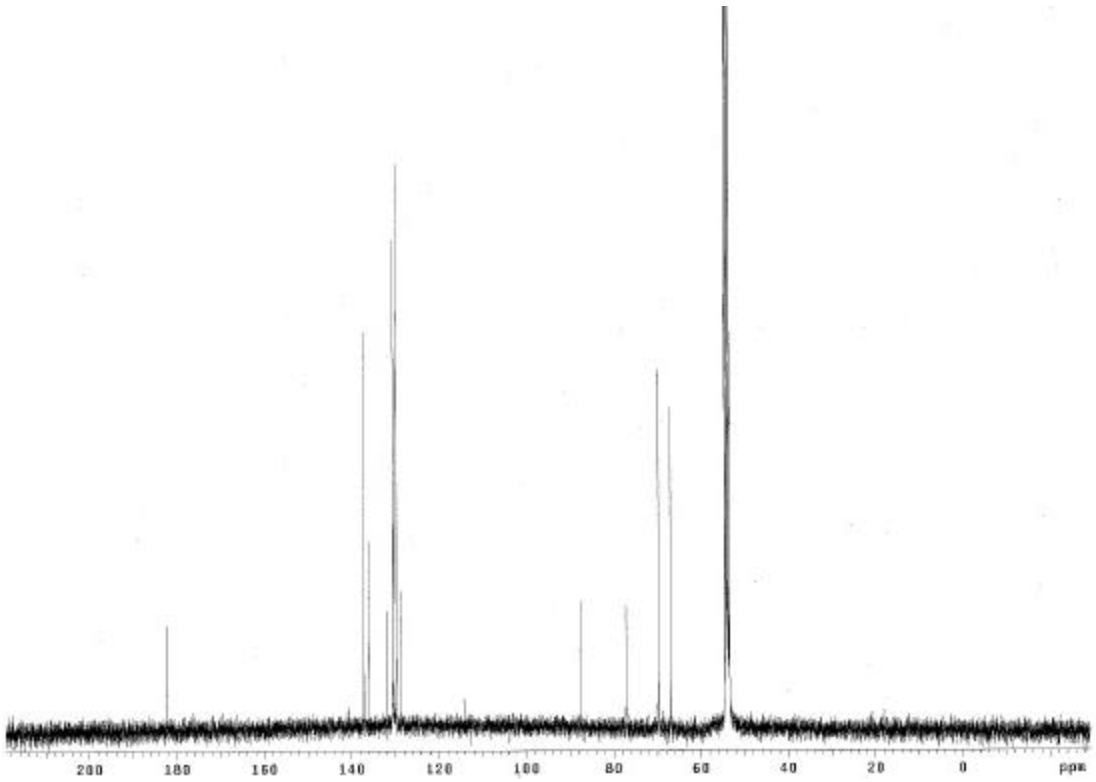
200
180
160
140
120
100
80
60
40
20
0
ppm

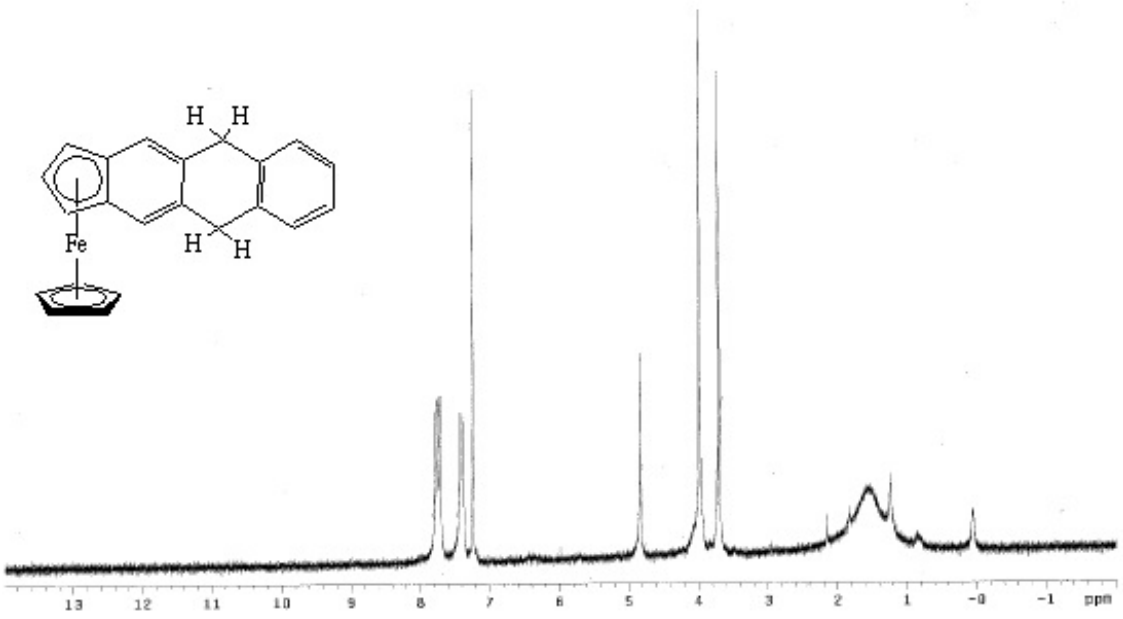
H H
Fe
H H
13 12 11 10 9 8 7 6 5 4 3 2 1 -0 -1 ppm

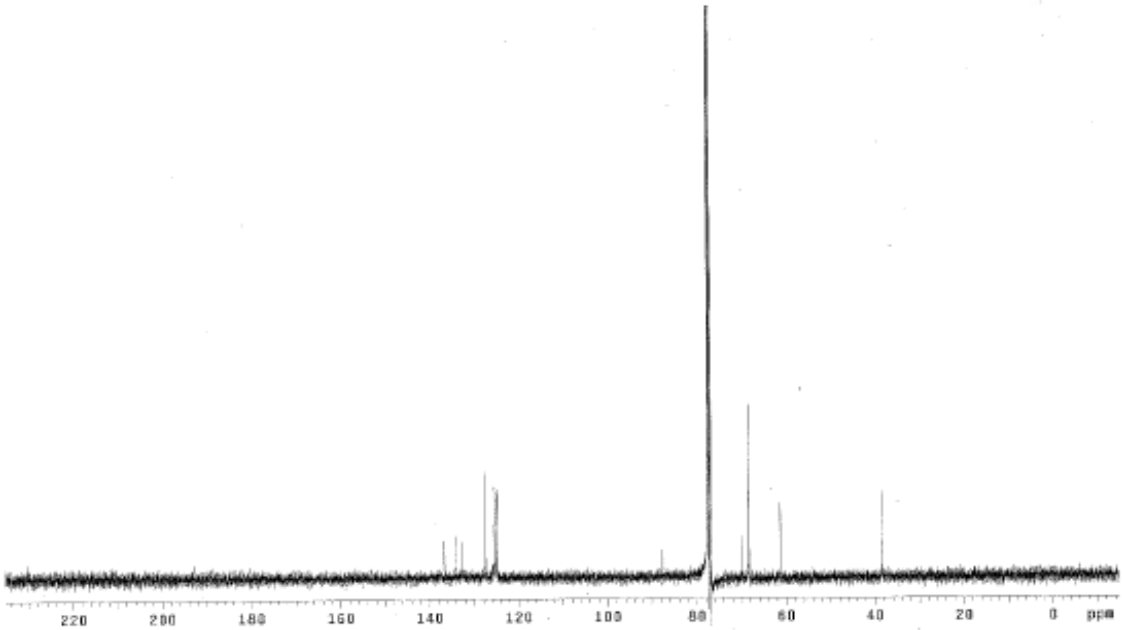
220 200 180 160 140 120 100 80 60 40 20 0 ppm

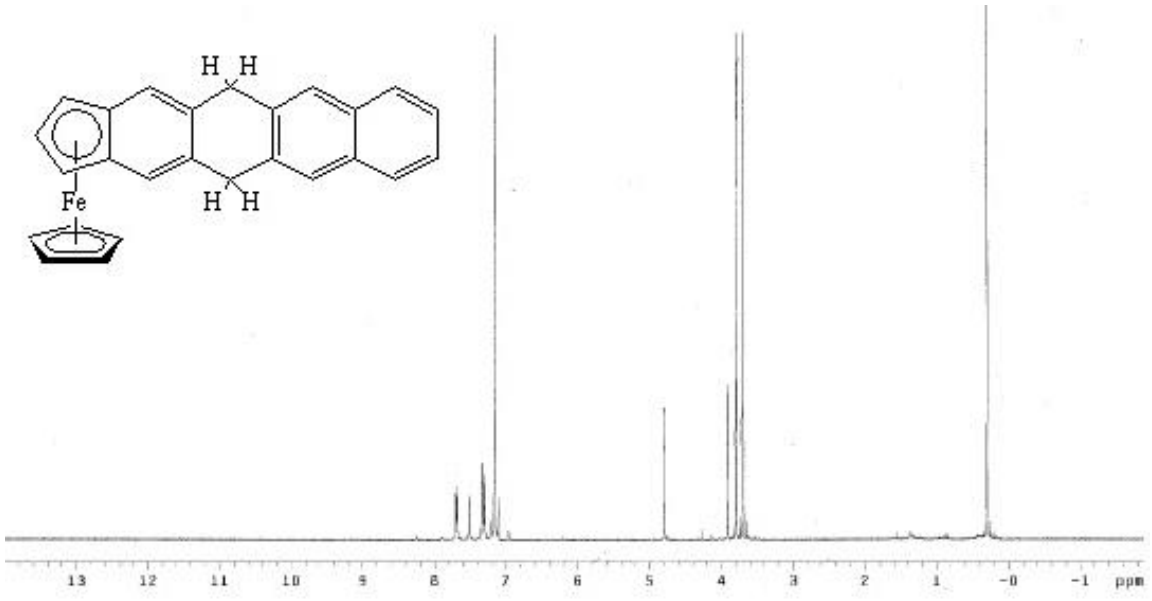
H H
Fe
H H
13 12 11 10 9 8 7 6 5 4 3 2 1 -0 -1 ppm

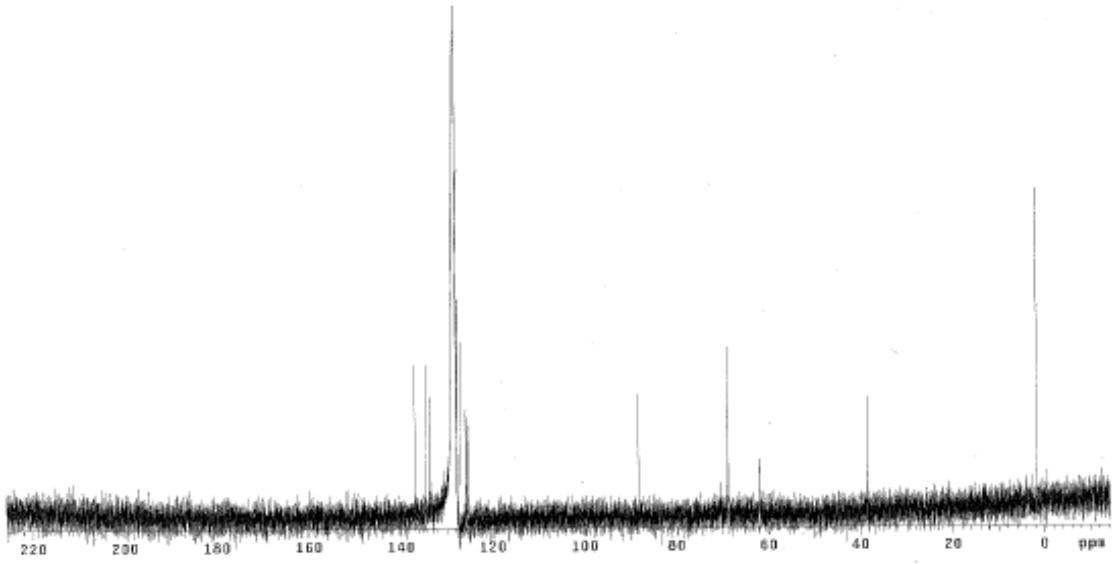
220 200 180 160 140 120 100 80 60 40 20 0 ppm

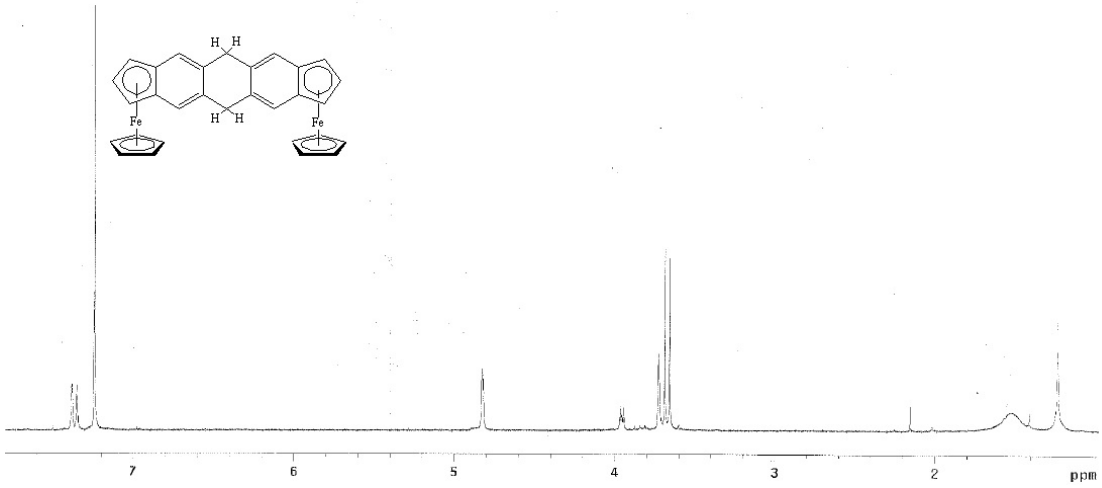
H H
H H
Fe
Fe
7
6
5
4
3
2
ppm

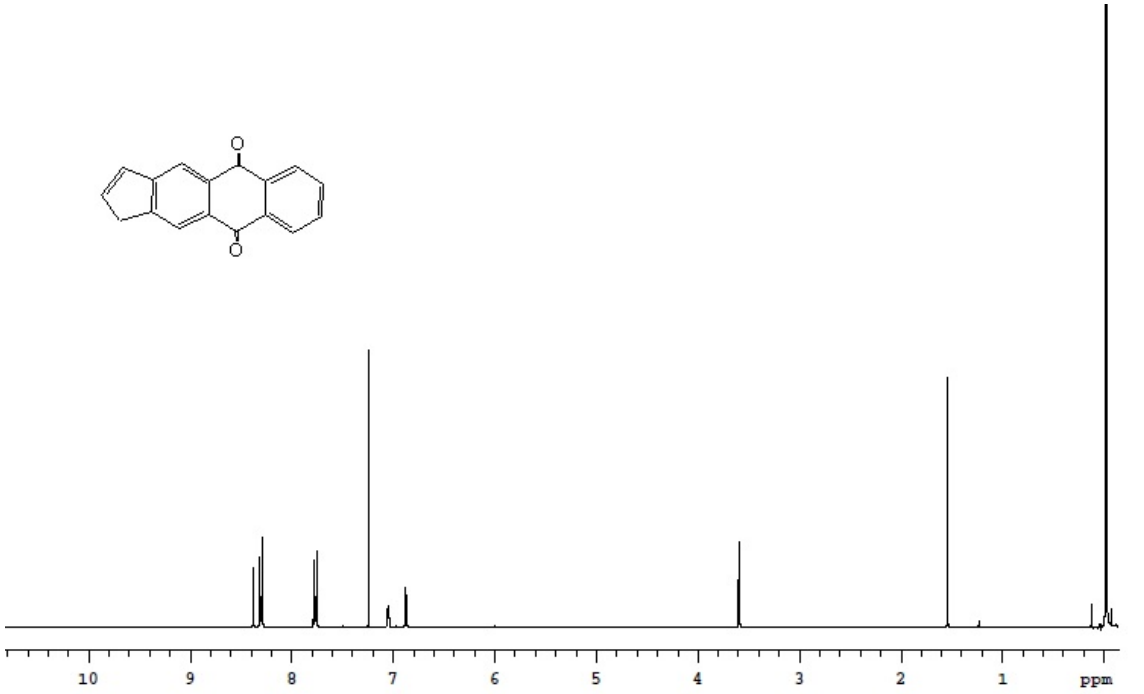
O
O
10
9
8
7
6
5
4
3
2
1
ppm

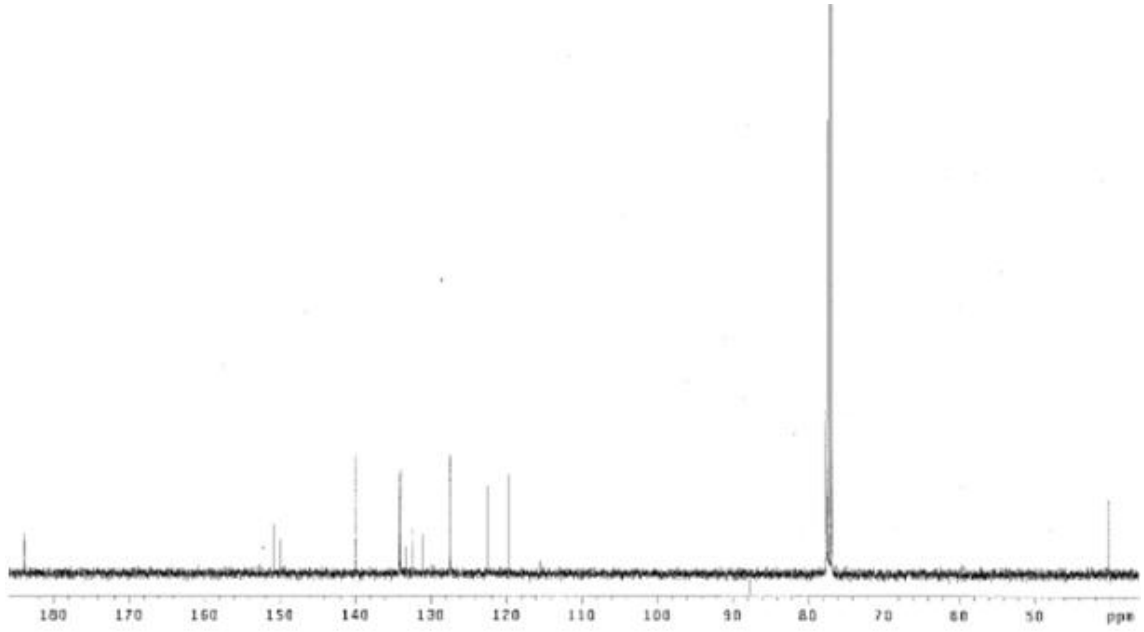
180
170
160
150
140
130
120
110
100
90
80
70
60
50
ppm

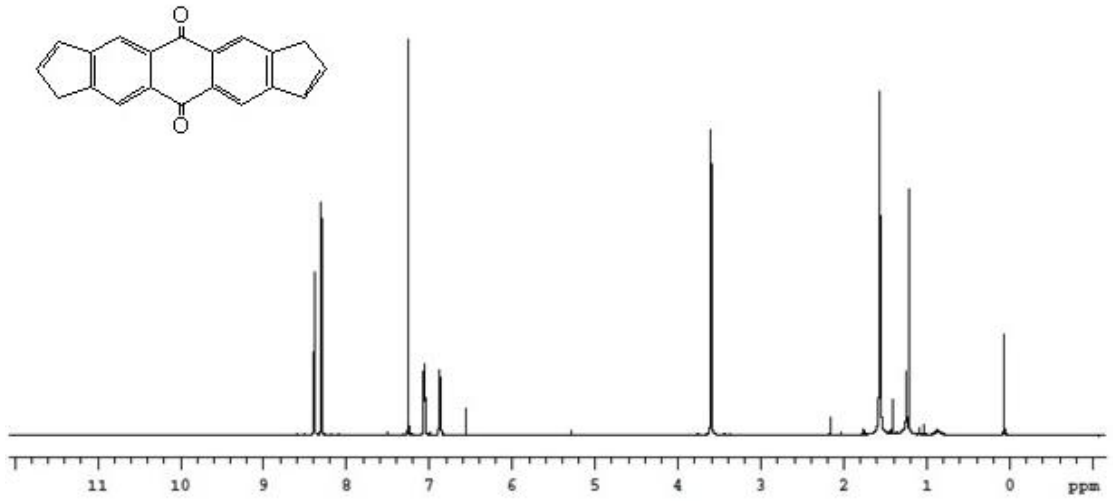
O
O
11
10
9
8
7
6
5
4
3
2
1
0
ppm

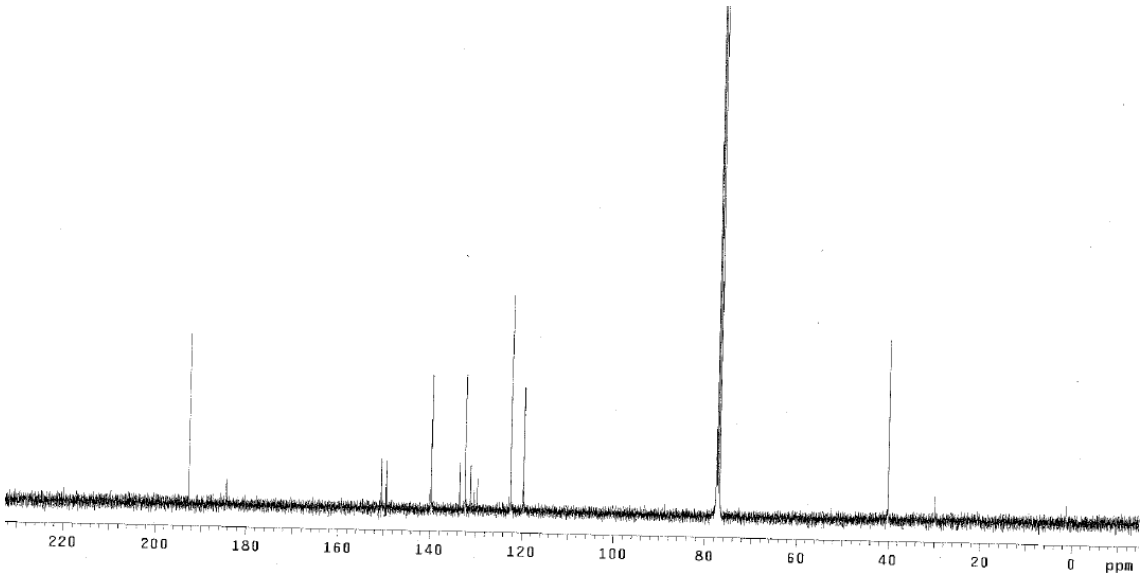
220
200
180
160
140
120
100
80
60
40
20
0
ppm

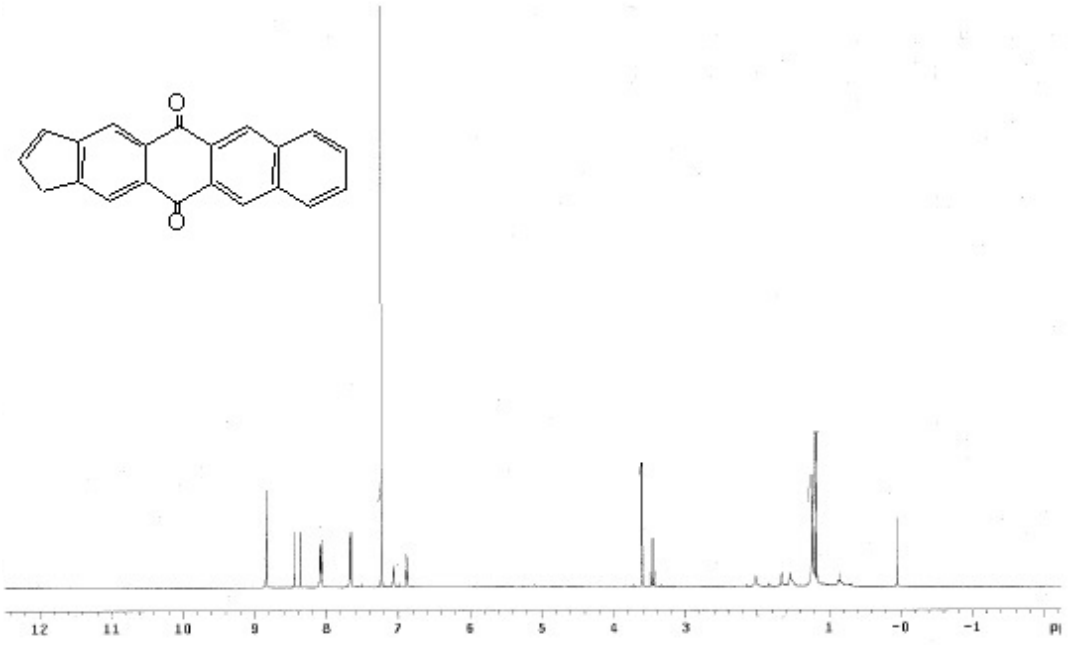
12
11
10
9
8
7
6
5
4
3
1
-0
-1

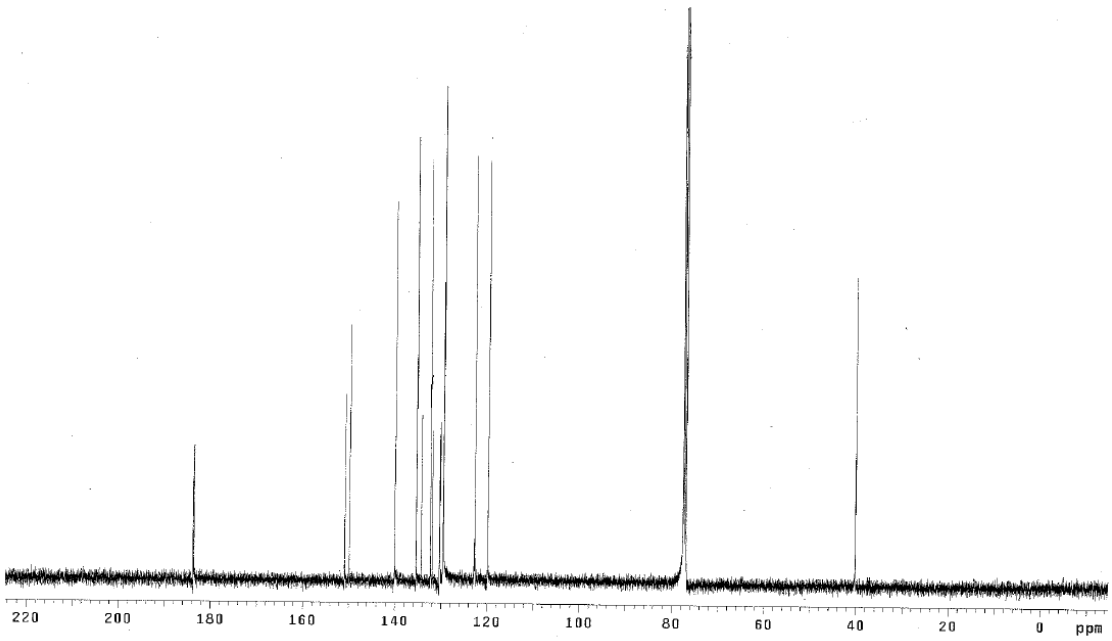
220
200
180
160
140
120
100
80
60
40
20
0
ppm

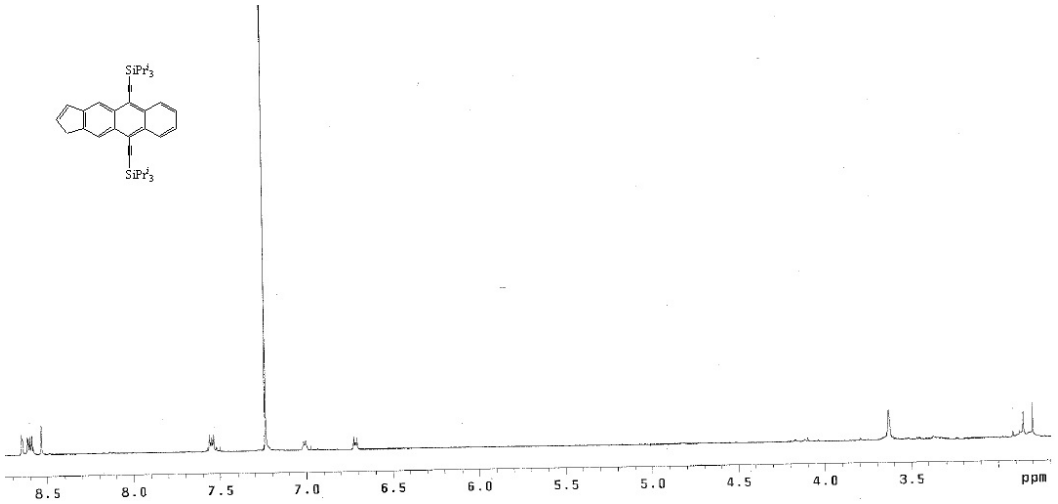
SiPr$^i_3$
SiPr$^i_3$
8.5
8.0
7.5
7.0
6.5
6.0
5.5
5.0
4.5
4.0
3.5
ppm

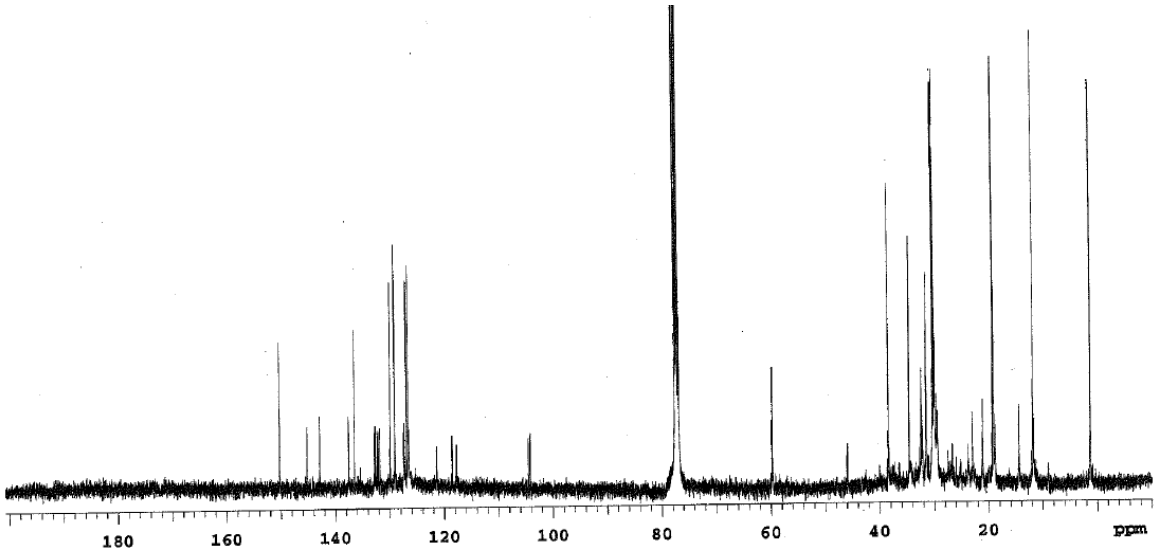
180
160
140
120
100
80
60
40
20
ppm

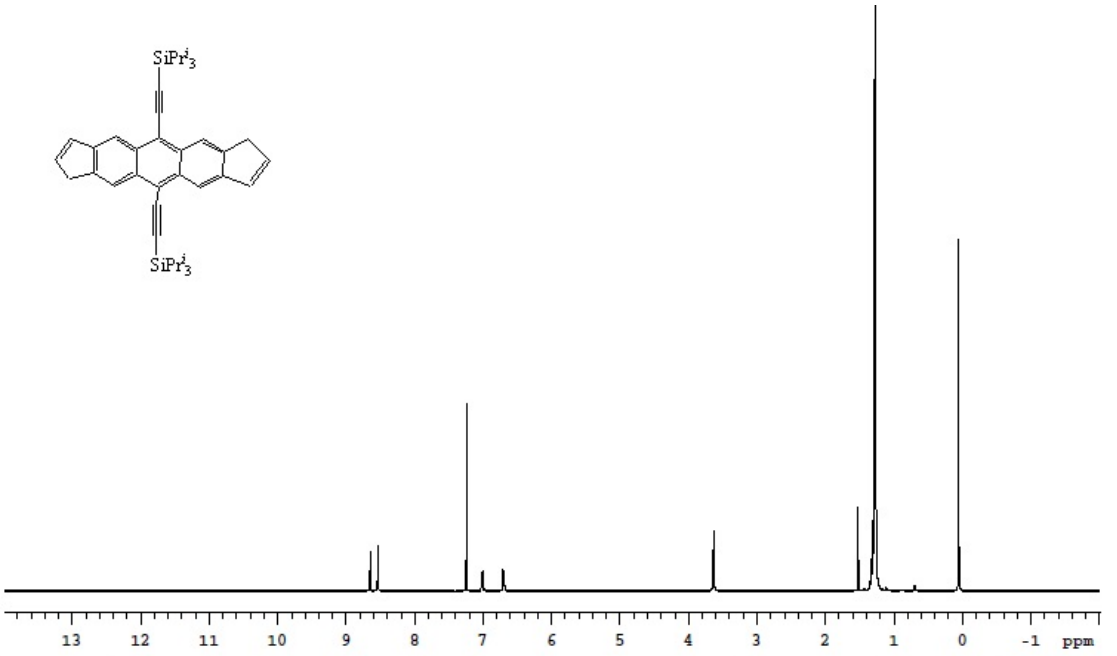
SiPr$^i_3$
SiPr$^i_3$
13 12 11 10 9 8 7 6 5 4 3 2 1 0 -1 ppm

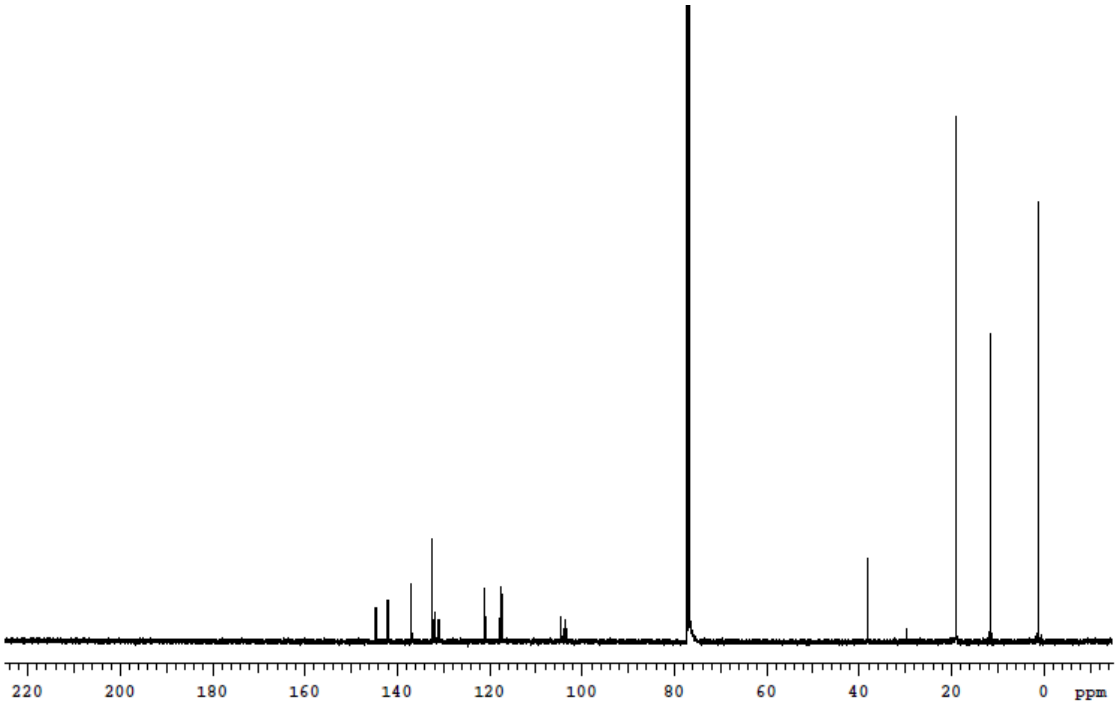
220 200 180 160 140 120 100 80 60 40 20 0 ppm

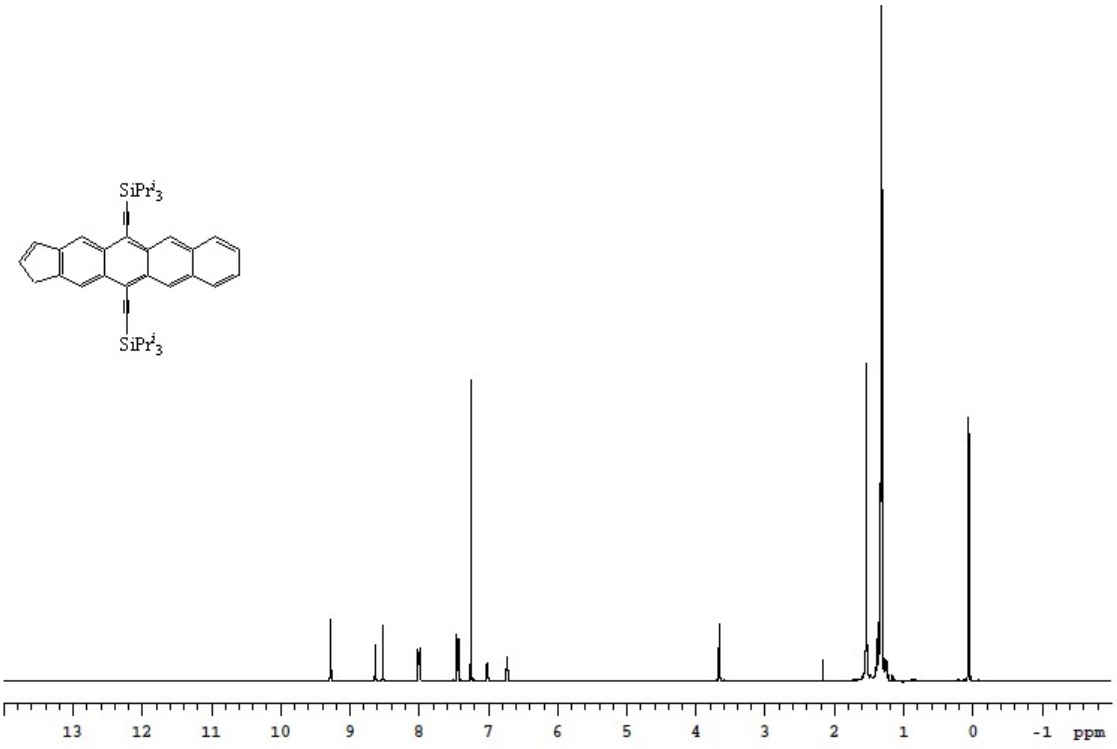
SiPr$^i_3$
SiPr$^i_3$
13 12 11 10 9 8 7 6 5 4 3 2 1 0 -1 ppm

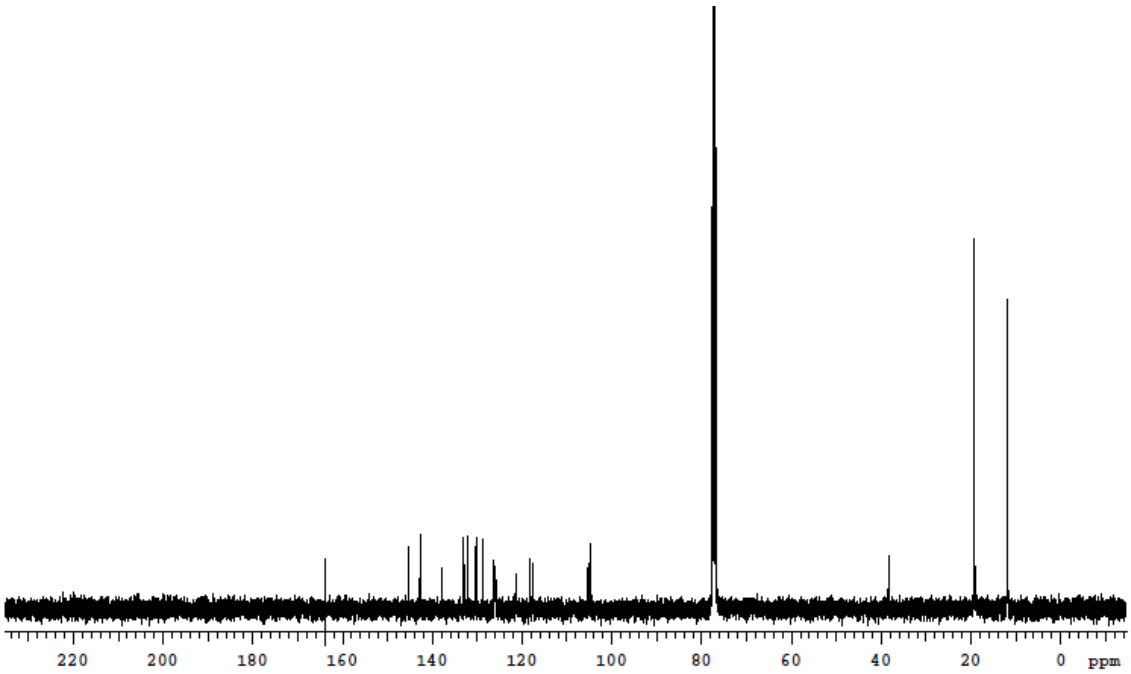
220 200 180 160 140 120 100 80 60 40 20 0 ppm

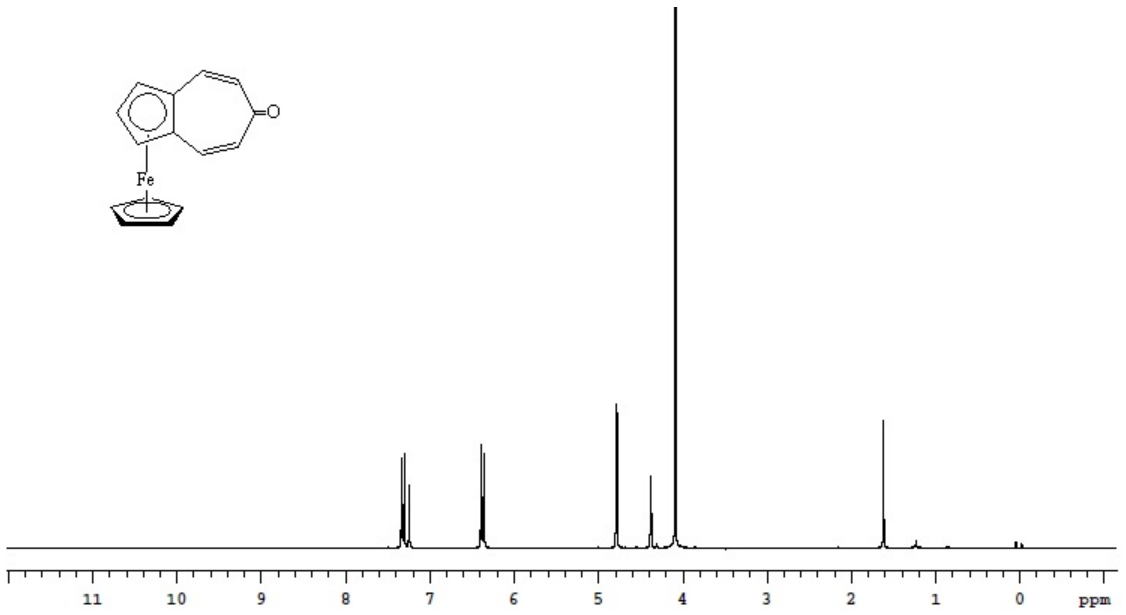
O
Fe
11
10
9
8
7
6
5
4
3
2
1
0
ppm

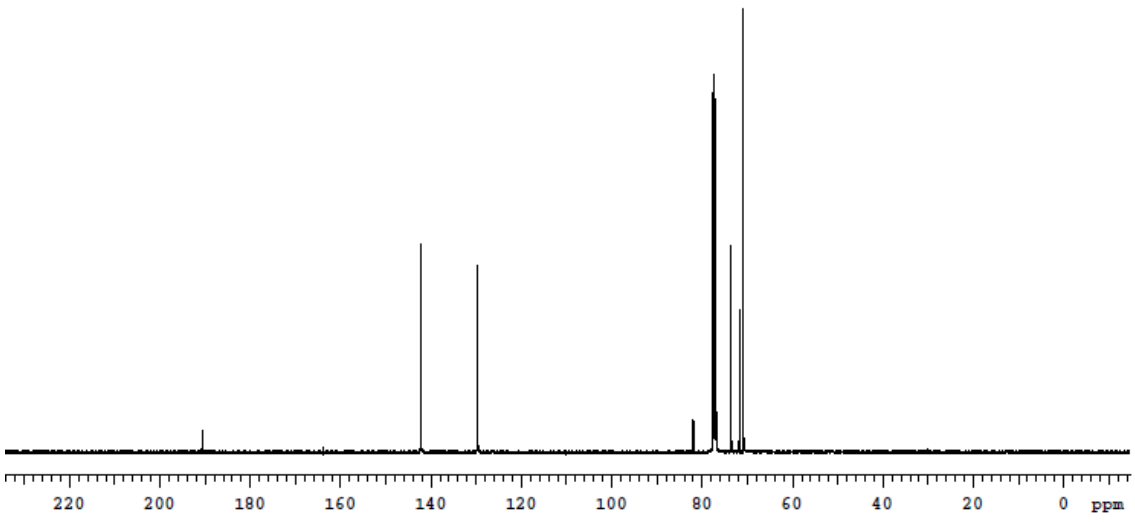
220
200
180
160
140
120
100
80
60
40
20
0
ppm

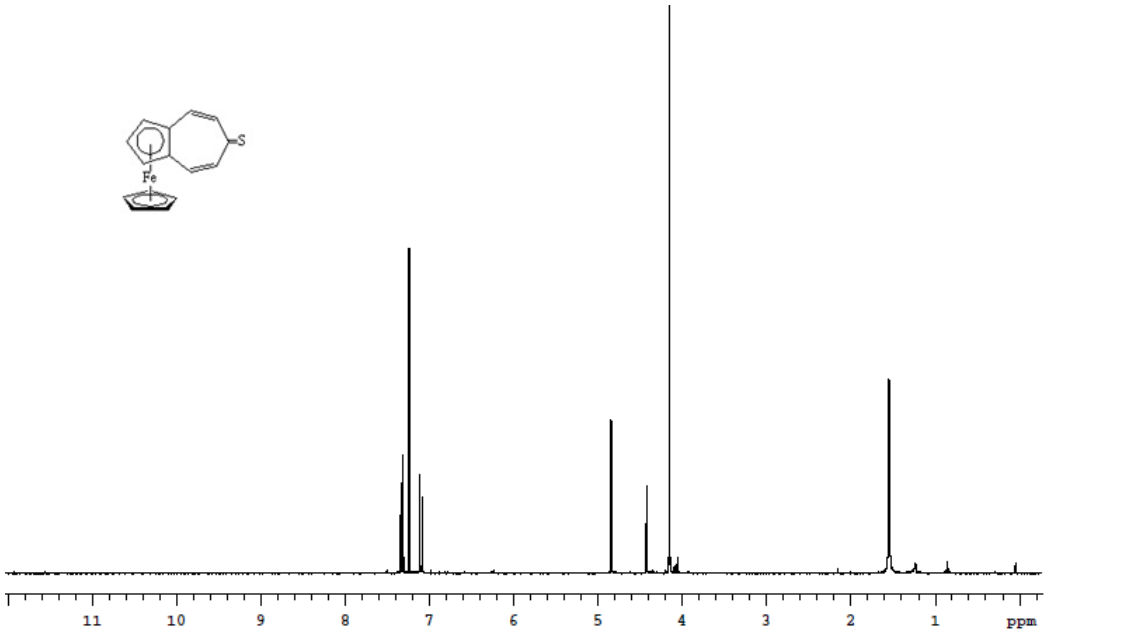
S
Fe
11
10
9
8
7
6
5
4
3
2
1
ppm

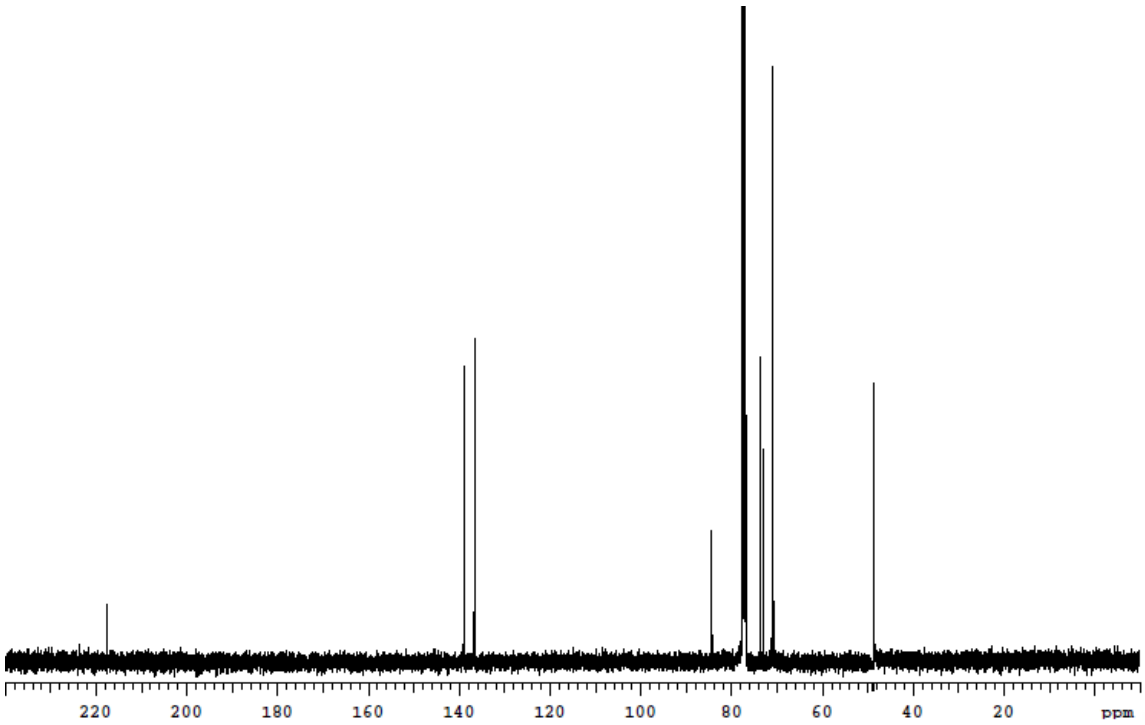
220
200
180
160
140
120
100
80
60
40
20
ppm

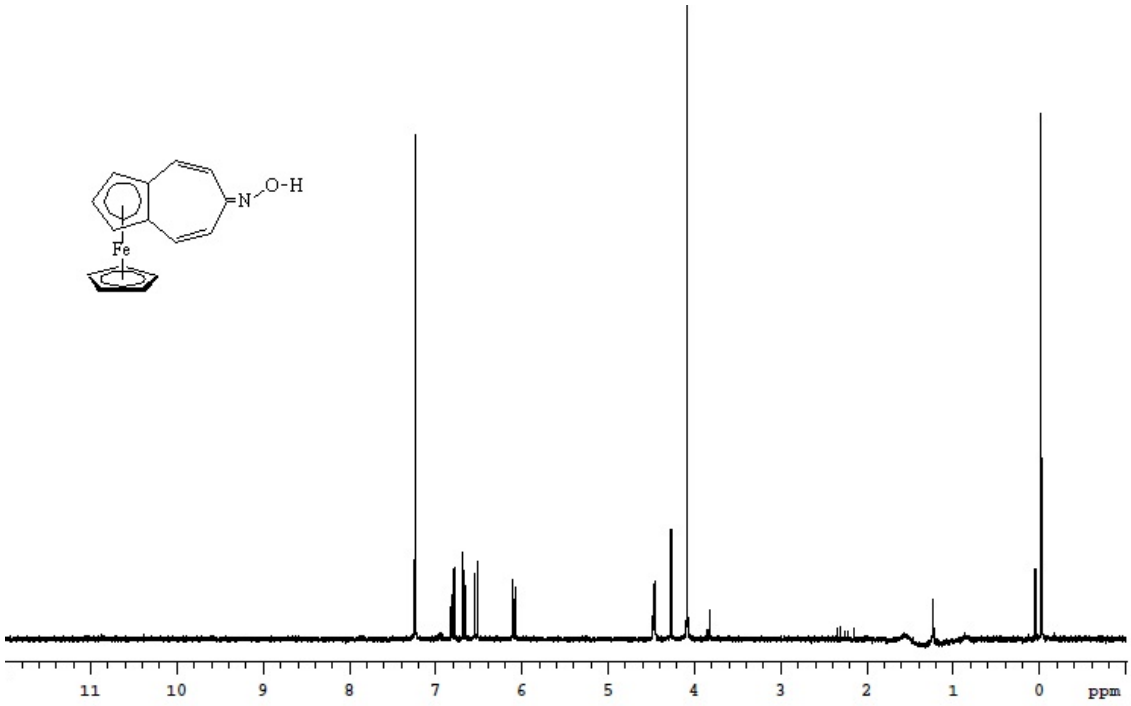
N
O-H
Fe
11
10
9
8
7
6
5
4
3
2
1
0
ppm

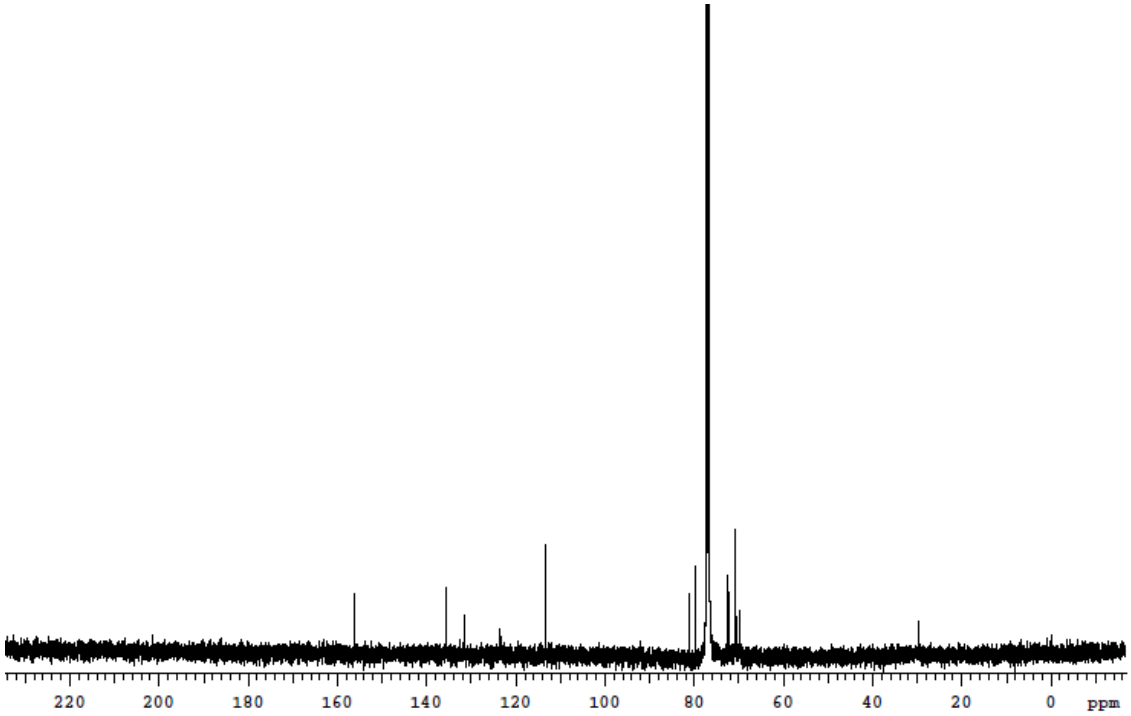
220
200
180
160
140
120
100
80
60
40
20
0
ppm

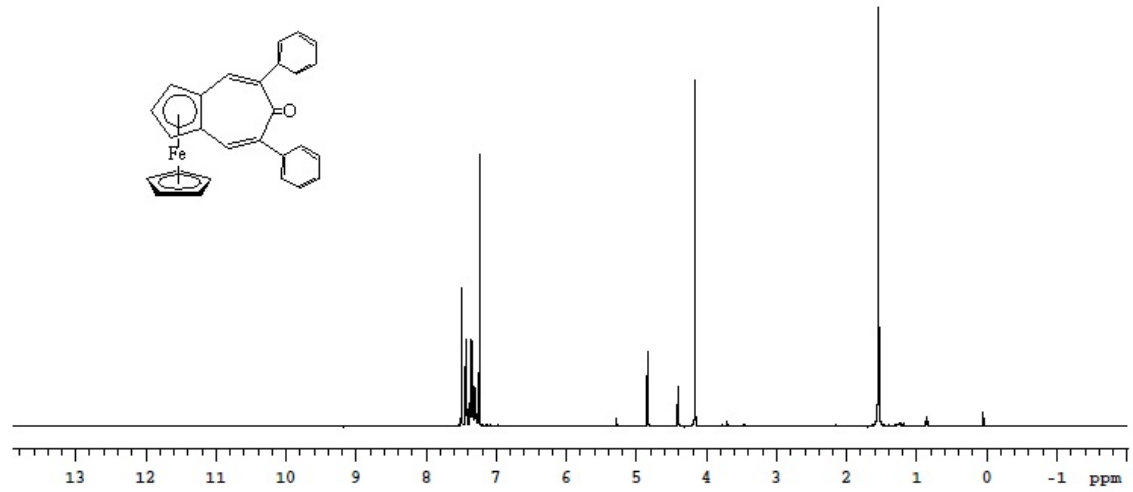
Fe
O
13
12
11
10
9
8
7
6
5
4
3
2
1
0
-1
ppm

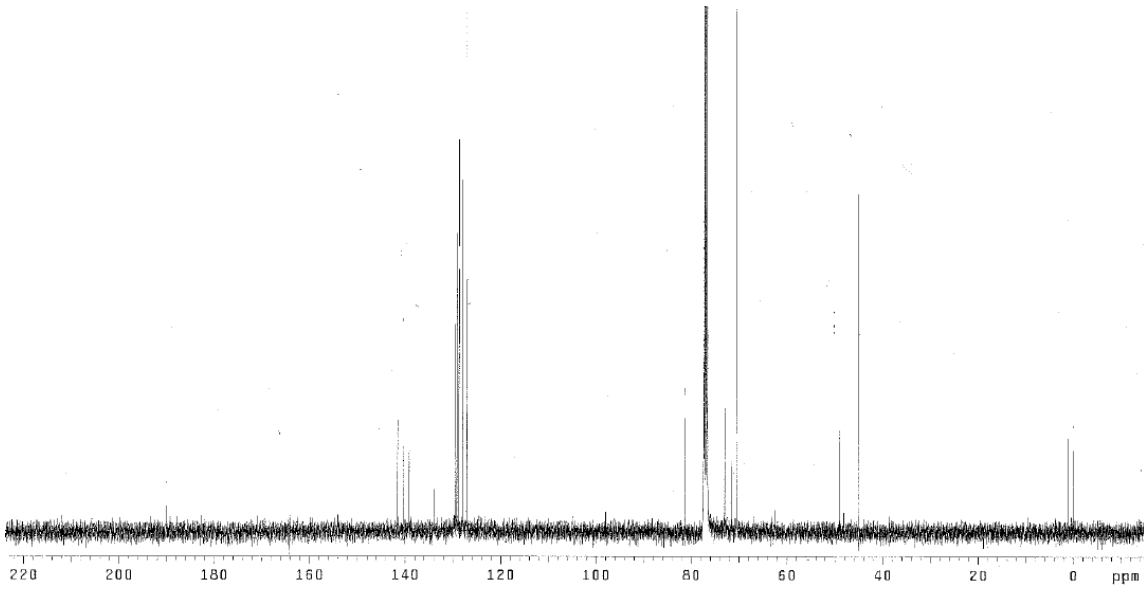
220
200
180
160
140
120
100
80
60
40
20
0
ppm

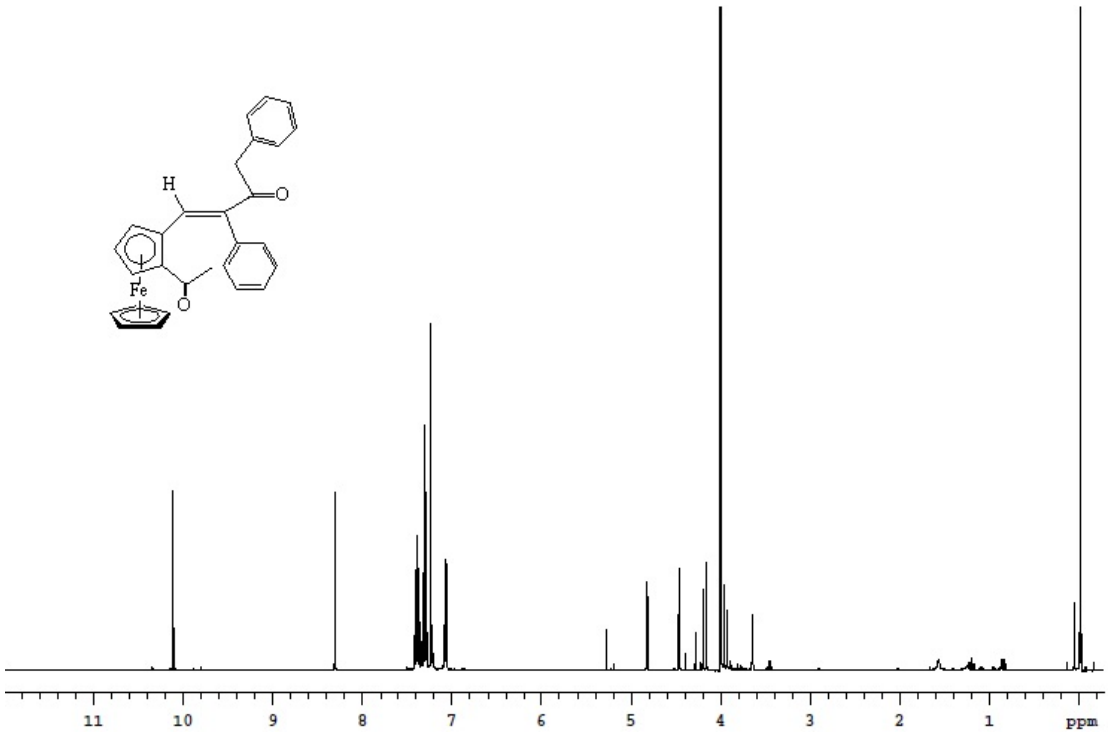
H
O
Fe
O
11
10
9
8
7
6
5
4
3
2
1
ppm

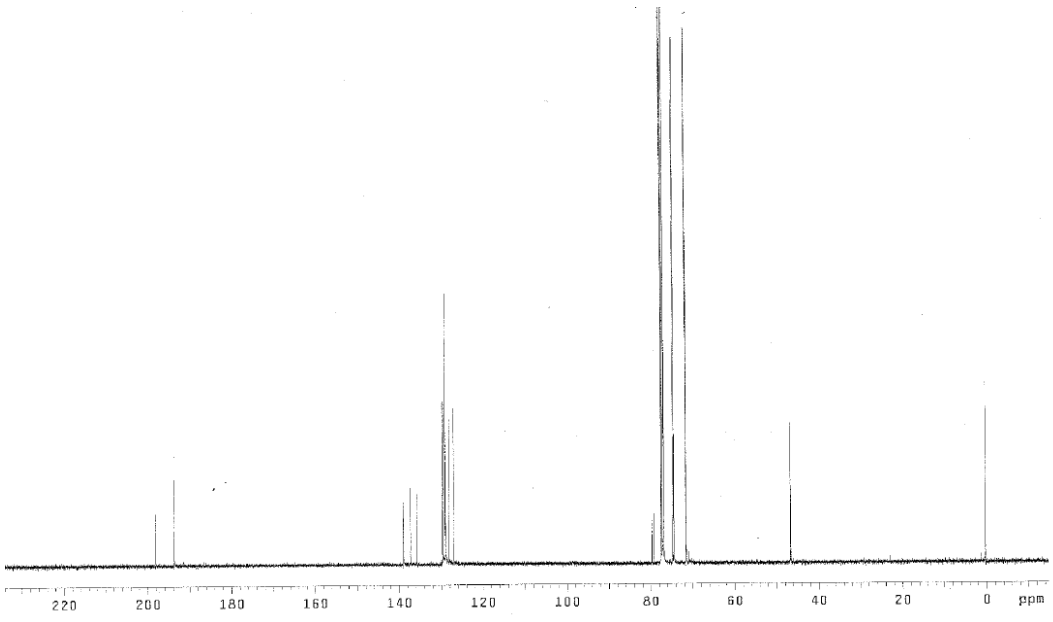
220
200
180
160
140
120
100
80
60
40
20
0
ppm

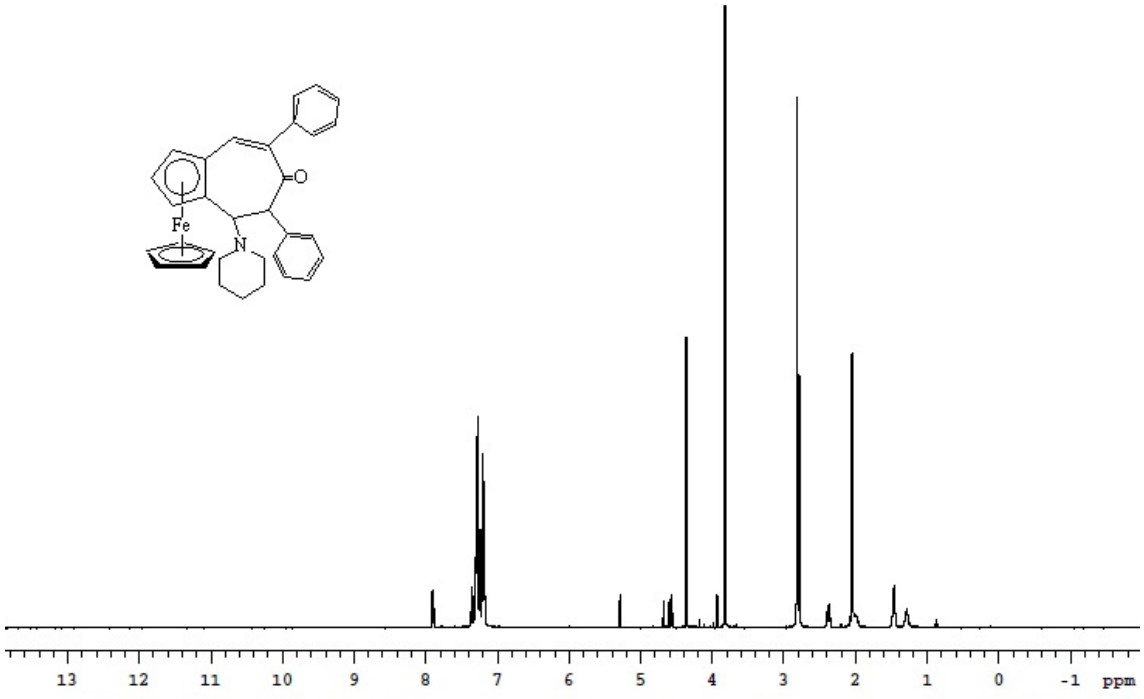
O
Fe
N
13
12
11
10
9
8
7
6
5
4
3
2
1
0
-1
ppm

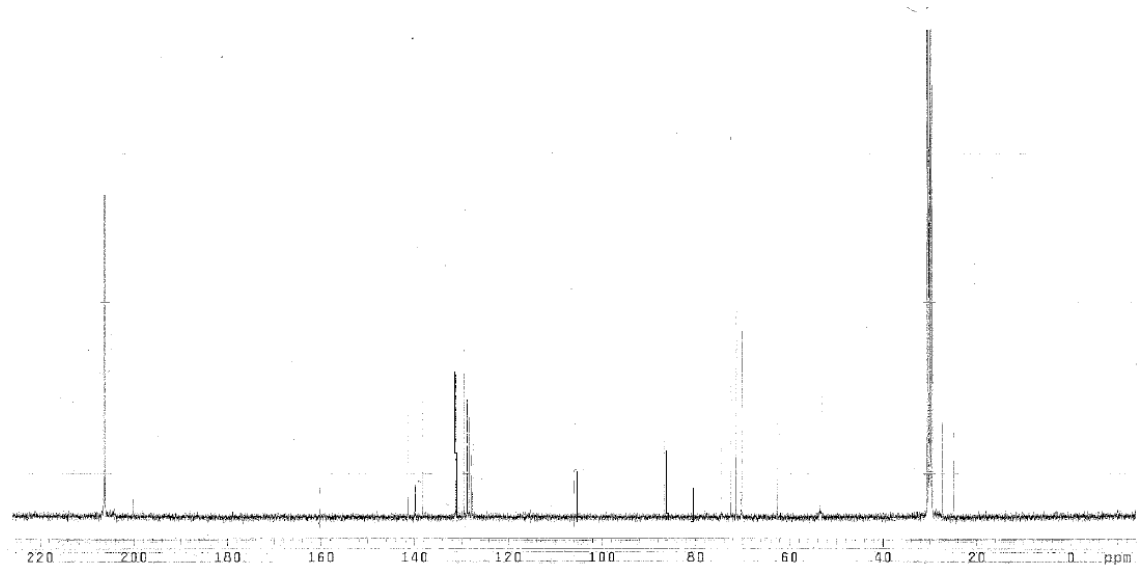
220
200
180
160
140
120
100
80
60
40
20
0
ppm

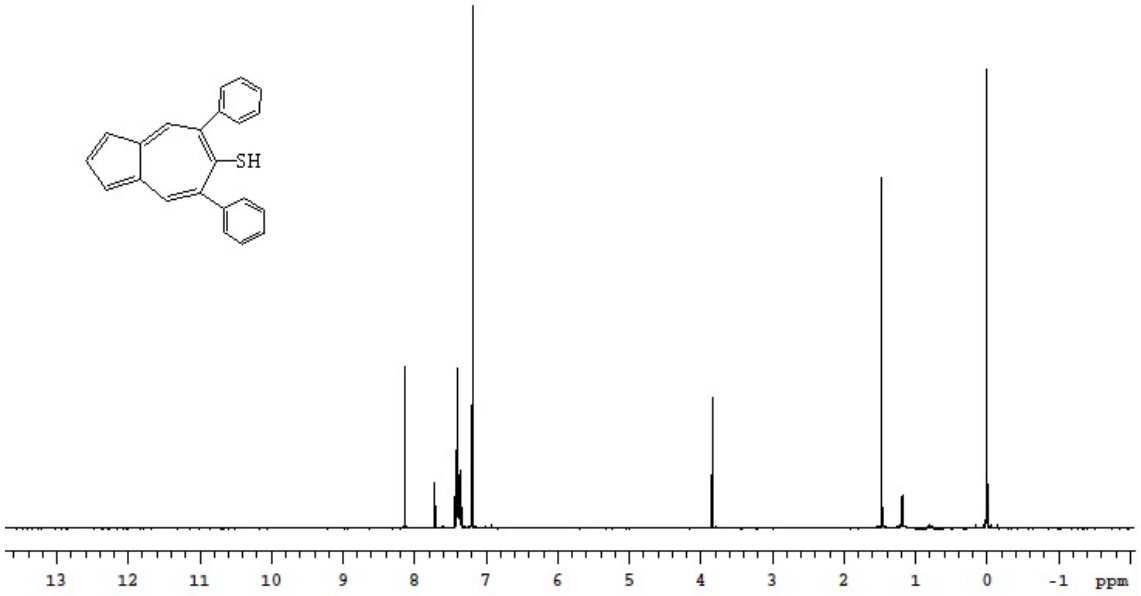
SH
13
12
11
10
9
8
7
6
5
4
3
2
1
0
-1
ppm

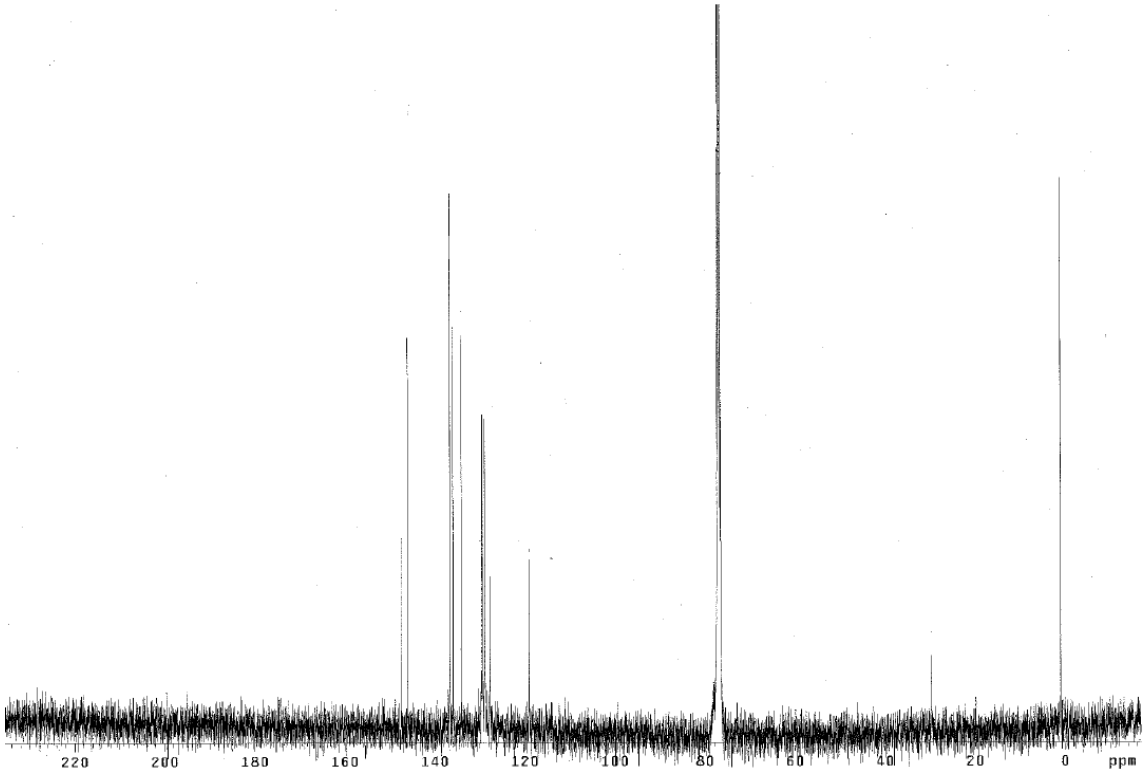
220
200
180
160
140
120
100
80
60
40
20
0
ppm

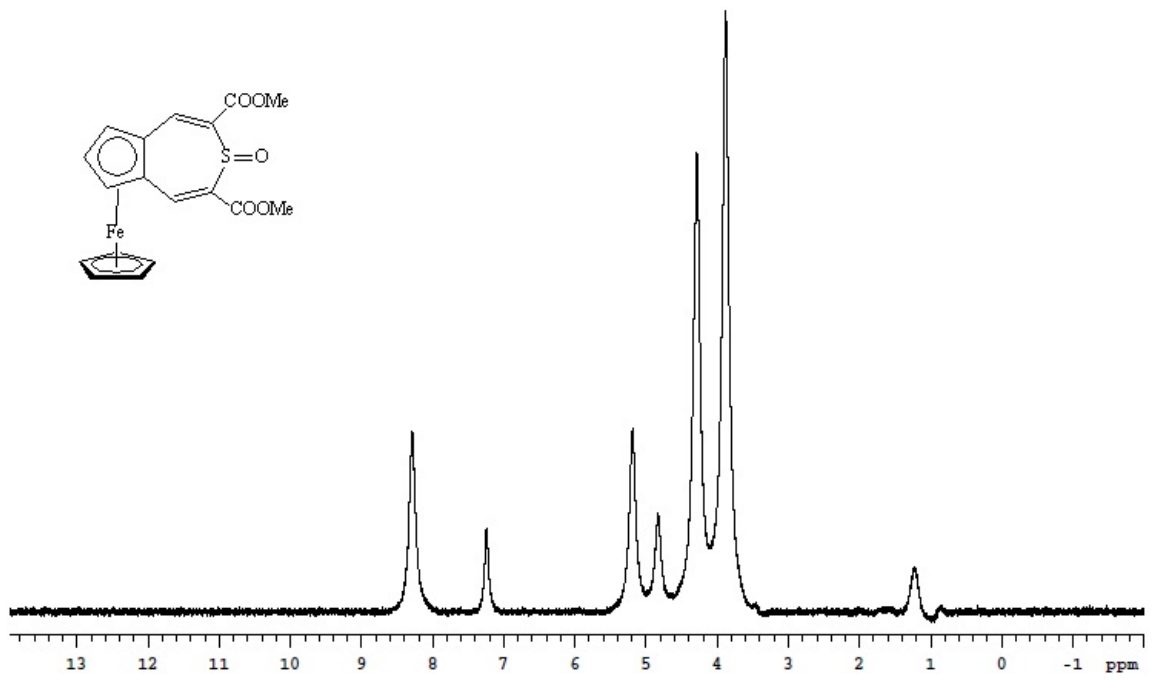
COOMe
S=O
COOMe
Fe
13 12 11 10 9 8 7 6 5 4 3 2 1 0 -1 ppm

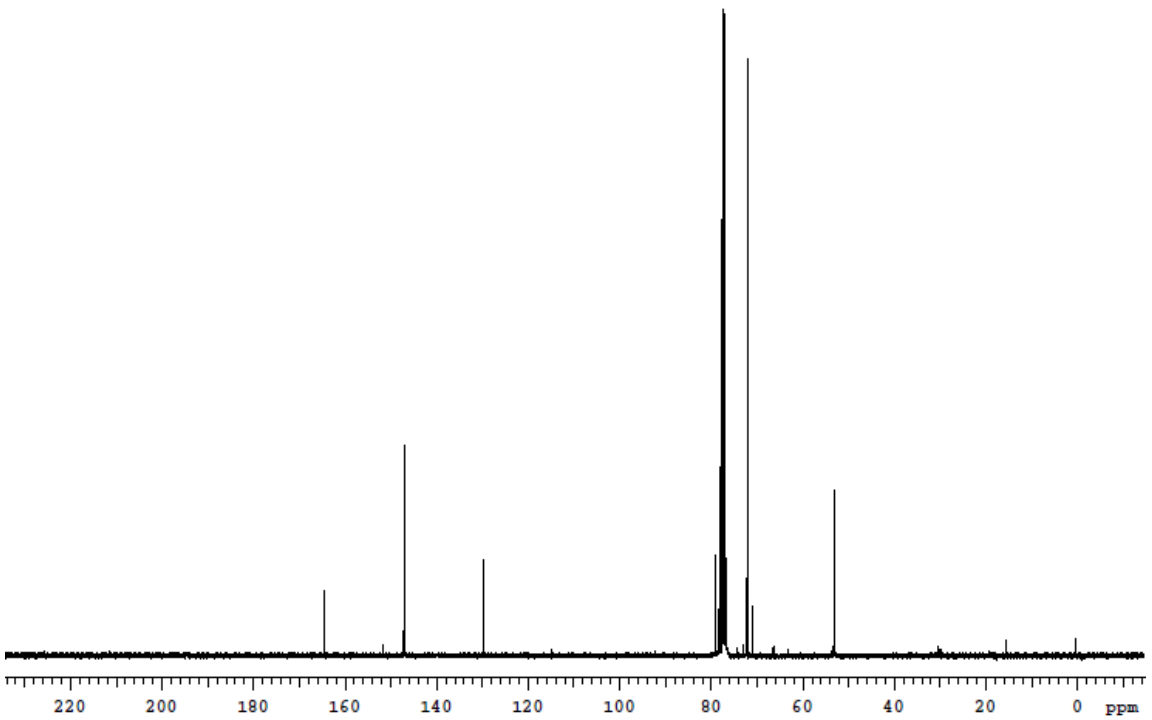
220 200 180 160 140 120 100 80 60 40 20 0 ppm

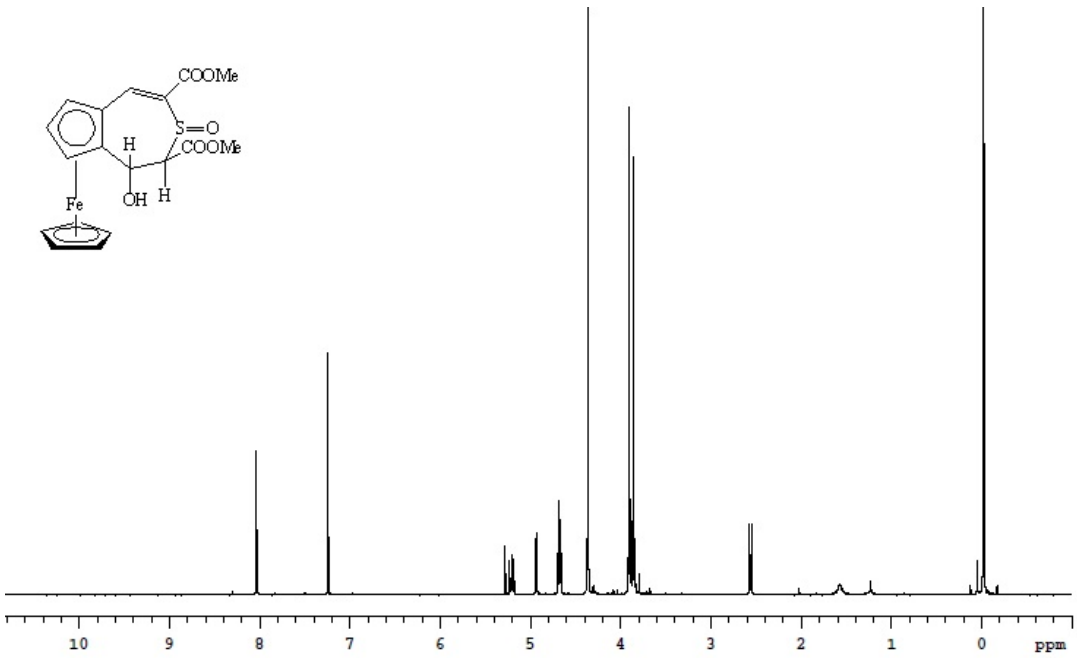
COOMe
S=O
COOMe
H
OH
H
Fe
10
9
8
7
6
5
4
3
2
1
0
ppm

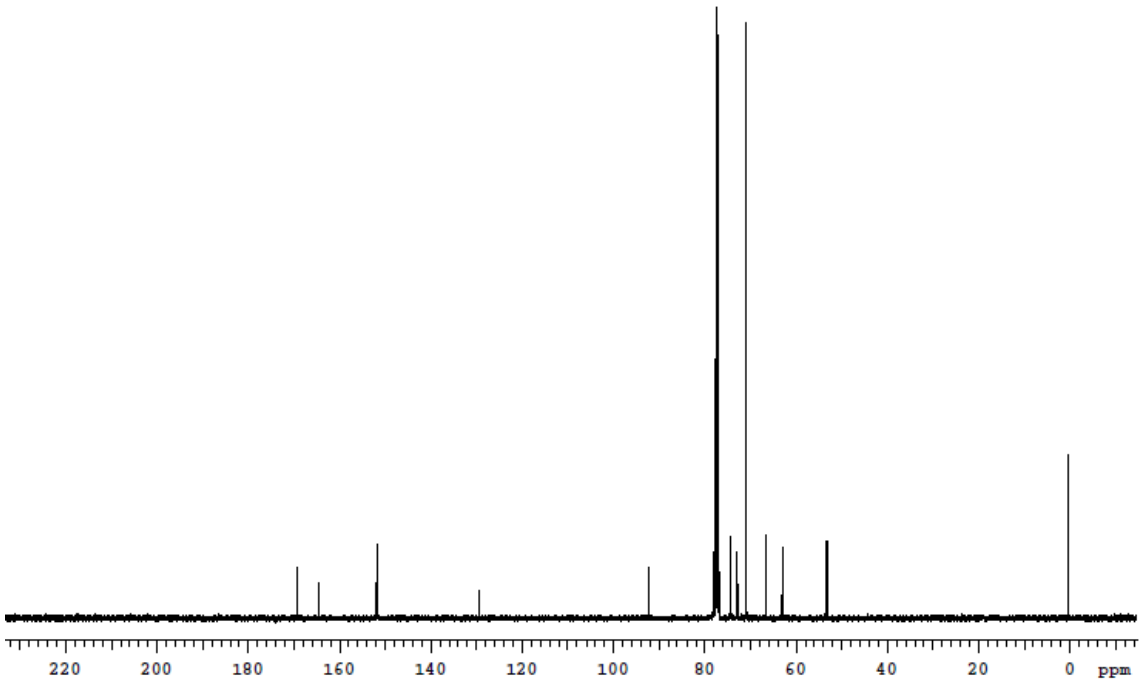
220
200
180
160
140
120
100
80
60
40
20
0
ppm

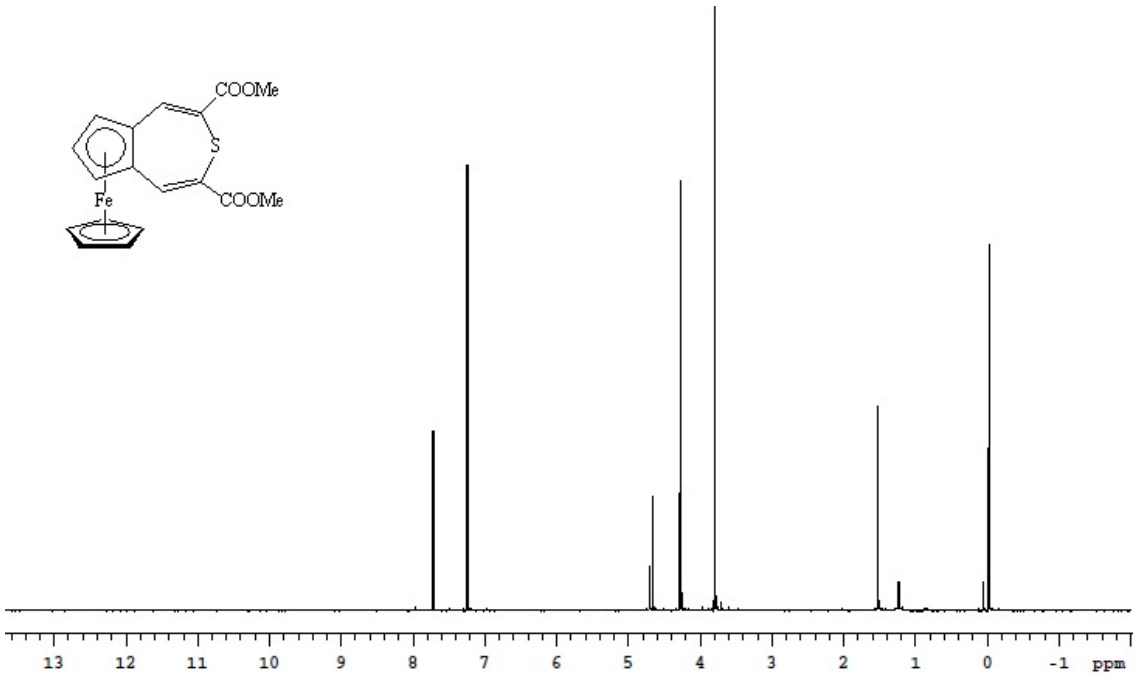
COOMe
S
COOMe
Fe
13
12
11
10
9
8
7
6
5
4
3
2
1
0
-1
ppm

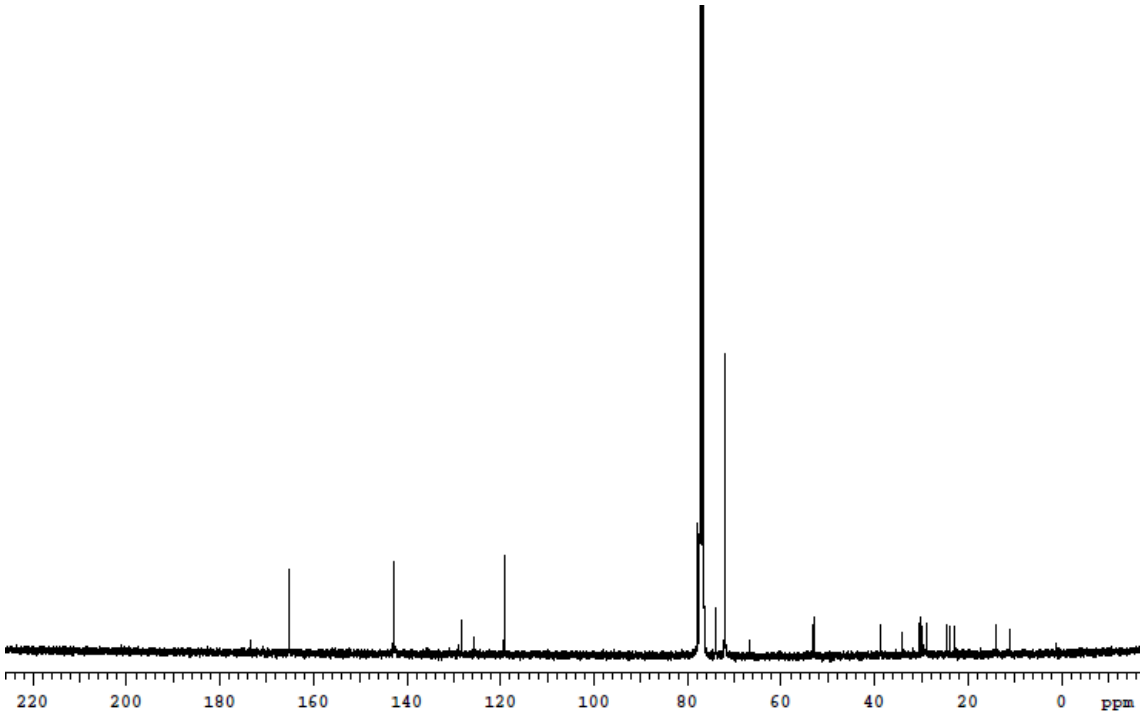
220
200
180
160
140
120
100
80
60
40
20
0
ppm

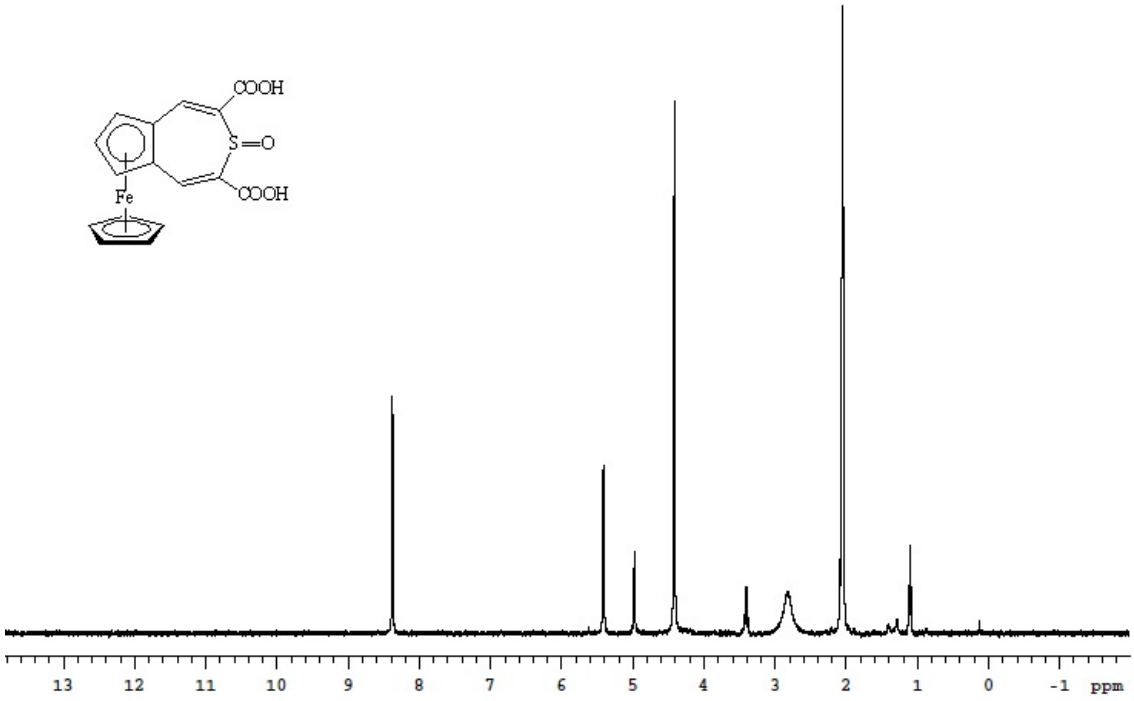
COOH
S=O
COOH
Fe
13 12 11 10 9 8 7 6 5 4 3 2 1 0 -1 ppm

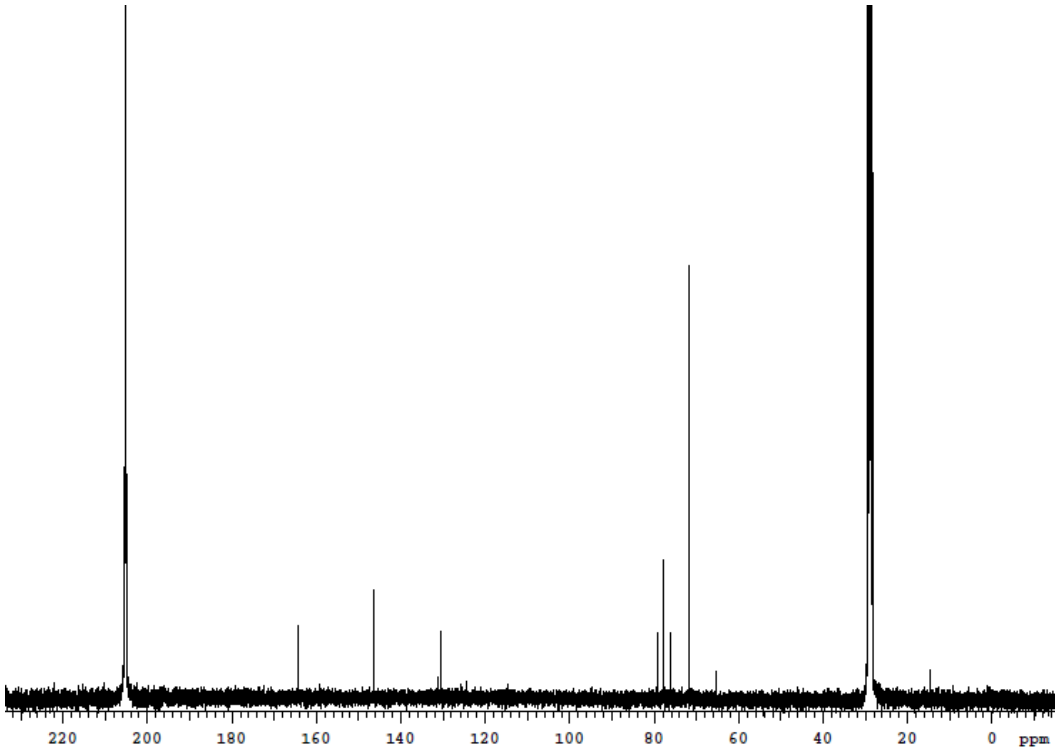
220 200 180 160 140 120 100 80 60 40 20 0 ppm

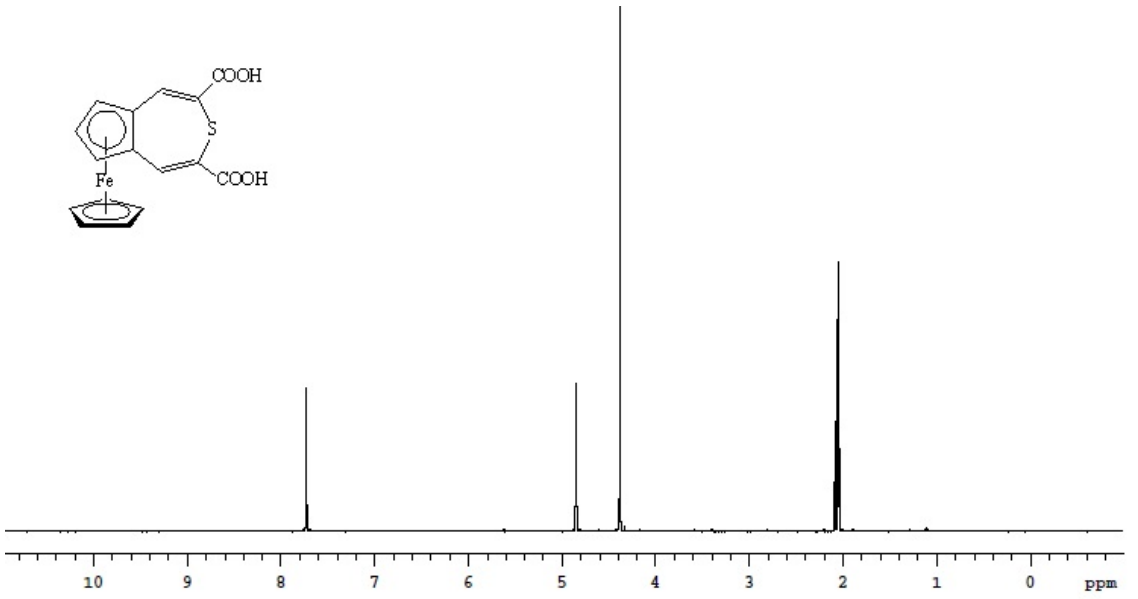
COOH
S
COOH
Fe
10
9
8
7
6
5
4
3
2
1
0
ppm

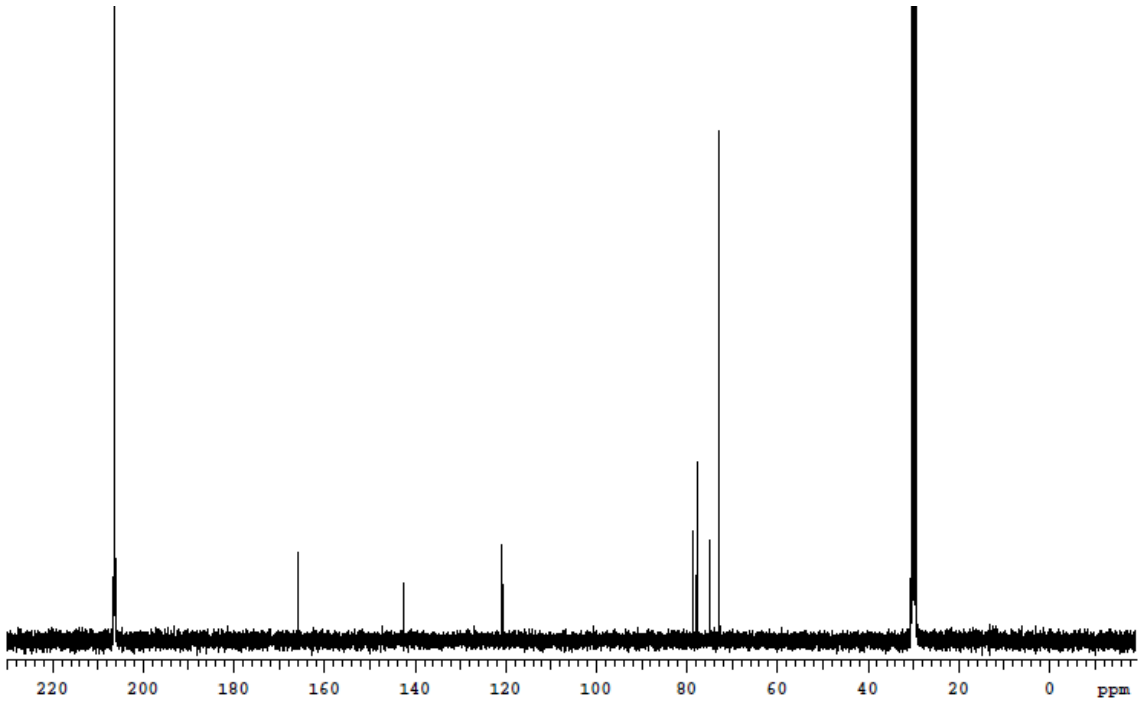
220
200
180
160
140
120
100
80
60
40
20
0
ppm

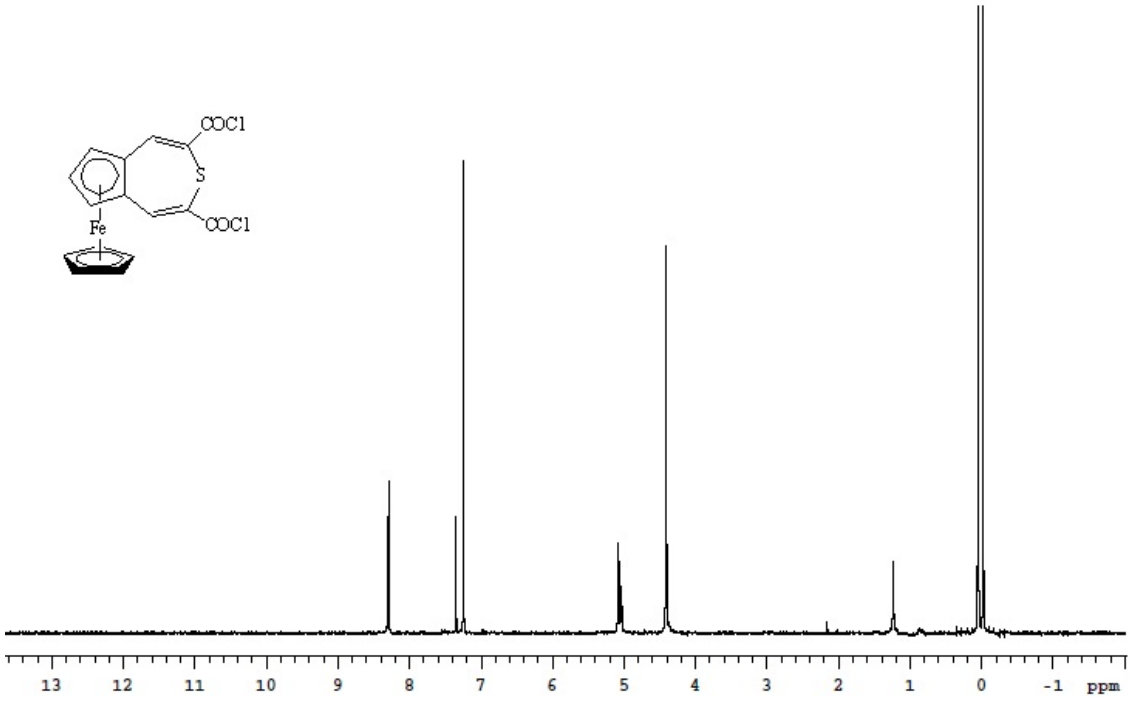
COCl
S
COCl
Fe
13
12
11
10
9
8
7
6
5
4
3
2
1
0
-1
ppm

References

1. (a) Cheng, Y.-J.; Yang, S.-H.; Hsu, C.-S. *Chem. Rev.* **2009,** *109*, 5868-5923; (b) Shirota, Y.; Kageyama, H. *Chem. Rev.* **2007,** *107*, 953-1010; (c) Katz, H. E.; Huang, J. *Ann. Rev. Mater. Res.* **2009,** *39*, 71-92.
2. Thomas, S. W.; Joly, G. D.; Swager, T. M. *Chem. Rev.* **2007,** *107*, 1339-1386.
3. Huitema, H. E. A.; Gelinck, G. H.; van der Putten, J. B. P. H.; Kuijk, K. E.; Hart, C. M.; Cantatore, E.; Herwig, P. T.; van Breemen, A. J. J. M.; de Leeuw, D. M. *Nature* **2001,** *414*, 599-599.
4. Steudel, S.; Myny, K.; Arkhipov, V.; Deibel, C.; De Vusser, S.; Genoe, J.; Heremans, P. *Nat. Mater.* **2005,** *4*, 597-600.
5. Sirringhaus, H. *Adv. Mater.* **2005,** *17*, 2411-2425.
6. Anthony, J. E. *Chem. Rev.* **2006,** *106*, 5028-5048.
7. Anthony, J. E. *Angew. Chem. Int. Ed.* **2008,** *47*, 452-483.
8. Allard, S.; Forster, M.; Souharce, B.; Thiem, H.; Scherf, U. *Angew. Chem. Int. Ed.* **2008,** *47*, 4070-4098.
9. Hoeben, F. J. M.; Jonkheijm, P.; Meijer, E. W.; Schenning, A. P. H. J. *Chem. Rev.* **2005,** *105*, 1491-1546.
10. Murphy, A. R.; Fréchet, J. M. J. *Chem. Rev.* **2007,** *107*, 1066-1096.
11. Zaumseil, J.; Sirringhaus, H. *Chem. Rev.* **2007,** *107*, 1296-1323.
12. Acton, O.; Ting Ii, G. G.; Ma, H.; Hutchins, D.; Wang, Y.; Purushothaman, B.; Anthony, J. E.; Jen, A. K. Y. *J. Mater. Chem.* **2009,** *19*, 7929-7936.
13. Dimitrakopoulos, C. D.; Malenfant, P. R. L. *Adv. Mater.* **2002,** *14*, 99-117.

14. Facchetti, A.; Yoon, M. H.; Marks, T. J. *Adv. Mater.* **2005,** *17*, 1705-1725.

15. Mas-Torrent, M.; Rovira, C. *Chem. Soc. Rev.* **2008,** *37*, 827-838.

16. Pesavento, P. V.; Chesterfield, R. J.; Newman, C. R.; Frisbie, C. D. *J. Appl. Phys.* **2004,** *96*, 7312-7324.

17. Horowitz, G. *Adv. Mater.* **1998,** *10*, 365-377.

18. Reese, C.; Roberts, M.; Ling, M.-m.; Bao, Z. *Mater. Today* **2004,** *7*, 20-27.

19. Sakamoto, Y.; Suzuki, T.; Kobayashi, M.; Gao, Y.; Fukai, Y.; Inoue, Y.; Sato, F.; Tokito, S. *J. Am. Chem. Soc.* **2004,** *126*, 8138-8140.

20. Herwig, P. T.; Müllen, K. *Adv. Mater.* **1999,** *11*, 480-483.

21. Panye, M. *University of Kentucky PhD* **2005**.

22. Afzali, A.; Dimitrakopoulos, C. D.; Graham, T. O. *Adv. Mater.* **2003,** *15*, 2066-2069.

23. Weidkamp, K. P.; Afzali, A.; Tromp, R. M.; Hamers, R. J. *J. Am. Chem. Soc.* **2004,** *126*, 12740-12741.

24. Huang, H. H.; Hsieh, H. H.; Wu, C. C.; Lin, C. C.; Chou, P. T.; Chuang, T. H.; Wen, Y. S.; Chow, T. J. *Tetrahedron Lett.* **2008,** *49*, 4494-4497.

25. Watanabe, M.; Chen, K.-Y.; Chang, Y. J.; Chow, T. J. *Acc. Chem. Res.* **2013,** *46*, 1606-1615.

26. Meng, H.; Bendikov, M.; Mitchell, G.; Helgeson, R.; Wudl, F.; Bao, Z.; Siegrist, T.; Kloc, C.; Chen, C. H. *Adv. Mater.* **2003,** *15*, 1090-1093.

27. Maulding, D. R.; Roberts, B. G. *J. Org. Chem.* **1969,** *34*, 1734-1736.

28. Picciolo, L. C.; Murata, H.; Kafafi, Z. H. *Appl. Phys. Lett.* **2001,** *78*, 2378-2380.

29. Purushothaman, B.; Bruzek, M.; Parkin, S. R.; Miller, A.-F.; Anthony, J. E. *Angew. Chem. Int. Ed.* **2011,** *50*, 6932-6932.

30. Swartz, C. R.; Parkin, S. R.; Bullock, J. E.; Anthony, J. E.; Mayer, A. C.; Malliaras, G. G. *Org. Lett.* **2005,** *7*, 3163-3166.

31. Takimiya, K.; Kunugi, Y.; Konda, Y.; Niihara, N.; Otsubo, T. *J. Am. Chem. Soc.* **2004,** *126*, 5084-5085.

32. Shinamura, S.; Osaka, I.; Miyazaki, E.; Nakao, A.; Yamagishi, M.; Takeya, J.; Takimiya, K. *J. Am. Chem. Soc.* **2011,** *133*, 5024-5035.

33. Laquindanum, J. G.; Katz, H. E.; Lovinger, A. J. *J. Am. Chem. Soc.* **1998,** *120*, 664-672.

34. Takimiya, K.; Shinamura, S.; Osaka, I.; Miyazaki, E. *Adv. Mater.* **2011,** *23*, 4347-4370.

35. Payne, M. M.; Parkin, S. R.; Anthony, J. E.; Kuo, C.-C.; Jackson, T. N. *J. Am. Chem. Soc.* **2005,** *127*, 4986-4987.

36. Tang, M. L.; Okamoto, T.; Bao, Z. *J. Am. Chem. Soc.* **2006,** *128*, 16002-16003.

37. Tang, M. L.; Reichardt, A. D.; Siegrist, T.; Mannsfeld, S. C. B.; Bao, Z. *Chem. Mater.* **2008,** *20*, 4669-4676.

38. Palayangoda, S. S.; Mondal, R.; Shah, B. K.; Neckers, D. C. *J. Org. Chem.* **2007,** *72*, 6584-6587.

39. Nguyen, M.-H.; Yip, J. H. K. *Organometallics* **2012,** *31*, 7522-7531.

40. Nguyen, M.-H.; Yip, J. H. K. *Organometallics* **2011,** *30*, 6383-6392.

41. Williams, K. A.; Boydston, A. J.; Bielawski, C. W. *Chem. Soc. Rev.* **2007,** *36*, 729-744.

42. Kaim, W.; Klein, A.; Glöckle, M. *Acc. Chem. Res.* **2000,** *33*, 755-763.

43. Holliday, B. J.; Swager, T. M. *Chem. Commun.* **2005**, 23-36.

44. Kowalski, K.; Winter, R. F. *J. Organomet. Chem.* **2009,** *694*, 1041-1048.

45. Fox, M. A.; Farmer, J. D.; Roberts, R. L.; Humphrey, M. G.; Low, P. J. *Organometallics* **2009,** *28*, 5266-5269.

46. Packheiser, R.; Ecorchard, P.; Rüffer, T.; Lohan, M.; Bräuer, B.; Justaud, F.; Lapinte, C.; Lang, H. *Organometallics* **2008,** *27*, 3444-3457.

47. Wilkinson, G.; Rosenblum, M.; Whiting, M. C.; Woodward, R. B. *J. Am. Chem. Soc.* **1952,** *74*, 2125-2126.

48. G. Alt, H.; Samuel, E. *Chem. Soc. Rev.* **1998,** *27*, 323-329.

49. (a) Hart-Davis, A. J.; Mawby, R. J. *J. Chem. Soc. A.* **1969**, 2403-2407; (b) Hart-Davis, A. J.; Mawby, R. J. *Journal of the Chemical Society A.* **1969**, 2403-2407.

50. Cramer, R.; Seiwell, L. P. *J. Organomet. Chem.* **1975,** *92*, 245-252.

51. Rerek, M. E.; Basolo, F. *J. Am. Chem. Soc.* **1984,** *106*, 5908-5912.

52. Rerek, M. E.; Ji, L.-N.; Basolo, F. *J. Chem. Soc., Chem. Commun.* **1983**, 1208-1209.

53. Westcott, S. A.; Kakkar, A. K.; Stringer, G.; Taylor, N. J.; Marder, T. B. *J. Organomet. Chem.* **1990,** *394*, 777-794.

54. Pauson, P. L.; Wilkinson, G. *J. Am. Chem. Soc.* **1954,** *76*, 2024-2026.

55. King, R. B.; Bisnette, M. B. *Inorg. Chem.* **1964,** *3*, 796-800.

56. Crisp, J. A.; Meier, R. M.; Overby, J. S.; Hanusa, T. P.; Rheingold, A. L.; Brennessel, W. W. *Organometallics* **2010,** *29*, 2322-2331.

57. Bradley, C. A.; Lobkovsky, E.; Chirik, P. J. *J. Am. Chem. Soc.* **2003,** *125*, 8110-8111.

58. Kim, D. H.; Lee, J. A.; Lee, B. Y.; Chung, Y. K. *J. Organomet. Chem.* **2005,** *690*, 1822-1828.

59. Foster, P.; Chien, J. C. W.; Rausch, M. D. *Organometallics* **1996,** *15*, 2404-2409.

60. Gonçalves, I. S.; Gamelas, C. A.; Pereira, C. C. L.; Romão, C. C. *J. Organomet. Chem.* **2005,** *690*, 1718-1725.

61. Kirillov, E.; Saillard, J. Y.; Carpentier, J. F. *Coord. Chem. Rev.* **2005,** *249*, 1221-1248.

62. Moss, J.; Thomas, J.; Ashley, A.; Cowley, A. R.; O'Hare, D. *Organometallics* **2006,** *25*, 4279-4285.

63. Alt, H. G.; Zenk, R. *J. Organomet. Chem.* **1996,** *526*, 295-301.

64. Samuel, E.; Setton, R. *J. Organomet. Chem.* **1965,** *4*, 156-158.

65. Kowala, C.; Wailes, P. C.; Weigold, H.; Wunderlich, J. A. *J. Chem. Soc., Chem. Commun.* **1974**, 993-994.

66. King, R. B.; Efraty, A.; Douglas, W. M. *J. Organomet. Chem.* **1973,** *56*, 345-355.

67. Decken, A.; MacKay, A. J.; Brown, M. J.; Bottomley, F. *Organometallics* **2002,** *21*, 2006-2009.

68. Moesges, G.; Hampel, F.; Schleyer, P. v. R. *Organometallics* **1992,** *11*, 1769-1770.

69. Peifer, B.; Bruce Welch, M.; Alt, H. G. *J. Organomet. Chem.* **1997,** *544*, 115-119.

70. Patsidis, K.; Alt, H. G.; Milius, W.; Palackal, S. J. *J. Organomet. Chem.* **1996,** *509*, 63-71.

71. Schertl, P.; Alt, H. G. *J. Organomet. Chem.* **1997,** *545–546*, 553-557.

72. Peifer, B.; Milius, W.; Alt, H. G. *J. Organomet. Chem.* **1998,** *553*, 205-220.

73. Johnson, J. W.; Treichel, P. M. *J. Am. Chem. Soc.* **1977,** *99*, 1427-1436.

74. Novikova, L. N.; Mazurchik, B. A.; Ustynyuk, N. A.; Kukharenko, S. V.; Strelets, V. V. *Russ. Chem. Bull.* **1994,** *43*, 299-303.

75. Katz, T. J.; Slusarek, W. *J. Am. Chem. Soc.* **1979,** *101*, 4259-4267.

76. Sudhakar, A.; Katz, T. J. *J. Am. Chem. Soc.* **1986,** *108*, 179-181.

77. Pammer, F.; Thiel, W. R. *Coord. Chem. Rev.* **2014,** *270–271*, 14-30.

78. Schröder, K.; Haase, D.; Saak, W.; Lützen, A.; Beckhaus, R.; Wichmann, S.; Schellenberg, J. *Organometallics* **2006,** *25*, 3824-3836.

79. Pammer, F.; Sun, Y.; May, C.; Wolmershäuser, G.; Kelm, H.; Krüger, H.-J.; Thiel, W. R. *Angew. Chem. Int. Ed.* **2007,** *46*, 1270-1273.

80. Pammer, F.; Sun, Y.; Pagels, M.; Weismann, D.; Sitzmann, H.; Thiel, W. R. *Angew. Chem. Int. Ed.* **2008,** *47*, 3271-3274.

81. Toganoh, M.; Sato, A.; Furuta, H. *Angew. Chem. Int. Ed.* **2011,** *50*, 2752-2755.

82. Payne, M. M.; Odom, S. A.; Parkin, S. R.; Anthony, J. E. *Org. Lett.* **2004,** *6*, 3325-3328.

83. Kerber, R. C. *Organometallic Chemistry II Iron, Ruthenium, and Osmium* **1994,** *7*, 102-185.

84. Rausch, M. D. *Can. J. Chem.* **1963,** *41*, 1289-1314.

85. Abd-El-Aziz, A. S. *Macromol. Rapid Commun.* **2002,** *23*, 995-1031.

86. Gagne, R. R.; Koval, C. A.; Lisensky, G. C. *Inorg. Chem.* **1980,** *19*, 2854-2855.

87. Beasley, C. A.; Murray, R. W. *Langmuir* **2009,** *25*, 10370-10375.

88. Linn, W. J.; Sharkey, W. H. *J. Am. Chem. Soc.* **1957,** *79*, 4970-4972.

89. Goetgheluck, S. P.; Delacroix, O.; Maciejewski, L.; Brocard, J. *Synthesis* **2000,** *10*, 1421-1426.

90. Malfait, S.; Pelinski, L.; Maciejewski, L.; Brocard, J. *Synlett.* **1997,** *7*, 830-832.

91. Marr, G.; Rockett, B. W.; Rushworth, A. *J. Organomet. Chem.* **1969,** *16*, 141-147.

92. Pokharel, U. R.; Selegue, J. P.; Parkin, S. *Organometallics* **2011,** *30*, 3254-3256.

93. Oatis, J. E.; Walle, T.; Daniell, H. B.; Gaffney, T. E.; Knapp, D. R. *J. Med. Chem.* **1985,** *28*, 822-824.

94. Chen, Z.; Amara, J. P.; Thomas, S. W.; Swager, T. M. *Macromolecules* **2006,** *39*, 3202-3209.

95. Otwinowski, Z.; Minor, W. In *Methods Enzymol.*, Charles W. Carter, Jr., Ed. Academic Press: 1997; Vol. 276, pp 307-326.

96. Sheldrick, G. *Acta Crystallogr. Sect. A: Found. Crystallogr.* **2008,** *64*, 112-122.

97. Lednicer, D.; Hauser, C. R. *Org. Synth. Coll.* **1973, 5, 434,** *1960, 40*, 31.

98. Rinehart, K. J.; Curby, R. J.; Sokol, P. E. *J. Am. Chem. Soc.* **1957,** *79*, 3420-3424.

99. Martin, E. L. *Org. Synth. Coll.* **1943, 2, 499,** *1935, 15*, 64.

100. Patwa, A. N.; Gupta, S.; Gonnade, R. G.; Kumar, V. A.; Bhadbhade, M. M.; Ganesh, K. N. *J. Org. Chem.* **2008,** *73*, 1508-1515.

101. Hill, E. A.; Richards, J. H. *J. Am. Chem. Soc.* **1961,** *83*, 4216-4221.

102. Weißenbacher, M.; Sturm, T.; Kalchhauser, H.; Kratky, C.; Weissensteiner, W. *Monatsh. Chem.* **2002,** *133*, 991-1009.

103. Sotiriou, C.; Lee, W.; Giese, R. W. *J. Org. Chem.* **1990,** *55*, 2159-2164.

104. Gao, B.; Yang, B.; Li, T.; Zhang, B. *Synth. Commun.* **2009,** *39*, 2973-2981.

105. Mayer, N. A.; Shklyar, C. A.; Ol'Dekop, U. A. *Russ. J. Gen. Chem.* **1980,** *11*, 2626.

106. Kündig, E. P.; Enríquez García, A.; Lomberget, T.; Bernardinelli, G. *Angew. Chem. Int. Ed.* **2006,** *45*, 98-101.

107. Pokharel, U. R. *University of Kentucky PhD* **2012**.

108. Takahashi, T.; Li, S.; Huang, W.; Kong, F.; Nakajima, K.; Shen, B.; Ohe, T.; Kanno, K. I. *J. Org. Chem.* **2006,** *71*, 7967-7977.

109. Niebel, C.; Lokshin, V.; Khodorkovsky, V. *Tetrahedron Lett.* **2008,** *49*, 7276-7278.

110. Niebel, C.; Lokshin, V.; Khodorkovsky, V. *Tetrahedron Lett.* **2010,** *51*, 949-951.

111. Makino, M.; Aihara, J.-i. *PCCP* **2008,** *10*, 591-599.

112. Kundig, E. P.; Lomberget, T.; Bragg, R.; Poulard, C.; Bernardinelli, G. *Chem. Commun.* **2004**, 1548-1549.

113. Kakkar, A. K.; Jones, S. F.; Taylor, N. J.; Collins, S.; Marder, T. B. *J. Chem. Soc., Chem. Commun.* **1989**, 1454-1456.

114. Kakkar, A. K.; Taylor, N. J.; Marder, T. B. *Organometallics* **1989,** *8*, 1765-1768.

115. Paddon, C. A.; Compton, R. G. *Electroanalysis* **2005,** *17*, 1919-1923.

116. Pommerehne, J.; Vestweber, H.; Guss, W.; Mahrt, R. F.; Bässler, H.; Porsch, M.; Daub, J. *Adv. Mater.* **1995,** *7*, 551-554.

117. Payne, M. M.; Parkin, S. R.; Anthony, J. E. *J. Am. Chem. Soc.* **2005,** *127*, 8028-8029.

118. Franken, P. A.; Hill, A. E.; Peters, C. W.; Weinreich, G. *Phys. Rev. Lett.* **1961,** *7*, 118-119.

119. Dalton, L. R.; Harper, A. W.; Ghosn, R.; Steier, W. H.; Ziari, M.; Fetterman, H.; Shi, Y.; Mustacich, R. V.; Jen, A. K. Y.; Shea, K. J. *Chem. Mater.* **1995,** *7*, 1060-1081.

120. Williams, D. J. *Angew. Chem. Int. Ed. Engl.* **1984,** *23*, 690-703.

121. Rentzepis, P. M.; Pao, Y. H. *Appl. Phys. Lett.* **1964,** *5*, 156-158.

122. Heilmeier, G. H.; Ockman, N.; Braunstein, R.; Kramer, D. A. *Appl. Phys. Lett.* **1964,** *5*, 229-230.

123. Qin, A.; Bai, F.; Ye, C. *J. Mol. Struc. Theochem* **2003,** *631*, 79-85.

124. Ray, P. C. In *Non-Linear Optical Properties of Matters*, Papadopoulos, M. G.; Sadlej, A. J.; Leszczynski, J., Eds. Springer: 2006; Vol. 1, pp 383-418.

125. Oudar, J. L.; Chemla, D. S. *J. Chem. Phys.* **1977,** *66*, 2664-2668.

126. Ahlheim, M.; Barzoukas, M.; Bedworth, P. V.; Blanchard-Desce, M.; Fort, A.; Hu, Z.-Y.; Marder, S. R.; Perry, J. W.; Runser, C.; Staehelin, M.; Zysset, B. *Science* **1996,** *271*, 335-337.

127. Calabrese, J. C.; Cheng, L. T.; Green, J. C.; Marder, S. R.; Tam, W. *J. Am. Chem. Soc.* **1991,** *113*, 7227-7232.

128. Green, M. L. H.; Marder, S. R.; Thompson, M. E.; Bandy, J. A.; Bloor, D.; Kolinsky, P. V.; Jones, R. J. *Nature* **1987,** *330*, 360-362.

129. Marder, S. R.; Perry, J. W.; Tiemann, B. G.; Schaefer, W. P. *Organometallics* **1991,** *10*, 1896-1901.

130. Alain, V.; Blanchard-Desce, M.; Chen, C.-T.; Marder, S. R.; Fort, A.; Barzoukas, M. *Synth. Met.* **1996,** *81*, 133-136.

131. Buemi, G.; Zuccarello, F.; Raudino, A. *J. Mol. Struc. Theochem* **1981,** *76*, 137-164.

132. Yumura, K.; Otani, H.; Mizuguchi, J. *Dyes Pigments* **1998,** *38*, 227-242.

133. Pluta, T.; Sadlej, A. J. *J. Chem. Phys.* **2001,** *114*.

134. Eckart, U.; Fu¨lscher, M. P.; Serrano-Andrés, L.; Sadlej, A. J. *J. Chem. Phys.* **2000,** *113*.

135. Otani, H.; Sato, Y.; Mizuguchi, J. *Dyes Pigments* **1997,** *35*, 205-217.

136. Giacomo, A. D.; Smyth, C. P. *J. Am. Chem. Soc.* **1952,** *74*, 4411-4413.

137. Mizuguchi, J.; Suzuki, T.; Matsumoto, S.; Otani, H. *J. Chem. Phys. B* **1999,** *103*, 426-430.

138. Leonard, N. J.; Miller, L. A.; Berry, J. W. *J. Am. Chem. Soc.* **1957,** *79*, 1482-1485.

139. Nozoe, T.; Mukai, T.; Takase, K.; Nagase, T. *P. Jpn. Acad.* **1952,** *28*, 477-482.

140. Takagi, K.; Nishikawa, Y.; Kunisada, H.; Yuki, Y. *Chem. Lett.* **2001,** *30*, 1244-1245.

141. Takagi, K.; Nishikawa, Y.; Nishioka, N.; Kunisada, H.; Yuki, Y. *J. Polym. Sci., Part A: Polym. Chem.* **2002,** *40*, 3927-3937.

142. Takagi, K.; Mori, K.; Kunisada, H.; Yuki, Y. *Polym. Bull.* **2004,** *52*, 125-132.

143. Sugiyasu, K.; Song, C.; Swager, T. M. *Macromolecules* **2006,** *39*, 5598-5600.

144. Cho, M. J.; Choi, D. H.; Sullivan, P. A.; Akelaitis, A. J. P.; Dalton, L. R. *Prog. Polym. Sci.* **2008,** *33*, 1013-1058.

145. Yesodha, S. K.; Sadashiva Pillai, C. K.; Tsutsumi, N. *Prog. Polym. Sci.* **2004,** *29*, 45-74.

146. Ariafard, A.; Lin, Z. *J. Organomet. Chem.* **2006,** *691*, 4545-4555.

147. Pauson, P. L.; Todd, K. H. *J. Chem. Soc. C* **1970**, 2315-2318.

148. Snyder, C. A.; Selegue, J. P.; Tice, N. C.; Wallace, C. E.; Blankenbuehler, M. T.; Parkin, S.; Allen, K. D. E.; Beck, R. T. *J. Am. Chem. Soc.* **2005,** *127*, 15010-15011.

149. Selegue, J. P.; Swarat, K. A. *J. Am. Chem. Soc.* **1993,** *115*, 6448-6449.

150. Wallace, C. E.; Selegue, J. P.; Carrillo, A. *Organometallics* **1998,** *17*, 3390-3393.

151. Tirouflet, J.; Moise, C. *C. R. Seances Acad. Sci., Ser. C* **1966,** *262*, 1889-1890.

152. Tice, N. *University of Kentucky PhD* **2006**.

153. Machiguchi, T.; Hasegawa, T.; Ohno, M.; Kitahara, Y.; Funamizu, M.; Nozoe, T. *J. Chem. Soc., Chem. Commun.* **1988**, 838-839.

154. Machiguchi, T.; Wada, Y.; Hasegawa, T.; Yamabe, S.; Minato, T.; Nozoe, T. *J. Am. Chem. Soc.* **1995,** *117*, 1258-1264.

155. Dunitz, J. D.; Orgel, L. E.; Rich, A. *Acta. Cryst.* **1956,** *9*, 373-375.

156. Machiguchi, T.; Mizuno, H.; Hasegawa, T.; Ishii, Y.; Otani, H. *Chem. Lett.* **1987**, 1893-6.

157. Kudoh, M.; Sudoh, S.; Katagiri, S.; Nakazawa, T.; Ishihara, M.; Jinguji, M.; Higashi, M.; Yamaguchi, H.; Miyatake, R.; Sugihara, Y.; Kabuto, C. *Bull. Chem. Soc. Jpn.* **2006,** *79*, 1240-1247.

158. Serrano Andres, L.; Pou Ame rigo, R.; Fu lscher, M. P.; Borin, A. C. *J. Chem. Phys.* **2002,** *117*, 1649.

159. Blankespoor, R. L.; Doyle, M. P.; Hedstrand, W. H.; Tamblyn, W. H.; Van Dyke, D. A. *J. Am. Chem. Soc.* **1981,** *103*, 7096-7101.

160. Mouanga, M.; Bercot, P. *Int. J. Electrochem. Sci.* **2011,** *6*, 1007-1013.

161. Hosoya, H.; Tanaka, J.; Nagakura, S. *Tetrahedron* **1962,** *18*, 859-874.

162. Yamaguchi, H.; Amako, Y.; Azumi, H. *Tetrahedron* **1968,** *24*, 267-277.

163. Richer, G.; Sandorfy, C. *J. Mol. Struc. Theochem* **1985,** *123*, 317-327.

164. Vernitskaya, T. y. V.; Efimov, O. N. *Russ. Chem. Rev.* **1997,** *66*, 443.

165. Chiang, C. K.; Druy, M. A.; Gau, S. C.; Heeger, A. J.; Louis, E. J.; MacDiarmid, A. G.; Park, Y. W.; Shirakawa, H. *J. Am. Chem. Soc.* **1978,** *100*, 1013-1015.

166. Roncali, J. *Chem. Rev.* **1992,** *92*, 711-738.

167. Kim, H.; Lee, H.; Seo, D.; Jeong, Y.; Cho, K.; Lee, J.; Lee, Y. *Chem. Mater.* **2015**.

168. Lange, U.; Roznyatovskaya, N. V.; Mirsky, V. M. *Anal. Chim. Acta* **2008,** *614*, 1-26.

169. Reynolds, J. R.; Elsenbaumer, R. L.; Skotheim, T. A. *Handbook of Conducting Polymers*. M. Dekker: New York, 1998.

170. Kanatzidis, M. G. *Chemical & Engineering News Archive* **1990,** *68*, 36-50.

171. Chittibabu, K. G.; Li, L.; Kamath, M.; Kumar, J.; Tripathy, S. K. *Chem. Mater.* **1994,** *6*, 475-480.

172. Patil, A. O.; Heeger, A. J.; Wudl, F. *Chem. Rev.* **1988,** *88*, 183-200.

173. Heywang, G.; Jonas, F. *Adv. Mater.* **1992,** *4*, 116-118.

174. Wudl, F.; Kobayashi, M.; Heeger, A. J. *J. Org. Chem.* **1984,** *49*, 3382-3384.

175. Roncali, J. *Chem. Rev.* **1997,** *97*, 173-206.

176. McCullough, R. D. *Adv. Mater.* **1998,** *10*, 93-116.

177. Brédas, J. L.; Heeger, A. J.; Wudl, F. *J. Chem. Phys.* **1986,** *85*, 4673-4678.

178. Cava, M. P.; Husbands, G. E. M. *J. Am. Chem. Soc.* **1969,** *91*, 3952-3953.

179. Tsubouchi, A.; Matsumura, N.; Inoue, H.; Yanagi, K. *J. Chem. Soc., Perkin Trans. 1* **1991**, 909-916.

180. Ishii, A.; Nakayama, J.; Kazami, J.; Ida, Y.; Nakamura, T.; Hoshino, M. *J. Org. Chem.* **1991,** *56*, 78-82.

181. Pozo-Gonzalo, C.; Khan, T.; McDouall, J. J. W.; Skabara, P. J.; Roberts, D. M.; Light, M. E.; Coles, S. J.; Hursthouse, M. B.; Neugebauer, H.; Cravino, A.; Sariciftci, N. S. *J. Mater. Chem.* **2002,** *12*, 500-510.

182. Kim, J.-H.; Song, C. E.; Kim, B.; Kang, I.-N.; Shin, W. S.; Hwang, D.-H. *Chem. Mater.* **2014,** *26*, 1234-1242.

183. Zhou, P.; Zhang, Z.-G.; Li, Y.; Chen, X.; Qin, J. *Chem. Mater.* **2014,** *26*, 3495-3501.

184. Fischer, E. O.; Öfele, K. *Chem. Ber.* **1958,** *91*, 2395-2399.

185. Fischer, E. O.; Goodwin, H. A.; Kreiter, C. G.; Simmons Jr, H. D.; Sonogashira, K.; Wild, S. B. *J. Organomet. Chem.* **1968,** *14*, 359-374.

186. Loft, M. S.; Widdowson, D. A.; Mowlem, T. J. *Synlett* **1992,** *1992*, 135-136.

187. Song, C.; Swager, T. M. *J. Org. Chem.* **2010,** *75*, 999-1005.

188. Nishino, K.; Takagi, M.; Kawata, T.; Murata, I.; Inanaga, J.; Nakasuji, K. *J. Am. Chem. Soc.* **1991,** *113*, 5059-5060.

189. Traynelis, V. J.; Yoshikawa, Y.; Sih, J. C.; Miller, L. J.; Livingston, J. R. *J. Org. Chem.* **1973,** *38*, 3978-3986.

190. Hess Jr, B. A.; Schaad, L. J.; Reinhoudt, D. N. *Tetrahedron* **1977,** *33*, 2683-2685.

191. Traynelis, V. J.; Love, R. F. *J. Org. Chem.* **1961,** *26*, 2728-2733.

192. Yasuoka, N.; Kai, Y.; Kasai, N.; Tatsuoka, T.; Murata, I. *Angew. Chem. Int. Ed. Engl.* **1976,** *15*, 297-297.

193. Yasuoka, N.; Kai, Y.; Kasai, N. *Acta Crystallogr. Sect. B.* **1975,** *31*, 2729-2731.

194. Hofmann, H.; Gaube, H. *Angew. Chem. Int. Ed. Engl.* **1975,** *14*, 812-813.

195. Scott, G. P. *J. Am. Chem. Soc.* **1953,** *75*, 6332-6333.

196. (a) Loudon, V. J. D.; Sloan, A. D. B. *J. Chem. Soc.* **1962**, 3262-3; (b) Schlessinger, R. H. *Non-Classical Sulphur Heterocycles, Department of Chemistry, University of Rochester, New York*, 158-165.

197. Schlessinger, R. H.; Ponticello, I. S. *J. Am. Chem. Soc.* **1967,** *89*, 7138-7139.

198. Cai, Z.; Zhang, H.; Geng, H.; Liu, Z.; Yang, S.; Luo, H.; Jiang, L.; Peng, Q.; Zhang, G.; Chen, J.; Yi, Y.; Hu, W.; Zhang, D. *Chem. Eur. J.* **2013,** *19*, 14573-14580.

199. Shirani, H.; Janosik, T. *J. Org. Chem.* **2007,** *72*, 8984-8986.

200. Emerson, G. F.; Watts, L.; Pettit, R. *J. Am. Chem. Soc.* **1965,** *87*, 131-133.

201. Amiet, R. G.; Pettit, R. *J. Am. Chem. Soc.* **1968,** *90*, 1059-1060.

202. Rosenblum, M.; North, B. *J. Am. Chem. Soc.* **1968,** *90*, 1060-1061.

203. Katz, T. J.; Acton, N. *J. Am. Chem. Soc.* **1972,** *94*, 3281-3283.

204. Grimme, W.; Koeser, H. G. *J. Am. Chem. Soc.* **1981,** *103*, 5919-5920.

205. Nishino, K.; Ishigami, S.; Tamura, Y.; Imagawa, K.; Ikutani, Y.; Murata, I. *Angew. Chem. Int. Ed. Engl.* **1988,** *27*, 1717-1718.

206. Levine, D. R.; Caruso, A.; Siegler, M. A.; Tovar, J. D. *Chem. Commun.* **2012,** *48*, 6256-6258.

207. Caruso, A.; Tovar, J. D. *J. Org. Chem.* **2011,** *76*, 2227-2239.

208. Caruso, A.; Tovar, J. D. *Org. Lett.* **2011,** *13*, 3106-3109.

209. Caruso, A.; Siegler, M. A.; Tovar, J. D. *Angew. Chem. Int. Ed.* **2010,** *49*, 4213-4217.

210. Levine, D. R.; Siegler, M. A.; Tovar, J. D. *J. Am. Chem. Soc.* **2014,** *136*, 7132-7139.

211. Ko, E. J.; Williams, C. M.; Savage, P. G.; Tsanaktsidis., J. *Org. Synth.* **2012,** *89*, 471-479.

212. Corvers, A.; De, G. A.; Godefroi, E. F. *Recl. Trav. Chim. Pays-Bas* **1973,** *92*, 1368-76.

213. Mineo, P.; Alicata, R.; Micali, N.; Villari, V.; Scamporrino, E. *J. Appl. Polym. Sci.* **2012,** *126*, 1359-1368.

214. Borai, M. E.; Megeed, M. F. A.; Fahmy, M. *Sulfur Lett.* **1985,** *3*, 1-5.

215. Hoogmartens, I.; Adriaensens, P.; Vanderzande, D.; Gelan, J.; Quattrocchi, C.; Lazzaroni, R.; Bredas, J. L. *Macromolecules* **1992,** *25*, 7347-7356.

216. Lu, P.; Sanchez, C.; Cornella, J.; Larrosa, I. *Org. Lett.* **2009,** *11*, 5710-5713.

217. Cairncross, A.; Roland, J. R.; Henderson, R. M.; Sheppard, W. A. *J. Am. Chem. Soc.* **1970,** *92*, 3187-3189.

218. Zhao, J. L.; Gou, X. F.; Hau, C. W.; Wang, L. Y. *Chinese J. Catal.* **2012,** *33*, 1262-1265.

Vita

Bidhya L. Maharjan was born in Kathmandu, Nepal. She enrolled at Tri-Chandra College, Kathmandu Nepal, where she majored in Chemistry/Biology and graduated with a B. Sc in 2001. She attended Tribhuvan University, Kathmandu Nepal and graduated in 2003 with a Master Degree in Chemistry. She enrolled in the graduate program at the University of Kentucky in January 2007 and joined the research group of Dr. John P. Selegue in May 2009. She is a member of the Kentucky Academy of Science, American Chemical Society and its Organic and Organometallic Divisions.

Awards

- First position in the Kentucky Academy of Sciences for oral presentation, University of Morehead, November 2013
- Outstanding Teaching Assistant Award, Department of Chemistry, University of Kentucky, May 2013

TEACHING EXPERIENCE

- **2010-2015:** Teaching Assistant for Organic Chemistry lab courses. University of Kentucky, Lexington. (CHE 233 & 231)
- **2009-2010:** Teaching Assistant for General Chemistry lab courses, University of Kentucky, Lexington. (CHE 111 & 113)
- **2005-2007:** Assistant Lecturer of Chemistry: Organic Chemistry lab, Department of Chemistry, Tribhuvan University, Nepal

PROFESSIONAL AFFILIATION

- American Chemical Society
- Kentucky Academy of Science
- Nepal Chemical Society

CONFERENCE ORAL PRESENTATIONS

- **2014:** American Chemical Society National Meeting, Dallas, TX: Synthetic Approaches to Ferrocene-Fused Tropones, Thiotropones and Tropone Oximes

- **2013:** American Chemical Society National Meeting, New Orleans, LA: Synthetic Approaches to Cyclopentadiene-Capped Acenes & Their Iron Complexes

- **2013:** Kentucky Academy of Science Annual Meeting, Morehead, KY: Synthetic Approaches to Cyclopentadiene-Capped Acenes & Their Iron Complexes

CONFERENCE POSTER PRESENTATIONS

- **2015:** Naff Symposium on Chemistry and Molecular Biology metals and Proteins, University of Kentucky, Lexington, KY: Synthesis and Characterization of Ferrocene-Fused Tropones, Thiotropones and Tropone Oximes

- **2012:** Naff Symposium on Chemistry and Molecular Biology metals and Proteins, University of Kentucky, Lexington, KY: Synthetic Approaches to Cyclopentadiene-Capped Acenes & Their Iron Complexes